СИСТЕМНІ ДОСЛІДЖЕННЯ ТА ІНФОРМАЦІЙНІ ТЕХНОЛОГІЇ

У номері:

- **Теоретичні та прикладні проблеми і методи системного аналізу**

- **Прогресивні інформаційні технології, високопродуктивні комп'ютерні системи**

- **Проблеми прийняття рішень та управління в економічних, технічних, екологічних і соціальних системах**

- **Теоретичні та прикладні проблеми інтелектуальних систем підтримання прийняття рішень**

- **Математичні методи, моделі, проблеми і технології дослідження складних систем**

SYSTEM RESEARCH AND INFORMATION TECHNOLOGIES

Шановні читачі!

Навчально-науковий комплекс «Інститут прикладного системного аналізу» Національного технічного університету України «Київський політехнічний інститут імені Ігоря Сікорського» видає міжнародний науково-технічний журнал

«СИСТЕМНІ ДОСЛІДЖЕННЯ ТА ІНФОРМАЦІЙНІ ТЕХНОЛОГІЇ».

Журнал публікує праці теоретичного та прикладного характеру в широкому спектрі проблем, що стосуються системних досліджень та інформаційних технологій.

Провідні тематичні розділи журналу:

Теоретичні та прикладні проблеми і методи системного аналізу; теоретичні та прикладні проблеми інформатики; автоматизовані системи управління; прогресивні інформаційні технології, високопродуктивні комп'ютерні системи; проблеми прийняття рішень і управління в економічних, технічних, екологічних і соціальних системах; теоретичні та прикладні проблеми інтелектуальних систем підтримання прийняття рішень; проблемно і функціонально орієнтовані комп'ютерні системи та мережі; методи оптимізації, оптимальне управління і теорія ігор; математичні методи, моделі, проблеми і технології дослідження складних систем; методи аналізу та управління системами в умовах ризику і невизначеності; евристичні методи та алгоритми в системному аналізі та управлінні; нові методи в системному аналізі, інформатиці та теорії прийняття рішень; науково-методичні проблеми в освіті.

Головний редактор журналу — ректор Національного технічного університету України «Київський політехнічний інститут імені Ігоря Сікорського», академік НАН України Михайло Захарович Згуровський.

Журнал «Системні дослідження та інформаційні технології» включено до переліку фахових видань ВАК України.

Журнал «Системні дослідження та інформаційні технології» входить до таких наукометричних баз даних: Scopus, EBSCO, Google Scholar, DOAJ, Index Copernicus, реферативна база даних «Україніка наукова», український реферативний журнал «Джерело», наукова періодика України.

Статті публікуються українською, російською та англійською мовами.

Журнал можна передплатити. **Наш індекс 23918.** Якщо ви не встигли передплатити журнал, його можна придбати безпосередньо в редакції за адресою: 03056, м. Київ, просп. Перемоги, 37, корп. 35.

Dear Readers!

Educational and Scientific Complex «Institute for Applied System Analysis» of the National Technical University of Ukraine «Igor Sikorsky Kyiv Polytechnic Institute» is published of the international scientific and technical journal

«SYSTEM RESEARCH AND INFORMATION TECHNOLOGIES».

The Journal is printing works of a theoretical and applied character on a wide spectrum of problems, connected with system researches and information technologies.

The main thematic sections of the Journal are the following:

Theoretical and applied problems and methods of system analysis; theoretical and applied problems of computer science; automated control systems; progressive information technologies, high-efficiency computer systems; decision making and control in economic, technical, ecological and social systems; theoretical and applied problems of intellectual systems for decision making support; problem- and function-oriented computer systems and networks; methods of optimization, optimum control and theory of games; mathematical methods, models, problems and technologies for complex systems research; methods of system analysis and control in conditions of risk and uncertainty; heuristic methods and algorithms in system analysis and control; new methods in system analysis, computer science and theory of decision making; scientific and methodical problems in education.

The editor-in-chief of the Journal is rector of the National Technical University of Ukraine «Igor Sikorsky Kyiv Polytechnic Institute», academician of the NASU Michael Zaharovich Zgurovsky.

The articles to be published in the Journal in Ukrainian, Russian and English languages are accepted. Information printed in the Journal is included in the Catalogue of periodicals of Ukraine.

СИСТЕМНІ ДОСЛІДЖЕННЯ ТА ІНФОМАЦІЙНІ ТЕХНОЛОГІЇ

2 • 2022

ЗМІСТ

SYSTEM RESEARCH AND INFORMATION TECHNOLOGIES

2 • 2022

CONTENT

ANALYSIS OF THE IMPACT OF RUSSIA'S MILITARY INVASION OF UKRAINE ON THE ENERGY INDEPENDENCE OF EUROPEAN COUNTRIES

M. ZGUROVSKY, M. KRAVCHENKO, K. BOIARYNOVA, O. ILYASH, K. KOPISHYNSKA, I. PYSHNOGRAIEV

Abstract. The article presents an analysis of the problems of energy independence and energy supply of European countries, given the impact of Russia's full-scale military invasion of Ukraine. This analysis is based on the Energy Freedom Index (*Ief*) developed by the authors, which aggregates sub-indices of energy potential, energy balance, and energy development. A rating of 142 countries of the world was formed according to the value of this index and the places of the EU countries and Ukraine in this rating were determined. Measures aimed at increasing the level of energy independence of European countries and Ukraine were analyzed. Diversification of supplies and accelerated transition to clean energy were proposed as the main measures. European countries have been clustered according to the level of economic and security losses due to the embargo on Russian energy resources. Four groups of countries have been identified in terms of their readiness to replace Russian energy resources and impose embargoes. The dynamics of the indicators of the energy freedom index and their dependence on Russian imports were analyzed, and measures to reduce this dependence were proposed.

Keywords: energy independence, energy freedom index, full-scale Russian invasion of Ukraine, reliance on Russian fossil fuels.

INTRODUCTION

The country's energy independence is a fundamental component of its sovereignty. It determines the self-sufficiency of the state in terms of energy resources, energy supply, and energy generation. In a narrower sense, energy independence determines the independence of one country from the energy resources of another and demonstrates the extent to which the economy relies on its imports to meet its energy needs. The European Union imports 90% of its gas consumption. Until recently, the share of the Russian Federation in these imports was 45% (Fig. 1). This is about 140 billion cubic meters of natural gas, of which 15 billion cubic meters were supplied in liquefied form. Russia also accounted for about 25% of oil and oil products imports and 45% of coal imports [1].

In 2021, the European Commission developed a program of gradual abandonment of Russian gas imports "Fit for 55". It presented a set of legislative proposals and initiatives to ensure that EU policies are in line with climate goals, but was rather slow, with a deadline of 2050.
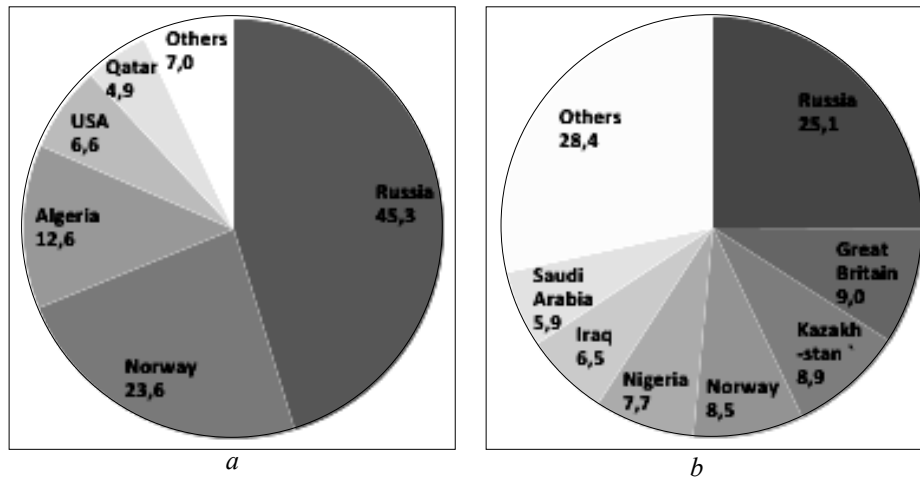
Fig. 1. Structure of imports of major energy sources in the European Union (%), 2021 [1]: *a* — natural gas; *b* — oil and oil products

The full-scale Russian invasion of Ukraine on February 24, 2024, exacerbated the problems in the energy market and necessitated an immediate review of the energy independence of the EU. This article examines the prerequisites for building such strategies and explores the possibilities of developing energy systems in Europe, given the significant reduction in dependence on Russian fossil fuels.

ENERGY INDEPENDENCE OF EUROPEAN COUNTRIES:

PREREQUISITES AND PROSPECTS

**Measures of the European Union to eliminate dependence
on Russian fossil fuels**

This situation shows that the countries of the European Union have been implementing the strategy of energy independence too slowly, probably because they saw an economic advantage in the use of imported Russian fuel resources. For each country, the ability to abandon Russian fossil fuels is determined by their energy systems' structure and state of development.

In the paper [2] we proposed a method of a quantitative assessment of the state of energy systems of countries in the form of an integrated index Energy Freedom Index *(Ief)*, which summarizes the characteristics of these systems by the following groups of indicators (subindices):

1. *Subindex of energy potential* (*Iep*) – determines the established potential of the country in terms of access to fuel and energy resources, namely to reserves of coal, natural gas and crude oil.

2. *Subindex of energy balance* (*Ieb*) – reflects the annual balance between total production and consumption of electricity and heat in the country.

3. *Subindex of energy development* (*Ied*) – demonstrates the ability of the country's energy system to develop, increase energy efficiency and increase the capacity of electricity generation facilities, including from renewable sources.

The integrated Energy Freedom Index is defined as the product of three subindexes (Table 1):

$$Ief = Iep \times Ieb \times Ied .$$

T a b l e 1. Characteristics of the components of the Energy Freedom Index (*Ief*)

Subindex	Characteristic	Calculation	Condition and meaning
1. Subindex of energy potential (*Iep*)	Determines the established potential of the country in terms of access to fuel and energy resources: coal, natural gas and crude oil reserves	The value of the total indicator of the overall explored reserves of coal, natural gas and crude oil, determined per capita. To determine the total indicator and reconcile the data, which differ both in units of measurement and in the range of values there was used a logistic normalization of data according to the formula: $$C_{\text{norm}}(x_{ij}) = (1 + e^{\frac{a - x_{ij}}{b}})^{-1} + 0.5,$$ here parameters a and b are calculated as the mean and standard deviation of the sample of countries under analysis	Larger subindex values within the range [0,1; 1,5] – greater potential. Average value is 1,0
2. Subindex of energy balance (*Ieb*)	Reflects the annual balance between total production and consumption of electricity and heat in the country	Ratio of annual production and annual energy consumption (both indicators – in million metric tons of oil equivalent). The volume of energy production includes: production and processing of coal, crude oil and leasing condensate, natural gas; electricity generation at nuclear and hydroelectric power plants; geothermal electricity generation; production of solar thermal and photovoltaic electricity and wind electricity; production of fuel from wood and biomass waste	Subindex value ≥ 1,0 – positive energy balance, the ability to meet the energy needs of the country's own production. Subindex value <1,0 – negative energy balance
3. Subindex of energy development (*Ied*)	Demonstrates the ability of the country's energy system to develop with the possibility of energy transition	Chain growth rate of the total installed capacity of all electricity generation facilities in the country. The total installed capacity of all electricity generation facilities consists of: power of fossil fuel electricity; hydraulic accumulators; hydroelectric power plants; nuclear electricity; geothermal electricity; electricity from biomass and waste; total electricity from renewable sources without taking into account hydropower. The value of the current year's subindex is defined as a percentage of the value of the indicator for the previous year	The value of the subindex of the base year 2000 = 1,0. Subindex value ≥ 1,0 – positive dynamics of development. Subindex value < 1,0 – negative dynamics of the decline

Table 2 shows the values of the Energy Freedom Index and its components for the EU and Ukraine (*Ief* values for 142 countries are given in [2]). The table also contains data on the share of energy imports from Russia in the structure of national consumption

In 2020, there have been significant changes in the EU economy and the electricity market in particular. Electricity consumption and imports decreased significantly, and fossil fuel use decreased accordingly. This was due to the slowdown in economic development due to the coronavirus pandemic and favorable weather conditions. The development of renewable generation (+80 TWh) and the increase in net imports (+13 TWh), mainly from Norwegian hydropower plants, also had a partial impact. In general, the carbon potential of the EU electricity in 2020 decreased by 14% compared to 2019 [3; 4].

T a b l e   2. Ranking of the EU and Ukraine by the value of the Energy Freedom Index and the relationship between the index and the share of energy imports from Russia in the structure of their national consumption [2; 3]

Place in the EU ranking 2020	Country	Ief 2019	Ief 2020	Index components 2020			Share of imports from Russia in national consumption	Correlation between Ief and the share of imports from Russia
				Subindex of energy potential	Subindex of energy balance	Subindex of energy develop-ment		
1	Ukraine	0,70	0,77	1,07	0,72	1,00	NA	NA
2	Bulgaria	0,59	0,76	1,00	0,69	1,11	0,40	0,20
3	Poland	0,58	0,63	1,05	0,59	1,01	0,37	-0,85
4	Denmark	0,70	0,61	0,95	0,98	0,65	0,16	-0,65
5	Czech Republic	0,55	0,59	1,00	0,63	0,94	0,24	-0,43
6	Sweden	0,68	0,59	0,94	0,63	1,00	0,08	0,57
7	Latvia	0,18	0,56	0,94	0,64	0,93	0,31	-0,29
8	Slovenia	0,47	0,55	0,97	0,55	1,03	0,10	0,10
9	France	0,48	0,54	0,94	0,58	0,99	0,09	-0,10
10	Romania	0,72	0,54	0,95	0,72	0,78	0,18	-0,58
11	Finland	0,42	0,49	0,94	0,52	1,00	0,45	0,09
12	Croatia	0,36	0,43	0,95	0,45	1,00	0,09	-0,08
13	Hungary	0,35	0,42	0,99	0,40	1,05	0,54	-0,28
14	Slovakia	0,32	0,40	0,95	0,41	1,03	0,60	-0,28
15	Germany	0,33	0,37	1,01	0,37	0,98	0,28	-0,65
16	Austria	0,35	0,32	0,94	0,42	0,82	0,03	0,10
17	Netherlands	0,39	0,32	0,95	0,35	0,95	0,55	-0,58
18	Portugal	0,23	0,31	0,94	0,35	0,94	0,05	0,49
19	Ireland	0,31	0,28	0,94	0,26	1,14	0,53	0,94
20	Greece	0,25	0,28	0,99	0,32	0,90	0,03	0,30
21	Spain	0,26	0,28	0,95	0,28	1,04	0,08	-0,39
22	Belgium	0,22	0,26	0,94	0,26	1,06	0,29	0,25
23	Italy	0,21	0,24	0,94	0,25	1,00	0,25	0,53
24	Lithuania	0,10	0,13	0,94	0,13	1,10	0,98	0,13
25	Estonia	0,18	0,10	0,94	0,11	1,01	0,16	-0,79
26	Luxembourg	0,03	0,05	0,94	0,05	1,00	0,03	0,36
27	Cyprus	0,04	0,05	0,94	0,05	1,03	0,05	-0,41
28	Malta	0,01	0,01	0,94	0,01	1,00	0,17	0,03

The Energy Freedom Index of the leaders of the European rating last year decreased – in Romania by 25%, in Denmark and Sweden – by 13%. Instead, for countries that have reduced fossil fuel consumption in 2020 – France, Germany, Belgium, Italy, and others – *Ief* has grown. The reduction in fossil fuel consumption and demand has also led to lower prices for all types of primary energy resources. Prices for coal, natural gas, and oil have been the lowest in twenty years, falling to 2000 levels.

In 2021, the EU was hit by an energy crisis. On the one hand, the post-pandemic economic recovery has increased natural gas consumption – in the EU as a whole by 4% compared to 2020. In particular, Slovakia increased gas consumption by 25%, Estonia – by 17%, Spain – by 13%, Italy – by 8%, France – by 3%, Germany – by 5% (Fig. 2, *a*). Only some countries have managed to reduce natural gas consumption. In particular, the Netherlands reduced gas consumption by 13%, Sweden – by 31%, Finland – by 23%, Lithuania – by 18% (Fig. 2, *b*).
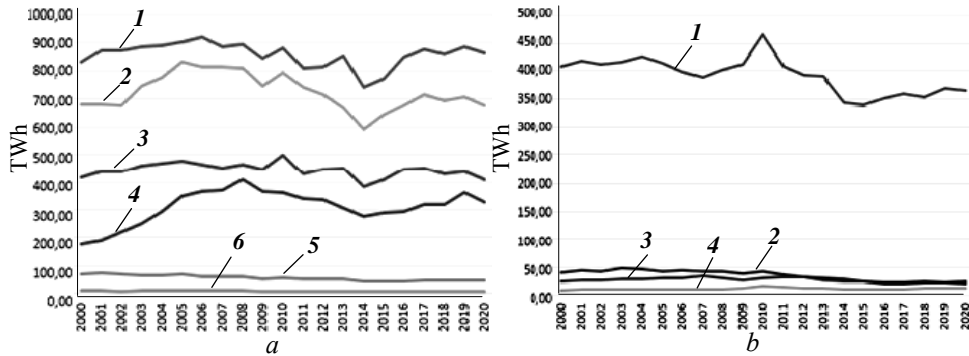
Fig. 2. EU natural gas consumption, 2000–2021 [7]; *a* — EU countries that have increased consumption by the beginning of 2021: *1* — Germany, *2* — Italy, *3* — France, *4* — Spain, *5* — Slovakia, *6* — Estonia; *b* — EU countries that have reduced consumption by the beginning of 2021: *1* — Netherlands, *2* — Finland, *3* — Lithuania, *4* — Sweden

On the other hand, the EU's own natural gas production decreased even more – by 13% compared to 2020. Quarterly production became lower than in the period 2015–2019 [6]. This showed that the reduction in domestic gas production in the EU is a long-term trend (Fig. 3).
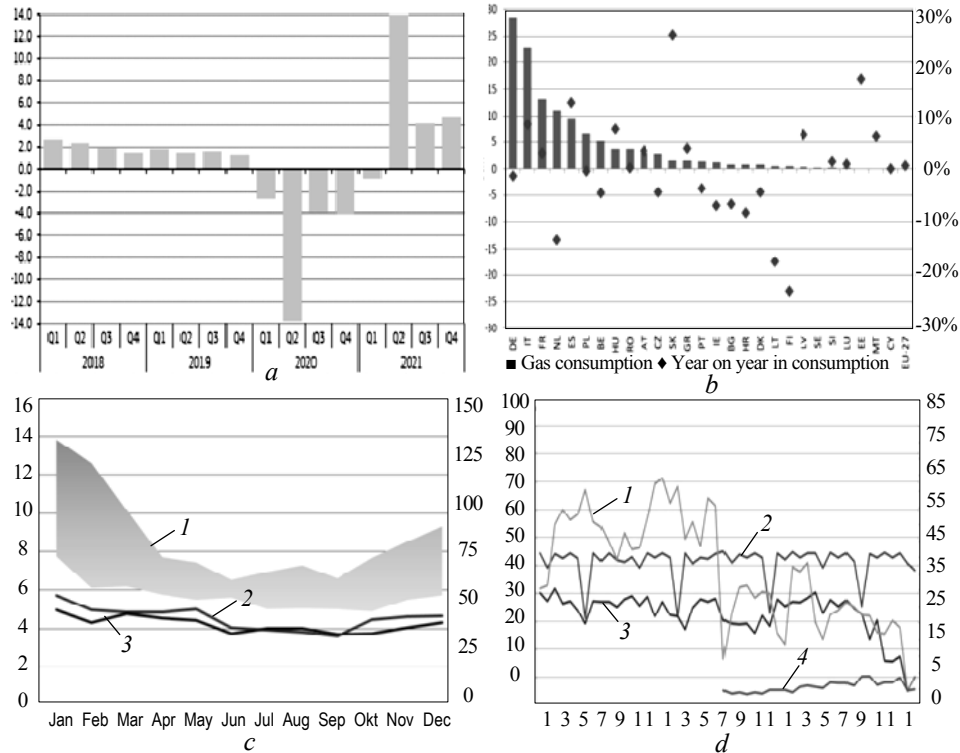
Fig. 3. EU energy market indicators, 2015–2021 [6]: *a* — GDP change year-on-year comparison (%); *b* — gas consumption in the fourth quarter of 2021, year-on-year change; *c* — monthly gas production EU: *1* — 2015–2019:, *2* — 2020, *3* — 2021; *d*— monthly imports of natural gas from Russia by supply route: *1* — Ukraine transit, *2* — Nord Stream, *3* — Belarus transit, *4* — Turkish transit

The full-scale Russian invasion of Ukraine at the end of February 2022 significantly affected the situation in the European energy market. Prices have risen unprecedentedly and consumption has fallen (Fig. 4). According to forecast data,

in 2022 the demand for natural gas is expected to decrease by about 6%, which will correspond to the level of 2020 [8].
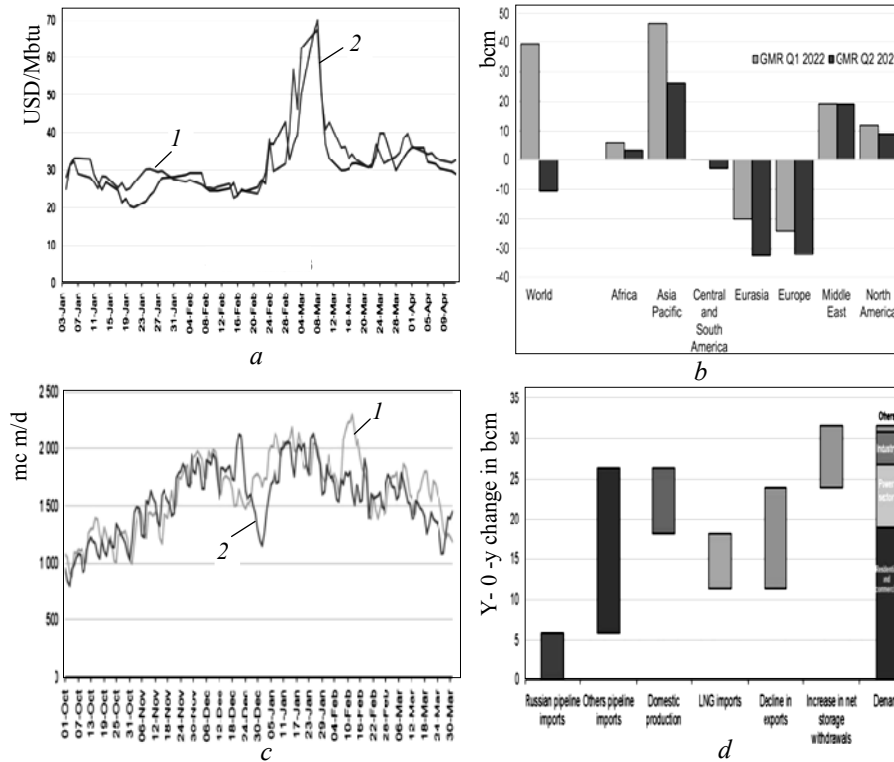
Fig. 4. EU energy market indicators, 2022 [8]: *a* — daily European month-ahead and Asian spot LNG prices: *1* — TIF, *2* — Asian spot LNG; *b* — natural gas consumption growth in the two latest issues of the Gas Market Report; *c* — daily natural gas demand: *1* — 2020/21, *2* — 2021/2022; *d* — natural gas balance, year-on-year change

Energy prices, which began to rise in 2021, jumped sharply – as of March 2022 by an average of 40% compared to December 2021 (Fig. 5).

In early March 2022, the price of natural gas in Europe set a new high and exceeded USD 3 800 per thousand cubic meters. As a result, the European Commission has presented a preliminary plan to eliminate dependence on Russian fossil fuels by 2030 REPowerEU [12].

Measures of the European Union to eliminate reliance on Russian fossil fuels

The dynamics of the energy independence index of countries such as Hungary, Germany, Slovakia, Ireland, Spain, etc., indicates the presence of energy potential, but their energy balance is low and energy development is slow. Lack of activities to increase energy independence, post-pandemic economic recovery and growing dependence on imported fuels have led to an energy crisis in these countries. Countries that had a high index, on the other hand, have greater opportunities to reduce their dependence on Russian fossil fuels.

According to the plan, by the end of 2022 it is expected to reduce EU demand for Russian gas by 100 billion cubic meters or two-thirds of the total. The strategy provides the implementation of two main directions [12]:
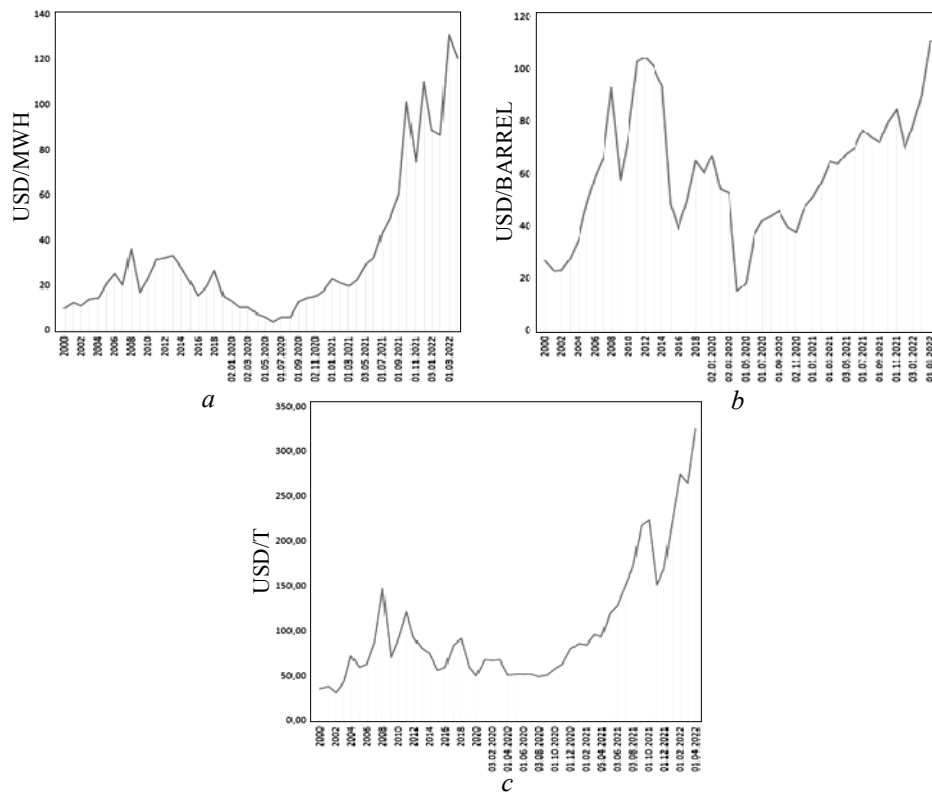
Fig. 5. Coal, natural gas, oil prices, 2000–2022 [9; 10; 11]: *a* — natural gas prices; *b* — oil prices; *c* — coal prices

The first direction is to diversify supplies and attract more renewable gas sources. In particular, it is planned to increase LNG imports (compensating for 60 billion cubic meters of gas), double sustainable biomethane production (compensating for 18 billion cubic meters of gas), increase production and imports of renewable hydrogen (20 million tons of hydrogen can compensate for 50 billion cubic meters of gas).

The second direction is to accelerate the transition to clean energy. In particular, it is planned to install photovoltaic panels on the roofs of residential buildings and enterprises, to double the speed of installing heat pumps. The commission also outlined measures to respond to rising energy prices in Europe and replenish gas supplies next winter. By the end of this year, about 25% of electricity can be generated by solar energy. In general, by the end of 2022 it is expected to reduce EU demand for Russian gas by 100 billion cubic meters or two-thirds of the total volume.

According to the REPowerEU plan, the European Commission has launched technical support for 17 EU member states to phase out Russian fossil fuels. The technical package of recommendations will allow states (Belgium, Bulgaria, Czech Republic, Estonia, Ireland, Greece, Spain, Croatia, Italy, Cyprus, Hungary, Poland, Portugal, Romania, Slovenia, Slovakia and Finland) to identify and implement political reforms and investments in such areas as diversifying energy supplies, accelerating the transition to renewable energy sources and improving energy efficiency [12].

A more detailed plan "A 10-Point Plan to Reduce the European Union's Reliance on Russian Natural Gas" was presented in March 2022 by the International

Energy Agency [13]. In order to ensure security and protect the EU from possible changes in energy supply, the European Parliament has also adopted regulations on measures to ensure security of gas supply (№2017/1938) and on conditions for access to natural gas transmission networks (№715/2009) [14].

In support of Ukraine and opposition to Russian armed aggression, the leaders of the European Union held an informal meeting in Versailles on March 10–11, 2022. The Versailles Declaration was signed as a result of the meeting. It also agreed to stop the import of Russian gas, oil and coal as soon as possible [15].

In general, the updated energy supply strategy of the EU countries envisaged by the above-mentioned acts is based on two main directions: diversification of supplies and accelerated transition to clean energy.

In the context of the second direction, the act of "green" taxonomy of the European Union was adopted, which sets out a number of provisions for changing the structure of energy supply. In particular, the most effective way to decarbonize the economy is direct electrification of end use. 66% of European electricity has already been decarbonized, of which 50% – due to nuclear energy [16]. Increasing the use of nuclear energy by EU countries is impossible. The planned construction of 14 new nuclear reactors in Europe, in particular in France, is not enough to prevent a gradual decline in the total installed capacity of existing reactors, which are nearing the end of their technical life. The new reactors will keep the share of nuclear energy in the structure of total energy production at 50% in 2035–2050.

Taking into account the climatic characteristics of the European region it is also impossible to use renewable energy for a full maximum. However, as an additional source, it is planned to increase the use of biomass, wind or solar energy from 32% to 40% of final energy consumption by 2030.

Thus, the main direction of increasing the level of energy independence of European countries from Russia is the diversification of gas supplies. With technical support from the EU, European countries are already taking steps to reduce or stop gas and oil imports from Russia, but most of the measures are planned for five years, as their rapid implementation is problematic. There are geographical difficulties in transporting LNG. Given the different volumes of Russian gas consumption and the different capacity of LNG infrastructure, countries have different options for its replacement, as shown in (Fig. 6, 7).
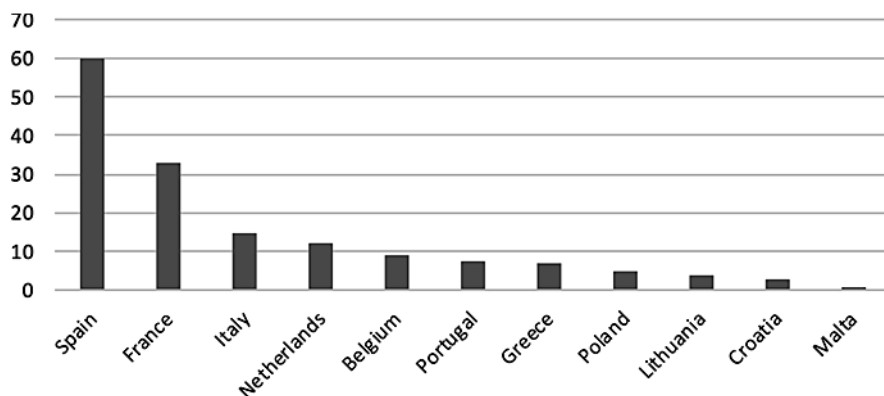
Fig. 6. Annual capacity of liquefied natural gas terminals (billion cubic meters per year), 2022 [17]
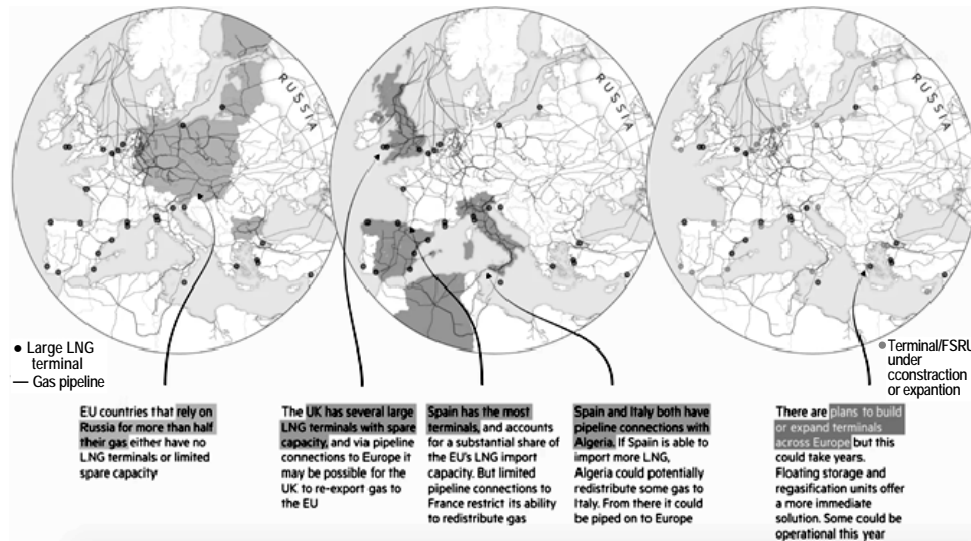
Fig. 7. Prospects for increasing LNG imports to EU countries [18]

The Baltic states were the first countries in Europe to completely stop importing Russian gas. From April 1, 2022, Russian natural gas will no longer flow to Latvia, Estonia and Lithuania. By the end of 2022, the Netherlands plans to abandon Russian oil, gas and coal.

The most difficult thing is to refuse to import Russian gas to its largest consumers – Germany, Italy and France. However, France has said it is ready to support an embargo on Russian oil and gas imports. Other countries, including Germany, are not ready to give up supplies from Russia. In case of a full embargo on imports from Russia, Germany will be able to replace only 20% of gas consumed by increasing coal combustion. At the same time, the German government has assured that it will not allow the Nord Stream 2 gas pipeline to start operating. Austria, which is 80% dependent on Russian natural gas, cannot abandon Russian natural gas in the nearest future, but the country has completely abandoned Russian oil [19].

Europe's efforts to gradually reduce gas imports from Russia are expanding the geography of supply. Already this year, the EU plans to increase liquefied gas supplies from the United States and Qatar by 50 billion cubic meters. The EU relies on Caspian producers to supply natural gas, which can supply up to 10 billion cubic meters for several months. This requires enhanced cooperation with Turkey, which is becoming a central link in alternative supply routes from Azerbaijan, Turkmenistan and Israel [20; 21]. Europe is focusing on the development of nuclear energy capacity, the generation of energy from renewable sources. New oil suppliers are being sought.

As of the end of April 2022, the EU's fifth package of sanctions has decided to impose an embargo only on Russian coal, which will take effect only in August. The European Union is currently developing the sixth package of sanctions that could affect oil and gas exports. However, some countries, such as Hungary and Slovakia, are unprepared for a total ban on Russian oil because it threatens their energy security. They will be given the time until the end of 2023 to enforce sanctions, one year more than other EU member states. In order to impose an oil embargo, the consent of the world's largest exporters is required. The UAE, Saudi Arabia, Iran, Venezuela, and others should increase oil production by a total of 10 million barrels per day. At the moment, there is the consent of some countries, but the full consent of all exporters is not yet. Therefore, the European Union admits that it will not be able to agree on the positions of all countries on the oil embargo.

Losses of European countries from the embargo on Russian energy resources and measures to reduce them

Russia's energy resources have become an important geopolitical factor. According to the Bruegel think tank, the EU pays 450 million and 400 million euros a day for oil and natural gas imports, respectively. This amount is equivalent to the estimated cost of 160 Caliber cruise missiles launched in Ukraine. In just two months of war, the EU has paid Russia more than 40 billion euros for oil and gas. This money has largely offset the impact of Western sanctions on Russia. The oil and gas sector brings in up to half of its budget revenues and more than half of its exports, and it sells 70% of its gas and 60% of its oil and petroleum products to Europe. In 2021, revenues from oil and gas exports in the federal budget of Russia amounted to 38,1% of total revenues, and profits – 119 billion dollars [22].

In response to the imposition of sanctions by European countries, on March 31, 2022, the President of Russia signed a decree defining new rules for the sale of natural gas to "unfriendly countries" from April 1. Countries-buyers should open special accounts with Gazprombank. The bank will accept payments in foreign currency and will convert it into rubles. Most EU and G7 countries have rejected this requirement, but about 10 countries, including Hungary and Italy, have already opened such accounts [23]. Due to the refusal to demand payment in rubles, Russia has already cut off gas supplies to Bulgaria and Poland. These countries have stated their readiness to stop Russian gas supplies and receive gas through alternative routes from Greece and Germany. But if a similar situation occurs with other, more vulnerable countries, it will require a partial revision of their energy strategy and structure.

All EU countries are taking active measures to replace Russian fuel with energy from other sources. However, as shown above, the level of their readiness and the time of replacement are different and are determined by the level of dependence, policies, and capabilities of countries. Different countries will have different consequences of the embargo on Russian fossil fuels, measured by losses in the country's economy and security.

For further research, a pairwise correlation analysis was conducted to determine the relationship between the Energy Freedom Index, which is a generalized measure of the country's ability to embargo, and the share of Russian energy imports in its total consumption, which is a measure of dependence on Russia (Fig. 8).

The correlation coefficient is interpreted as follows:

1. Positive coefficient:

• the growth of the Energy Freedom Index is associated with the growth of energy imports from Russia;

• the decrease in the Energy Freedom Index is associated with a decrease in energy imports from Russia.

2. Negative coefficient:

• the growth of the Energy Freedom Index is associated with a decrease in energy imports from Russia;

• the decrease in the Energy Freedom Index is associated with the growth of energy imports from Russia.

The density of the relationship between variables in the interval $[0; \pm 0,1)$ – absent, in the interval $[\pm 0,1; \pm 0,3)$ – low, in the interval $[\pm 0,3; \pm 0,5)$ – medium, and in the interval $[\pm 05; \pm 1]$ – high.
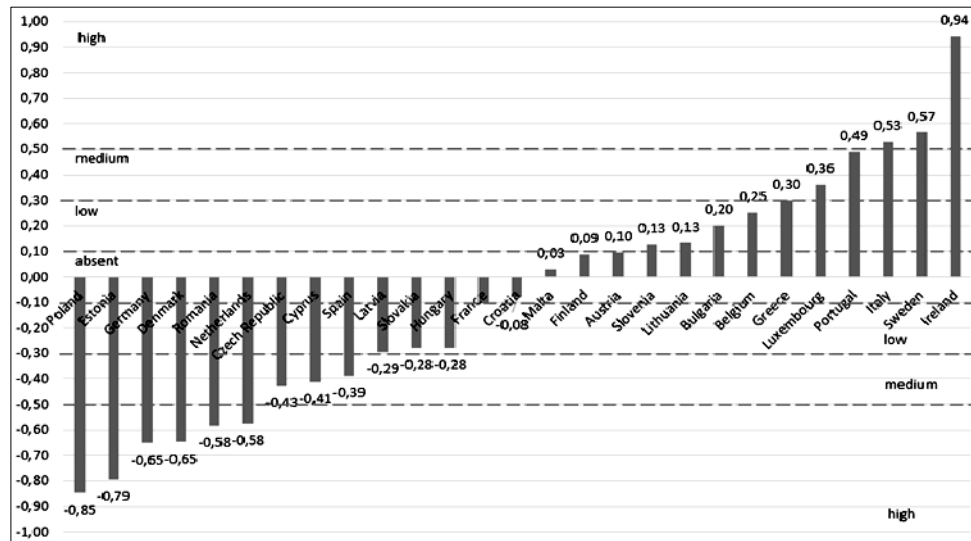
Fig. 8. Correlation coefficient and density of the relationship between the Energy Freedom Index (*Ief*) and the share of imports of Russian energy resources in the structure of their total consumption (*Imrf*) for the UE countries

Based on the results of the analysis, it is possible to group countries on the basis of the relationship between their energy freedom and the share of Russian energy imports as:

• countries with a high and medium density of the inverse relationship between their energy freedom and the share of imports of Russian energy (Poland, Estonia, Germany, Denmark, Romania, the Netherlands, the Czech Republic, Cyprus and Spain);

• countries with a low level of direct and inverse relationship between their energy freedom and the share of imports of Russian energy (Latvia, Slovakia, Hungary, Slovenia, Austria, Belgium, Lithuania);

• countries for which the relationship between their energy freedom and the share of imports of Russian energy has not been established (Croatia, France, Malta, Finland);

• countries with a high and medium density of direct relationship between their energy freedom and the share of imports of Russian energy (Greece, Luxembourg, Portugal, Italy, Sweden and Ireland).

Among the established groups of countries, only the first can show that for these countries, increasing dependence on energy imports from Russia may reduce the level of their energy independence and vice versa. The rest of the groups have either a weak and no correlation between variables, or results that contradict the hypothesis about the nature of the relationship between the energy freedom of countries and energy imports from Russia.

Thus, the correlation analysis does not allow to clearly identify patterns of dependence of countries on energy imports from Russia and to determine which of them are willing to abandon such imports and take measures to reduce this dependence.

Another approach to grouping countries takes into account the risk of refusing to import energy resources. The grouping of countries in the two-dimensional field of parameters – Energy Freedom Index (*Ief*) and the share of imports of Russian energy resources in the structure of total consumption (*Imrf*) – provided an opportunity to distribute countries according to the level of risk. According to the results of grouping for 2020 data (Fig. 9):
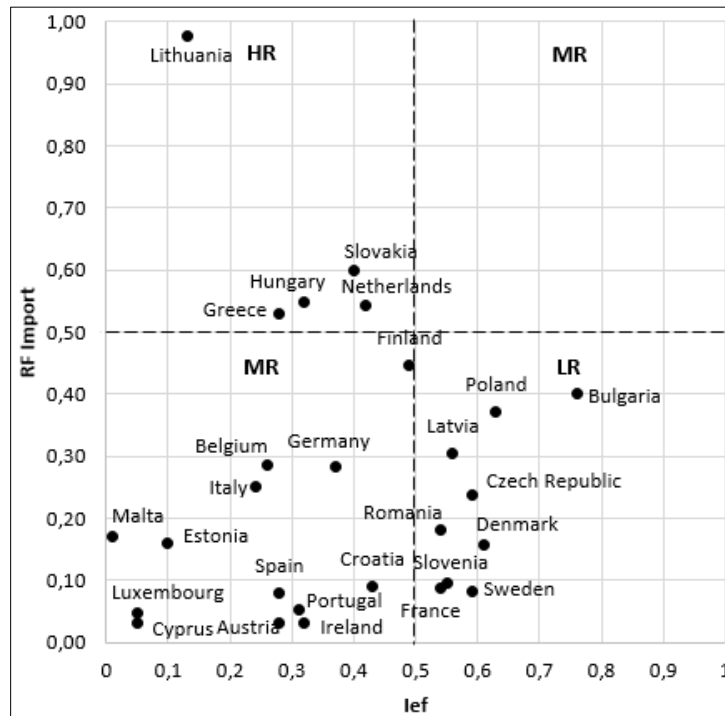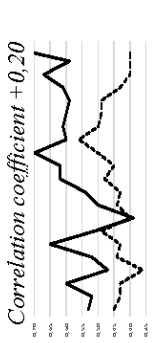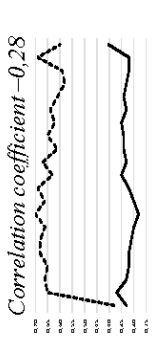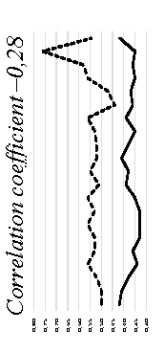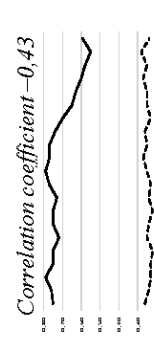
Fig. 9. The grouping of countries in the two-dimensional field of parameters – Energy Freedom Index (*Ief*) and the share of imports of Russian energy resources in the structure of total consumption (*Imrf*)
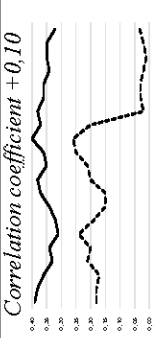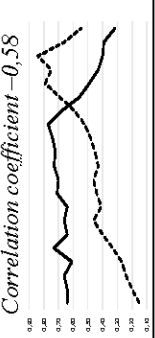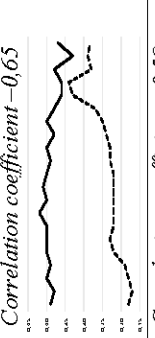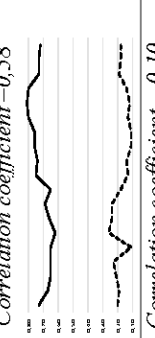
• in the high-risk zone (HR) were countries whose index is below average, and which have more than half of Russian energy resources in the structure of total consumption: *Ief* < 0,50; *Imrf* > 0,50 (Greece, Lithuania, Netherlands, Slovakia, Hungary);

• in the medium-risk zone (MR) were countries whose index is below average, but which have less than half of Russian energy resources in the structure of total consumption: *Ief* < 0,50; *Imrf* < 0,50 (Austria, Belgium, Estonia, Ireland, Spain, Italy, Cyprus, Luxembourg, Malta, Germany, Portugal, Croatia);

• in the low-risk zone (LR) were countries whose index is above average, and which have less than half of Russian energy resources in the structure of total consumption: *Ief* > 0,50; *Imrf* <0,50 (Bulgaria, Denmark, Latvia, Poland, Romania, Slovenia, France, Czech Republic, Sweden).

Both of the abovementioned approaches to grouping do not take into account the measures taken by the countries to reduce dependence on energy imports from Russia (which in this case oppose risky measures), so they cannot be used to measure final risk and determine their readiness for the embargo. In addition, the country's readiness to implement the proposed EU embargo is largely determined by its political interests. To this end, the countries were analyzed in the context of a set of measures they took to eliminate Russian dependence and preparedness for the embargo.

To date (since the countries are in the process of making final decisions), four groups of countries can be identified (Table 3) according to the degree of their readiness to replace Russian energy sources and impose an embargo:

T a b l e 3. Comparative analysis of European countries by groups of measures to eliminate dependence on Russian energy imports and readiness for embargo

Country	Dynamics of changes Ief (solid line) and $Imrf$ (dashed line)	Implemented actions on the embargo	Diversification	Use of clean energy	Reduction of energy intensity	Increasing own production and (or) construction of own LNG terminals
1	2	3	4	5	6	7
Group 1						
Bulgaria	*Correlation coefficient +0,20*	Refusal to renew the contract after the expiration of this year	Agreement with Azerbaijan on increasing gas supplies.			Use of a new pipeline with Greece
Slovakia	*Correlation coefficient –0,28*	Cessation of veto, but focus on oil-based relief based on oil-based production from Russia	Searching for a solution			Development of strategies for the introduction of new technologies of other types of oil refining
Hungary	*Correlation coefficient –0,28*	Refusal of the embargo. Ban on the supply of coal from Russia	Searching for a solution			
Czech Republic	*Correlation coefficient –0,43*	Needs an extension or exemption from the oil embargo	Use of Shell's TAL oil pipeline			

Group 2

1	2	3	4	5	6	7
Austria	Correlation coefficient +0,10	Cessation of veto, refusal of the oil and gas company OMV to import oil from Russia				Production of shale gas by new methods
Netherlands	Correlation coefficient −0,58	Cessation of veto, however, the focus on relief from the embargo is based on oil-based production from Russia				Changing oil refining technologies
Germany	Correlation coefficient −0,65	Significant impact on the economy due to transportation conditions	Energy partnership agreements with Qatar			Use of LNG acceptance terminals from tankers
Romania	Correlation coefficient −0,58	OMV Petrom's refusal to import oil		Strategic partnership between Romania, Hungary, Slovakia, and Poland on the development of hydrogen networks		Resumption of gas production on the Black Sea shelf
France	Correlation coefficient −0,10	Readiness for the embargo				Resumption of NPP construction

1	2	3	4	5	6	7
			Group 3			
Belgium	*Correlation coefficient +0,25*	Not interested in the energy embargo				Development of nuclear energy
Italy	*Correlation coefficient +0,53*	Significant dependence on fossil fuels from Russia, however, the embargo is maintained	Establishing cooperation with Algeria on fossil fuel imports			Cooperation with Spain on planning the construction of the pipeline
Lithuania	*Correlation coefficient +0,13*	Complete cessation of energy imports from Russia		Development of green energy		Import via LNG terminal in Klaipeda
Poland	*Correlation coefficient –0,85*	Full support for the embargo, a ban on coal imports, disconnection from gas supplies to Russia	Gas supply agreement with Estonia			Increasing own production
Finland	*Correlation coefficient +0,09*	Focus on joining NATO			Reduction of natural gas consumption	

Group 4

1	2	3	4	5	6	7
Greece	Correlation coefficient +0,30	Support for the embargo				Construction of LNG floating stations
Denmark	Correlation coefficient –0,65	Support for the embargo		Focus on green energy		Resumption of the Baltic Pipe pipeline project from Norway to Poland
Estonia	Correlation coefficient – 0,79	Refusal to import until the end of the year				Creation of receiving capacities in ports
Ireland	Correlation coefficient +0,94	Full support for the abandonment of fossil fuels from Russia		Focus on the use of nuclear, wind and solar energy		
Spain	Correlation coefficient –0,39	Support for the embargo, use of LNG regasification				Cooperation with Italy on planning the construction of the pipeline
Cyprus	Correlation coefficient –0,41	Support for the embargo, concerns about declining profitability of shipping	Focus on gas supplies from the eastern Mediterranean			

1	2	3	4	5	6	7
Latvia	Correlation coefficient −0,29	Support for the emsbargo	Use of gas reserves. Focus on the use of Lithuanian terminals			
Luxembourg	Correlation coefficient −0,36	Agreement with the refusal of coal	Neutrality in imports of Russian gas and oil			
Malta	Correlation coefficient +0,03	Independence from t he import of fuel resources from Russia	Focus on diversification of energy sources			
Portugal	Correlation coefficient +0,49	Support for the embargo		Focus on renewable energy sources		
Slovenia	Correlation coefficient +0,10	Support for the embargo	Focus on cooperation with Croatia on gas supplys			

- *Group 1* – countries for which the refusal to import fuel resources from Russia threatens the greatest losses in the economy, and which need and may receive a delay in the imposition of embargoes (Hungary, Czech Republic, Slovakia and Bulgaria);
- *Group 2* – countries that are heavily dependent on fuel imports from Russia, and at the beginning of the sixth package of sanctions have some controversy over the imposition of the embargo (Netherlands, Austria, Germany, Romania, France);
- *Group 3* – countries that have significant or moderate dependence on imports of fuel imports from Russia, but support the embargo (Lithuania, Belgium, Italy, Finland, Poland);
- *Group 4* – countries that have low dependence on fuel imports from Russia and support the embargo (Greece, Estonia, Ireland, Spain, Cyprus, Luxembourg, Malta, Portugal, Slovenia, Denmark, Latvia).

Measures envisaged by the strategy of elimination of EU dependence taken by certain countries (anti-risk measures) can be divided into four categories: diversification; use of clean energy; reduction of energy consumption; the increase of own energy production and (or) construction of own LNG terminals.

Group 1 — Bulgaria (LR), Czech Republic (LR), Slovakia (HR), Hungary (HR). This group of countries includes both high-risk and low-risk countries, which have low or not very high dependence on Russian energy imports. As can be seen from Table 3, all countries in this group have already increased their energy independence index in 2020 and reduced the share of Russian fuel imports. The analysis showed that for the countries of this group, the primary measure to reduce dependence is the diversification of fuel suppliers.

Bulgaria has the highest index and declining dynamics of imports from Russia, which is already taking measures to diversify — liquefied gas supplies from the US at lower prices than from Russia, supplies from Azerbaijan, and in the long run - LNG use through terminals in Greece and Turkey [24]. The Czech Republic, with fairly strong reserves of coal, oil and gas, is mainly focused on imports from Russia. The lack of differentiation policy in the past determines the urgent need for its implementation. In particular, the Czech company Mero acquired a stake in Shell's TAL oil pipeline [25]. In addition, the Czech Republic has a significant level of biogas production potential. These countries are quite capable of overcoming the risk that will arise as a result of the energy embargo from Russia.

Slovakia currently has a sufficient level of gas in its storage facilities to meet its needs, but it is completely dependent on oil imports from Russia due to the technological features of refineries. Hungary is heavily dependent on Russian fuel, especially oil, and has a low level of supply diversification. Receiving Russian gas in transit through Bulgaria, under the threat of its suspension, the country needs new sources of supply and changes in energy policy. However, for Hungary and Slovakia, the search for alternatives to Russian imports is a long one, and cannot be implemented quickly.

Group 2 — Netherlands (HR), Austria (MR), Germany (MR), Romania (LR), France (KR). This group includes countries with high, medium and low risk — those that at the beginning of the sixth package of EU sanctions had controversy over the imposition of embargo. In the countries of this group there is an inverse relationship between the increase in the level of Energy Freedom Index and the share of fuel imports from Russia in domestic consumption.

At the same time, the Energy Freedom Index in 2020 increased only in Germany and France, while in other countries it decreased. In Austria, when the share of fuel imports from Russia in domestic consumption decreased, the level of the Energy Freedom Index also decreased. This shows that the country's energy dependence is moderate. Austria has long had Kazakhstan, Libya and Iran as key oil suppliers, but high dependence on gas has caused the country to hesitate in deciding on an embargo. Germany, which has a developed industry, needs much more energy than it produces. The supply of fuel resources is limited by pipelines, which complicates the diversification process. The country is considering the supply of liquefied natural gas from Qatar, which will allow the gradual abandonment of Russian gas, for this purpose will be used terminals to receive gas from tankers. The partnership agreed with Qatar includes not only LNG supplies, but also the development of renewable energy sources, as well as energy efficiency measures [26]. Romania's measures are aimed at the development of foreign economic activity and gas production from the Black Sea shelf. However, these projects are long. The Netherlands is currently unable to completely cut off all fossil fuel supplies from Russia, but is refusing to transport it, and the country is focused on import diversification. To this end, floating regasification plants (LNG terminal) are being leased for future LNG gas uptake in Emshaven, Groningen [27]. France receives about 70% of its electricity from nuclear energy. The country has abandoned its previous government's policy of reducing the share of nuclear generation, and this year announced plans to build six new reactors and consider building eight more. This provides the country with a high level of energy security. Thus, the countries of this group have the opportunity to replace imported fossil fuels from Russia, so an embargo is possible. The threat of loss of energy independence that could occur in the event of further dependence on Russia can be eliminated (as shown in Table 3).

Group 3 — Lithuania (HR), Belgium (MR), Italy (MR), Finland (MR), Poland (LR). This group of countries includes high, medium and low risk countries - those that have supported or expressed the readiness to impose an embargo. With the exception of Lithuania, the countries of this group have a low level of dependence on Russian fossil fuels. The defining feature of the countries of this group is the growth of the Energy Freedom Index and the decline in the share of fuel imports from Russia in domestic consumption, which indicates an intensification of efforts in these areas. Poland is actively looking for opportunities to diversify supplies and increase its own production. With an expanded LNG terminal, the country is stepping up the commissioning of the Baltic Pipeline, which will provide it with gas connections with Lithuania and Slovakia [28]. Italy is focusing on diversification and finding new suppliers, and Algeria is currently being considered as such. In addition, the possibility of building a pipeline to supply gas from Spain is being discussed. Belgium has a strong nuclear power industry but is an importer of fuel resources. Although a fairly high proportion of them imported from Russia, the country has taken steps to diversify its sources of supply, importing oil from Iran and Saudi Arabia and gas from Qatar, the Netherlands and Norway. Lithuania's economy is heavily dependent on Russian fuel imports, but the country was one of the first to abandon it. Currently, the country is focused on imports through the LNG terminal in Klaipeda from other suppliers and the development of green energy. Finland is focusing on new gas import agreements, including an agreement with Estonia. A characteristic feature of Group 3 countries is the low level of LNG use.

Group 4 — Greece (HR), Estonia (MR), Ireland (MR), Spain (MR), Cyprus (MR), Luxembourg (MR), Malta (MR), Portugal (MR), Slovenia (MR), Denmark (MR), Latvia (MR). This group of countries includes countries with high, medium and low risk - those that have low dependence on imports of fuel resources from Russia and support the embargo, because they risk the least. The level of their energy independence is determined mainly by other factors. With the exception of Denmark, Estonia and Ireland, all countries in the group have seen an increase in the Energy Freedom Index in recent years. Latvia, which transported gas from Russia, is now relying on the supply of liquefied gas through the Klaipedos Nafta terminal [29] and is stepping up its green energy policy. Luxembourg has the ability to quickly give up Russian coal but needs oil and gas. The Slovenian government, although it has not given up on Russian fuel, has expressed its readiness to support EU actions in this direction. The country is now focusing on obtaining liquefied natural gas from a terminal in Croatia. Estonia had a high level of gas supplies from Russia, but decided on a strategy of diversification, in particular, the ports will be set up to receive liquefied natural gas. Spain was still the largest importer of LNG from the United States — in 2021 its share rose to 65% [6; 8]. Almost all of Ireland's imports are to the UK, the country focuses on the development of renewable energy sources. Countries such as Cyprus, Greece, and Malta are located in warm natural climates, fossil fuels are used only for industrial purposes. However, the key industry of these countries is shipping, they are engaged in the transportation of oil by sea, and in the embargo see a certain threat of loss of traffic [30]. Greece is focused on the construction of new LNG floating stations. To this end, a project has been launched to build a floating liquefied natural gas terminal in Alexandroupolis [31]. The terminal is scheduled to be completed by the end of 2023, which will identify Greece as the center of EU gas reserves.

Risks and losses of Ukraine's energy as a result of the military invasion of the Russian Federation

In 2019, the Energy Freedom Index of Ukraine was 0,70 and ranked 49th out of 142 countries in the overall ranking [2]. Among the EU countries, only Romania and Denmark were ahead of it.

It should be noted that in 2020 Ukraine's Energy Freedom Index increased by 10% to 0,77 and the overall Ief and energy potential subindex surpassed all EU countries, and the energy balance subindex ranked 3rd. The high energy potential and the general trend of growing energy independence allowed Ukraine to develop an export-oriented energy policy. It had every prospect of becoming a competitive and full-fledged player in the European energy market.

At the same time, Ukraine depends on oil imports by about 83%, 33% on natural gas imports, and 50% on coal imports [32]. This situation is due to the lack of incentives for the development of own energy production, significant depletion of explored fields, and constant changes in government regulation on the rent for hydrocarbon production. Over the past few years, the state has paid more attention to eliminating dependence on gas imports. Therefore, in 2021, imports of oil and petroleum products from Belarus to Ukraine exceeded 2,86 billion dollars, and imports of these resources from Russia amounted to about 3,43 billion dollars [33].

Even before the beginning of the military aggression on February 24, 2022, Ukraine was actively implementing measures to reduce energy dependence on Russia. Such measures have received additional support from other countries. Thus, Energoatom and all its stations were transferred to the Paris Center of the World Association of Nuclear Operators (until now, Ukrainian nuclear power plants were part of the Moscow center WANO). All operating nuclear power plants are operating stably, despite losses. It was planned to build a storage facility for spent nuclear fuel. Ukraine has refused to purchase Russian nuclear fuel. Currently, fuel reserves for WWER-1000 reactors will be enough for two years. During this period, it is planned to equip one of the Ukrainian enterprises with a production line for assembling Westinghouse fuel assemblies.

The Ukrainian power system has finally disconnected from the power systems of Russia and Belarus and joined the European Network of Transmission System Operators for Electricity (ENTSO-E). Accession provides a bilateral advantage: on the one hand, it is an opportunity for European business to work in the energy market of Ukraine, on the other — the development of the European energy market by domestic companies.

Military action has halted the active development of renewable energy that has been observed in Ukraine in recent years. Solar energy suffers the most due to the large area of damaged industrial solar generation facilities. Thus, according to various estimates, 30–40% of solar power plants in the regions affected by the Russian invasion were affected (1120–1500 MW of installed capacity). More than two thirds of all wind power plants have been shut down. 10–15% of the installed capacity of bioenergy facilities was affected [34].

Gas imports from Europe are uninterrupted, in March 2022 the volume of imports amounted to 10 million cubic meters per day. Hungary provides the maximum volume of Ukraine daily imports (about 4,5 million cubic meters per day) [35]. The GTS operators of Slovakia and Poland also provided additional guaranteed capacity for gas imports to Ukraine.

Ukraine is also currently undergoing changes in the market for imports of oil and oil products, where Russia and Belarus used to be key suppliers. The search for new suppliers and the damage caused by hostilities at the largest domestic refineries, Kremenchuk and Shebelynsky, provoked a shortage in the market and a significant increase in product prices.

The outlined measures will increase the level of Ukraine's energy independence, as well as ensure full participation in the European electricity market in the postwar period. However, repairing the damage will require global financial support.

CONCLUSIONS

1. Analysis of the energy independence of the European Union, after the Russian military intervention in Ukraine, showed significant negative consequences. Unflexible and multi-vector energy policy of industrialized EU countries, and their underutilization of energy potential, including the development of renewable energy, and low energy balance have led to import dependence on one energy supplier, and limited opportunities to use their own energy sources. The consequence of such an imbalance is the economic dependence of countries with developed economies on the Russian Federation, which has a predominantly raw-materials-based economy.

2. For a long time, European countries have been increasing their dependence on Russia's fuel resources through slow implementation of reforms, differentiation of suppliers, and development of energy infrastructure, considering it economically feasible to use existing exporters and traditional transit infrastructure. The energy crisis of 2021 revealed the following problems of Europe's energy system:

- limited gas transportation capacity;
- inadequate geographical location or insufficient length of existing gas pipelines in the EU;
- lack of LNG terminals and seaports in some countries;
- failure of the existing level of developing renewable energy to meet energy needs.

3. In such circumstances, the implementation of the strategy of energy independence of European countries from the Russian Federation should focus on two basic areas:

- diversification of supplies;
- accelerated transition to the production and use of clean energy.

Studies have shown that both directions have significant limitations and could lead to a complete abandonment of Russian energy at best in 2030, which significantly complicates the imposition of a full embargo on energy imports from this country until 2030.

4. An alternative to a full embargo could be a sharp reduction in energy imports, imposing a 40% tariff on it, which would reduce imports by about 80%. This will reduce economic losses for the countries, which are most dependent on Russian energy. The economic effect of changing energy supply strategies for European countries will depend on the replacement and redistribution of energy between sectors.

5. The study of the level of energy independence of European countries provided an opportunity to identify four key groups of countries on this indicator:

- with a high level of energy independence and a low level of risk of its loss;
- with a sufficient level of energy independence and an acceptable level of risk of its loss;
- with an acceptable level of energy independence and an increased level of risk of its loss;
- with a low level of energy independence and a high level of risk of losing it.

The analysis showed that in the first and second groups of countries, there are those who have an increased risk of losing energy independence due to the embargo on energy from Russia. These risks must be minimized through the introduction and implementation of planned EU measures aimed at diversifying supplies and accelerating the transition to the production and use of clean energy.

6. Russia's full-scale military invasion of Ukraine has led to the irreparable destruction and destabilization of the country's energy system, which was previously closely integrated with the respective systems of Russia and Belarus. As a result of hostilities, the largest domestic refineries, Kremenchuk and Shebelynsky, were damaged. There were destabilized energy supply chains from Europe, which led to a significant deficit in the energy market and a significant increase in product prices. In response to all the devastating phenomena since February 24, 2022, Ukraine has joined the ENTSO-E integrated power system of continental Europe, disconnected from the energy systems of Russia and Belarus, and established supply chains for oil products from Europe. Despite the fighting and the capture

of the largest Zaporizhzhya nuclear power plant in Europe by Russian troops, Ukraine's energy system has been operating smoothly throughout the Russian aggression. These measures are gradually increasing the level of Ukraine's energy independence and should ensure its full participation in the European market in the postwar period. However, repairing large-scale damage will require global political and financial support.

REFERENCES

1. Statistical office of the European Communities*, General and regional statistics,* 2021. [Online]. Available: https://ec.europa.eu/eurostat.

2. "Index of Energy Freedom of countries and regions of the world: methods of calculation and analysis", (in Ukrainian), in *Foresight: challenges of energy independence of countries and regions of the world in mid-term (until 2025) and long-term (until 2030) time horizons*, M.Z. Zgurovsky, Ed. Kyiv, Ukraine: Igor Sikorsky KPI, Polytechnica PH, 2021, pp. 9–31.

3. International Energy Agency, *Reliance on Russian Fossil Fuels Data Explorer*, March, 2022. [Online]. Available: https://www.iea.org/reports/reliance-on-russian-fossil-fuels-data-explorer.

4. European Commission: *Quarterly Report on European Electricity Markets,* 2021. [Online]. Available: https://ec.europa.eu/energy/sites/default/files/quarterly_report_ on_european_ electricity_ markets_ q4_2020.pdf.

5. European Commission, *Gas and electricity market reports,* 2020. [Online]. Available: https://energy.ec.europa.eu/data-and-analysis/market-analysis_en.

6. European Commission: *Quarterly report on European gas markets,* 2021. [Online]. Available: https://energy.ec.europa.eu/system/files/2022-04/Quarterly%20report%20 on%20European%20gas%20markets_Q4%202021.pdf.

7. *Our World in Data*. [Online]. Available: https://ourworldindata.org/grapher/gas-consumption-by-country?tab=chart&time=2000..latest&country=LTU~ NLD~FIN~SWE.

8. International Energy Agency, *Gas Market Report,* Q2-2022, 2022. [Online]. Available: https://iea.blob.core.windows.net/assets/cfd2441e-cd24-413f-bc9f-eb5ab7d82076/GasMarketReport%2CQ2-2022.pdf.

9. bp: *Statistical Review of World Energy – all data, 1965-2000.* [Online]. Available: https://www.bp.com/en/global/corporate/energy-economics/statistical-review-of-world-energy.html.

10. OECD: *Energy prices are spiking.* March 17, 2022. [Online]. Available: https://www.oecd.org/coronavirus/en/data-insights/energy-prices-are-spiking.

11. Trading economics: *Coal.* [Online]. Available: https://tradingeconomics.com/ commodity.

12. European Comission, *REPowerEU: Joint European action for more affordable, secure and sustainable energy*, March 08, 2022. [Online]. Available: https://ec.europa.eu/commission/ presscorner/detail/en/ip_22_1511.

13. International Energy Agency: *A 10-point plan to reduce the European Union's reliance on Russian natural gas*, March 6, 2022. [Online]. Available: https://www.iea.org/reports/ a-10-point-plan-to-reduce-the-european-unions-reliance-on-russian-natural-gas.

14. European Parliament: *MEPs back plans to restock gas reserves before next winter,* April 07, 2022. [Online]. Available: https://www.europarl.europa.eu/news/es/press-room/ 20220401IPR26536/el-pe-apoya-el-plan-para-almacenar-gas-de-cara-al-proximo-invierno.

15. Council of the European Union: *Versailles Declaration,* March 11, 2022. [Online]. Available: https://www.consilium.europa.eu/media/54773/20220311-versailles-declaration-en.pdf.

16. J. Buzek et al., "An exchange of views on the second EU Taxonomy Delegated Act", *European Energy Forum*, March 03, 2022. [Online] Available: http://www. euro-peanenergyforum.eu/ events/exchange-views-second-eu-taxonomy-delegated-act.

17. L. Boehm, "Russia's war on Ukraine: Implications for EU energy supply", *European parliamentary research service*, March 01, 2022. [Online]. Available: https:// epthink-tank.eu/ 2022/03/ 01/russias-war-on-ukraine-implications-for-eu-energy-supply.

18. H. Dempsey, N. Kommenda, L. Hook, C. Campbell, C. Nevitt, and S. Joiner, "Can the EU wean itself off Russian gas?", *Financial Times,* April 19, 2022. [Online]. Available: https://ig.ft.com/europes-race-to-replace-russian-gas.

19. "Austria has given up Russian oil", (in Ukrainian), *Ukrainian multimedia platform for broadcasting*, April 21, 2022. [Online]. Available: https://www.ukrinform.ua/ rubric-world/3463443-avstria-vidmovilasa-vid-rosijskoi-nafti.html.

20. I. Surwillo and V. Slakaityte, "With energy at play in the Ukraine war, everybody pays", *Danish Institute for International Studies*, March 17, 2022. [Online]. Available: https://www.diis.dk/en/research/with-energy-play-in-the-ukraine-war-everybody-pays.

21. M. Saglam, "Can Turkey benefit from Europe's quest to reduce Russian gas?", *Al-Monitor*, March 09, 2022. [Online]. Available: https://www.al-monitor.com/ origi-nals/2022/03/can-turkey-benefit-europes-quest-reduce-russian-gas.

22. J. Liboreiro, "After coal, the EU faces an uphill battle to ban Russian oil and gas", *Euronews*, April 12, 2022. [Online]. Available: https://www.euronews.com/my-europe/2022/04/12/after-coal-the-eu-faces-an-uphill-battle-to-ban-russian-oil-and-gas.

23. E. Fomina, "The European Union will increase LNG purchases from the United States to replace Russian gas", (in Russian), *Deutsche Welle,* April 01, 2022. [Online]. Available: https://www.dw.com/ ru/es-uvelichit-zakupki-spg-iz-ssha-dlya-zameny-rossijskogo-gaza/a-61324346.

24. "Bulgaria agrees to supply gas from US at lower prices than Gazprom", (in Ukrainian), *Economichna pravda*, May 11, 2022. [Online]. Available: https://www.epravda.com.ua/news/2022/05/11/686912.

25. "The Czech Republic has found something to replace oil from Russia", (in Ukrainian), *Economichna pravda*, May 6, 2022. [Online]. Available: https://www.epravda.com.ua/news/2022/05/6/686711.

26. S. Romashenko "Germany and Qatar agree long-term energy partnership", (in Russian), *Deutsche Welle*, March 20, 2022. [Online]. Available: https://p.dw. com/p/48kUR.

27. "Netherlands's Gasunie leases second floating LNG terminal to replace Russian gas" (in Ukrainian), *Business Tzenzor*, May 11, 2022. [Online]. Available: https://biz.censor.net/n3340621.

28. "Poland wants to give up Russian gas from 2023. The current contract expires in December", (in Ukrainian), *Forbes*, March 17, 2022. [Online]. Available: https://forbes.ua/news/_polshcha-z-2023-roku-planue-povnistyu-vidmovitisya-vid-kupivli-rosiyskogo-gazu-chinniy-kontrakt-zavershuetsya-u-grudni-17032022-4760.

29. O. Ananyeva and O. Khmarna, "Sponsors of the war: who in the EU supports and who blocks the ban on oil and gas from Russia", (in Ukrainian), *Evropeyska pravda*, April 20, 2022. [Online]. Available: https://www.eurointegration.com.ua/articles/ 2022/04/20/7138073.

30. "Some countries have begun to question the effectiveness of the oil embargo against Russia", (in Ukrainian), *Comments*, May 4, 2022. [Online]. Available: https://politics.comments.ua/ua/news/foreign-policy/okremi-kraini-pochali-sumnivatisya-v-efektivnosti-naftovogo-embargo-proti-rosii-697982.html.

31. "Greece becoming Europe energy gateway?", *Ekathimerini*, May 04, 2022. [Online]. Available: https://www.ekathimerini.com/economy/1183473/greece-becoming-europe-energy-gateway.

32. IEA: *Ukraine energy profile*. [Online]. Available: https://www.iea.org/reports/ukraine-energy-profile.

33. State Statistics Committee: *Countries by commodity structure of foreign trade*. [Online]. Available: http://www.ukrstat.gov.ua/operativ/operativ2021/zd/kr_tstr/arh_kr_2021.htm.

34. "Green energy in Ukraine is on the verge of bankruptcy. What's next?", (in Ukrainian), *Ekonomichna Pravda*, April 10, 2022. [Online]. Available: https://www.epravda.com.ua/columns/2022/04/10/685513.

35. *Official site of GTS Ukraine Operator LLC*. [Online]. Available: https://tsoua.com.

INFORMATION ON THE ARTICLE

Michael Z. Zgurovsky, ORCID: 0000-0001-5896-7466, National Technical University of Ukraine "Igor Sikorsky Kyiv Polytechnic Institute", Ukraine, e-mail: zgurovsm@hotmail.com

Maryna O. Kravchenko, ORCID: 0000-0001-5405-0159, National Technical University of Ukraine "Igor Sikorsky Kyiv Polytechnic Institute", Ukraine, e-mail: marina.kravchenko.kpi@gmail.com

Kateryna O. Boiarynova, ORCID: 0000-0001-5879-2213, National Technical University of Ukraine "Igor Sikorsky Kyiv Polytechnic Institute", Ukraine, e-mail: boyarinovaea@ukr.net

Olha I. Ilyash, ORCID: 0000-0002-7882-3942, National Technical University of Ukraine "Igor Sikorsky Kyiv Polytechnic Institute", Ukraine, e-mail: oliai@meta.ua

Kateryna O. Kopishynska, ORCID: 0000-0002-1609-2902, National Technical University of Ukraine "Igor Sikorsky Kyiv Polytechnic Institute", Ukraine, e-mail: kopishynska@ukr.net

Ivan O. Pyshnograiev, ORCID: 0000-0002-3346-8318, National Technical University of Ukraine "Igor Sikorsky Kyiv Polytechnic Institute", Ukraine, e-mail: pyshnograiev@gmail.com

АНАЛІЗ ВПЛИВУ ВІЙСЬКОВОГО ВТОРГНЕННЯ РОСІЇ В УКРАЇНУ НА ЕНЕРГЕТИЧНУ НЕЗАЛЕЖНІСТЬ КРАЇН ЄВРОПИ / М.З. Згуровський, М.О. Кравченко, К.О. Бояринова, О.І. Іляш, К.О. Копішинська, І.О. Пишнограєв

Анотація. Подано аналіз проблем енергетичної незалежності та енергопостачання країн Європи з огляду на вплив повномасштабного воєнного вторгнення Росії в Україну. Наведений аналіз ґрунтується на розробленому авторами Індексі енергетичної незалежності (Energy Freedom Index – *Ief*), який агрегує субіндекси енергетичного потенціалу, енергетичного балансу та розвитку енергетики. Сформовано рейтинг 142 країн світу за значенням вказаного індексу та визначено місця країн Європейського Союзу і України у цьому рейтингу. Проаналізовано заходи, спрямовані на підвищення рівня енергетичної незалежності європейських країн та України. До головних заходів віднесено: диверсифікація постачань та прискорений перехід на чисту енергетику. Проведено кластеризацію країн Європи за рівнем утрат в економіці та безпеці внаслідок ембарго на російські енергоносії. Виділено чотири групи країн за ступенем їх готовності до заміни російських енергоносіїв та запровадження ембарго. Проаналізовано динаміку показників індексу енергетичної незалежності, їх залежності від російського імпорту та запропоновано заходи для зменшення цієї залежності.

Ключові слова: енергетична незалежність, індекс енергетичної незалежності, повномасштабне вторгнення Росії в Україну, залежність від російського викопного палива.

DEVELOPMENT OF A HYBRID METHOD FOR CALCULATION OF SOFTWARE COMPLEXITY

T.H. KAZIMOV, T.A. BAYRAMOVA

Abstract. The use of code metrics allows software developers and project managers to evaluate various features of the software (to be built or already in existence), predict workload, determine software complexity and reliability, and quantify the quality of software systems being developed. Articles written in recent years have proposed various methods for solving this problem. However, there is still no very effective approach to measuring software complexity. This article provides a brief overview of existing software complexity metrics and proposes a new hybrid method for computing software complexity. The proposed hybrid method for evaluating software complexity combines the key features of the Halsted, Maccabe, and SLOC metrics and also allows for a more efficient assessment of complexity.

Keywords: software engineering, software complexity, complexity metrics, hybrid method.

INTRODUCTION

One of the most dynamically developing spheres of modern life is information technology. Today, people's lives are organized in such a way that even people who are far from information technology use them to achieve their goals. The introduction of automated information systems not only reduces the number of operations performed by a person, but also creates new problems. As software grows in size and complexity, the number of bugs increases. Software projects that at first glance appear to be successful may be stopped due to such errors, or the code may be rewritten. This leads to a slight increase in budget expenditures. The world's leading software companies are working on these problems. Various standards organizations (ISO/IEC, IEEE) have developed hundreds of standards covering all stages of software life to improve its quality. Software quality is a complex and multifaceted concept. After the advent of computers in the defense industry in the 1970s, metrics began to emerge to evaluate software performance and quality management.

Software measurement is one of the most important issues in developing quality software. In the words of Tom DeMarco [1], "you can't control what you can't measure".

At the moment, a large number of different software metrics have been developed. Software metrics fall into three categories (Fig.1):

- ● **Product metrics** are product characteristics such as performance, design, size, quality level, and complexity.
- ● **Process Metrics**. These metrics are used to improve software development and maintenance processes.
- ● **Project Metrics**. These metrics describe the performance and characteristics of the project.

Among these indicators, software complexity indicators are of particular importance. In the 10th edition of Sommerville's book Software Engineering, he noted that one of the most important tasks in the development of the modern software industry is the management of software complexity [4]. Research shows that when the project size approaches 5 million lines, the number of defects begins to increase dramatically (Fig. 2). This can be explained by the significant complication of large-scale projects [5].
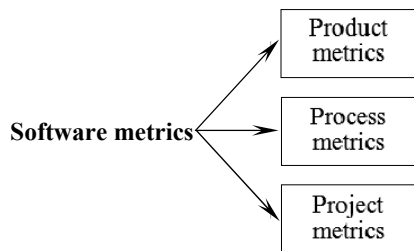
Fig. 1. Software metrics
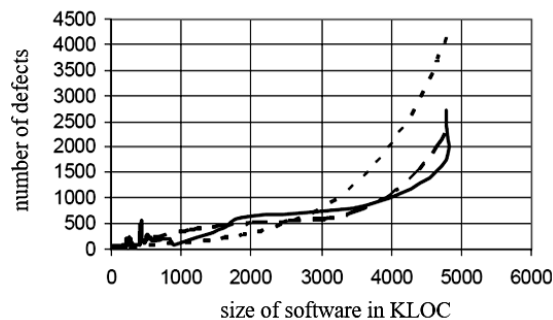
Fig. 2. Dependence of KLOC

Complexity is the degree where it is difficult to verify and understand the design or application of a system or component. The problem of software complexity estimation is widely studied in the field of software engineering. The complexity of the software may vary depending on the choice of algorithm, design, choice of programming language, writing code. Research shows that increasing complexity increases the number of bugs in software, which makes it difficult (in some cases impossible) to maintain and improve programs and makes it difficult to test certain modules. The legibility of the program code directly depends on the level of complexity of the program. The relationship between indicators of software complexity and various attributes of a software system is shown in Fig. 3.

The importance of program complexity indicators can be illustrated as follows [7]:

✓ Difficulty metrics can help people predict and sustain projects.

✓ Complexity metrics can help estimate the amount of programming and development costs, and estimate maintenance costs.
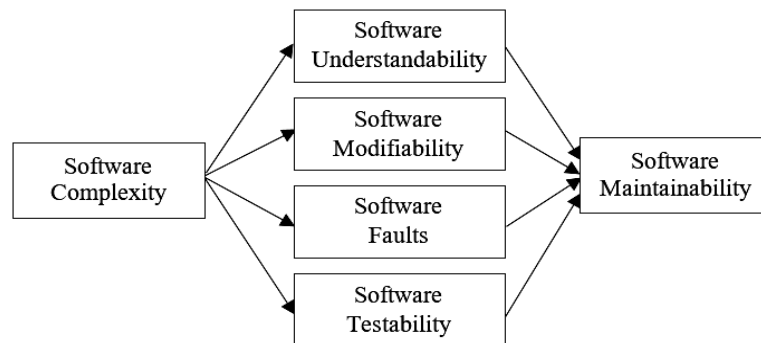
Fig. 3. Software complexity and various attributes of a software

  ✓ Difficulty scores can help you choose the most suitable program with the same functionality. The less complex the programs, the better they are.
  ✓ Complexity measures can be used to predict defects or errors [8].
  ✓ By determining the complexity of software systems, the overall workload and personal contribution of each person working on software modules to the overall work can be assessed in evaluating the performance of software developers [9].

RELATED WORK

Application of program code metrics allows professionals who work on the project to evaluate various feauters of existing or to be created software, to predict the scope of work, quantitatively characterize these or other project solutions, to evaluate quality of prepared systems, complexity and realiability of software [9–13].

  The large amount of data and functionality required in today's enterprise systems presents many challenges for software developers. It is difficult to maintain a balance between software complexity and ease of use, which are indicators of the quality of software, as the complexity of the software increases and its use becomes more difficult. To ensure the quality of the software and the high level of project management, it is necessary to control the complexity and other related characteristics. Large companies such as SAP and Oracle are currently losing market share due to the cost and complexity of the software product [14].

  Numerous studies show that complexity leads to an increase in the number of vulnerabilities in software. Programmers face a number of challenges when trying to make changes to complex software components. Software developers should strive for minimal complexity, as increasing complexity creates security risks that not only damage the business, but also damage its reputation. Violation of safety measures can also pose a serious threat to human health. Some experts deliberately complicate the same program so that they do not write it twice. It is necessary to simplify the management of software security. The authors substantiate the relationship between security and software complexity (Fig. 4) [15].

  Different software development organizations use different metrics to measure and maintain the quality of software code. In [16, 17], the authors

conducted comparative analytical studies using Halstead metrics and proved that software complexity metrics can be used to measure various characteristics. The authors analyzed the program code written for the same function in the programming languages Python, C, JavaScript, and Java. The complexity of these program codes was calculated based on the Halstead scores. Experience has shown that python is more convenient and simpler, while Java is a modern, powerful, but complex programming language. They showed that program performance is important throughout the life of a project, and they concluded that early calculations have a direct impact on fixing errors and thus saving time and budget.
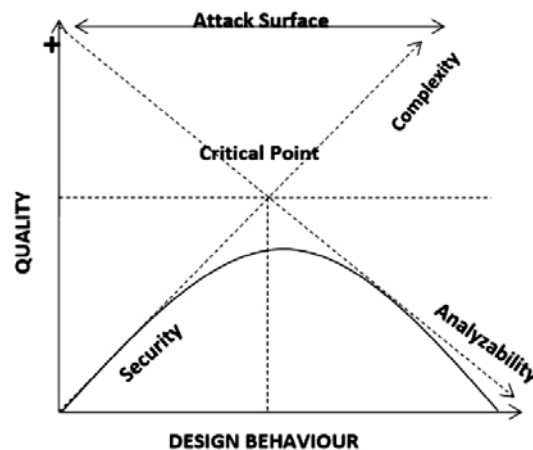
Fig. 4. Security and software complexity

In [18], the authors point out that the main reason for software vulnerabilities is its complexity. Failure to discover software vulnerabilities in a timely manner can jeopardize confidentiality, completeness, and availability. Studies of 12 programs, differing in characteristics and sizes, have shown that the complexity of all software components (size, structure, etc.) is important for predicting vulnerabilities.

In their articles, Shin and William examined code complexity metrics that can be used to predict software vulnerabilities, and concluded that the more complex the software code, the more vulnerabilities. Their results showed a correlation between difficulty scores and vulnerabilities in the Mozilla JavaScript Engine [19].

In [20], the authors investigated the influence of complexity, coupling and cohesion on the number of vulnerabilities in a program. Experiments with Mozilla Firefox have empirically proven that there is a relationship between these parameters and vulnerabilities in the program. Vulnerabilities cannot be discovered in the early stages of software development. Metrics such as complexity, coupling and cohesion can be calculated early. Calculating these metrics can help software developers identify potential vulnerabilities.

In [21], the authors presented a new approach to measuring the quality of software using fuzzy metrics obtained as a result of software design. This metric begins with an assessment of the difficulty rating for each class, which is itself assessed based on the difficulty rating of the class attributes and the difficulty rating of the class methods. Then, to assess the quality metrics of the fuzzy code,

they followed a pattern to explain the relationship between class complexity and LOC for that class, and between method complexity and LOC for that method.

The paper [23] examines the problem of software complexity and its impact on software errors. Having studied various studies, the authors came to the conclusion that with the increase in the complexity of the software system, the threats to its security also increase. While most studies have shown that bugs in software systems are related to their complexity, some researchers have noted that the relationship between complexity and the occurrence of bugs is weak [24].

The software development process, including documentation, design, software, testing, and support, can be measured statistically. Thus, the quality of the software can be effectively controlled. Software metrics are very important in software engineering research [25] provides a summary of software metrics and their types. The authors note that measuring the complexity of software is an integral part of software performance and affects the price and reliability of software products.

Software users assume there are no bugs in the program, but software developers know that it is very difficult, and in some cases impossible, to write program code without bugs. This complexity is mainly due to the intrinsic complexity of the program and the problems that arise when developing and testing the program. In [26], the authors demonstrated the relationship between the complexity of software and its reliability in each specific case.

In [27], the authors analyzed aspects influencing the complexity of the program based on various metrics. A large amount of program code to some extent affects the programmer's thought process and leads to more errors in the program. At the same time, if the number of modules and branches in the program is large, the volume of information exchange is large, and the program is very complex, this will cause problems for the program testers and reduce the quality of testing.

Software complexity plays an important role in reducing the effort required to build and maintain software, and in improving testing efficiency and software quality. The more complex the solution of the program, the more errors it creates [28] examines four software metrics, their importance, strengths and weaknesses. The authors come to the conclusion that each method covers a part and takes into account a certain group of parameters. Therefore, it is important to use a combination of these metrics to measure software complexity.

HYBRID SOFTWARE COMPLEXITY CALCULATION METHOD

The hybrid software complexity method presented in this study combines the advantages of the SLOC, Halstead, Maccab metrics and the module connectivity metric.

Number of lines of code (LOC). When assessing the complexity of a software product, three groups of indicators are usually used: indicators that determine the size of the program, indicators of the complexity of the program flow, and complexity of the data flow of the program. The first group is more common because the metrics are simple. The program size traditionally means the number of source lines of the program (SLOC – Source Lines Of Code) [29].

Lines of Code (LOC) or Source Lines of Code (SLOC) are used to measure the size of a program by counting the number of lines in the text of the program's source code. LOC measures the amount of code, can be used to compare or evaluate programs that use the same programming language and are coded using the same coding standards. Lines of code are completely dependent on the programming language and may differ during the conversion of the program code to any other programming language. This indicator cannot be considered effective in assessing complexity.

Halsted metric. M.H. Halsted was the first researcher to write a mathematical formulation of software metrics [30]. Table 1 shows the main Halsted metrics.

T a b l e 1. Halsted metrics

Program dictionary	$h = h_1 + h_2$
Program length	$N = N_1 + N_2$
Program scope	$V = N \log_2 h$
Program complexity	$D = (h_1/2)(N_2/h_2)$
Implementation effort or program comprehensibility	$E = DV$
Expected number of errors in the program	$B = E0{,}667/3000$

The Halsted metric is based on four measurable program characteristics:

h_1 — the number of unique program operators;

h_2 — the number of unique software operands;

N_1 — total number of program operators;

N_2 — total number of program operands.

McCabes cyclomatic complexity. McCabe proposed this metric in 1976. McCabe's cyclomatic complexity metric is one of the most common indicators for evaluating software complexity. This indicator is calculated based on the control-flow graph of the program and is an indicator of the complexity of the control structures.

The formula for calculating cyclomatic complexity is as follows:

$$C = e - n + 2p,$$

where e — the number of edges of the graph; n — the number of nodes of the graph; p — the number of connected components.

This method takes into account all kinds of cyclic and conditional operators, as well as the complexity of their logical predicates. Linear operators are ignored here. Despite the passage of 45 years, it remains relevant because it more accurately expresses the complexity of the fundamental structures of software. The author of the metric notes the high correlation of the metric with errors. Therefore, the use of this metric to evaluate errors is reasonable and logical. Cyclomatic complexity allows not only to estimate the labor costs and the cost of software projects, but also to make the necessary management decisions taking into account risks [32, 33].

The program module coupling metric distinguishes between data communication, data structure, control, common area (global data), content, as well as external communication, message communication, subclass communication, time communication, and no communication. The advantages of these metrics are that they were developed back in the 80s, are well studied, are often used, and the calculation of values for metrics is automated. These metrics are intended for structured programming, but can be applied to object-oriented programming.

A hybrid method for calculating the complexity of a program code. The proposed method provides an integrated approach to the complexity of the software system and takes into account the following disavantages of the McCabe and Halsted metrics and LOC:

- it cannot be argued that a program with the maximum number of lines of code is more complex, sometimes a small program can be quite complex;

- linear, cyclic, conditional operators in the system of Halsted metrics have the same complexity, which is not true;

- all cyclic, conditional operators in the McCabe metrics system have the same complexity, which is not true. It is assumed that the more nested cyclic and conditional (multiple branching) statements, the more complex the program code becomes and the greater the likelihood that the programmer can make a logical error;

- models do not take into account the inter-module structural complexity of the software, which generates a significant number of defects.

In this method, the main parameters affecting the complexity are the algorithmic complexity of each program module, the number of standard called programs ready for use, and the total number of intermodule links.

When solving problems algorithmically, it often becomes necessary to create a cycle containing another cycle in its body. Such loops are called nested loops. Sometimes you have to check several conditions in a row. To solve the problem of redundancy, you can nest conditional statements inside each other. This is called multiple branching of conditional statements. Nested loops and multiple branches in the code complicate it. At the same time, the number of interacting modules and standard software applications available in these modules directly affects the complexity of the program.

The complexity of the program code can be calculated using the formula (higher value is considered better):

$$C = \log_2 E + \log_2(N - n) + r,$$

where N — the number of all operators in the program code; n — total number of conditional and cyclic operators; r — the number of intermodular couplings; E — parameter depending on the number of cyclic and conditional operators in the program code. This parameter is calculated using the following formula:

$$E = \sum_{i=0}^{n} (i+1)m_i, \quad (i = 0, 1, ..., n),$$

m_i is the total number of conditional and cyclic operators in which conditional and cyclic statements of number *i* are nested. (For example, if there are 2 cyclic statements in the program code and three nested cyclic statements in each of them, then $i = 3$, $m_3 = 2$).

Let's calculate the complexity of two programs written in C++ (Fig. 5 and 6). First, we received an expert assessment of the complexity of these programs based on the assessment of 3 experts on a 10-point scale. All experts rated the algorithm in Fig. 6 as complex, since this algorithm has more nested cyclic and conditional operators. The calculation results are shown in Table 2.

```
 1   #include<iostream>
 2   using namespace std;
 3    int main {}
 4   {
 5    int n=3;
 6    int a[n][n];
 7    int m=0
 8   for {int i=1; i<=n;i++}
 9    for {int j=1; j<=n;j++}{
10         cin>>a[i][j];
11         if (a[i][j]==i+j)
12        m=m+1;
13       else
14         m=m;
15   }
16
17   if(m>0)
18    for {int i=1; i<=n;i++}
19     for {int j=1; j<=n;j++}{
20
21        if (a[i][j]==i+j)
22          cout<<a[i][j];
23        else
24           continue;
25   }
26   else
27    cout<<"No such element";
28   return 0;
29   }
```
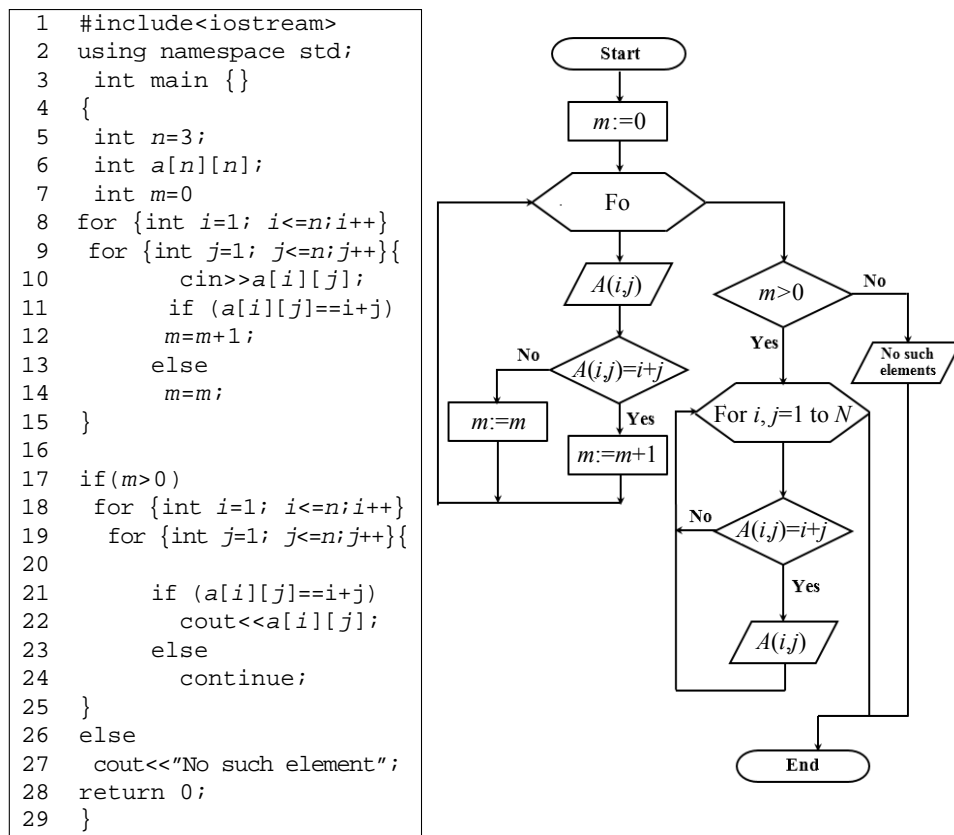

Fig. 5. Finding complexity of program 1

T a b l e 2. Software complexity metrics

Complexity metrics	Calculation	Program 1		Program 2	
LOC	Number of lines of code		27		30
Expert assessment			3		4
MacCabe	For a single program $C = e - n + 2$	e=15; n=12	6	e=17, n=13	6

Complexity metrics	Calculation	Program 1		Program 2	
Hybrid	$E = \sum_{i=0}^{n}(i+1)m_i$ $C = \log_2 E + \log_2(N-n) + r$	$N=108, \backslash$ $n=5, r=0,$ $m_0=3$ $(i=0)$ $m_1=2$ $(i=1),$	9,49	$N=101,$ $n=5, r=0,$ $m_0=3$ $(i=0),$ $m_1=0$ $(i=1),$ $m_2=1$ $(i=2),$ $m_3=1$ $(i=3)$	9,58

```
1    #include<iostream>
2    using namespace std;
3    int main {}
4    {
5      int n;
6      cin>>n;
7      int z[n];
8      for (int i=1; i<=n;i++){
9        cin>>z[i];
10     }
11   if (n>1)
12     for (int i=1; i<=n-1;i++){
13     int v=z[i];
14     int I=i;
15     for (int j=i+1;<=n;j++)
16     {
17       if(z[j]<v)
18       {
19         v=z[j];
20         I=j
21       {
22     {;
23     if (I==1)
24     continue;
25     else{
26     z[I]=z[i]
27     z[i]=v;
28     }}
29     return 0;
30     }
```
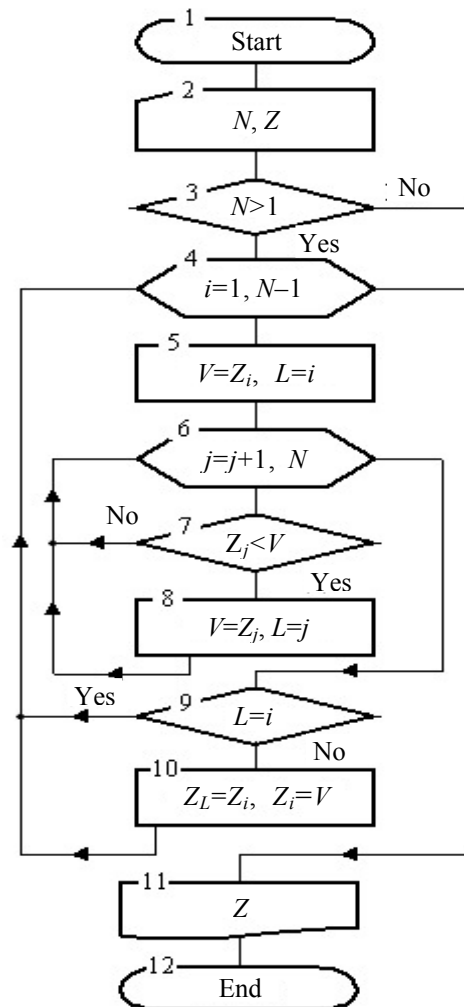

Fig. 6. Finding complexity of program 2

As can be seen from Table 2 according to McCabe, the complexity of programs is the same, because in this method all conditional and cyclic operators have the same level of complexity. The hybrid method takes into account the nesting of cycles, so the result is closer to the expert assessment.

In another example, let's calculate the complexity of a program code written for the same function in C++ and Java using the metrics mentioned above (Fig. 7 and 8). Depending on the chosen programming language, the complexity may increase. Calculating the complexity will help you choose the simpler of the two programs. The calculation results are shown in Table 3.

```
 1  Public Class
 2  {
 3
 4  Public static void main
                (String[]args)
 5
 6  {
 7    int arr[10]={1,9,0,5,6,7,
                8,2,4,3};
 8    int length = 10;
 9    int result[]=new int (10);
10    result=QuickSort (arr,0,
                length-1);
11  }
12
13  Static int [] QuickSort (int
                []a,int r)
14
15    if (I<r)
16
17  {
18    int i=I;
19    int j=r;
20    int k = (int)((I+r)/2);
21    int pilot = a[k];
22
23    do
24    {
25        while (a[i].less (pilot))
26          i++
27        while (pilot.less (a[i]))
28          j--;
29
30        if (i<=j)
31        {
32            int t = a[i];
33            a[i] = a[j];
34            a[j] = t;
35
36            i++;
37            j++;
38
39        }
40    }
41    while (i<j)
42
43  a=QuickSort{a,i,j};
44  a=QuickSort{a,i,r};
45  }
46
47  return a;
48
49  } //end of QuickSort
50
51
52  } // end of class QS
```

Fig. 7. Quick sort implementation code in C++

```
 1  #include<iostream>
 2  using namespace std;
 3
 4  int main()
 5
 6  {
 7
 8    int A[]={}1,9,0,5,6,7,8,2,3,4
 9    intlength = 10;
10    quickSort(A,0,length-1);
11
12
13  void quicksort(int A[],int
                F,int L)
14  {
15    int pivotIndex;
16
17    if (F<L)
18
19    Partition(A,F,L,pivotindex;
20    quicksort(A,F,pivotindex-1);
21    quicksort(A,pivotindex+1,L);
22    }
23  }
24
25  void partition(int A[],int F,
            int L,int & pivotindex)
26  {
27    int piv = A[F];
28    int lastS1 = F;
29    int firstUnknown = F+1;
30
31    for(firstUnknown = F+1;++
                firstUnknown)
32    {c
33    if (A[firstUnknown]<pivot)
34      {++lastS1;
35        Swap(A[firstUnknown],
                A[lastS1]);
36    }
37    }
38    Swap(A[F],A[lastS1]);
39    pivotindex=lastS1;
40
41  }
42
43  void Swap(int & x,int & y)
44  {
45    int temp = x;
46    X=y;
47    Y-temp;
48  }
```

Fig. 8. Quick sort implementation code in Java

T a b l e 3 . Software complexity of C++ and Java programs

Complexity metrics	Calculation	C++		Java	
LOC	Number of lines of code		48		52
MacCabe	For a single program $C = e - n + 2$	e=28, n=26	4	e=29, n=25	6
Halstead	$D = (h_1/2) * (N_2/h_2)$	N_1=142 N_2=57 h_1=25 h_2=21	33,92		39,75
Hybrid	$E = \sum_{i=0}^{n} (i+1)m_i$ $C = \log_2 E + \log_2 (N-n) + r$	N=142, n=3, r=0, m_1=1 (i=1), m_0=2 (i=0)	9,11	N=133, n=5, r=0, m_0=3 (i=0), m_1=1 (i=1), m_2=1 (i=2)	10

CONCLUSİON

Software complexity metrics are one of the key aspects of software process management. Complexity makes software difficult to understand, which creates problems when maintaining a software system and adding new functions to it. In the articles of recent years, various methods of solving this problem have been proposed. Numerous studies in the field of software complexity metrics suggest that there is no universal metric for assessing the complexity of any program code. The use of any metric, hybrid metric, or multiple metrics depends on the specific problem. This article proposes a new hybrid method for calculating the complexity of software, the effectiveness of which is substantiated by experiments. The proposed metric makes it possible to clarify (due to additional indicators) the complexity of software modules of a large class separately from the known metrics. Based on the above, it is concluded that software metrics are important at the stages of the project life cycle and, with early application of program metrics, help to largely overcome the presence of errors and, thus, save time and money.

REFERENCES

1. T. DeMarco, *Controlling Software Projects*. Yourdon Press, New York, 1982, 816 p.
2. S. Reddivari and J. Raman, "Software Quality Prediction: An Investigation Based on Machine Learning", *2019 IEEE 20th International Conference on Information Reuse and Integration for Data Science (IRI)*, pp. 115–122. doi: 10.1109/IRI.2019.00030.
3. A.V. Smirnov, "Methods for assessing and managing the quality of software", *Izvestia ETU "LETI"* no. 2, pp. 20–25, 2019.
4. I. Somerville, *Software engineering*, 10th edition. Pearson, 2015, 816 p.
5. S.A. Yaremchuk, "Method for estimating the number of software defects using complexity metrics", *Radioelectronic and computer systems*, no. 5, pp. 212–218, 2012.
6. P.A. Laplante, *Dictionary of computer science, engineering and technology*. CRC Press, 2017, 560 p.
7. J. Rashid, T. Mahmood, M.W. Nisar, "A Study on Software Metrics and its Impact on Software Quality", *Technical Journal, University of Engineering and Technology (UET), Taxila, Pakistan*, vol. 24, no. 1, pp. 1–14, 2019.

8. T. Honglei, S. Wei and Z. Yanan, "The Research on Software Metrics and Software Complexity Metrics", *2009 International Forum on Computer Science-Technology and Applications*, pp. 131–136, 2009. doi: 10.1109/IFCSTA.2009.39.

9. T.H. Kazimov and T.A. Bayramova, "Evaluating Key Performance Indicators for Software Development", *IV International Congress on New Trends in Science, Engineering and Tehcnology*, pp. 99–105, 2020.

10. Shweta, S. Sharma, and R. Singh, "Analysis of correlation between software complexity metrics", *International Journal of Innovative Science, Engineering & Technology*, vol. 2 issue 8, August 2015.

11. S. McIntosh et al., "An empirical study of the impact of modern code review practices on software quality", *Empirical Software Engineering*, 21, pp. 2146–2189, 2016. Available: https://doi.org/10.1007/s10664-015-9381-9.

12. S. Bhatia and J. Malhotra, "A survey on impact of lines of code on software complexity", *2014 International Conference on Advances in Engineering & Technology Research (ICAETR – 2014)*, pp. 1–4, 2014. doi: 10.1109/ICAETR.2014.7012875.

13. A. Ghazarian, "A Theory of Software Complexity", *2015 IEEE/ACM 4th SEMAT Workshop on a General Theory of Software Engineering*, pp. 29–32, 2015. doi: 10.1109/GTSE.2015.11.

14. M. Khan, F. Ahmad, and M.A. Khanum, "Literature review on software complexity, software usability and software deliverability", *International Journal of Advanced Research in Computer Science*, vol. 9, no. 2, pp. 438–441, 2018. doi: 10.26483/ijarcs.v9i2.5853.

15. M. Alenezi and M. Zarour, "On the relationship between software complexity and security", *International Journal of Software Engineering & Applications (IJSEA)*, vol. 11, no. 1, pp. 51–60, 2020.

16. S.A. Abdulkareem and A.J. Abboud, "Evaluating Python, C++, JavaScript and Java Programming Languages Based on Software Complexity Calculator (Halstead Metrics)", *2nd International Scientific Conference of Engineering Sciences (ISCES 2020) 16th-17th December, Diyala, Iraq, IOP Conference Series: Materials Science and Engineering*, vol. 1076, pp. 1–9, 2020. doi: 10.1088/1757-899X/1076/1/012046.

17. Nikhil Govil, "Applying Halstead Software Science on Different Programming Languages for Analyzing Software Complexity", *Proceedings of the Fourth International Conference on Trends in Electronics and Informatics (ICOEI 2020)*, pp. 939–943, 2020. doi: 10.1109/ICOEI48184.2020.9142911

18. Y. Javed, M. Alenezi, M. Akour, and A. Alzyod, "Discovering the relationship between software complexity and software vulnerabilities", *Journal of Theoretical and Applied Information Technology*, vol. 96, no. 14, pp. 4690–4698, 2018.

19. Y. Shin, "Exploring Complexity Metrics as Indicators of Software Vulnerability", in *the 3rd International Doctoral Symposium on Empirical Software Engineering, Kaiserslautern, Germany,* October 8, 2008.

20. I. Chowdhury and M. Zulkernine, "Can complexity, coupling, and cohesion metrics be used as early indicators of vulnerabilities?", *Proceedings of the 2010 ACM Symposium on Applied Computing – SAC '10*, 2010. doi:10.1145/1774088.1774504.

21. O. Masmali and O. Badreddin, "Towards a Model-based Fuzzy Software Quality Metrics", *8th International Conference on Model-Driven Engineering and Software Development*, pp.139–148, 2020.

22. Tong Yi and Chun Fang, "A Novel Method of Complexity Metric for Object-Oriented Software", *International Journal of Digital Multimedia Broadcasting*, vol. 2018, pp. 1–9, 2018. Available: https://doi.org/10.1155/2018/7624768

23. S. Moshin Reza, M. Mahfujur Rahman, H. Parvez, O. Badreddin, and S. Al Mamun, "Performance Analysis of Machine Learning Approaches in Software Complexity Prediction", *Proceedings of International Conference on Trends in Computational and Cognitive Engineering. Advances in Intelligent Systems and Computing*, vol. 1309, pp. 27–39, 2021. doi: 10.1007/978-981-33-4673-4_3.

24. P. Morrison, K. Herzig, B. Murphy, and L. Williams, "Challenges with applying vulnerability prediction models", in *Proceedings of the 2015 Symposium and Bootcamp on the Science of Security*, pp. 1–9, 2015.

25. Mohd. Kamran Khan et al., "Literature review on software complexity, software Usability and software deliverability", *International Journal of Advanced Research in Computer Science*, 9 (2), pp. 438–441, 2018.

26. M. Devon Simmonds, "Complexity and the Engineering of Bug-Free Software", *Proceedings of the International Conference on Frontiers in Education: Computer Science and Computer Engineering (FECS), Athens*, pp. 94–100, 2018.

27. T. Hariprasad, G. Vidhyagaran, K. Seenu, and C.Thirumalai, "Software complexity analysis using halstead metrics", *2017 International Conference on Trends in Electronics and Informatics (ICEI), Tirunelveli*, pp. 1109–1113, 2017. doi: 10.1109/ICOEI.2017.8300883.

28. A. Athar Khan, M. Amjad, Sajeda M. Amralla, and Tahera H. Mirza, "Comparison of Software Complexity Metrics", *International Journal of Computing and Network Technology*, no. 1, pp.19–26, 2016.

29. G.R. Choudhary, S. Kumar, K. Kumar, A. Mishra, and C. Catal, "Empirical analysis of change metrics for software fault prediction", *Computers & Electrical Engineering*, vol. 67, pp. 15–24, 2018. Available: https://doi.org/10.1016/ j.compeleceng. 2018.02.043.

30. N. Govil, "Applying Halstead Software Science on Different Programming Languages for Analyzing Software Complexity", *2020 4th International Conference on Trends in Electronics and Informatics (ICOEI)(48184)*, pp. 939–943, 2020. doi: 10.1109/ICOEI48184.2020.9142911.

31. L. Pudovkina and V. Sinyaiev, "Applying empirical models and halstead metrics to evaluate the quality of application software", *Open Information and Computer Integrated Technologies*, no. 86, pp.190–197, 2019. doi: 10.32620/oikit.2019.86.14

32. T.J. McCabe, "A Complexity Measure", in *IEEE Transactions on Software Engineering*, vol. SE-2, no. 4, pp. 308–320, 1976. doi: 10.1109/TSE.1976.233837.

33. H. Liu, X. Gong, L. Liao and B. Li, "Evaluate How Cyclomatic Complexity Changes in the Context of Software Evolution", *2018 IEEE 42nd Annual Computer Software and Applications Conference (COMPSAC)*, pp. 756–761, 2018. doi: 10.1109/COMPSAC.2018.10332.

INFORMATION ON THE ARTICLE

Tofig Kazimov (Hasanaga), ORCID: 0000-0001-9245-6731, Institute of Information Technology of Azerbaijan National Academy of Sciences, Azerbaijan, e-mail: tofig@mail.ru

Tamilla Bayramova (Adil), ORCID: 0000-0002-8377-3572, Institute of Information Technology of Azerbaijan National Academy of Sciences, Azerbaijan, e-mail: toma_b66@mail.ru

РОЗРОБЛЕННЯ ГІБРИДНОГО МЕТОДУ ОБЧИСЛЕННЯ СКЛАДНОСТІ ПРОГРАМНОГО ЗАБЕЗПЕЧЕННЯ / Т.Г. Казімов, Т.А. Байрамова

Анотація. Застосування показників програмного коду дозволяє розробникам програмного забезпечення і керівникам проектів оцінювати різні функції програмного забезпечення, яке буде створено або вже існує, прогнозувати робоче навантаження, визначати складність і надійність програмного забезпечення і надавати кількісні характеристики якості розроблюваних програмних систем. У працях останніх років пропонуються різні методи вирішення цієї проблеми. Утім досі немає ефективного підходу до вимірювання складності програмного забезпечення. Подано стислий огляд існуючих метрик складності програмного забезпечення. Запропоновано новий гібридний метод обчислення складності програмного забезпечення, який об'єднує ключові характеристики метрик Холстеда, Маккабі і SLOC, а також дозволяє більш ефективно оцінювати складність.

Ключові слова: програмна інженерія, складність програмного забезпечення, метрики складності, гібридний метод.

COMPARATIVE ANALYSIS OF THE EFFECTIVENESS OF USING FINE-GRAINED AND NESTED PARALLELISM TO INCREASE THE SPEEDUP OF PARALLEL COMPUTING IN MULTICORE COMPUTER SYSTEMS

V. MARTELL, A. KOROCHKIN, O. RUSANOVA

Abstract. The article presents a comparative analysis of the effectiveness of using parallelism of varying granularity degrees in modern multicore computer systems using the most popular programming languages and libraries (such as C#, Java, C++, and OpenMP). Based on the performed comparison, the possibilities of increasing the efficiency of computations in multicore computer systems by using combinations of medium- and fine-grained parallelism were also investigated. The results demonstrate the high potential efficiency of fine-grained parallelism when organizing intensive parallel computations. Based on these results, it can be argued that, in comparison with more traditional parallelization methods that use medium-grain parallelism, the use of separately fine-grained parallelism can reduce the computation time of a large mathematical problem by an average of 4%. The use of combined parallelism can reduce the computation time of such a problem to 5,5%. This reduction in execution time can be significant when performing very large computations.

Keywords: multicore computer system, core, thread, tasks, parallelism, granularity, fork-join, speedup coefficient, fine-grained parallelism, nested parallelism, combined parallelism.

INTRODUCTION

Classical von Neumann architecture is not designed for parallel computing; all commands execute in one sequence strictly one after another. Each such individual sequence that operates on the machine at the current time is a process. ISO 9000:2000 [1] defines a process as a set of interconnected and interacting actions that convert input data into output. A computer program in itself is only a passive sequence of instructions, while a process is the direct execution of those instructions.

The concept of process is inextricably linked with the concept of thread. The execution thread is the smallest unit of processing, the execution of which can be assigned by the operating system kernel [2]. Implementation of execution threads and processes in different operating systems differs from each other, but in most cases, the execution thread is within the process. Multiple threads can exist within the same process and share resources such as memory, while processes do not share these resources. In particular, the execution thread hare process instructions (its code) and its context (the values of the variables they have at any given time).

Thus, in the framework of von Neumann or single-core architecture, parallelism is usually realized by time multiplexing: the processor switches between different threads. This context switching is called pseudo-parallelism and usually

occurs often for the user to perceive the execution of threads or tasks as simultaneous [3]. In such systems, there are effective time schedulers in standby mode (blocked) [4]. Scheduling is based on the principle of priorities, for example, in most cases, some user input has a higher priority than some computations, so if the central processor unit (CPU) receives an input signal, a priority interrupt occurs and the CPU processes its, which allows the user to control most of process, such as urgently terminate some of them.

However, in the present stage, this approach no longer ensures compliance with the requirements for computer systems. And with the emergence of multi-core and multiprocessor architecture, the question arose of the organization of real parallelism, when at the point of time each individual core or processor performs its own thread. In multiprocessor and multi-core systems, threads or tasks can run simultaneously, with each processor or core processing a separate thread at the same time. The operating systems of such computers are much more complex and voluminous because, for such architectures to function effectively, their components must also exchange data (communicate and synchronize), and do so in a timely, fast, and with minimal computational downtime. Planners of such operating systems plan the distribution of captures by the thread of cores both in time and space [4]. So, even parallel threads are not all the same. In addition to the level of their priority, you can enter another measure for them – quantitative, one that is based on the volume of the basic unit in the program.

PROBLEM ANALYSIS AND TASK STATEMENT

Each individual elementary parallel computation in modern multi-core computer systems (MCS) can be represented as a granule. Depending on how many such elementary calculations (parallel within the system, but consecutive within one thread) each thread contains, and how many communications (i.e. interruptions of parallelism) were conducted between such threads, we can introduce the concept of "granularity".

Granularity is a measure of the ratio of the number of calculations performed in a parallel problem to the number of communications [5]. The degree of granularity varies from fine-grained to coarse-grained.

It should be noted that the granularity classifications available in different sources differ slightly, especially for coarse- and medium-grained parallelism, so the following classification will be taken as a basis in this article:

1. Coarse-grained parallelism: each parallel calculation is quite independent of the others, and requires a relatively rare exchange of information with other calculations. The units of parallelism are large and independent programs that include thousands of commands [6].

2. Medium-grained parallelism: units of parallelization are individual procedures that are called in separate threads and include hundreds of commands. It is usually organized by both the programmer and the optimizing compiler. Most general-purpose parallel computers are primarily focused on this category of parallelism [7].

3. Fine-grained parallelism: each parallel calculation is quite small and elementary, consists of dozens of commands. Usually, the units that are parallelized are elements of expressions or individual iterations of a loop. They usually have

little or no relationship between the data. The amount of work associated with a parallel task is low and the work is evenly distributed among the processors. Hence, fine-grained parallelism facilitates load balancing [8].

The very term "fine-grained parallelism" refers to the simplicity and speed of any computational action. A characteristic feature of fine-grained parallelism is the approximate equality of computational intensity and data exchange. This level of parallelism is often used by the parallelizing (vectorizing) compiler [9], as well as recently in asynchronous programming. This work focuses on medium- and fine-grained parallelism.

Fine-grained parallelism has a long history: it is the most "ancient" kind of parallelism. The development of his theory took place simultaneously with the development of the theory of successive calculations and is associated with the name of the already mentioned John von Neumann. His theoretical model of a calculator with fine-grained parallelism is widely known – "cellular automaton" [10]. But, when in the process of development of computer technology there were opportunities and capacities for the organization of full-fledged threads of medium-grained and coarse-grained parallelism, there was some decline in interest in fine-grained parallelism. However, the decline in interest changed when technological advances, on the one hand, led to the fact that medium- and coarse-grained parallels somewhat exhausted their significant development, and on the other hand allowed to create a unified architecture within which at different stages of program implementation could move on parallelism of various degree of granularity, i.e. on some parts of programs to use the classical mechanism of threads, and on others fine-grained parallelisms, like tasks or parallel loops.

Against the background of renewed interest in fine-grained parallelism in modern programming languages and libraries, along with the tools for organizing parallel computations by creating a set of classic full-fledged medium-grain threads, there are tools for computing within fine-grained parallelism. Most often, these are tools for parallelizing loops or small sets of similar commands.

However, it also led to conflicts in the design stages of modern parallel software. Currently, there are two opposing approaches to creating the architecture of such software: on the one hand, you can represent the parallel part of the program in the format of medium-grained structures (classical threads), on the other hand, all calculations can be represented in the form of small tasks. At the same time, if we can say that the classical concept of threads is not very suitable for modern back-end problems, in contrast to the concept of tasks, then in the field of high-load and intensive scientific calculations, solving classical problems can be presented using both threads and tasks.

At the same time, given the above-described nature of parallelism in modern MCS, as well as modern flexible tools for organizing different levels of parallelism in languages and libraries of parallel programming, we can assume that there is space and opportunities for effective solving of computational problems with simultaneous use of both mechanisms. This combination is called "Nested parallelism".

Therefore, the purpose of this work is to research the possibilities of improving the execution time of parallel programs in MCS through the use of fine-grained parallelism, the optimal combination of medium and fine-grained parallelism (nested parallelism), as well as the use of modern software instruments of their implementation.

FINE-GRAINED PARALLELISM IMPLEMENTATIONS OVERVIEW

Among the most popular languages and libraries currently used in high-load computing, fine-grained parallelism tools are implemented in the OpenMP library (which is usually used in combination with C++), Java and C# languages [11–14].

OpenMP

Fine-grained parallelism is represented by a special preprocessor directive **#pragma omp parallel for**, which refers to the work-sharing directives. Such directives are not used only for parallel code execution; they are used for the logical distribution of a group of threads to implement these control logic constructs. The #pragma omp for directive informs that when running a loop in parallel mode, loop iterations must be distributed between a group of threads. Execution of the following program code:

1. int size=100; //the number of calculation iterations
2. #pragma omp parallel for
3. for(int i = 0; i < size; i++)
4. Calculations();
5. ShowResults();

in the four-processor system would happen as shown in Fig. 1. This distribution is used by default and is called static scheduling.
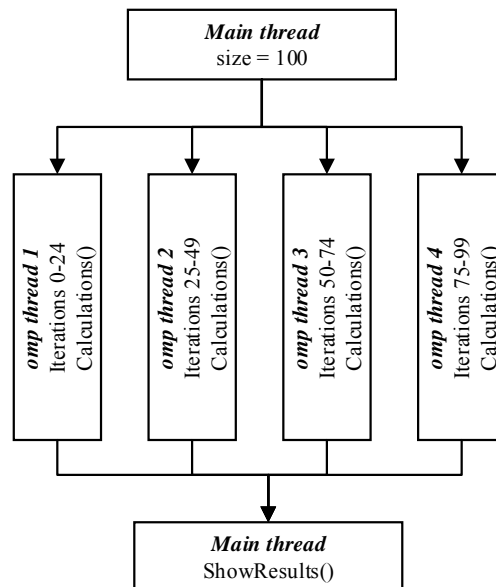
Fig. 1. The scheme of distribution loop iterations in parallel threads using OpenMP

OpenMP also provides another, more flexible types of scheduling, such as dynamic scheduling, runtime scheduling, and guided scheduling. The special section is used to set up one of these modes. The following code scheme shows the format of this section: **schedule *(algorithm name)* num_threads *(number of iterations)***. This mechanism is used when different iterations perform different amounts of work and determine whether a thread that has already completed its iteration will be able to take over part of the work of another thread.

When writing more complex parallel programs, one of the key tasks to solve is the problem of thread synchronization. In OpenMP, implicit barrier synchronization is at the end of each #pragma omp parallel and parallel for block. There are also manual synchronization tools, such as barriers that can be created using the #pragma omp barrier directive.

With writing the parallel program, the second main task that needs to be figured out is the mutual exclusion problem, which avoids the situation so-called "race condition", when a large number of threads will behave unpredictable or be blocked due to access to the same area of memory, which, for example, contains some variable (shared resource), which used in all threads. With the large number of threads created with the application of fine-grained parallelism, this problem is particularly acute. OpenMP provides the ability to use special nonblocking tools to solve the problem of mutual exclusion, such as the directive #pragma omp atomic, as well as modifiers of the directive #pragma omp parallel for: shared, private, firstprivate, lastprivate or reduction. Manual means of solving the problem of mutual exclusion are represented by such constructions as locks and critical sections.

Java

Developers are offered extremely flexible and powerful tools for implementing fine-grained parallelism based on the Fork-Join model, realized in built-in package **java.util.concurent**.

A recursive algorithm is used to implement this model in Java, which described in the following paragraph:

1. The check on the possibility of dividing the actions of this thread into two smaller tasks.

2. If the check is successful, the distribution is performed (Fork), by creating new threads for each new task. In each new thread, the algorithm begins anew. The thread that performed the distribution is blocked until both created threads have finished their work, and then it performs the final collection of the result.

3. If the check is not successful (the limit of the so-called "grain of parallelism" is reached), then the calculations are performed in this thread, after which the connection with the generated thread occurs (Join).

This implementation contains two classes: **RecursiveAction** and **RecursiveTask**. When it is necessary to calculate a specific numeric value of a large function (such as the sum of vector elements), it is better to use Recursive Task. In the case of general operations, the results of which are not a specific number, RecursiveAction works better. By inheriting these classes and describing the computer's own overload, the developer can customize the work to solve a specific problem, which is extremely effective.

An example of using the RecursiveAction class to implement fine-grained parallelism in Java organizing a parallel loop as an example is shown in the listing below:

```
1   class ParallelFor extends RecursiveAction {
2       private int from, to;
3       volatile final int GRAIN = 25;
4       public ParallelFor(int from, int to) {
5           this.from = from;
6           this.to = to;
7       }
8       protected void compute() {
```

```
9        int len = to - from;
10       // Stop condition of main recursion
11       if (len < GRAIN)
12          work(from, to);
13       else {
14          int mid = (from + to) >>> 1;
15          ForkJoinTask<Void> parallelFor1 =
16             = new ParallelFor(from, mid).fork();
17          ForkJoinTask<Void> parallelFor2 =
18             = new ParallelFor(mid, to).fork();
19          parallelFor1.join();
20          parallelFor2.join();
21       }
22    }
23 }
24 // Parallel loop startup is performed using the invoke()
25 // method called on the instance of the ForkJoinPool class
26 ForkJoinPool pool = new ForkJoinPool();
27 pool.invoke(new ParallelFor(from, to));
```

The variable *GRAIN* determines the depth of the partition, in other words, the amount of work, after achieving which, the thread will start to perform it, rather than making further parallelization. The *work()* method may contain certain basic parameterized calculations, which performance is expected from each Fork-Join task after reaching the maximum depth of parallelization. For example, after setting the initial values of the variables *GRAIN* = 25, *from* = 0, *to* = 100, we obtain a parallel execution of the loop of 100 iterations discussed in the previous subsection, in which each of the Fork-Join tasks will receive 25 iterations for processing. However, unlike OpenMP, the structure of the generated threads and their control hierarchy will be treelike, as shown in Fig. 2.
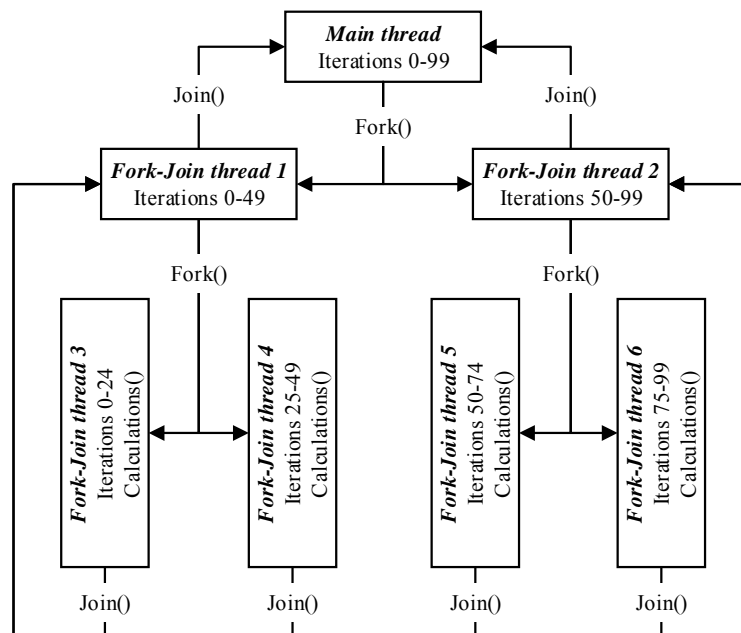
Fig. 2. The scheme of distribution loop iterations in Fork-Join parallelization using Java

The resulting structure is more complex than the one in OpenMP. Nevertheless, according to the results provided in the next chapter, such an approach to fine-grained parallelism proved to be no less effective.

C#

C# also provides the ability to implement fine-grained parallelism. All the necessary functionality for this is contained by a static class **System.Threading.Tasks.Parallel**, namely by its three main methods **Parallel.For()**, **Parallel.ForEach()**, **Parallel.Invoke()** and their various overloads. Parallel.For and Parallel.ForEach provide parallel execution of for and foreach loops, respectively. The override methods presented in this class are aimed to maximize the parameterization of parallelism, depending on the specific task being implemented.

Each method described above is based on a mechanism similar to the one used in Java. Nonetheless, it has also been simplified with a mechanism for delegating and anonymous methods. Developers are not required to manually write the entire recursive part and the regulation of grain parallelism, this is the responsibility of the execution environment. Therefore, in practice, the implementation of fine-grained parallelism becomes extremely simple and has almost no different from the classical single-threaded approach.

The following piece of code provides a similar parallelization to the previous loop of a hundred iterations:

```
1   Parallel.For(0, 100, i => {
2       Calculation();
3   });
```

Although parallelization in C# occurs by the very same mechanism as in OpenMP, through the simplifying, that assures the virtual environment of the CLR execution, the resulting threads' structure and their hierarchy of management will be similar to that in the OpenMP library.

Also in C# are realized the tools for the organization of fine-grained parallelism manually, similar to corresponding tools in Java. The *Task* class (**System.Threading.Tasks**) is responsible for this. The formed tasks can be performed in one or more threads. The official documentation of this programming language recommends using them primarily for asynchronous programming. In fact, the tools for organization parallel loops in C# discussed above are high-level abstractions constructed using Tasks.

NESTED (COMBINED) PARALLELISM

This approach is based on the use of two types of parallelism in the parallel program: medium-grained and fine-grained. The program includes a set of traditional threads for the number of MCS cores. Each of these threads additionally implements internal (fine-grained) parallelism by creating subthreads using appropriate Fork-Join tools. The initial number of traditional threads can be reduced in order to provide fine-grained parallelism with free processor resources. A parallel thread interaction scheme for such a program for the test system and the task (discussed in the next section) implemented by OpenMP tools as an example, can be represented as shown in Fig. 3.
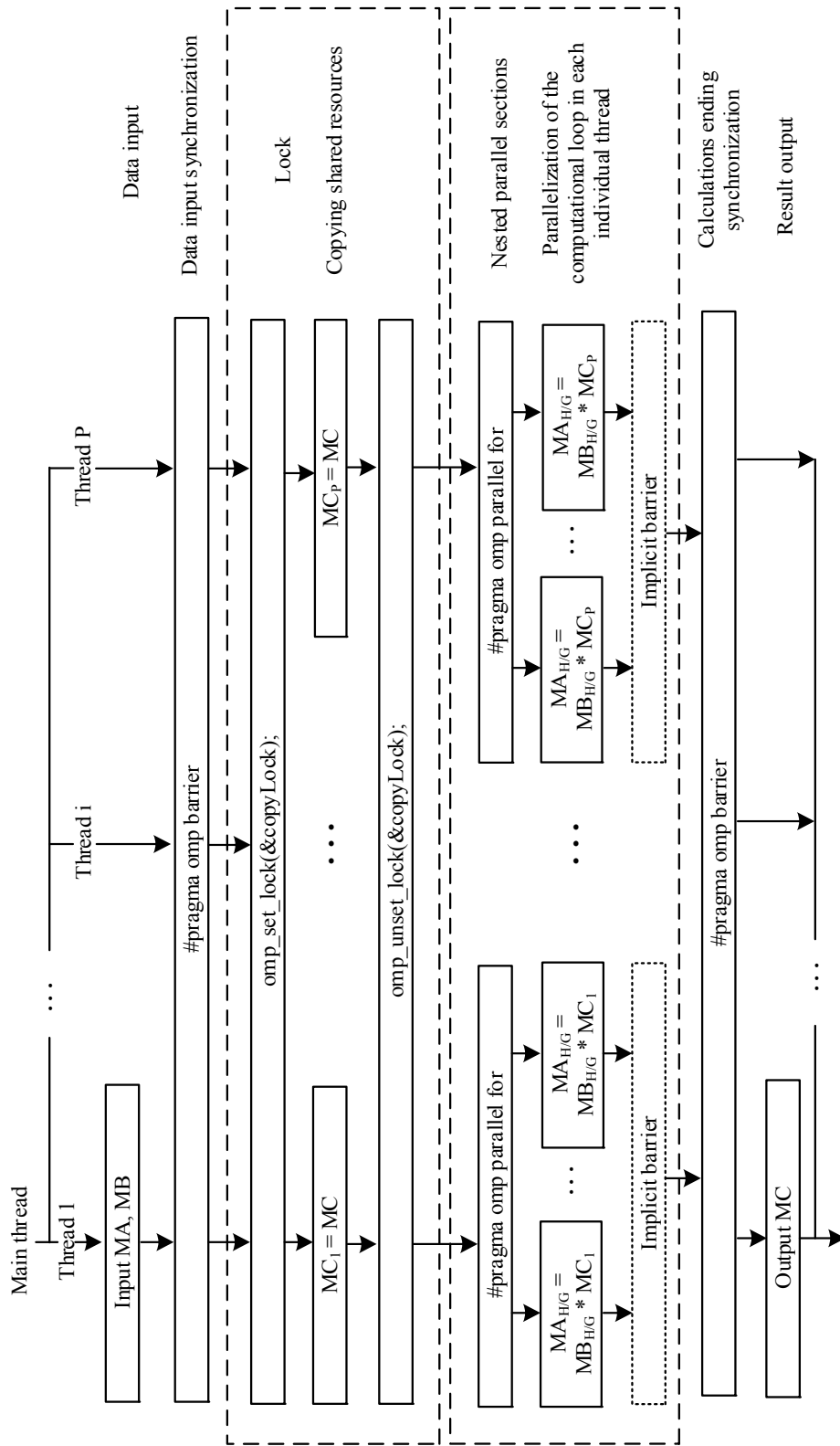
Fig. 3. The scheme of the interaction of threads within the model of nested parallelism implemented by OpenMP tools using the problem of two square (*N*N*) matrices multiplication as an example

Support for nested parallelism in OpenMP is enabled manually. There are two ways to do this:

1. By calling **omp_nested true** command before compiling the program.

2. By calling **omp_set_nested(1)** procedure in the program code.

Both methods set the environment variable ***omp_nested*** to the value of true. However, the second method is more preferable because it provides better portability of the code, because there is no guarantee that on computers where the code will run in the future, will be manually set the appropriate value of the variable *omp_nested*.

Unlike OpenMP, Java and C# do not require any additional operations to activate compiler support for nested parallelism.

EXPERIMENTAL TESTING

Selection a problem for testing

For the most transparent comparative testing, the problem of multiplying two square matrices of large dimension ($N * N$ elements of 64-bit type double) was chosen as an example of a typical problem from the field of high-load computing:

$$MA = MB + MC. \tag{1}$$

Due to the large number of elementary mathematical operations, which can be differently and in different quantities distributed between threads or tasks, the program to solve this problem can be properly implemented using all types of parallelism, while always maintaining high-intensity computations, with minimal downtime for synchronization and data exchange, which is important for more transparent comparative performance testing.

In addition, the choice of this problem for comparative testing of different types of parallelism is also ideal in terms of its coverage of all models of data exchange and interaction between threads or tasks. In medium-grained parallelism, it contains the required fragment of the copy of the shared resource (matrix *MC*) between the threads. In fine-grained parallelism, there is an interaction of tasks without copying shared resources (a direct reference to matrices elements), which is just more typical for applied implementations of this type of parallelism. And in nested parallelism, these two approaches of parallel interaction with shared resources are combined. Therefore, it can be argued that this problem contains all the characteristic cases that occur in solving other common mathematical problems in parallel programs.

Description of the mathematical model of the test problem

The mathematical algorithm for performing this problem (1) is reduced to *N*-fold repetition of the calculation:

$$a_{ij} = \sum_{k=1}^{N} b_{i,k} c_{k,j}, \tag{2}$$

where a_{ij}, b_{ij}, c_{ij} are the corresponding elements of the ith row and j^{th} column of the matrices *MA, MB, MC*; i and j lie in the range from 1 to N.

Therefore, the total number of elementary operations that must be performed to obtain solution (1) is equal to N^3.

With this in mind, the following parallel mathematical algorithm was chosen [15]:

$$MA_H = MB_H + MC, \tag{3}$$

where H is a rounded up number equal to the quotient of the division N/P and MA_H, MB_H are the corresponding rectangular matrices of dimensions H by N elements of the matrices MA and MB [15].

It is worth noting that in this case, the variable P can be either equal to the number of cores available in the system (medium-grained parallelism), or be less than this number (no parallelism, some variants of nested parallelism), or significantly larger than it (fine-grained parallelism).

Each thread implements H repetitions of the algorithm (2), while calculating the Hth part (3) of the total program's result.

Since this algorithm provides for frequent access to all elements of the MC matrix from each thread, an important point is that when creating threads, each of them gets its own instance of this matrix, which eliminates conflicts between threads for capturing and owning shared resources. However, such copying is valid only for medium-grained parallelism; for fine-grained and nested parallelism, such copying does not occur.

Description of the test software and hardware complex

Testing of programs was carried out in two identical MCSs. Their main characteristics are shown in Table 1.

T a b l e 1. The main characteristics of the test MCSs

Hardware	
Processor	AMD Phenom II
Processor architecture	K10
Number of cores	6
RAM capacity	8 Gb
RAM type	DDR3
Sofrware	
Operation system	Windows 7
OpenMP version	3.1
C++ compiler	MC++ (MSVC)
JVM version	1.8
.NET Framework version	4.7
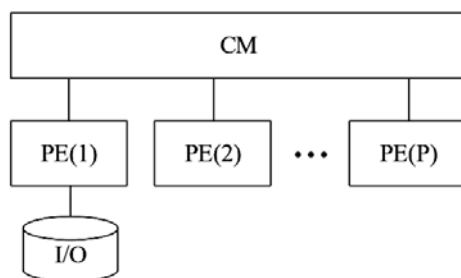
MA, MB, MC

Fig. 4. The test hardware and software complex schematic structure

The software structure is aligned with the hardware structure (primarily for medium-grained part of computing), and it includes both manual and automatic scalability. The schematically formed structure of the hardware and software test complex is shown in Fig. 4.

The following symbols are introduced into this diagram:

1. PE(i) — the processing ele-

ment (processor or core). Its index corresponds to the number of this element, and lies in the range from 1 to P inclusive, where P is the number of all processing elements in the test system. At the software level, each physical processor element corresponds to a software-generated thread.

2. CM — the common (shared) memory (RAM for example), to which each processor element is connected, and with the help of which they communicate with each other.

3. I/O - an I/O device that is connected to one of the processor elements (or to one of the cores, since in fact the processing of I/O signals will ultimately be processed by one of the physical cores of the system), and which provides input of initial data and output of results.

4. MA, MB, and MC are matrices that make up the multiplication operation (1). Moreover, the MA and MB matrices are multipliers and are entered from the I/O device (for large dimensions, random input is used, the execution time of which is not taken into account in the overall test result), and the MC matrix is the result that is output by this device at the end of all calculations (the execution time measurement is stopped just before the output).

Tests results

Table 2 shows the results of testing parallel programs for the operation of matrix multiplication for different values of *N* (dimension of matrices). Presented the execution time of programs that were built with:

- using medium-grained parallelism through the thread mechanism;
- using fine-grained parallelism through the parallel loops and/or fork-join mechanisms described in the previous section;
- using nested (combined) parallelism, when each thread additionally uses parallel processing through the parallel loops and/or fork-join constructs.

Based on the actual time indicators obtained, the acceleration coefficients (speedup coefficients) of the considered programs are calculated. The speedup coefficient of a parallel program is the ratio of the execution time of a program without parallelism on one computing core to the execution time of a similar program with parallelism on $_P$ computing cores and shows how much the program execution time is reduced in a parallel system [15]. Calculated using the formula

$$SC = \frac{T_1}{T_p},$$

where T_1 is the actual running time of the program without applying parallelism, and T_p is the actual running time of a similar program using parallelism in $_P$ computing cores. Ideally, this coefficient is equal to the number of cores, but in practice, this coefficient is always several tenths less than the number of cores. This is due to the presence of other background processes in the system, which also occupy a certain place in the kernel operation plan.

Below are graphs (Fig. 5) showing the dependence of the speedup coefficients for all three types of parallelism on the values of *N*.
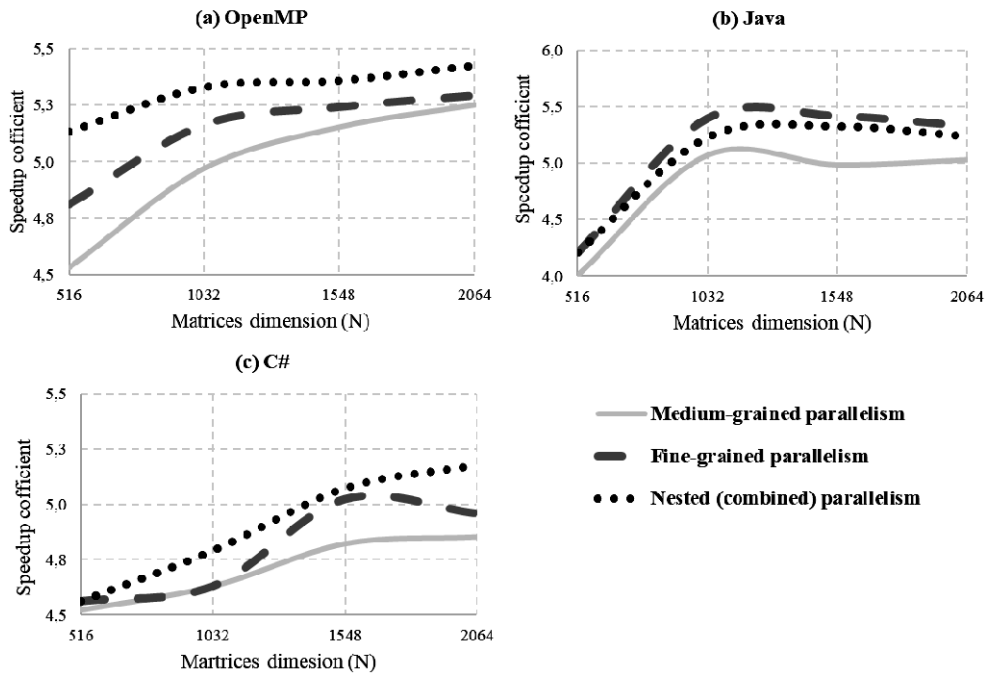
Fig. 5. The dependence of the average speedup coefficients of test parallel programs on the type of parallelism used in them, and on the software tools for its implementation: OpenMP (via C ++) (a), Java (b) and C# (c) in solving the problem of two square matrices multiplication

Additionally, more detailed testing of fine-grained parallelism was conducted in order to identify ways to increase its efficiency. At this stage, those test programs from the developed package were tested, which were written using only fine-grained parallelism. Multiple measurements of the time of the multiplication operation of two matrices with a dimension of 1500*1500 elements were performed. The dependence of execution time on the number of software implemented threads was checked. Fig. 6 demonstrate the detected time dependence on the number of created tasks. More detailed results are provided in Table 2 and 3.
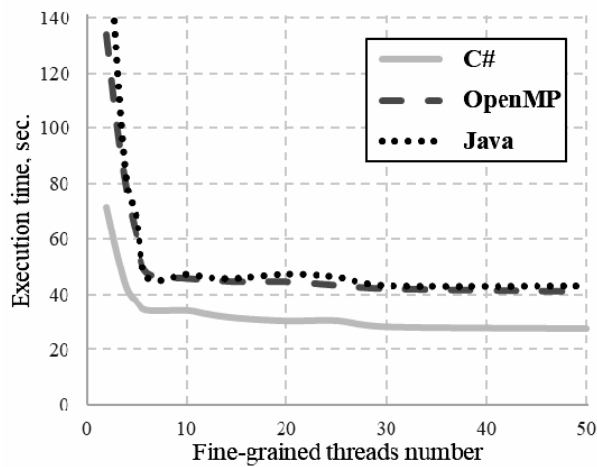
Fig. 6. The dependence of fine-grained parallelism execution time on the number of created threads

T a b l e 2. The results of testing the performance of test parallel programs developed using different types of parallelism (or without using parallelism – as a control sample) and various software tools for its implementation in solving the problem of two square matrices multiplication

N	Computing time (sec)					
	Medium-grained			Fine-grained		
	OpenMP	Java	C#	OpenMP	Java	C#
516	1,7	0,2	1,2	1,6	0,2	1,1
1032	13,3	3,3	9,8	12,8	2,9	9,8
1548	46,7	14,0	35,6	45,9	12,1	34,1
2064	111,7	38,5	79,8	110,8	33,5	78,1
N	Computing time (sec)					
	Nested			Non-parallel		
	OpenMP	Java	C#	OpenMP	Java	C#
516	1,5	0,2	1,1	7,7	8,0	5,2
1032	12,4	3,1	9,5	66,1	66,9	45,5
1548	44,9	13,0	33,8	240,6	250,2	171,4
2064	108,1	35,5	74,8	586,5	640,1	387,1

T a b l e 3. The results of fine-grained parallelism testing in solving the problem of two square matrices multiplication using various software tools for its implementation

Number of threads	Computing time (sec)		
	C#	Java	OpenMP
2	71,309	133,944	190,618
3	55,1	101,41	125,12
4	42,099	77,393	79,894
5	37,202	60,942	68,167
6	34,222	47,532	46,157
10	34,113	45,551	47,202
12	32,841	45,117	46,011
15	31,405	44,37	45,7
20	30,404	44,33	47,196
25	30,511	43,101	46,21
30	28,329	41,9	43,15
50	27,683	40,88	43,01

CONCLUSIONS AND FUTURE WORK

The results obtained during testing showed the effectiveness of MCS in the implementation of the considered mathematical problem solution by using Java and C# languages and OpenMP library. Additionally, reduction of the programs execution time with the application of the parallelism of any degree of grain is possible (speedup coefficient values are in the range of 4,0–5,5). The best result in terms of program execution time was obtained for the C#.

Medium-grained parallelism showed sufficient efficiency, but had the worst result. At the same time, the speedup achieved by OpenMP tools is constantly increasing with the amount of data processed. While using the C# and the Java tools, speedup remains at approximately the same level.

Using fine-grained parallelism was also effective, in which case the speedup coefficient increases steadily with increasing data volume. This type of parallelism was most effective in C#.

Furthermore, additional testing of fine-grained parallelism revealed a declining exponential dependence between the number of threads, which is allowed to create by the program, and the time of its operation. As mentioned in Section 3, the main reason for this is a larger number of fine-grained tasks (threads) that access physical processing elements (cores) and shared resources, which leads to significant downtime due to the problem of mutual exclusion. The optimal number of fine-grained tasks is in the range of 5 to 20, regardless of how it was organized.

Nested (combined) parallelism showed its effectiveness and allowed to increase speedup coefficient when it is used in C# language and OpenMP library. Moreover, there is an increase of speedup coefficient with increasing amount of processed data, which is one of the most important arguments for the feasibility of this approach in the MCS.

It could be assumed that the efficiency of using nested parallelism will increase with an increasing number of cores in the MCS, where:

1. There will be additional processor resources for its implementation.

2. It is possible to reduce the size of grains.

3. There will be an optimal ratio between the number of streams and sub-threads.

Besides, the efficiency of nested parallelism implemented in OpenMP can be improved by more efficient implementation of the powerful sub-threads management system embedded in the library, similar to how it was done in the fork-join model. Since the identified patterns of change in program execution time and speedup coefficients, in general, are preserved for all considered means of organizing parallelism, it can be argued that this approach will be effective regardless of the language or library by which it will be organized.

Therefore, it can be argued that the use of fine-grained and/or combined (nested) parallelism in most cases is an effective approach to the implementation of parallel computing in multi-core computer systems.

Possible directions of work continuation:

1. Testing formed hypotheses in larger and more powerful multi-core computer systems.

2. Testing formed hypotheses on a number of more applied problems.

3. Check the statement about the effectiveness of fine-grained and combined parallelism, regardless of the instruments of its organization, compared with medium-grained parallelism.

From the point of view of the development of high-level instruments of fine-grained parallelism realization in modern parallel programming languages and libraries:

1. Adaptation of existing computational planning methods to the realities of fine-grained and nested parallelism.

2. Adaptation of existing effective processing queue management policies to the realities of fine-grained and nested parallelism.

REFERENCES

1. *ISO 9000:2000 Quality management systems – Fundamentals and vocabulary.* Available: https://www.iso.org/standard/29280.html

2. L. Lamport, "How to Make a Multiprocessor Computer That Correctly Executes Multiprocess Programs", *IEEE Transactions on Computers*, vol. C-28, no. 9, pp. 690–691, 1979. doi: 10.1109/TC.1979.1675439.

3. A.C. Wayne, S.J. Procter, and T.E. Anderson, "The nachos instructional operating system", in *USENIX Winter 1993 Con-ference (USENIX Winter 1993 Conference).* San Diego, CA: USENIX Association, Jan. 1993. doi: 10.1.1.181.878.

4. B.S. Tanenbaum and H. Bos, *Modern Operating Systems*, 4th ed. USA: Prentice Hall Press, 2014. doi: 10.5555/2655363.

5. J.E. Moreira, D. Schouten, and C.D. Polychronopoulos, "The performance impact of granularity control and functional parallelism", in *Proceedings of the 8th International Workshop on Languages and Compilers for Parallel Computing, ser. LCPC'95*, pp. 581–597. Berlin, Heidelberg: Springer-Verlag, 1995. doi: 10.5555/645673.665710.

6. K. Hwang, *Advanced Computer Architecture: Parallelism, Scalability, Programmability*, 1st ed. McGraw-HillHigher Education, 1992. doi: 10.5555/541880.

7. R. Miller and Q.F. Stout, *Parallel Algorithms for Regular Architectures: Meshes and Pyramids*. Cambridge, Mass: MITPress, 1996. doi: 10.5555/249608.

8. B. Blaise, *Introduction to Parallel Computing*. [Online]. Available: https://hpc.llnl.gov/training/tutorials/introduction-parallel-computing-tutorial/

9. J.L. Hennessy and D.A. Patterson, *Computer Architecture, Fifth Edition: A Quantitative Approach*. Morgan Kaufmann Publishers Inc., 2011. doi: 10.5555/1999263.

10. O. Bandman, "Composing fine-grained parallel algorithms forspatial dynamics simulation", in *Proceedings of the 8th International Conference on Parallel Computing Technologies, ser. PaCT'05*, pp. 99–113. Berlin, Heidelberg: Springer-Verlag, 2005. doi: 10.1007/11535294_9.

11. D. Lea, "A java fork/join framework", in *Proceedings of the ACM2000 Conference on Java Grande, ser. JAVA '00*, pp. 36–43. New York, NY, USA: Association for Computing Machinery, 2000. doi: 10.1145/337449.337465.

12. P.E. Hadjidoukas, G.C. Philos, and V.V. Dimakopoulos, "Exploiting fine-grain thread parallelism on multicore architectures", *Sci. Program.*, vol. 17, no. 4, pp. 309–323, Dec. 2009. doi: 10.1155/2009/249651.

13. P. Czarnul, "Assessment of OpenMP master-slave implementations for selected irregular parallel applications", *Electronics*, vol. 10, no. 10, 2021. doi: 10.3390/electronics10101188.

14. J. Ponge, *Fork and Join: Java Can Excel at Painless Parallel Programming Too!* [Online]. Available: https://www.oracle.com/technical-resources/articles/java/fork-join.html

15. O. Rusanova and A. Korochkin, "Scheduling problems for parallel and distributed systems", *Ada Lett.*, vol. XIX, no. 3, pp. 195–201, Sep. 1999. doi: 10.1145/319295.319323.

INFORMATION ON THE ARTICLE

Valerii V. Martell, ORCID: 0000-0002-1749-5818, National Technical University of Ukraine "Igor Sikorsky Kyiv Polytechnic Institute", Ukraine, e-mail: valerii.martell@gmail.com

Aleksandr V. Korochkin, ORCID: 0000-0003-4650-2316, National Technical University of Ukraine "Igor Sikorsky Kyiv Polytechnic Institute", Ukraine, e-mail: avcora@gmail.com

Olga V. Rusanova, ORCID: 0000-0003-0145-3012, National Technical University of Ukraine "Igor Sikorsky Kyiv Polytechnic Institute", Ukraine, e-mail: olga.rusanova.v@gmail.com

ПОРІВНЯЛЬНИЙ АНАЛІЗ ЕФЕКТИВНОСТІ ВИКОРИСТАННЯ ДРІБНОЗЕРНИСТОГО ТА ВКЛАДЕНОГО ПАРАЛЕЛІЗМУ ДЛЯ ЗБІЛЬШЕННЯ ПРИШВИДШЕННЯ ПАРАЛЕЛЬНИХ ОБЧИСЛЕНЬ У БАГАТОЯДЕРНИХ КОМП'ЮТЕРНИХ СИСТЕМАХ / В.В. Мартелл, О.В. Корочкін, О.В. Русанова

Анотація. Подано результати порівняльного аналізу ефективності використання паралелізму різного ступеня зернистості в сучасних багатоядерних комп'ютерних системах з використанням найпопулярніших натепер мов програмування та бібліотек (таких як C#, Java, C++ та OpenMP). Досліджено можливості підвищення ефективності обчислень у багатоядерних комп'ютерних системах за допомогою комбінацій середньо- та дрібнозернистого паралелізму. Отримані результати демонструють високу потенційну ефективність використання дрібнозернистого паралелізму для організації інтенсивних паралельних обчислень. На підставі цих результатів можна стверджувати, що порівняно з більш традиційними методами розпаралелювання, які використовують паралелізм із середньою зернистістю, використання окремо дрібнозернистого паралелізму може скоротити час обчислення великої тестової математичної задачі в середньому на 4% , а використання комбінованого паралелізму — до 5,5%. Це скорочення часу виконання доцільне в разі виконання надвеликих обчислень.

Ключові слова: багатоядерна комп'ютерна система, ядро, потік, завдання, паралелізм, зернистість, fork-join, коефіцієнт пришвидшення, дрібнозернистий паралелізм, вкладений паралелізм, комбінований паралелізм.

INTELLIGENT DECISION SUPPORT SYSTEMS IN THE DEVELOPMENT OF MEGALOPOLIS INFRASTRUCTURE

O. TROFYMCHUK, A. STENIN, M. SOLDATOVA, I. DROZDOVICH

Abstract. From the point of view of the management theory, a megapolis is a complex non-stationary spatial system. The problem of making innovative decisions on the development of their infrastructure is caused by the presence of a large amount of information, its uncertainty and inconsistency. This article discusses the principles of building intelligent decision support systems of a situational type for the innovative development of the infrastructure of megacities. Solutions are formed by logico-analytical processing of data on the situation in general and special cases of situations for the considered subject of the megalopolis infrastructure. For the practical implementation of the decision-making mechanism, the article proposes a linguistic-numerical method for determining the potentially best alternative and a fuzzy situational algorithm for managing the subjects of the megalopolis infrastructure, based on the structural generality of the situations of a fuzzy situational network. The obtained results were tested on two real infrastructure subjects of Kyiv.

Keywords: megapolis, infrastructure entities, intelligent decision support system, linguo-numerical evaluation of alternatives, fuzzy situational algorithm.

INTRODUCTION

From the point of view of the management theory, any megalopolis is a complex non-stationary spatial system. For objects of this kind, two main features are characteristic: the dependence of the parameters of the component parts of the object on their spatial location and the variability of these parameters over time. The study of such objects with sufficient versatility to obtain practically significant results, taking into account the fact that experimental effects on them for various reasons (limited time frames, the risk of irreversible changes, the high cost of experiments, etc.) are usually impossible or undesirable. It is possible to perform almost only by modeling possible situations [1–3]. Especially difficult is the problem of making effective decisions on the development of the megalopolis infrastructure, which is associated with large amounts of information, its uncertainty and inconsistency. This problem can solved by using intelligent decision support systems (IDSS). IDSS is a decision support system with embedded artificial intelligence techniques exhibiting some or all of the abilities indicative of intelligent behavior. At the same time, one of the main properties of the intelligence of this system is the ability to generate, analyze, display, search and design a solution that is not explicit and ready in the system [4–6, 18].

A review of publications on the problems of information IDSS in the field of infrastructure development of megacities shows that at present the use of intelligent information technologies in this area is mainly limited to the creation of reference and search engines. Hence, the task of creating fully functional systems that support all the main stages of decision-making — from the collection and storage of initial information to the presentation of a reasonable version of the optimal solution-remains relevant.

STATEMENT OF RESEARCH PROBLEMS

Let be $A_1, A_2,...A_n$ — a set of alternatives. Alternatives may or may not specified at the time of the decision. Let's also define criteria for evaluating alternatives $K_1, K_2,...K_n$, which are verbal gradations of quality $X_q = x_q^1,...,x_q^m$, where is the gradation number ($q = \overline{1, N}$), m — a set of values of estimates, or otherwise the scale of the criterion. For discrete scales, the number of gradations is usually small $m = 2,...,5$. Discrete scales are ordered in descending order (x_q^1 — best, x_q^m — worst). Utility of the *i*-th alternative A_i to the multi-criteria problem denote by. Sometimes it is allowed that, although in the general case. In addition, introduce solution classes, defined and ordered by quality (from best to worst). Then, if $U(A_i) \in C_u$, but $U(A_j) \in C_v$ and $u < v$, then $U(A_i) > U(A_j)$, i.e., the utility of the *i*-th alternative is higher, since it corresponds to a better class of solutions. This problem refers to the static problem of determining the optimal solution by determining the potentially best alternative. In addition to this task, the article deals with the dynamic problem of determining the potentially best alternative associated with the operational management of a dynamic object in uncertain conditions of its operation. The solution of these problems in this article carried out within the framework of the IDSS of the situational type based on the method of linguo-numerical estimates and a fuzzy situational control algorithm.

Literature review

When determining the rational solution to a particular problem that arises in the urban economy, as a rule, it is necessary to take into account a large number of uncertain and contradictory factors. Uncertainty is an integral part of decision-making processes for most infrastructure subjects of megapolis [7]. The uncertainty is primarily due to the incompleteness of knowledge about the problem solved and the inability fully take into account the reaction of the environment, i.e. the current situation. Inconsistency arises due to ambiguity in the assessment of situations, errors in the choice of priorities, which, in the end, greatly complicates decision-making. Research shows that decision-makers without additional analytical support tend to use simplified and sometimes contradictory decision-making rules. In this case, the most effective tool for making a potentially better decision is intelligent Decision Support Systems (IDSS). It should note that modern IDSS is based on the use of specialized information storage (Data Warehouse) and OLAP (On-Line Analytical Processing) technologies — operational data analysis. The main purpose of OLAP technologies is dynamic multidimensional data analysis using an effective Data mining tool, modeling and forecasting [8–10].

It is extremely difficult and almost impossible to reduce tasks with the above uncertainties by precisely set goals. To do this, you need to "remove" the uncertainty. One of the most common methods of withdrawal is the subjective assessment of a specialist (expert, manager), which determines his preferences. At present, the subjective assessment has proved to be the only possible basis for combining the heterogeneous physical parameters of the problem solved into a single model that allows evaluating possible solutions. Taking into account the factor of subjectivity of the decision-maker (LPR) in decision-making violates the fundamental principle of the methodology of operations research: the search for an objectively optimal solution. The recognition of the right of the decision-maker to the subjectivity of the decision is a sign of the emergence of a new paradigm, characteristic of another scientific direction — decision-making under many criteria. On the other hand, when making decisions on many criteria, there is also an objective component. Usually, this component includes restrictions imposed by the external environment on possible solutions (availability of resources, time constraints, environmental requirements, social situation, etc.) [11, 12].

Decision-making problems usually divided into well structured, weakly structured and unstructured. The first problem of a substantial relationship between the main characteristics can expressed quantitatively. Unstructured problems characterized by the fact that their description dominated by qualitative factors that are difficult to formalize, and the quantitative relationships between these factors usually not defined. The intermediate position occupied by weakly structured problems that combine quantitative and qualitative dependencies, and uncertainty has a dominant component. Unstructured decision-making problems are the most complex and characteristic of the infrastructure subjects of megalopolis. These problems are problems of unique choice in the sense that each time the problem either new to the decision-maker, or has new features compared to a previously encountered similar problem [13].

IDSS of situational type

To solve the above problems, the most effective is the situational IDSS, the structure of which shown in Fig. 1.
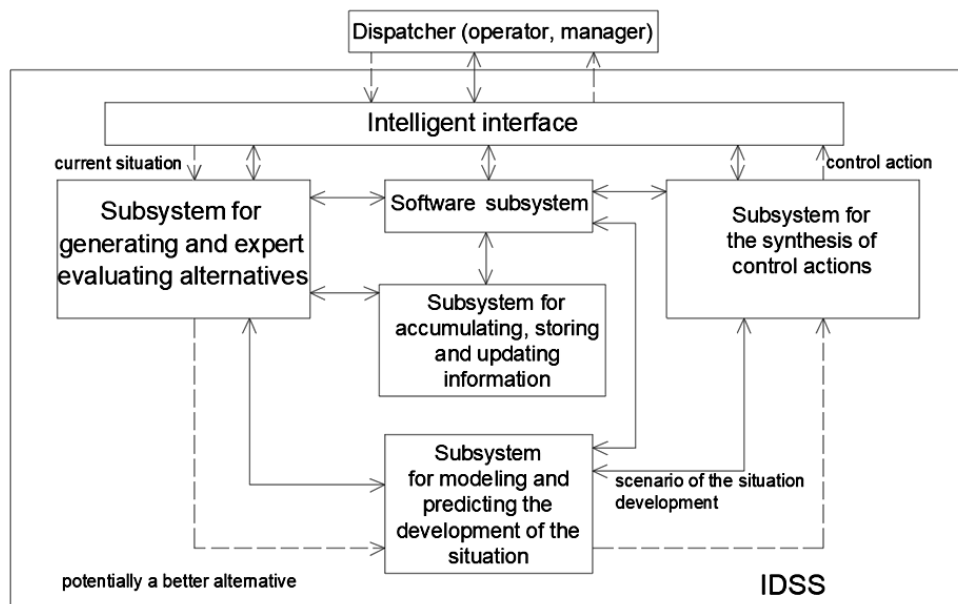
Fig. 1. Situational type IDSS structure

In the dialogue with the expert, the situational IDSS provides automated configuration of the parameters of the subject of the studied megalopolis infrastructure by entering the basic system of concepts, attributes, values, relations between them, as well as the types of situations that are typical processes and interactive user interface in the process of its functioning. The model of the process of functioning of the subject of the megalopolis infrastructure defined as a set of "regular" situations that represent a fuzzy situational network (FSN) (Fig. 2).
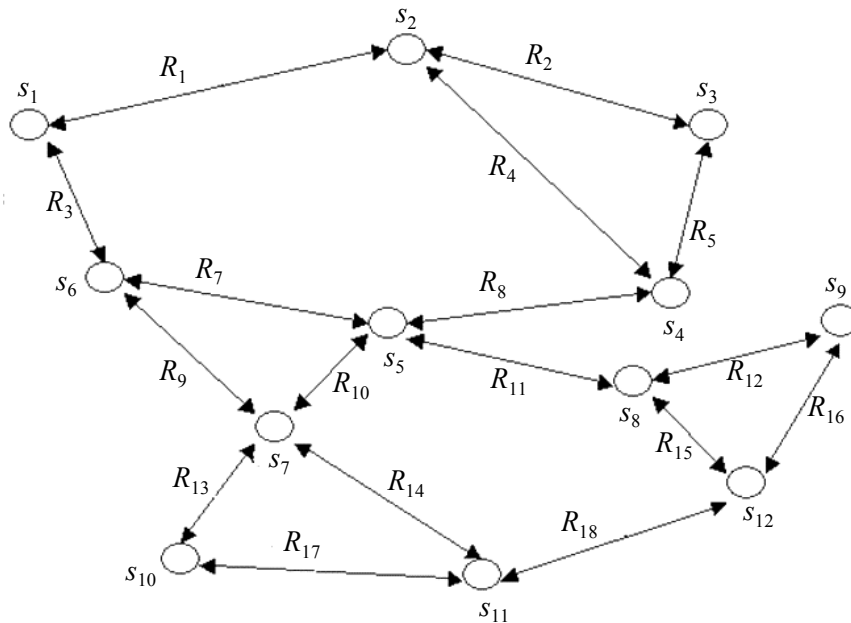
Fig. 2. FSN IDSS of situational type

Decisions about the situation formed by logical and analytical processing of data about the situation in general and special cases of situations for the considered subject of the megalopolis infrastructure. It assumed that the functioning of the studied subject of urban infrastructure described on the 'regular' situations, previously synthesized in the subsystem of generation and expert evaluation of alternatives. Subsystem also identifies for them the potentially best alternatives (PBA) of rational solutions and control actions.

A ready-made FSN used to determine the sequence of actions or transition paths between any source and target situation, and this process can fully automated. An example of a fragment of such a network is shown in Fig. 2, where S_i is the *i*-th regular situation, R_i is the functions that characterize the cost degree normalized in the range [0,1] during the mutual transition from S_i to S_j and vice versa.

To analyze the consequences of the use of certain management alternatives for current situations, the appropriate scenarios implemented in the subsystem of modeling and forecasting the development of the situation.

For the selected situation, depending on the goals and conditions of its implementation, the rational control formed in the subsystem for the synthesis of control actions.

Taking into account the specifics of the infrastructure of megacities in the ISPR of the situational type in the subsystem of accumulation, storage and updating

of information, the corresponding requirements for the main structural unit of this subsystem — the knowledge representation model (KRM) should formulated. This concerns the system of concepts, the adequacy of the content and correspondence of the formulated knowledge to the studied processes, and the suitability for performing the required actions. A complete description of the situation does by the expert, if there is a complete set of indicators that characterize this situation. To take into account many factors, the original set of indicators can divided into fragments that combine indicators that form a relatively independent semantic group. Thus, the task of assessing the situation in the functioning of a megalopolis subject can divided into a number of specific tasks. The solutions generated by the particular problems are indicators of a higher degree of generalization, which serve as the initial data for the particular problems of the next level of the hierarchy, etc. This process of decomposition of the overall assessment task leads to the formation of a multi-level hierarchy of related input-output private tasks. They solution allows to form a system of solutions for individual aspects and a general decision on the degree of compliance of the current situation with the goals of the management in the subject of the megalopolis infrastructure.

Each task (subtask) in the accepted interpretation is a set of functional dependencies that describe the initial situation and the solution to the situation. Using the subsystem of logical inference of the generalized assessment of the situation and the formation of explanations, the rules built and the KRM updated. The solution of the applied problem carried out by applying the rules from the KRM database to the data about the current situation.

In other words, when creating an KRM, it is necessary to actually describe the semantic content of the functioning of the subject of the megalopolis infrastructure, which guarantees their processing by formal methods. Currently, many KRM have developed. Having a generic name, they differ in the ideas underlying them, in terms of mathematical validity.

Obviously, for the above-mentioned situational IDSs, the closest CRM is the frame model based on the concept of Marvin Minsky. His concept is that the frame model is a systematized psychological model of a person's memory and consciousness. In this sense, it is as close as possible to the creative activity of a person, including the development of the infrastructure of a megalopolis [14, 15].

For the frame KRM, the data structure is a connected tree structure of nodes and rules of formalized data accumulated by experts for the subjects of the megalopolis infrastructure. In this case, the linguistic variable ω_n of the frame KRM can described by the following expression:

$$\omega_n = (n, T(n), U, G, M),$$

where $T(n)$ is a term — set of n values that represent the names of fuzzy variables; U is the domain of definition of each fuzzy variable; G is a syntactic procedure that serves to expand the set $T(n)$ to generate new elements; M is a special semantic procedure for forming a fuzzy set.

Knowledge Z is defined as a tuple of a set of objects Q with a set of implementations of relations F between them and a set of actions N that are performed on elements of Q, i.e.

$$Z = \langle Q, F, N \rangle, \tag{1}$$

Production rules can written as sets of fuzzy utterances $\widetilde{L}$:

$$\widetilde{L} = (\text{IF } (a_1 \text{ THEN } \beta_1) \text{ AND...AND } (\beta_l) \, \alpha_k \text{ THEN}),$$

where α is a generalized linguistic variable defined on the set of input parameters; β is a generalized linguistic variable defined on the set of output variables; k, l is the order of these variables.

For the frame KRM IDSS, the data structure of which is a coherent structure of formalized data on the subjects of the megalopolis infrastructure, the formation and selection of a potentially better alternative (rational solution) implemented on the linguistic-numerical method proposed below.

A linguo-numerical method for determining a potentially better alternative

The main task of the situational type IDSS is to determine the potentially best solution for the current situation, which can be static (for example, choosing the rational location for the construction of a supermarket) and dynamic (for example, passenger traffic management). Since alternatives to solutions in this IDSS can formed both quantitatively and verbally, a linguistic-numerical method for determining the potentially best alternative (PBA) proposed. The following is an example of a linguistic rating scale:

very low → 2, low → 3, average → 4, high → 5, very high.

To date, there is a large selection of methods for evaluating the generated set of alternatives and selecting the best alternatives [11, 13]. These decision-making methods for evaluating and selecting potentially better alternatives are effective with a small power of the set of evaluated alternatives (no more than 5–10). To evaluate the set of high-power alternatives, which corresponds to the above-mentioned tasks of managing the subjects of the megalopolis infrastructure, it proposed to use intelligent methods, in particular, fuzzy logic methods, which allow for automatic ranking of alternatives based on decision rules.

To enable the evaluation of alternatives based on linguistic variables, the scheme of the fuzzy inference procedure is used (Fig. 3) [16].
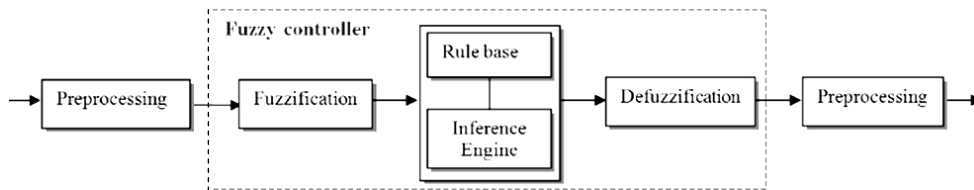
Fig. 3. The scheme of the fuzzy inference procedure

Since in the KRM, the reason corresponds to the KRM frame, which contains a ready-made mechanism for implementing this reason (sub-goal), the procedure for general fuzzy inference is greatly simplified. In addition, since the parameters that can qualitatively evaluated by the studied subject of the city infrastructure have a different physical nature, the natural requirement for its objective assessment is the introduction of a single normalized rating scale in a certain range at the fuzzification stage.

Let the attributes that form the alternatives A_i contain both numerical (quantitative) and linguistic variables (qualitative). In this case, each variable is assigned a belonging function. In this case, we will use the universal scale [0,1] to evaluate preferences. In other words, for the set $x \in [0,1]$ and the membership function $\mu : x \to [0,1]$, the fuzzy set is defined as

$$\widetilde{A} = \{(x, \mu_A(x)) \mid x \in X\} . \tag{2}$$

The belonging function (1) quantifies the membership of the elements of the set of alternatives A, defined by $x \in A$ to the fuzzy set $\widetilde{A}$, with normalized variables $\widetilde{x}$ A value of 0 means that the element does not include a fuzzy set, and 1 means that the element is completely described by this set. Among the most well-known and used belonging functions, the most convenient and universal for the variables under consideration are linear and trapezoidal functions of the form [6, 7, 18]:

The graphs of the belonging functions correspond to the ascending (Fig. 4, *a*) and descending (Fig. 4, *b*) preference scales, respectively. Thus, for all quantitative evaluations of max and min values of the variable a_{ij} and b_{ij} are known, and for all linguistic (verbal) ratings, they are determined by the maximum and minimum number of linguistic scale (see example linguistic scale).
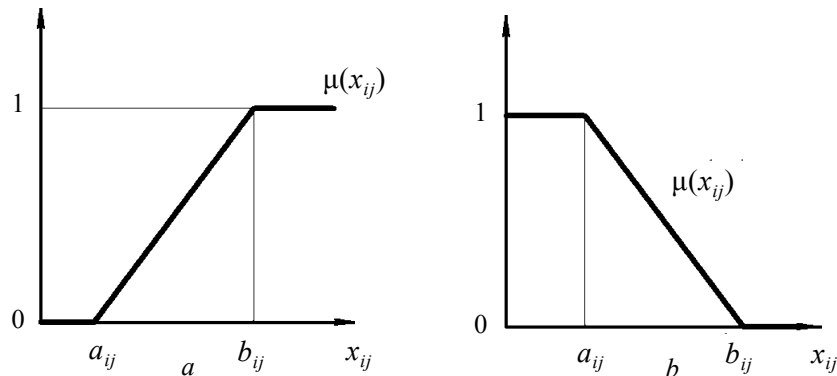
Fig. 4. Graphs of belonging functions

The potentially best alternative determined by the formula

$$\widetilde{A}_{iopt} = \max J_i = \sum_{i=1}^{n} x_{ij} \quad (j = 1,2,...,m) , \tag{3}$$

where $\widetilde{x}_{ij}$ — I variable of the j alternative.

The practical use of this method has shown the identity of its results to the well-known methods PARK, ORKLASS, QUERY, CORD, etc. [13], but the complexity of the decision-making process of the proposed method is significantly lower. This is due to the lack of a procedure for pairwise comparison of the selected parameters of the studied subject of the megalopolis infrastructure. The most effective application of this approach to the assessment and selection of the PBA of the studied subject of the megalopolis infrastructure is expedient with a large number of characteristic parameters of this subject.

Fuzzy situational control subjects of infrastructure of the megapolis

Let the current situation of a megalopolis infrastructure subject described as a fuzzy situation of the following type:

$$S_{TEK} = \{M_{s_i}(x_i) / x_i\}, \; x_i \in X, \qquad (4)$$

where the function of belonging to a linguistic variable x_i, describing the current situation.

Since each linguistic variable corresponds to the j-th term from the set of terms of KRM, the formula (4) can written as:

$$S_i = \{M_{M_{s_i(x_i)}}(T_j^i) / T_j^i\}, \; j = \overline{1, M}; \; i = \overline{1, N}; \; x_i \in X,$$

where j-th term i-th linguistic variable.

To determine the control action for the current state you want to compare this situation fuzzy fuzzy with each situation from a set of existing KRM in the test subject of city's infrastructure "regular" situations, which on the basis of expert methods elaborated by standard control actions.

From the point of view, the most convenient measure of proximity can considered the degree of fuzzy inclusion of the situation, which characterized by a certain inclusion threshold determined by the developer, based on the conditions in which the subject of the megalopolis infrastructure operates. The inclusion threshold defined, as well as the belonging functions, in the normalized range [0, 1] as follows:

$$t_{incl} \in [\alpha_{\min}, 1],$$

where the lower limit of the range of the degree of inclusion, usually. In this case, we can talk about how fuzzy the signs of the current STEK situation are indistinctly included in the fuzzy values of the corresponding signs of the situation [2, 6].

If a "regular" situation found that is sufficiently close to this current one, then from the set of alternatives for this "regular" situation, the PBA for which the control action implemented selected. If such proximity not found, then the current situation processed in the subsystem for generating and expert evaluation of alternatives, after which its dynamic assessment is carried out for the found PBA in the subsystem for modeling and predicting the development of the situation. Further, in the subsystem of synthesis of control actions, the corresponding control formed. This situation then transferred to the category of "regular". The algorithm for implementing fuzzy situational control based on IDSS shown by the dotted arrows in Fig. 1.

In addition, if the external working conditions of the studied subject of the megalopolis infrastructure change, it becomes necessary to move from one "regular" situation to another. The possible transition from one "regular" situation to another carried out with the help of some strategy.

The strategy is described by the optimal FSN route between the current fuzzy situation $s_i \in S$ and the target situation $s_c \in S$. Transitions are determined by R_i solutions, which correspond to a certain degree of cost. The total number of situations and transitions between them in the FSN describing the real subjects of

the megalopolis infrastructure can be very large. To simplify the search task, management strategies use various optimization methods (for example, the dynamic programming method).

Given that the subjects of the megalopolis infrastructure in most cases have mutual independence of the values of the features, it proposed to use the FSN compression method based on the definition of "community structures". Community structures Oi that have non-empty intersections with each other called neighbors, and the set of vertices of the intersection area of two neighboring structures called the transition area of community structures. For the fragment of the FSN (Fig. 2), the structures of generality of situations with the costs of mutual transitions have the form shown in Fig. 5.
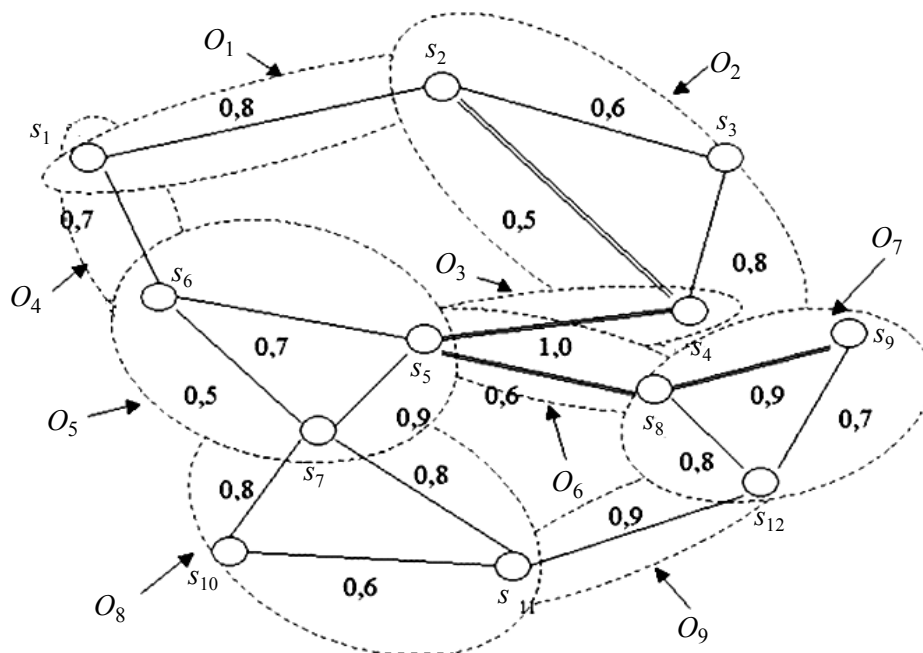
Fig. 5. Community structures of FSN IDSS

The essence of the proposed approach based on the NSS compression method for the given NSS fragment is as follows. As an optimality criterion in the conditional example, we use use the minimum of total costs. The path that has the minimum cost considered optimal. Let's determine the optimal transition from s_2 to s_9. Given that $O_2 \cap O_9 = \varnothing$ (empty set), it is not possible to go from s_2 to s_9 using a single local control solution. Since there are no pairs of vertices adjacent to each other from the number belonging to O_2 and O_9, we proceed to find the shortest possible path between all pairs of vertices of the sets O_2 and O_9. The shortest path $L = (O_2, O_3, O_6, O_7)$. Moving to the transition points of neighboring structures of the common path L, we get the control strategy: $C(s_2, s_9) = (s_2, s_4, s_5, s_8, s_9)$. The desired path in Fig. 2 highlighted with a dotted line.

Practical implementation of the results obtained

The researches in the article was carried out within the framework of research work "Research of methods and tools for creating a hybrid computing technology for constructing a quasi-formalized forecasting model in conditions of data heterogeneity and non-normative deviations in organizational management systems" (S/R 0117U002448). The obtained results tested on two real subjects of the infrastructure of Kiev.

Construction of social objects. Assessed the appropriateness of the choice of the construction site of a supermarket. The expert group suggested the following criteria: price, population density within a radius of 1 km, the presence of competitors, infrastructure connections, the number of places for car Parking, access places through public transport and the visibility of the supermarket from the nearby major streets, as well as data on these criteria. Four possible supermarket construction sites were evaluated (alternatives var. 1 — var. 4). In one of them, a supermarket built in Kiev. Expert assessments listed in Table 1.

T a b l e 1. Initial expert assessments

x_{ij}	Variables	Alternatives			
		var. 1	var. 2	var. 3	var. 4
x_{1j}	The number of places for car Parking, max	400	300	250	150
x_{2j}	Presence of the competitors, min	1 (few)	5 (many)	3 (average)	5 (many)
x_{3j}	Population density in 1 km radius, max	200	4500	6000	7000
x_{4j}	The cost of the placement, million UAH, min	6	16	12	20
x_{5j}	The flow of public transport, max	1 (low)	3 (average)	5 (high)	7 (very high)
x_{6j}	Main street visibility, max	5 (good)	5 (good)	3 (average)	1 (bad)
x_{7j}	Infrastructure, max	3 (average)	3 (average)	5 (good)	7 (very good)

After the procedure of fuzzification and normalization of linguistic variables according to the formula (2) and Fig. 4, *a*) and Fig. 4, *b*), we summarize their values in Table 2.

T a b l e 2. Sum of data

Variables	Alternatives			
	var. 1	var. 2	var. 3	var. 4
$\widetilde{x}_{1j}$	1	0,6	0,4	0,0
$\widetilde{x}_{2j}$	1	0,33	0,66	0,33
$\widetilde{x}_{3j}$	0	0,63	0,85	1
$\widetilde{x}_{4j}$	1	0,285	0,57	0
$\widetilde{x}_{5j}$	0	0,33	0,66	1
$\widetilde{x}_{6j}$	0,66	0,66	0,33	0
$\widetilde{x}_{7j}$	0,33	0,33	0,66	1
$\sum_{i=1}^{7} x_{ij}$	3,99	3,165	4,13	3,33

Then, using the formula (3), we obtain the following estimates of alternative options: 3,99; 3,165; 4,13; 3,33, from which it follows that the potentially best alternative (PBA) is the alternative var. 3, which confirmed the feasibility of this supermarket construction site. It should note that the alternative var.1 is also of interest to the decision-maker.

Public transport. Today, the development and effective management of transport is unthinkable without the development and application of intelligent control systems. The process of transportation of passengers by urban passenger transport based on the observance of the schedule of movement of vehicles along the route in accordance with the pre-established schedule of movement. In most motor transport companies of Ukraine, the management of the passenger transportation process controlled by the dispatcher for compliance with the traffic schedule.

Due to the transience of changing road situations, the lack of complete information about the situation on the route, the presence of many uncertainties when receiving it, it is impossible to build a reliable forecast of the development of the situation over a long time interval. Thus, the decision-making by the dispatcher takes place in a difficult situation and requires a lot of psycho-physiological stress from the dispatcher [17, 8].

To assess the effectiveness and sustainability of the decisions made by the dispatcher in the process of managing the movement of public transport, one of the bus routes in Kiev selected for the study. The scheme of implementation of control solutions for fuzzy situational management of public transport traffic shown in Fig. 6. The use of a fuzzy situational algorithm for controlling the movement of urban transport for 3 weeks made it possible to increase the efficiency of transport on this route (Fig. 7, red line). In addition, the dispatcher with the help of the ISPR could quickly make operational decisions on the "emergency" situations that arose, which reduced the economic losses of the transport company.
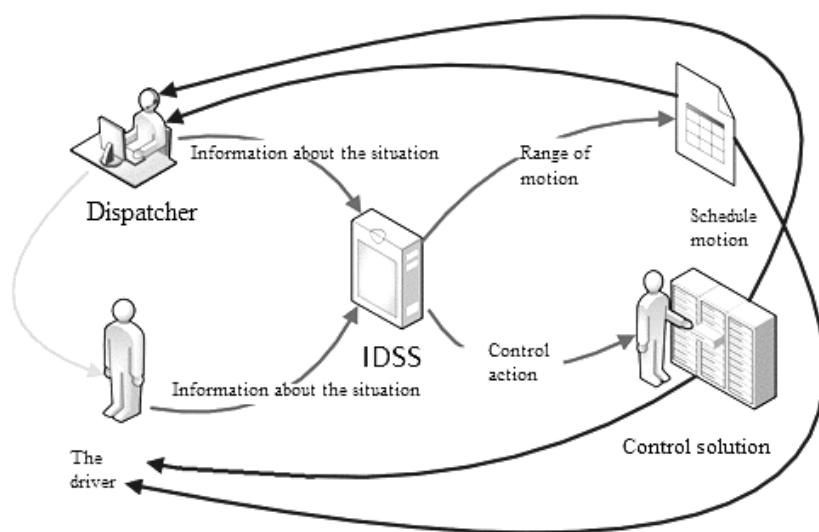
Fig. 6. Fuzzy situational control
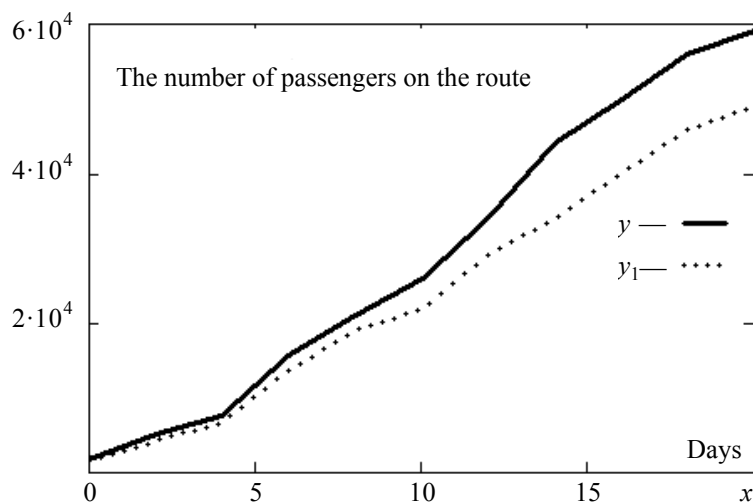
Fig. 7. Loading schedule

The article proposes an intelligent decision support system, the main elements of which are a fuzzy situational network and a frame model for representing the knowledge of the subjects of the megalopolis infrastructure. This allows us to formalize the "regular" situations that arise in the course of the activities of the subjects of the megalopolis infrastructure using the theory of fuzzy sets, and then determine the optimal control actions for them. If it is necessary to move from one "regular" situation to another with minimal costs, an algorithm based on the structural generality of situations is used. When an "unregular" current situation occurs, its maximum proximity to one of the "regular" situations determined and linguo-numerical alternatives to decision-making generated. The selection of the potentially best ones based on a logical inference scheme. After that, the optimal control action for this current situation synthesized and identified in the knowledge representation model as "regular".

CONCLUSION

The article proposes an intelligent decision support system, the main elements of which are a fuzzy situational network and a frame model for representing the knowledge of the subjects of the megalopolis infrastructure. This allows us to formalize the "regular" situations that arise in the course of the activities of the subjects of the megalopolis infrastructure using the theory of fuzzy sets, and then determine the optimal control actions for them. If it is necessary to move from one "regular" situation to another with minimal costs, an algorithm based on the structural generality of situations is used. When an "unregular" current situation occurs, its maximum proximity to one of the "regular" situations determined and linguo-numerical alternatives to decision-making generated. The selection of the potentially best ones based on a logical inference scheme. After that, the optimal control action for this current situation synthesized and identified in the knowledge representation model as "regular".

REFERENCES

1. V. Bourdakis, "Low Tech Approach to 3D Urban Modeling", *Architecture in Computro (26th eCAADe Conference Proceedings)*, Antwerpen, Belgium, 2008, pp. 959–964.

2. A.A. Sholomitsky, A.A. Lunev, and O.M. Tarasova, "Technology of three-dimensional modeling of cities", *Scientific Bulletin of the Nizhny Novgorod State University*, Nizhny Novgorod, no. 2, pp. 57–62, 2011.

3. M. Carrozzino, F. Tecchia, and M. Bergamasco, *Urban procedural modeling for real-time rendering*. Available: http://www.isprs.org /proceedings/XXXVIII/5-W1/pdf/carrozzino_etal_2.pdf

4. V.P. Osipov, T.V. Sivakova, V.A. Sudakov, and Yu.I. Nechaev, "Intellectual core of the decision support system", *Preprints of the IPM named after M.V. Keldysh*, no. 205, 23 p., 2018. doi: 10.20948/prepr-2018-205.

5. V.P. Karelin, "Intellectual technologies and artificial intelligence systems for decision support", *Bulletin of the Taganrog Institute of Management and Economics*, no. 2, pp. 79–84, 2011.

6. E.A. Engel, "Models and methods of intellectual support for manager decision making", *Journal of Siberian state University of science and technology*, no. 4, pp. 106–112, 2011.

7. O. Tikhanychev, "About information support of decision-making support", *International Journal "Software Products and Systems"*, vol. 27, pp. 311–315, 2018. doi: 10.15827/0236-235X.122.311-315

8. R. Bavad and Jean-Charles Pomerol, "An "Intelligent" DSS for the Reinforcement of Urban Electrical Power Networks", *Conference: Decision Support Systems: Experiences and Expectations, Proceedings of the IFIP TC8/WG8.3 Working Conference on Decision Support Systems: Experiences and Expectations, Fontainebleau, France, 30 June – 3 July 1992*, pp. 153–165.

9. G. Phillips-Wren, "Decision Support Systems", *in book: Multicriteria Decision Aid and Artificial Intelligence*. Loyola University Maryland, 2013, pp. 25–44. doi: 10.1002/9781118522516.ch2.

10. A. Kaklauskas, "Intelligent Decision Support Systems. In book: Biometric and Intelligent Decision Making Support", *Intelligent Systems Reference Library*. Vilnius Gediminas Technical University, 2015, pp. 31–85. DOI: 10.1007/978-3-319-13659-2_2.

11. V.P., Karelin and O.L. Kuzmenko, "Choosing the best management solution with fuzzy source data and multiple criteria", *Izvestiya VUZov. The North Caucasus region. Technical sciences*, no.1, pp. 158–165, 2006.

12. A.A. Evseeva, D.A. Krasnikova, and A.A. Kazakov, "Modern approaches to solving multi-criteria problems", *Scientific and methodological electronic Journal "Concept"*, vol. 3, pp. 2801–2805, 2013. Available: http://e-koncept.ru/2013/53563.htm.

13. A. Stenin, I. Drozdovych, and M. Soldatova, "Situational management of urban engineering networks with intelligent support for dispatching decisions", *Proceedings of the Third International Workshop on Computer Modeling and Intelligent Systems (CMIS-2020) Zaporizhzhia, Ukraine, April 27 – May 1, 2020*, pp. 118–131. Available: http://ceur-ws.org/Vol-2608

14. M.L. Minsky, "A Framework for Representing Knowledge", in Patrick Henry Winston (ed.), *The Psychology of Computer Vision*. New York: McGraw-Hill, 1975, pp. 211–277.

15. M.K. Hasan, "A Framework for Intelligent Decision Support System for Traffic Congestion Management System", *Engineering, Kuwait University*, vol. 2, pp. 270–289, 2010. doi: 10.4236/eng.2010.24037

16. A.A. Akhrem, M.R. Ashinyants, and S.A. Petrov, "Fuzzy logical conclusion in the decision-making system", *Proceedings of the Institute of System Analysis of the Russian Academy of Sciences*, vol. 29, pp. 265–275, 2007.

17. A. Stenin, O.I. Lisovichenko, I.G. Drozdovich, and S.A. Stenin, "Analysis of passenger traffic and situational management of urban transport", *Bulgarian Journal for Engineering Design*, no. 40, pp.7–12, 2019.

18. O.M. Trofymchuk and P.I. Bidyuk, *Decision support systems, modeling, forecasting, risk Estimation*. LAP LAMBERT Academic Publishing, 2019, 179 p.

INFORMATION ON THE ARTICLE

Oleksandr M. Trofymchuk, ORCID: 0000-0003-3358-6274, Institute of telecommunications and global information space of NAS of Ukraine, Ukraine, e-mail: itc_nasu@ukr.net

Aleksandr A. Stenin, ORCID: 0000-0001-5836-9300, National Technical University of Ukraine "Igor Sikorsky Kyiv Polytechnic Institute", Ukraine, e-mail: alexander.stenin@yandex.ua

Maria A. Soldatova, ORCID: 0000-0003-1233-1272, National Technical University of Ukraine "Igor Sikorsky Kyiv Polytechnic Institute", Ukraine, e-mail: benten1093@gmail.com

Irina G. Drozdovich, ORCID: 0000-0002-4216-2417, Institute of telecommunications and global information space of NAS of Ukraine, Ukraine, e-mail: irinashitikova54@gmail.com

ІНТЕЛЕКТУАЛЬНІ СИСТЕМИ ПІДТРИМАННЯ ПРИЙНЯТТЯ РІШЕНЬ У РОЗВИТКУ ІНФРАСТРУКТУРИ МЕГАПОЛІСУ / О.М. Трофимчук, О.А. Стенін, А.О. Солдатова, І.Г. Дроздович

Анотація. Мегаполіс з точки зору теорії управління являє собою складну нестаціонарну просторову систему. Проблему прийняття інноваційних рішень щодо розвитку їх інфраструктури зумовлено наявністю великого обсягу інформації, її невизначеністю і суперечливістю. У роботі розглянуто принципи побудови інтелектуальних систем підтримання прийняття рішень ситуаційного типу для інноваційного розвитку інфраструктури мегаполісів. Рішення формуються шляхом логіко-аналітичного оброблення даних про ситуацію в цілому і окремих випадках ситуацій для розглянутого суб'єкта інфраструктури мегаполісу. Для практичної реалізації механізму прийняття рішень запропоновано лінгвочисловий метод визначення потенційно кращої альтернативи та нечіткий ситуаційний алгоритм управління суб'єктами інфраструктури мегаполісу, заснований на структурній спільності ситуацій нечіткої ситуаційної мережі. Отримані результати протестовано на двох реальних об'єктах інфраструктури Києва.

Ключові слова: мегаполіс, інфраструктурні об'єкти, інтелектуальна система підтримання прийняття рішень, лінгво-числове оцінювання альтернатив, нечіткий ситуаційний алгоритм.

ТОПОЛОГІЧНА ОПТИМІЗАЦІЯ СИМЕТРИЧНОГО КЛЕЙОВОГО З'ЄДНАННЯ ВНАПУСК

С.С. КУРЄННОВ

Анотація. Розглянуто задачу оптимізації профілю шарів, що з'єднані внапуск за допомогою проміжного клейового шару. З'єднання оцінюється за моделлю Фолькерсена, згідно з якою несучі шарі розглядаються як стрижні, які працюють лише на стискання–розтягування, а клейовий шар працює лише на зсув. Метою оптимізації є проєктування конструкції з'єднання мінімальної маси за умов виконання обмежень на міцність клейового шару та мінімально припустиму товщину несучих шарів. Профіль несучих шарів описано за допомогою розкладання в ряд Фур'є. Пряму задачу зі знаходження напруженого стану з'єднання стрижнів перемінної товщини розв'язано за допомогою методу скінченних різниць. Задачу оптимізації зведено до пошуку коефіцієнтів ряду Фур'є та довжини з'єднання. Застосовано генетичний алгоритм оптимізації. Розв'язано модельну задачу.

Ключові слова: тришарова конструкція, топологічна оптимізація, генетичний алгоритм.

ВСТУП

Клейові з'єднання внапуск є невід'ємною частиною сучасних композитних конструкцій. Поширеність їх застосування зумовлена такими якостями, як мала маса, технологічність, герметичність, висока аеродинамічна ефективність тощо. Але відомим недоліком з'єднань внапуск є концентрація напружень у клейовому шарі біля кінців з'єднання [1–4]. З метою підвищення міцності з'єднань та зниження концентрації напружень застосовуються певні конструктивні заходи, такі як утворення напливу з надлишків клею на краю склейки, створення фасок на кінцях з'єднуваних шарів, застосування функціонально-градієнтних клеїв, уведення у з'єднання поперечних та поздовжніх силових елементів тощо [5]. Зазвичай проектування з'єднання зводиться до пошуку оптимальної довжини склейки за умов постійних за довжиною конструкції пружних та геометричних параметрів шарів. Одним з ефективних заходів зі зниження концентрації напружень у клейовому шарі є застосування з'єднань зі змінною товщиною шарів, з'єднань «на вус». Застосування сучасних адитивних технологій, таких як 3D друк, дозволяє надавати елементам конструкції будь-якої складної форми. Це ставить перед проектувальниками нові завдання, такі як топологічна та структурна оптимізація конструкцій, тобто пошук не одного певного параметра оптимізації, а невідомої функції, яка описує геометрію конструкції або її внутрішню структуру. Але навіть у двовимірній постановці такі задачі наштовхуються на труднощі, зумовлені надвеликою розмірністю задачі [6, 7]. Крім того, отримані результати можуть бути неприйнятними з технологічних, конструктивних або інших міркувань, які не враховано під час постановки задачі [8]. У цій ситуації перспективним напрямом може стати поєднання класичних матема-

тичних моделей стрижнів, балок та пластин і методу дискретизації конструкції з методами оптимізації на основі генетичних еволюційних алгоритмів. Це дозволяє зменшити розмірність задачі без суттєвих утрат у точності математичної моделі.

ПОСТАНОВКА ЗАДАЧІ

Схему з'єднання внапуск показано на рис. 1.
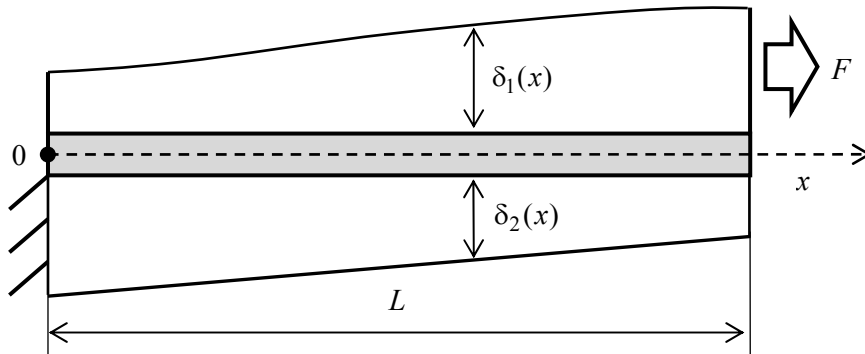
Рис. 1. Схема з'єднання внапуск

Товщина несучих шарів $\delta_1(x)$ і $\delta_2(x)$, товщина з'єднувального шару постійна за довжиною з'єднання і дорівнює δ_0. Довжина з'єднання L. Перший шар навантажено поздовжнім зусиллям F.

Вважаємо, що матеріали обох несучих шарів однакові. Оскільки за моделлю Фолькерсена [1, 4] несучі шари розглядаються як стрижні, які працюють тільки на розтягування–стискання, то із симетрії крайових умов для шарів випливає симетрія товщини несучих шарів, тобто $\delta_1(x) = \delta_2(L - x)$.

Розглянемо диференціальний елемент з'єднання, який показано на рис. 2.
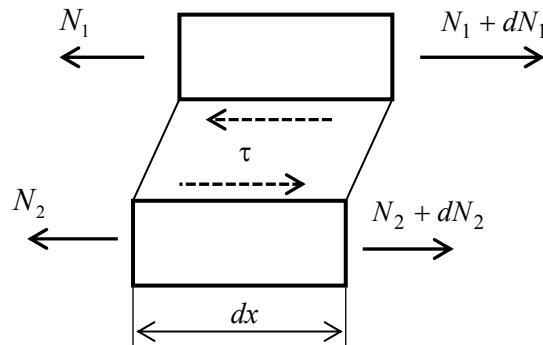
Рис. 2. Рівновага диференціального елемента з'єднання

У несучих шарах діють поздовжні зусилля N_1 і N_2; дотичні напруження у клейовому шарі позначимо через τ. Будемо вважати, що дотичні напруження постійні за товщиною клейового шару. Рівняння рівноваги несучих шарів мають вигляд

$$\frac{dN_1}{dx} - \tau = 0, \quad \frac{dN_2}{dx} + \tau = 0. \tag{1}$$

З іншого боку, $N_i = \delta_i \sigma_i = \delta_i E_i \dfrac{dU_i}{dx}$, де $i = 1,2$; σ_i — нормальні напруження у відповідному шарі; E_i — модуль пружності відповідного шару; U_i — поздовжні переміщення шару i.

Дотичні напруження у клейовому шарі пропорційні різниці поздовжніх переміщень несучих шарів [1]:

$$\tau = P(U_1 - U_2)\,, \tag{2}$$

де $P = \dfrac{G_0}{\delta_0}$ — жорсткість клейового шару на зсув; G_0 — модуль зсуву клею; δ_0 — товщина клейового шару.

Диференціюючи рівняння (2) та застосовуючи очевидне рівняння $N_1 + N_2 = F$, отримуємо рівняння

$$\frac{d^2 N_1}{dx^2} - P\left(\frac{1}{E_1 \delta_1(x)} + \frac{1}{E_1 \delta_1(x)}\right) N_1 = -\frac{PF}{E_2} \frac{1}{\delta_2(x)} \tag{3}$$

із крайовими умовами $N_1(0) = 0$ і $N_1(L) = F$.

Зауважимо, що у випадку постійної товщини несучих шарів рівняння (3) має відомий аналітичний розв'язок [1]. Але навіть за умов лінійного розподілу товщини за довжиною з'єднання це рівняння аналітичних розв'язків немає. Тому для знаходження напруженого стану з'єднань зі змінними параметрами застосовуються числові методи, зокрема метод скінченних різниць [9, 10].

Задачу оптимізації можна сформулювати таким чином: необхідно знайти такий розподіл товщини несучого шару $\delta_1(x)$ та довжину з'єднання L, за яких маса з'єднання (з точністю до постійного множника) досягає мінімуму

$$V = \int\limits_0^L \delta_1(x)dx \to \min$$

і виконується умова міцності з'єднання

$$\tau(x) = \frac{dN_1}{dx} \le \tau_{\max}\,.$$

На невідому товщину $\delta_1(x)$ також накладено умову $\delta_1(x) \ge \delta_{\min}$, яка є наслідком технології виробництва. Товщина другого несучого шару $\delta_2(x)$ знаходиться із $\delta_1(x)$ автоматично завдяки симетрії конструкції, і тому в задачу не входить. Дотичні напруження у клеї знаходимо з рівняння (1) як похідну від нормальних зусиль N_1, які, у свою чергу, залежать від невідомої товщини $\delta_1(x)$ через диференціальне рівняння (3).

ПОБУДОВА РОЗВ'ЯЗКУ

Для розв'язання задачі застосуємо дискретизацію області $x \in [0; L]$, для чого розіб'ємо її на $N+1$ вузлових точок x_k з нумерацією від 0 до N на кін-

цях відрізка $x = 0$ і $x = L$. Застосувавши п'ятиточковий скінченно-різницевий шаблон, рівняння (3) запишемо у вигляді

$$-n_{k-2}^{(1)} + 16n_{k-1}^{(1)} - \alpha_k n_k^{(1)} + 16n_{k+1}^{(1)} - n_{k+2}^{(1)} = -\frac{12h^2F}{E_2}\frac{P}{\delta_k^{(2)}} \,, \tag{4}$$

де $n_k^{(1)} = N^{(1)}(x_k)$; $h = \dfrac{L}{N}$ — шаг дискретизації; $\delta_k^{(i)} = \delta^{(i)}(x_k)$,

$\alpha_k = 12P_k h^2\left(\dfrac{1}{E_2\delta_k^{(2)}} + \dfrac{1}{E_1\delta_k^{(1)}}\right) + 30$; $k = 0, 1, ..., N$.

Із крайових умов випливає $n_0^{(1)} = 0$ і $n_N^{(1)} = F$, а також $n_{-1}^{(1)} = -n_1^{(1)}$, $n_{-2}^{(1)} = -n_2^{(1)}$, $n_{N-1}^{(1)} = -n_{N+1}^{(1)}$, $n_{N-2}^{(1)} = -n_{N+2}^{(1)}$. Це дозволяє звести задачу зі знаходження зусиль у вузлових точках за відомою товщиною несучих шарів $\delta_k^{(i)}$ до системи лінійних рівнянь.

Відповідно до рівняння (1) маємо

$$\tau_k = \frac{n_{k-2}^{(1)} - 8n_{k-1}^{(1)} + 8n_{k+1}^{(1)} - n_{k+2}^{(1)}}{12h} \,. \tag{5}$$

Для пошуку оптимальних значень товщини несучих шарів у вузлових точках застосовуємо метод генетичної оптимізації. Для цього можна взяти за шукані змінні $\delta_k^{(i)}$. Але, якщо товщина несучих шарів у сусідніх точках суттєво відрізняється (що може трапитися внаслідок мутацій), то розв'язок системи (4) та дотичні напруження у клейовому шарі (5) мають неправдоподібний характер (модель напруженого стану втрачає адекватність). Тому доцільно шукати $\delta_k^{(i)}$ серед функцій, які мають певну гладкість. Це випливає також з тих міркувань, що шуканий розподіл товщини за довжиною з'єднання найімовірніше буде описуватися гладкою функцією, або функцією лише з кількома кутовими точками. Тому запропоновано застосувати для опису форми несучих шарів ряд Фур'є за косинусами на інтервалі $\xi \in [0; 1]$:

$$y(\xi) = \frac{a_0}{2} + \sum_{n=1}^{M} a_n \cos \pi n\xi \,. \tag{6}$$

Якщо розбити інтервал $\xi \in [0; 1]$, як і інтервал $x \in [0; L]$, на $N+1$ вузлових точок ξ_k, то можна описати форму першого несучого шару за допомогою довжини L та товщини у вузлових точках $\delta_k^{(1)}$, які можна розрахувати за допомогою рівняння (6) як

$$\delta_k^{(1)} = y(\xi_k) = \frac{a_0}{2} + \sum_{n=1}^{M} a_n \cos \pi n\xi_k \,. \tag{7}$$

При цьому $\delta_k^{(2)} = \delta_{N-k}^{(1)}$.

Форма (7) зручна для знаходження маси несучого шару

$$V = \int_0^L \delta_1(x)dx = \frac{a_0}{2}L \,. \tag{8}$$

Щільність матеріалу у формулі (8) вважаємо рівною одиниці, оскільки конкретне значення щільності не впливає на результат оптимізації. Застосування саме косинусів у формулі (7) має перевагу над синусами завдяки тому, що у даному випадку на кінцях інтервалу, у точках $\xi = 0$ і $\xi = 1$, значення функції може відрізнятися від нуля і набувати будь-якого значення, на відміну від розкладання в ряд Фур'є за синусами.

Таким чином, невідомими параметрами, які необхідно знайти в результаті оптимізації, є довжина з'єднання L та набір коефіцієнтів $a_0, a_1,..., a_M$, які описують зміну товщини несучого шару вздовж з'єднання.

Для реалізації генетичного алгоритму необхідно створити фітнес-функцію, яка б давала змогу ранжувати різні розв'язки (особини) за якістю і наближеністю до оптимуму. Вочевидь ця функція має містити масу (площу) конструкції (8) та штрафи за перевищення напружень у клейовому шарі максимально припустимих значень $\tau_{\max}$, а також за те, що товщина несучого шару менша за мінімально припустиму $\delta_{\min}$. Таким чином, можемо, наприклад, фітнес-функцію записати у такій формі:

$$\Phi = L\frac{a_0}{2} + \begin{cases} Z_1 \dfrac{\max\limits_k (|\tau_k|)}{\tau_{\max}}, & \max\limits_k(|\tau_k|) > \tau_{\max}; \\ 0, & \max\limits_k(|\tau_k|) \le \tau_{\max}; \end{cases} + \begin{cases} Z_2 \dfrac{\delta_{\min}}{\min\limits_k(\delta_k)}, & \min\limits_k(\delta_k) < \delta_{\min}; \\ 0, & \min\limits_k(\delta_k) \ge \delta_{\min}. \end{cases} \quad (9)$$

Тут Z_1 і Z_2 — великі числа, які визначають величину штрафу за вихід розв'язку у неприпустиму область; $\max\limits_k(|\tau_k|)$ — максимальні значення абсолютних значень дотичних напружень у клейовому шарі за всіма вузловими точками у ділянці склеювання (5); $\min\limits_k(\delta_k)$ — мінімальна товщина несучого шару за всіма вузлами у ділянці склеювання.

Таким чином, якщо розв'язок (набір L та $a_0, a_1,..., a_M$) є припустимим, то фітнес-функція (9) дорівнює площі несучого шару (8). Але якщо напруження у клейовому шарі хоча б в одній вузловій точці перевищують припустимі, або (та) товщина несучого шару хоча б в одній вузловій точці менша за припустиму, то до площі додаються ще штрафні доданки. Таким чином, для розв'язання задачі оптимізації необхідно знайти такий набір L та $a_0, a_1,..., a_M$, який мінімізує функцію (9).

Для розв'язання поставленої задачі оптимізації застосуємо генетичний алгоритм [11, 12], який складається з таких етапів:

1. Побудова початкової популяції векторів $\vec{h}^{(j)}$, де $j = 1,..., N_g$ (N_g — кількість особин у популяції). Кожен вектор (особина) містить компоненти $L^{(j)}$ та $a_0^{(j)}, a_1^{(j)},..., a_M^{(j)}$.

2. За даними наборами параметрів обчислення відповідних значень $\Phi_j = \Phi(\vec{h}^{(j)})$ за формулою (9). Для цього необхідно за значеннями коефіцієнтів $a_0^{(j)}, a_1^{(j)},..., a_M^{(j)}$ і $L^{(j)}$ знайти товщини несучих шарів у вузлових точках та шаг дискретизації $h^{(j)} = L^{(j)} N^{-1}$, розв'язати пряму задачу зі знахо-

дження поздовжніх зусиль у першому несучому шарі (4), і знайдені результати застосувати для знаходження дотичних напружень у клейовому шарі (5).

3. *Селекція.* Ранжуємо наявні в популяції вектори $\vec{h}^{(j)}$ згідно з відповідними значеннями фітнес-функції Φ_j.

4. Відбір з популяції $2k$ (де $2k < N_g$) елементів $\vec{h}^{(j)}$. Імовірність потрапляння у вибірку може залежати або від номера в ранжованому списку або від значень Φ_j, Необхідно, щоб у вибірку потрапляли найкращі особини $\vec{h}^{(j)}$ з популяції, які мають менші значення фітнес-функції.

5. *Вибір батьків.* Розбиваємо $2k$ відібраних особин на пари і отримуємо k пар батьків.

6. *Схрещування.* Випадковим чином обираємо для кожної нової особини параметрів $L^{(j)}$ та $a_0^{(j)}, a_1^{(j)},...,a_M^{(j)}$ з обох батьківських особин. У результаті даної операції отримуємо популяцію k нових особин.

7. *Мутація.* У реалізованій версії алгоритму мутації відбуваються лише з деякою невеликою часткою компонентів векторів $\vec{h}^{(j)}$ особин, які виникли в результаті схрещування. Мутація полягає в зміні значень компонентів вектора на деяке незначне відхилення. Величина випадкового відхилення може описуватися, наприклад, розподілом Гауса з нульовим математичним сподіванням, а значення дисперсії бути пропорційною абсолютному значенню коефіцієнта a_n. Тобто більші за абсолютним значенням коефіцієнти Фур'є мутують з більшою дисперсією, а менші — з меншою. Якщо коефіцієнт a_n дорівнює нулю, то внаслідок мутацій середньоквадратичне відхилення набуває певного фіксованого значення σ_0.

8. Після внесення змін до генного коду нащадки повертаються в основну популяцію, яка збільшується з N_g до $N_g + k$ особин. Після цього особини знову ранжуються за значеннями фітнес-функції Φ_j і k гірших особин вилучаються з популяції.

9. *Перевірка критерію зупину.* Якщо критерію зупину (наприклад, задана кількість циклів розмноження K) не досягнуто — повернення до пункту 4.

МОДЕЛЬНА ЗАДАЧА

Розглянемо приклад застосування запропонованої методики для проєктування з'єднання. Беремо такі параметри $E_1 = E_2 = 70$ ГПа, $G_0 = 0,8$ ГПа, $\delta_0 = 0,1$ мм, мінімальна припустима товщина несучого шару $\delta_{\min} = 0,7$ мм, максимальні припустимі дотичні напруження у клейовому шарі $\tau_{\max} = 25$ МПа. З'єднання, навантажене зусиллям $F = 500$ кН/м. Нехай кількість особин у популяції $N_g = 50$. Для розв'язання задачі зі знаходження напруженого стану з'єднання обрано $N = 50$ точок дискретизації. Для опису функції зміни товщини несучих шарів за довжиною з'єднання застосовано $M = 30$

членів ряду Фур'є. У початковій популяції довжину з'єднання взято однаковою у всіх особин $L = 50$ мм, а розподіл товщини за довжиною з'єднання — лінійним, за яким товщина першого шару змінюється від випадкових значень товщини: від $0,7-3$ мм при $x = 0$ до 3 мм при $x = L$. Кількість особин, обираних для схрещування, — $2k = 16$. Імовірність мутації довжини з'єднання та мутації коефіцієнтів a_n беремо 0,2. Середньоквадратичне відхилення за мутацій довжини з'єднання $\sigma = 0,1$ мм коефіцієнт варіації за мутацій коефіцієнтів a_n становив $c_v = 0,005$ і фіксований додаток $\sigma_0 = 10^{-8}$. Кількість циклів $K = 25000$. Для більшої точності виконано 10 таких еволюційних моделювань, а отримані результати (довжину з'єднання і товщину несучих шарів у вузлових точках) осереднено. Знайдена оптимальна довжина з'єднання $L = 41,3$ мм. Результати достатньо стабільні — середньоквадратичне відхилення за 10 числовими експериментами становить 0,8 мм.

Графіки оптимальної товщини шарів зображено на рис. 3.
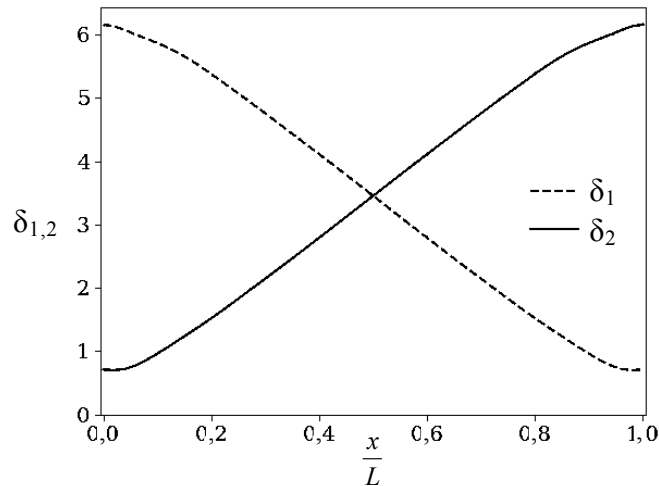
Рис. 3. Оптимальна товщина несучих шарів у мм

Відповідні дотичні напруження у клейовому шарі показано на рис. 4.
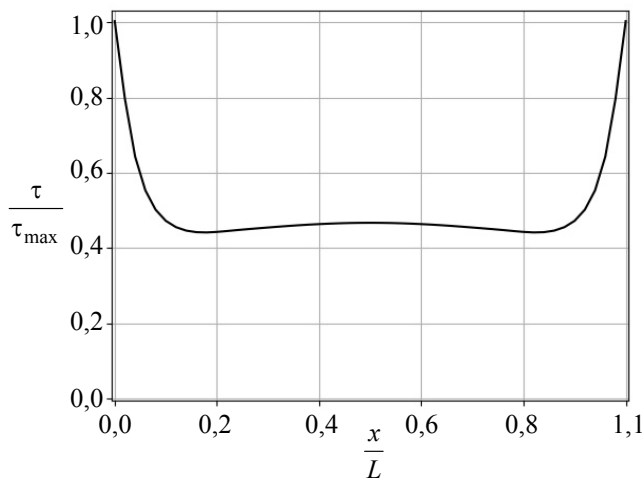
Рис. 4. Дотичні напруження у клейовому шарі

Як видно з графіків, у результаті оптимізації товщина навантажених кінців несучих шарів збільшилась більше ніж удвічі порівняно з відповідними значеннями у початковій популяції і перевищує 6 мм. Ненавантажені кінці мають мінімально припустиму за умовами задачі товщину 0,7 мм. На більшій частині довжини з'єднання товщина змінюється за лінійним законом. Дотичні напруження у клейовому шарі також на більшій частині довжини з'єднання постійні, хоча біля кінців з'єднання спостерігається концентрація напружень.

ВИСНОВКИ

1. Запропоновано методику оптимізації форми клейового з'єднання внапуск, яка забезпечує мінімум маси конструкції. Методика ґрунтується на спільному застосуванні класичних моделей механіки і методу скінченних різниць з генетичними алгоритмами оптимізації.

2. Завдяки гнучкості еволюційних алгоритмів оптимізації не складає труднощів розвинути запропонований підхід на більш точні математичні моделі з'єднань, які враховують вигин конструкції і напруження відриву у клейовому шарі, а також на інші задачі, які можуть бути зведені до одновимірних [3, 13, 14].

3. У фітнес-функцію може бути додані додаткові члени, які враховують міцність несучих шарів, обмеження на величину переміщень та більш складні критерії міцності клейового шару [2].

4. Перехід від неперервних змінних до дискретних дозволяє розв'язувати задачі оптимізації не тільки для клейових з'єднань внапуск, але і для багаторядних болтових з'єднань та комбінованих клеєболтових.

5. Подальший розвиток запропонованої методики розв'язання задач топологічної оптимізації, яка основана на поєднанні методу скінченних різниць та генетичних алгоритмів, можна також спрямувати на розв'язання двовимірних задач оптимізації шаруватих конструкцій [15–19].

Якщо умови задачі такі, що припустимий розв'язок не існує (наприклад, завелике навантаження F), то, призначивши у рівняння (9) $Z_2 > Z_1$ у результаті оптимізації отримуємо розв'язок, який можна реалізувати фізично ($\delta_k^{(1)} \geq \delta_{\min}$), але який лише мінімізує напруження у з'єднанні, утім не забезпечує виконання умови міцності з'єднання.

ЛІТЕРАТУРА

1. L.F.M.da Silva, P.J.C. das Neves, R.D. Adams, and J.K. Spelt, "Analytical models of adhesively bonded joints. Part I: Literature survey", *Int. Journal Adhes. & Adhesiv*, vol. 29, pp. 319–330, 2009. doi: 10.1016/j.ijadhadh.2008.06.005.

2. S.S.Kurennov, "Refined Mathematical Model of the Stress State of Adhesive Lap Joint: Experimental Determination of the Adhesive Layer Strength Criterion", *Strength Mater*, vol. 52, pp. 779–789, 2020. doi: 10.1007/s11223-020-00231-5.

3. S.S. Kurennov, K.P. Barakhov, and A.G. Poliakov, "Stressed State of the Axisymmetric Adhesive Joint of Two Cylindrical Shells under Axial Tension", *Materials Science Forum*, vol. 968, pp. 519–527, 2019. doi: 10.4028/www.scientific.net/ msf.968.519.

4. E.H. Wong and J. Liu, "Interface and interconnection stresses in electronic assemblies – A critical review of analytical solutions", *Microelectronics Reliability*, vol. 79, pp. 206–220, 2017. doi: 10.1016/j.microrel.2017.03.010.

5. J. Kupski and S. Teixeira de Freitas, "Design of adhesively bonded lap joints with laminated CFRP adherends: Review, challenges and new opportunities for aerospace structures", *Composite Structures*, vol. 268, 113923, 2021. doi:10.1016/j.compstruct.2021.113923.

6. R.H. Kaye and M. Heller, "Through-thickness shape optimisation of bonded repairs and lap joints", *Int. Journal of Adhesion & Adhesives*, vol. 22, pp. 7–21, 2002.

7. R.Q. Rodríguez, R. Picelli, P. Sollero, and R. Pavanello, "Structural shape optimization of bonded joints using the ESO method and a honeycomb-like mesh", *Journal of Adhesion Science and Technology*, vol. 28:14-15, pp. 1451–1466, 2014. doi: 10.1080/01694243.2012.698112.

8. H. Ejaz, A. Mubashar, I.A. Ashcroft, E. Uddin, and M. Khan, "Topology Optimisation of Adhesive Joints Using Non-Parametric Methods", *International Journal of Adhesion and Adhesives*, vol. 81, pp. 1–10, 2018. doi: 10.1016/j.ijadhadh.2017.11.00.

9. F. Thamm, "Stress Distribution in Lap Joints With Partially Thinned Adherends", *The Journal of Adhesion*, vol. 7:4, pp. 301–309, 1976. doi: 10.1080/00218467608075061.

10. Y.S. Karpov, "Jointing of high-loaded composite structural components. Part 2. Modeling of stress-strain state", *Strength Mater*, vol. 38, pp. 481–491, 2006. doi: 10.1007/s11223-006-0067-9.

11. V. Sineglazov, K. Riazanovskiy, and O. Chumachenko, "Multicriteria conditional optimization based on genetic algorithms", *System Research and Information Technologies*, no. 3, pp. 89–104. 2020. doi: 10.20535/SRIT.2308-8893.2020.3.07.

12. Y. Bodyanskiy, A. Shafronenko, and I. Pliss, "Credibilistic fuzzy clustering based on evolutionary method of crazy cats", *System Research and Information Technologies*, no. 3, pp. 110–119, 2021. doi: 10.20535/SRIT.2308-8893.2021.3.09.

13. S. Kurennov, N. Smetankina, V. Pavlikov, D. Dvoretskaya, and V. Radchenko, "Mathematical Model of the Stress State of the Antenna Radome Joint with the Load-Bearing Edging of the Skin Cutout", *International Conference on Reliable Systems Engineering (ICoRSE) - 2021. ICoRSE 2021. Lecture Notes in Networks and Systems*, vol. 305, 2022. doi: 10.1007/978-3-030-83368-8_28.

14. K. Barakhov, D. Dvoretska, and O. Poliakov, "One-Dimensional Axisymmetric Model of the Stress State of the Adhesive Joint", *Lecture Notes in Networks and Systems*, vol. 188, pp. 310–319, 2021. doi: 10.1007/978-3-030-66717-7_26.

15. A. Kondratiev and V. Gaidachuk, "Weight-based optimization of sandwich shelled composite structures with a honeycomb filler", *Eastern-European Journal of Enterprise Technologies*, vol. 1(1), pp. 24–33, 2019. doi: 10.15587/1729-4061.2019.15492.

16. L. Tong and X. Sun, "Shape optimization of bonded patch to cylindrical shell structures", *International journal for numerical methods in engineering*, vol. 58, pp. 793–820, 2003. doi: 10.1002/nme.802.

17. C.H. Wang and A.J. Gunnion, "Optimum shapes of scarf repairs", *Composites Part A: Applied Science and Manufacturing*, vol. 40(9), pp. 1407–1418, 2009. doi: 10.1016/j.compositesa.2009.02.009.

18. S.S. Kurennov, O.G. Polyakov, and K.P. Barakhov, "Two-Dimensional Stressed State of an Adhesive Joint. Nonclassical Problem", *Journal of Mathematical Sciences*, vol. 254(1), pp. 156–163, 2021. doi: 10.1007/s10958-021-05295-5.

19. S.S. Kurennov, "Determining Stresses in an Adhesive Joint with a Longitudinal Unadhered Region Using a Simplified Two-Dimensional Theory", *Journal of Applied Mechanics and Technical Physics*, vol. 60(4), pp. 740–747, 2019. doi: 10.1134/s0021894419040199.

INFORMATION ON THE ARTICLE

Sergey S. Kurennov, ORCID: 0000-0002-3835-3288, National Aerospace University "Kharkiv Aviation Institute", Ukraine, e-mail: kurennov.ss@gmail.com

TOPOLOGICAL OPTIMIZATION OF A SYMMETRIC SINGLE-LAP ADHESIVE JOINT / S.S. Kurennov

Abstract. The profile optimization problem for layers overlapped with an interjacent adhesive layer is considered. The joint is considered according to the Volkersen model, according to which the base layers are considered as rods that act only in stress-strain, and the adhesive layer acts only in shear. The aim of the optimization is to design a joint structure of minimum mass under the strength restrictions for the adhesive layer and the minimally allowable base layer thickness. The base layers profile is described by a Fourier series expansion. The direct stress state problem for the joint of variable thickness rods is solved by the finite difference method. The optimization problem is reduced to the problem of determining Fourier series coefficients and the joint length. A genetic optimization algorithm was used. The model problem is solved.

Keywords: three layer construction, topological optimization, genetic algorithm.

HYBRID CONVOLUTION NETWORK FOR MEDICAL IMAGES PROCESSING AND BREAST CANCER DETECTION

Yu. ZAYCHENKO, M. NADERAN, G. HAMIDOV

Abstract. In this paper, the breast cancer detection problem using convolutional neural networks (CNN) is considered. The review of known works in this field is presented and analysed. Most of them rely only on feature extraction after the convolutions and use the precision of classification of malignant tumors as the main criterion. However, because of the huge number of parameters in the models, the time of computation is very large. A new structure of CNN is developed — a hybrid convolutional network consisting of convolutional encoder for features extraction and reduction of the complexity of the model and CNN for classification of tumors. As a result, it prevented overfitting the model and reduced training time. Further, while evaluating the performance of the convolutional model, it was suggested to consider recall and precision criteria instead of only accuracy like other works. The investigations of the suggested hybrid CNN were performed and compared with known results. After experiments, it was established the proposed hybrid convolutional network has shown high performance with sensitivity, precision, and accuracy of 93,50%, 91,60%, and 93%, respectively, and requires much less training time in the problem of breast cancer detection as compared with known works.

Keywords: breast cancer detection, hybrid convolutional network, encoder, classification sensitivity, dimensionality reduction.

INTRODUCTION

Breast cancer is a very common cancer among women between the ages of 35 and 55 [1]. Diagnosing breast cancer is frequently discussed as a classification problem within neural networks. Detecting and diagnosing breast cancer in early stages is critical in saving women's lives. Detecting this cancer in its early stages can help prevent the spread of cancer to other organs/tissues allowing doctors to help the patient before it is too late. Early detection requires methods that are systematic and dependable, allowing healthcare professionals to accurately distinguish between benign and malignant tumors [2]. For these reasons, the exact detection and classification of breast tumors is extremely important for public health and to the lives of cancer patients [3].

There are four types of breast cancer: in situ, invasive ductal carcinoma, inflammatory breast cancer, and metastatic cancer [4]. Breast cancer detection is important in developing countries, where the number of patients is dramatically

higher. Moreover, detecting breast cancer is a challenging and time-consuming task requiring doctors to manually label scans. Although, there are supervised and unsupervised machine learning algorithms that assist doctors. According to the World Health Organization (WHO) [5], a mammography scan is more efficient and cost-effective for breast cancer detection. Although it is more expensive than other medical images, the quality of the image is superior to other medical scans and therefore mammography scans, from the BreakHis dataset [6] have been used in this work.

The main goal of this work is the development and investigation of hybrid convolutional network to increase the sensitivity and to reduce the complexity of the model for breast cancer detection. A convolutional autoencoder was proposed to extremely decrease the computation time.

REVIEW OF PREVIOUS WORKS

There are a lot of studies that consider breast cancer detection using CNNs. However, most of them rely on the accuracy in their experiments, but accuracy in any cancer detection is not the only valid factor that should be considered [7]. In these tasks, the sensitivity of models should be considered to understand how many times the model misclassified cancer. Authors in [8] proposed a state-of-the-art convolutional neural network (DenseNet) for breast cancer detection using Breast Cancer Histology images (BACH) with an accuracy of 85,6%. The misclassification rate for cancer class was 14,4% on average. In their work, the sensitivity (on average for 4 classes) of ResNet 50 was compared with their proposed CNN at 76% and 79% respectively.

Compared with pre-existing CNN models (VGG-16, VGG19, Xception, Resnet, Inception) with 80% accuracy in multiclass classification, authors in [9] proposed a model where the accuracy was 83,97% on average for two classes (Benign and Malignant). The proposed model was a combination of Inception and Resnet using the BreakHis data set, which contains 7909 mammography scans with four magnification factors (40X, 100X, 200X and 400X).

In [10], it was stated that because of the architecture of DenseNet, in which all layers are fully connected to every previous layer, and with a short connection between those layers near the input and output, the model could be trained more efficiently and accurately.

In [11] a DenseNet network authors proposed model which achieved high processing performances with 95,4% of accuracy. The Authors claim they first used weights from Imagenet and fine-tuned the model to train DenseNet. All convolutional parts of the network were frozen but the fully connected layer was trainable. Authors in [12] used an atrous DenseNet that achieves multi-scale feature extraction by integrating the atrous convolutions to the dense block. The authors in [12] compared two datasets, BACH and CCG, in which the average class accuracy for the proposed model was 82,50% and 87,05% respectively for each dataset.

A new model of convolutional neural network was proposed in [13], where the authors used 400 images with 40x magnification for training data and 200 for validation data. In [13] three different ConvNet architectures were evaluated: 1) a 3-layer ConvNet architecture, 2) a 4-layer ConvNet architecture, and 3) a deeper

6-layer ConvNet architecture. The 3-layer ConvNet included one convolution, one pooling and one fully connected layer. The 4-layer had two convolutional and two pooling layers and the last layer was fully connected. The 6-layer ConvNet architecture comprises four convolutional and pooling layers with 16 units, a fully connected layer. According to the results in [13], deep architectures shows better result with 1,06% accuracy.

Authors in [14] proposed semi-supervised learning (SSL) using convolutional neural networks. The accuracy of the developed model was 82,43% and the area under the curve (AUC) observed in their study was 88,18%. There were 1874 pairs of mammogram images used during the experiments. Moreover, the authors developed three data weighing equations using exponential function, Gaussian function, and Laplacian function. Based on results [14], comparing two other weighting equation, the exponential function has shown better results with 82,43%, 81,00% and 72,26% for labelling accuracy, sensitivity and specificity respectively.

In [16] authors applied Principal component analysis (PCA) for Hybrid Fuzzy CNN Network. The idea of using PCA was to reduce the number of extracted features. In their work, the authors proposed a model where CNN VGG 16 was used for feature extraction and FNN NEFClass was used for image classification.

DATASET

The open source BreakHis dataset was used during the experiment. The dataset includes two classes benign and malignant tumors. The dataset is also separated into four magnification zooms 40X, 100X, 200X and 400X; 5000 images were used for training and 350 images were used for testing. Fig. 1 illustrates some input images that were used for training the model. Fig. 1, *a–d* belong to the benign category and Fig. 1, *e–h* belong to the malignant category.
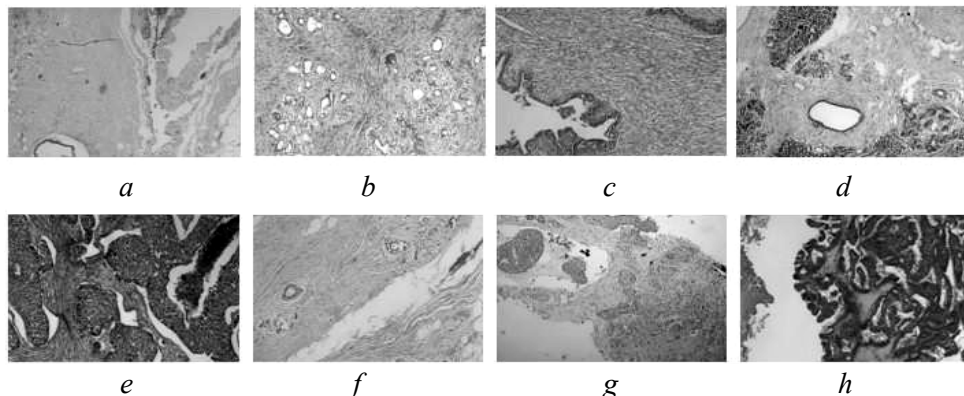
Fig. 1. Sample of input images: *a* — adenosis; *b* — fibroadenoma; *c* — phyllodes_tumor; *d* — Tubular_adenoma; *e* — Ductal_carcioma; *f* —Lobular_ carcioma; *g* — Muconous carcinoma; *h* — Papillary carcioma

ARCHITECTURE AND TRAINING OF CONVOLUTIONAL AUTOENCODER

The aim of the autoencoder is to learn a compressed distributed representation for the given data typically for the purpose of dimensionality reduction. On the other

hand, there is a principal component analysis (PCA) for the same task (reduction dimensionality). However, there are some advantages [17] of using autoencoder like: 1) autoencoder can represent both linear and non-linear transformations in encoding but PCA can perform only linear transformations; 2) it could be more efficient in terms of model parameters to learn several layers with an autoencoder rather than one massive transformation with PCA; 3) it gives a representation as the output of each layer and having multiple representation of different dimensions is more practical.

One of the reasons a convolutional autoencoder was used during experiments is because it is very challenging to find significantly sized datasets with labels and autoencoder is an unsupervised model that does not require the dataset to be labelled. Another advantage of the autoencoder is that it makes the model smaller. Respectively, the model would have less parameters and as a result, the time of computation and training will drastically decrease. For example, in Dense Net there are a total of 58,420,802 parameters and 7,037,504 of them are not trainable. However, in the proposed convolutional autoencoder there are 2,940,865 parameters and only 3,840 of them are non-trainable.

Fig. 2 illustrates the architecture of an autoencoder. In the autoencoder there are layers between the input and output and the sizes of these layers are smaller than the input layer. For example, the input vector has a dimensionality of N which means that the output will also have a dimensionality of N. The input goes through a layer of size P, where the value of P is less than N. The autoencoder receives unlabelled input which is then encoded to reconstruct input. The important part of autoencoder is the Bottleneck approach for representation learning.
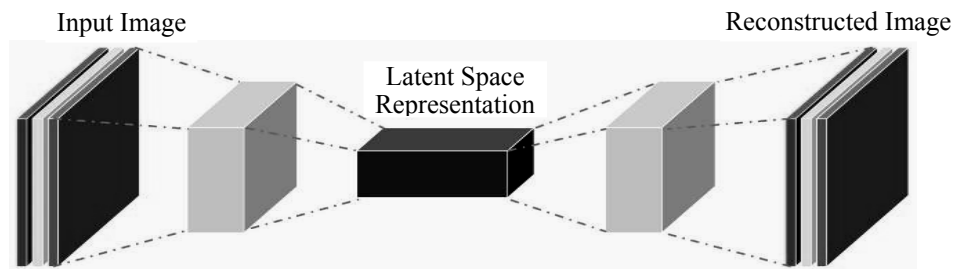
Fig. 2. The architecture of an autoencoder

In the current work, several architectures of convolutional autoencoder were used during the experiment. The convolutional autoencoder was modified with 18 encoding layers and 14 decoding layers. There were eight convolutional and two max pooling layers in encoder. In decoder there were six convolutional and two upsampling layers. Batch normalization was used between each convolutional layer. The proposed convolutional autoencoder was trained in a way, that the model would extract informative features (Codes) during the encoding process, and the decoder could then reconstruct the original input image of the encoder. The model could recreate the original image, even though some noises were applied to the scans. A comparison of the input images and reconstructed images is shown in Fig. 3. After creating a successful autoencoder-model, the output of the encoder will be used with a fully connected layer to create a full model (Convolutional Autoencoder).
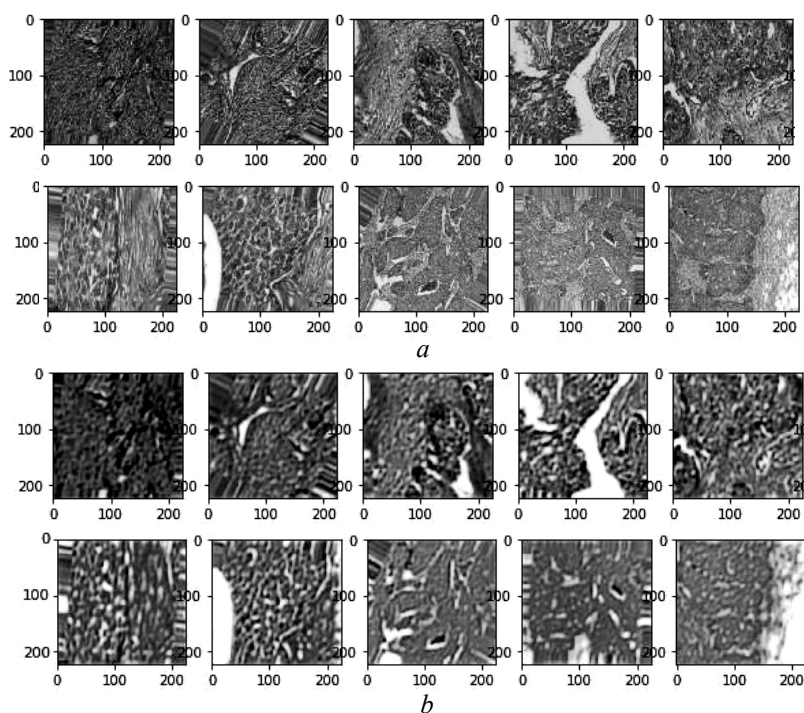
Fig. 3. On scans (*a*) noises were added, and scans (*b*) are reconstructed to original test data

The accuracy of the recreated test data for convolutional autoencoder was 79,38%.

EXPERIMENTAL INVESTIGATIONS AND ANALYSIS

For training an autoencoder there are four parameters that it is needed to be set. The first one is code size. The code size represents the number of nodes in the middle layer and smaller size results in more compression. The second parameter is the number of layers and the autoencoder could be as deep as we want it to be. Another parameter is the loss function. The last parameter is the number of nodes per layer. The number of nodes per layer decreases with each subsequent layer of the encoder and increases back in the decoder. Also, the decoder is symmetric to the encoder in terms of layer structure.

The Adam optimizer with learning rate 0,001 was used for training Dense-Net whereas, in convolutional autoencoder the RMSprop ($lr = 0,001$) has shown better results.

All scans were pre-processed, before being used to train the model by resizing, normalizing and dimensionality reduction methods. In this paper, all experiments were developed using Jupyter Labs, Tensorflow 2 and Python 3. The programs were implemented on a virtual machine with an NVIDIA Tesla GPU and eight Intel CPUs.

Fig. 4, *a* and *b* illustrate how the loss for training and validation data was changed. Multiple tests were done using different numbers of epochs. It was found that 250 epochs provided better results compared to larger number of

epochs like 500. The more epochs, the more chance the model will have overfitting. According to Fig. 6, it is better to use learning rate 0,001 for the current model. However, this parameter could be different for other models.
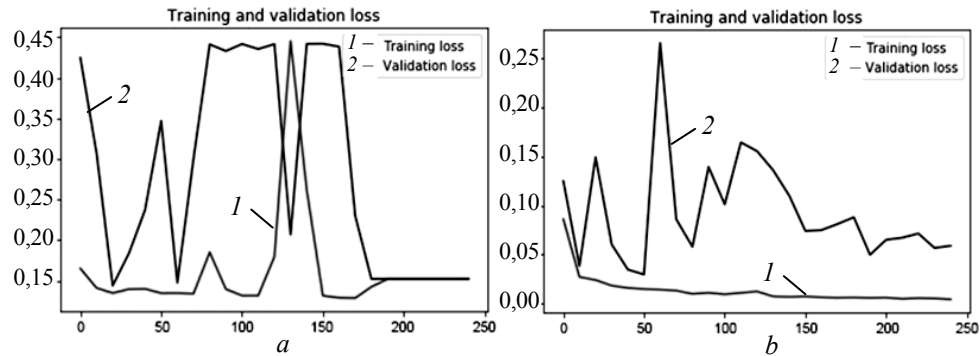
Fig. 4. Loss comparison for training and validation data with learning rate 0,01 and 0,001 on (*a*) and (*b*) respectively

In previous work [17], a modified Inception V3 was proposed for breast cancer detection. In this work a hybrid convolutional network was proposed using a fine-tuned DenseNet121 and modified convolutional autoencoder. In the proposed hybrid convolutional network, the convolutional autoencoder was used as a feature extraction and the DenseNet was used as a classifier. Fig. 5 demonstrates the architecture of the proposed model.
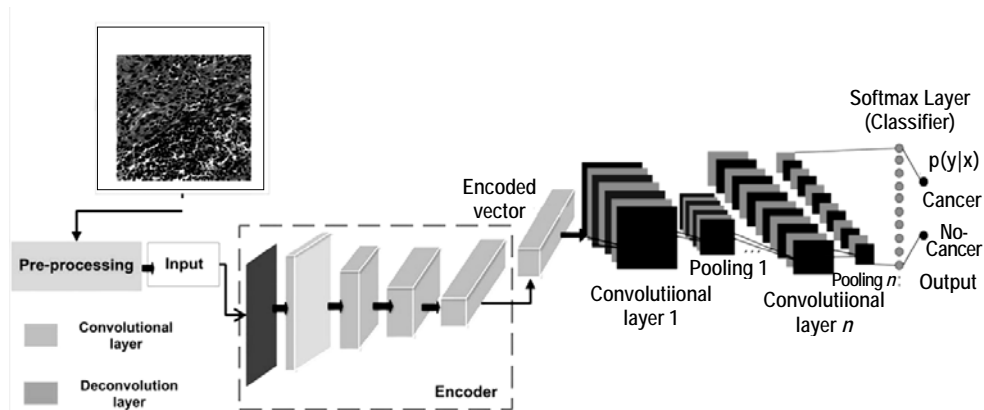
Fig. 5. Modified architecture of hybrid convolutional network

Table 1 shows the result of the proposed model for each class.

T a b l e 1. The results of breast cancer recognition using a convolutional autoencoder

Class	Precision, %	Recall, %	F1-Score, %	Support
Class 0	90	95	93	747
Class 1	95	90	92	1626
Weighted ayg	93,2	93,5	93,3	2373

The experiment proves that it is not necessary to have large data sets to train a convolutional autoencoder from scratch. Comparatively, training the DenseNet

and Inception-v3 convolutional networks from scratch, require a large number of input images. Thus, the convolutional autoencoder has a simplified model, and training time is significantly reduced compared to DenseNet or Inception-v3. Fig. 6 illustrates the performance of the model with different number of input data as training data.

Also, the appearance and image quality of the input data significantly affect the performance of the model. BreakHis and Breast histology datasets were used for comparison. In the table 2 shows the performance of the model with different input data.
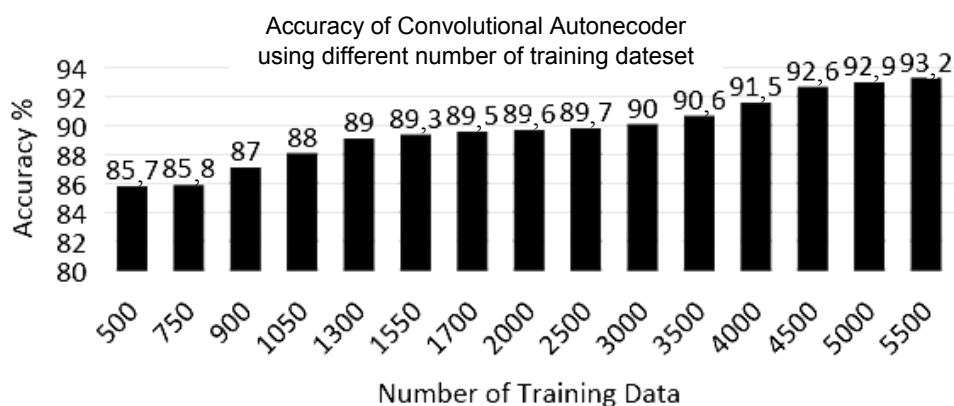
Fig. 6. Accuracy of proposed model for different size of data sets

T a b l e 2 . Comparison of the quality of the model of the convolutional autoencoder for different datasets

Factors/Datasets	BreakHis, %	Breast histology, %
Accuracy	93	90,5
Precision	93,2	91,6
Recall	93,5	92,40
F1-Score	93,3	92

Table 3 shows three different deep convolutional networks that were used for the current task. According to table 3, the hybrid convolutional network has shown better results as compared to other methods, the training time was lower. There are plenty of studies for breast cancer detection using deep learning, and most of them rely only on accuracy. However, sensitivity (recall) is the most important factor that should be kept in mind while training deep neural networks. With recall it is possible to assess whether the network predicts cancer as a cancer, so in the current work both recall and precision of the model were considered.

T a b l e 3 . Result of comparison different models for detecting breast

CNN models	Factors			
	Precision, %	Recall, %	F1 score, %	Training Time
Modified Inception V3 [17]	66,66	85,70	74,99	27h
DenseNet 121	75,73	86,1	80,84	24h
Hybrid convolutional neural network	91,60	93,50	92,5	13h

Based on the data from table 3 and table 1, it can be concluded that the sensitivity of the model (recall) when using a convolutional autoencoder gives a better result compared to Inception-v3. It should also be noted that only 5% of class 0 (cancer), was misclassified.

CONCLUSION

1. In this paper, a hybrid convolutional neural network was developed, and investigated in the problem of breast cancer detection. In the proposed hybrid convolutional network the convolutional autoencoder was used as a feature extraction while CNN DenseNet was used as a classifier.

2. In the experiments it was determined that sensitivity, precision and accuracy of the proposed model were 93,50%, 91,60% and 93% respectively. The comparison with known CNN was performed which has shown the proposed hybrid CNN has higher sensitivity (recall) than known CNN models.

3. Besides the hybrid CNN has fewer parameters compared to DenseNet, as a result, the model is less complex and prevents overfitting. Moreover, the used autoencoder is an unsupervised model and does not require labeled data.

4. In addition, during the experiments it was established that hybrid CNN requires less training time as compared with known CNN models.

REFERENCES

1. K. Polat et al., "A new classification method for breast cancer diagnosis: feature selection artificial immune recognition system (FS-AIRS)", *Advances in Natural Computation*, pp. 830–838, 2005.
2. M.R. Senapati et al., "Local linear wavelet neural network for breast cancer recognition", *Neural Computing and Applications*, 22 (1), pp. 125–131, 2013.
3. A. Marcano-Cedeno, J. Quintanilla Dominguez, and D. Andina, "Breast cancer classification applying the artificial metaplasticity algorithm", *Neurocomputing*, 74 (8), pp. 1243–1250, 2011.
4. *Diagnostic Mammogram*. Available: https://www.nationalbreastcancer.org/ diagnosticmammogram.
5. *Breast cancer: prevention andcontrol*. Available: https://www.who.int/news-room/ fact-sheets/ detail/breast-cancer.
6. *Breast Cancer Histopathological Database (BreakHis)*. Available: https://web.inf. ufpr.br/vri/databases/breast-cancer-histopathological-database-breakhis/.
7. *Inverse Relationship Between Precisionand Recall*. Available: https://datascience. stackexchange.com/questions/49117/inverserelationship-between-precision-and-recall
8. G. Arestaa et al., "BACH: grand challenge on breast cancer histology images", *Medical Image Analysis*, ELSEVIER 2019.
9. *BreakHist-Dataset-Image-Classification*. Available: https://github.com/Anki0909/ BreakHist-Dataset-Image-Classification
10. Gao Huang, Zhuang Liu, and Kilian Q. Weinberger, "Densely Connected Convolutional Networks", *arXiv:1608.06993v3*, 2018.
11. Majid Nawaz, Adel A. Sewissy, and Taysir Hassan A. Soliman, "MultiClass Breast Cancer Classification using Deep Learning Convolutional Neural Network", *International Journal of Advanced Computer Science and Applications*, vol. 9, no. 6, 2018.
12. Yuexiang Li, Xinpeng Xie, Linlin Shen, and Shaoxiong Liu, "Reversed Active Learning based Atrous DenseNet for Pathological Image Classification", *arXiv:1807.02420*, 2018.

13. A. Cruz-Roa et al., "Accurate and reproducible invasive breast cancer detection in whole-slide images: A Deep Learning approach for quantifying tumor extent", *Sci. Rep.*, 7, 46450, 2017. doi: 10.1038/srep46450.

14. Wenqing Sun, Tzu Liang (Bill) Tseng, Jianying Zhang, and Wei Qian (2016). "Enhancing deep convolutional neural network scheme for breast cancer diagnosis with unlabeled data", *Computerized Medical Imaging and Graphics*. doi: 10.1016/j.compmedimag.2016.07.004

15. *Comparison PCA and Autoencoder*. Available: https://towardsdatascience.com/ dimensionality-reduction-pca-versus-autoencoders-338fcaf3297d

16. Y. Zaychenko and G. Hamidov, "Hybrid Fuzzy CNN Network in the Problem of Medical Images Classification and Diagnostics", in *Advances in Natural Computation, Fuzzy Systems and Knowledge Discovery, ICNC-FSKD 2019, Advances in Intelligent Systems and Computing*, vol. 1074. Springer, Cham, 2020.

17. M. Naderan, Yu. Zaychenko, and A. Napoli, "Using convolutional neural networks for breast cancer diagnosing", *System Research and Information Technologies*, no. 4, pp. 85–93, 2019.

18. M. Naderan, "Review methods for breast cancer detection using artificial intelligence and deep learning methods", *System Research & Information Technologies*, no. 1, pp. 98–101, 2021.

INFORMATION ON THE ARTICLE

Yuriy P. Zaychenko, ORCID: 0000-0001-9662-3269, Institute for Applied System Analysis of the National Technical University of Ukraine "Igor Sikorsky Kyiv Polytechnic Institute", Ukraine, e-mail:zaychenkoyuri@ukr.net

Maryam Naderan, Institute for Applied System Analysis of the National Technical University of Ukraine "Igor Sikorsky Kyiv Polytechnic Institute", Ukraine, e-mail: ma.nederan@gmail.com

Galib Hamidov, "Azerishiq", Azerbaijan, e-mail: galib.hamidov@gmail.com

ГІБРИДНА ЗГОРТКОВА МЕРЕЖА ДЛЯ ОБРОБЛЕННЯ МЕДИЧНИХ ЗОБРАЖЕНЬ ТА ВИЯВЛЕННЯ РАКУ МОЛОЧНОЇ ЗАЛОЗИ / Ю.П. Зайченко, М. Надеран, Г. Гамідов

Анотація. Розглянуто проблему виявлення раку молочної залози з використанням згорткових нейронних мереж (ЗНМ). Наведено огляд та аналіз праць з цієї галузі. Зазначається, що більшість з них засновано на вилученні ознак у результаті згортки з використанням як основного критерію точність класифікації пухлин. Унаслідок великого обсягу параметрів, що оптимізуються, час навчання дуже тривалий. Розроблено нову структуру ЗНМ — гібридну мережу, що складається з енкодера для отримання первинних ознак і скорочення розмірності моделі та декількох шарів згортки для класифікації пухлин. Це дало змогу запобігти перенавченню мережі та скоротити час навчання. Для оцінювання якості класифікації запропоновано використовувати критерій чутливості (до злоякісних пухлин) разом із критерієм точності на відміну від відомих праць. Це дозволило скоротити відсоток пропуску злоякісних пухлин. Проведено експериментальні дослідження розробленої гібридної згорткової мережі та порівняно з іншими працями. Установлено, що гібридна ЗНМ має високі показники якості класифікації, а також чутливість до ракових пухлин і точність класифікації 93,50%, 91,60% відповідно і потребує значно менше часу на навчання класифікації пухлин молочної залози порівняно з відомими працями.

Ключові слова: виявлення раку молочної залози, гібридна згорткова мережа, кодер, чутливість класифікації, зменшення розмірності.

SIMULATIONS OF NEW COVID-19 PANDEMIC WAVES
IN UKRAINE AND IN THE WORLD
BY GENERALIZED SIR MODEL

I. NESTERUK

Abstract. New waves of the COVID-19 pandemic in Ukraine, which began in the summer of 2021, and after holidays in the middle of October 2021, were characterized by the almost exponential growth of smoothed daily numbers of new cases. This is a matter of great concern and the need to immediately predict the epidemic dynamics in order to assess the maximum possible values of new cases, the risk of infection, and the number of deaths. The generalized SIR-model and corresponding parameter identification procedure were used to simulate and predict the dynamics of two new epidemic waves in Ukraine and one worldwide. Results of calculations show that new cases in Ukraine will not stop appearing before November 2022. The pandemic can continue for another ten years if the global situation with vaccination, testing, and treatment does not change.

Keywords: COVID-19 pandemic, epidemic waves, epidemic dynamics in Ukraine, global pandemic dynamic, mathematical modeling of infection diseases, SIR model, parameter identification, statistical methods..

INTRODUCTION

The COVID-19 pandemic dynamics in Ukraine was discussed in [1–14]. To predict the first wave of the pandemic, the classical SIR model [15–17] and the statistics-based method of its parameter identification [18] were used. To simulate new epidemic waves, a numerical method of their detection [4, 19], a generalized SIR-model [20], and a corresponding parameter identification procedure [21] were developed. In particular, eleven epidemic waves were simulated for Ukraine [5, 8–11] and five pandemic waves for the whole world [5].

The calculations of the 11th pandemic wave (based on the accumulated numbers cases reported by Ukrainian national statistics [22, 23] in the period May 23 – June 5, 2021) predicted the end of this wave on August 25, 2021 with the number of cases 2,226,797 (see [11]). As of August 25, 2021 the real number of cases accumulated in Ukraine was 2,278,171 (see Table 1). It means that the predicted saturation level was exceeded only 2,26% (after 81 days of observation). The obtained high accuracy of the method allows us to hope for a fairly accurate forecast for next pandemic waves in Ukraine (12th and 13th) and in the whole world (6th), to which this study is devoted. Some results concerning the 12th epidemic wave in Ukraine are already available in [13].

DATA

We will use the data set regarding the accumulated numbers of laboratory-confirmed COVID-19 cases and deaths in Ukraine from national sources [22, 23].

The corresponding numbers V_j, d_j and moments of time t_j (measured in days) are shown in Table 1 for the period of July to November 2021. The values V_j, corresponding to the previous moments of time, can be found in [4, 8–10]. The period T_{c11}: May 23 – June 5, 2021 has been used in [10] for SIR simulations of the eleventh epidemic wave in Ukraine. Here we use the datasets, corresponding to the period T_{c12}: September 29 – October 12, 2021 to simulate the 12th wave and the period T_{c13}: October 28 – November 10, 2021 for the 13th wave. Other V_j and t_j values will be used to control the accuracy of predictions.

T a b l e 1. Cumulative numbers of laboratory-confirmed COVID-19 cases and deaths in Ukraine in the summer and autumn of 2021 according to the national statistics [22, 23]

Day in corresponding month of 2021	Number of cases in July, V_j	Number of cases in August, V_j	Number of cases in September, V_j	Number of cases in October, V_j	Number of cases in November, V_j	Number of deaths in October, d_j	Number of deaths in November, d_j
1	2236497	2253534	2290848	2447222	2955693	56649	68727
2	2237202	2254361	2293541	2455189	2979086	56775	69447
3	2237579	2255345	2296155	2460010	3006463	56889	70146
4	2237823	2256397	2297534	2469856	3032951	57206	70842
5	2238364	2257478	2298307	2482518	3058014	57526	71635
6	2238974	2258532	2300504	2497643	3075433	57840	72084
7	2239591	2259151	2303276	2514005	3088501	58081	72557
8	2240246	2259451	2306939	2529913	3107489	58331	73390
9	2240753	2260232	2310554	2541257	3130772	58463	74206
10	2241043	2261354	2314423	2550089	3155519	58700	74857
11	2241217	2262601	2316619	2562085	3179577	59052	75601
12	2241698	2263864	2317824	2578394	3203149	59523	76302
13	2242245	2265217	2321156	2597275	3217639	59935	76705
14	2242868	2265912	2325796	2610899	3228441	60137	77147
15	2243605	2266329	2331540	2623882	3244749	60414	78085
16	2244196	2267219	2338164	2635170	3263417	60633	78754
17	2244495	2268666	2344398	2644694	3284008	60810	79506
18	2244677	2270226	2348381	2660273	–	61348	–
19	2245275	2271826	2350646	2679185	–	61843	–
20	2245930	2273558	2355805	2701600	–	62389	–
21	2246656	2274561	2362559	2725385	–	63003	–
22	2247419	2275171	2370425	2748614	–	63486	–
23	2248164	2275863	2379483	2769405	–	63872	–
24	2248450	2276590	2387750	2784039	–	64202	–
25	2248663	2278171	2392397	2803159	–	64936	–
26	2249344	2280203	2395404	2825733	–	65628	–
27	2250061	2282285	2401956	2851804	–	66204	–
28	2250907	2284191	2411622	2878674	–	66852	–
29	2251869	2284940	2423379	2904872	–	67393	–
30	2252785	2286296	2435413	2922302	–	67729	–
31	2253269	2288371	–	2936238	–	68027	–

To estimate the mortality rate in Ukraine (ratio of accumulated number of deaths d_j to accumulated number of cases V_j), let us take figures d_j corresponding different days: 52,286 (June 26, 2021); 52,665 (July 13, 2021); 52,981 (August 2, 2021); 53,789 (August 30, 2021); 54,550 (September 15, 2021); 57,526 (October 5, 2021); 59,052 (October 11, 2021), [22, 23]. Taking corresponding V_j values we can calculate the mortality rates $m_i = d_j * 1000/V_j$ (per thousand of cases) for the listed days: 23,40; 23,49; 23,50; 23,52; 23,40; 23,17; 23,05. Thus, the mortality rate is rather stable (its variation during June to October 2021 is only 0,47). We will use the average value $m = 23,36$ to predict the number of deaths in Ukraine during the new 12th and 13th pandemic waves.

We will use the data set regarding the accumulated numbers of laboratory-confirmed COVID-19 cases in the whole world from the COVID-19 Data Repository by the Center for Systems Science and Engineering (CSSE) at Johns Hopkins University (JHU) [24]. The numbers V_j and moments of time t_j (measured in days) corresponding to the version of JHU data available on November 18, 2021 are shown in Table 2 for the period of May to November 2021. The period T_{c6}: September 29 – October 12, 2021 will be used for SIR simulations of the sixth pandemic wave in the whole world. Other V_j and t_j values will be used to control the accuracy of predictions.

T a b l e 2. Cumulative numbers of laboratory-confirmed COVID-19 cases in the whole world in the summer and autumn of 2021 according to the JHU datasets [24]

Day in corresponding month of 2021	Number of casesin May, V_j	Number of cases in June, V_j	Number of cases in July, V_j	Number of cases in August, V_j	Number of cases in September V_j	Number of cases in October, V_j	Number of cases in November, V_j
1	152276590	171272898	182726434	198444595	218595466	234356127	247171157
2	152951570	171758996	183167695	199022653	219272430	234701054	247599693
3	153630578	172248309	183544382	199660021	219990395	235008467	248117984
4	154438256	172667912	183872893	200335410	220474967	235452671	248643609
5	155280720	173067049	184242453	201024324	220914961	235872200	249157004
6	156150815	173390272	184695883	201846052	221355380	236384642	249569269
7	156983904	173710775	185159327	202397022	222080699	236816997	249914970
8	157770675	174077854	185639668	202838586	222712220	237290992	250391584
9	158412936	174497701	186147179	203492405	223349675	237622759	250871092
10	159031606	174947362	186574219	204141032	223983497	237937441	251442851
11	159770619	175368288	186944737	204869528	224439880	238319075	251956201
12	160530984	175741060	187381421	205580294	224808018	238751674	252542169
13	161256546	176044679	187901397	206385979	225409164	239214456	252974728
14	161974329	176352002	188442853	206919889	225960250	239658510	253318827
15	162603295	176723278	189014972	207383880	226527940	240115116	253860137
16	163152581	177121944	189613250	208062469	227104401	240449869	254382438
17	163691215	177514452	190087192	208745487	227697551	240764659	–
18	164313944	177921297	190518240	209473681	228234315	241178794	–
19	164986139	178270695	191014762	210189272	228594983	241619751	–
20	165265741	178573040	191544693	210979353	229128857	242090131	–
21	165892200	178866758	192103503	211519485	229597662	242546214	–
22	166471396	179238527	192667887	211965954	230135505	243030920	–
23	166948481	179676298	193357870	212670361	230646900	243390258	–

Continued Table 2

Day in corresponding month of 2021	Number of cases in May, V_j	Number of cases in June, V_j	Number of cases in July, V_j	Number of cases in August, V_j	Number of cases in September V_j	Number of cases in October, V_j	Number of cases in November, V_j
24	167400782	180081192	193829848	213357235	231194181	243705625	–
25	167933373	180503102	194275173	214087524	231560977	244135761	–
26	168502846	180869106	194815533	214823164	231909080	244576866	–
27	169057033	181180563	195425745	215568802	232381444	245088017	–
28	169557476	181508885	196070028	216116120	232830308	245545805	–
29	170039483	181888509	196722877	216562642	233332705	246049111	–
30	170431363	182285486	197453162	217249144	233817106	246429566	–
31	170810073	–	197963310	217868234	–	246749382	–

GENERALIZED SIR MODEL AND DATA SMOOTHING PROCEDURE

The generalized SIR-model relates the number of susceptible S, infectious I and removed persons R for a particular epidemic wave i, [9, 20]. The exact solution of the set of non-linear differential equations uses the function

$$V(t) = I(t) + R(t),\qquad(1)$$

corresponding to the number of victims or the cumulative laboratory-confirmed number of cases versus time t [9, 20]. Its derivative:

$$\frac{dV}{dt} = \alpha_i SI\qquad(2)$$

yields the estimation of the average daily number of new cases. When the registered number of victims V_j is a random realization of its theoretical dependence (1), the exact solution presented in [9, 20] depends on five parameters (α_i is one of them). The details of the optimization procedure for their identification can be found in [21].

Since daily numbers of new cases are random and characterized by some weekly periodicity, we will use the smoothed daily number of accumulated cases:

$$\overline{V}_i = \frac{1}{7} \sum_{j=i-3}^{j=i+3} V_j,$$

and its numerical derivative:

$$\left.\frac{d\overline{V}}{dt}\right|_{t=t_i} \approx \frac{1}{2}(\overline{V}_{i+1} - \overline{V}_{i-1})\qquad(3)$$

to estimate the smoothed number of new daily cases [4, 5, 10, 19].

RESULTS AND DISCUSSION

The optimal values of SIR-model parameters and other characteristics of the 12th and 13th pandemic waves in Ukraine and the 6th wave in the whole world are calculated and listed in Table 3. The corresponding SIR curves are shown in

Figs. 1 and 2 by blue and brown lines for Ukraine and green lines for the world. Black lines illustrate the results of SIR simulation of the eleventh epidemic wave in Ukraine published in [11]. It can be seen that the optimal values of SIR parameters are very different (even for 12th and 13th epidemic waves in Ukraine). Close values were obtained only for the average times of spreading the infection $1/\rho_i$. The assessments of the pandemic wave durations (corresponding the moment when the number of infectious persons becomes less that unit) are very pessimistic (November, 2022 for Ukraine and December 2031 for the whole world). A similar long epidemic wave was also predicted for India [25].

T a b l e   3 . Optimal values of parameters and other characteristics of the 12th and 13th COVID-19 pandemic waves in Ukraine and the 6th wave in the whole world

Characteristics	12th epidemic wave in Ukraine, i=12, [13]	13th epidemic wave in Ukraine, i=13	6th pandemic wave in the whole world, i=6
Time period taken for calculations T_{ci}	September 29 – October 12, 2021	October 28 – November 10, 2021	September 29 – October 12, 2021
I_i	25,261.4089164122	73,492.9652436053	1,550,494.67573132
R_i	2,399,050.73394073	2,801,190.17761354	231,782,051.609983
N_i	3,790,400	7,237,600	334,411,200
ν_i	1,137,541.61656928	4,252,588.61675970	101736415.543763
α_i	2.63670321714285e-07	6.7868529452959e-08	2.84345358576434e-09
ρ_i	0.299935964004210	0.288616935787874	0.289282775580724
$1/\rho_i$	3.33404499630449	3.46480014164856	3.45682523956893
r_i	0.997536473683354	0.998339758268927	0.999305866880929
$S_{i\infty}$	845,264	3,503,575	84,981,994
$V_{i\infty}$	2,945,136	3,734,025	249,429,206
Final day of the epidemic wave	June 16, 2022	November 13, 2022	December 2031

The saturation levels (final sizes) $V_{i\infty}$ of the 12th wave in Ukraine and 6th global wave are already exceeded (compare corresponding values in Tables 1–3). As of November 17, 2021 the real accumulated number of deaths – 79,506 – registered in Ukraine (see Table 1) has already exceeded the figure 68,764 predicted in [13] for the end of 2021 with the use of *V(t)* curve for 12th epidemic wave. This discrepancy can be explained by the sharp increase in the daily number of new cases which occurred after long holidays October 14–17, 2021 (see red "crosses" in Figs. 1 and 2). These changes in the epidemic dynamics indicate the beginning of a new (13th) wave in Ukraine. The calculations allow us to estimate the new saturation level $V_{13\infty}$= 3,734,025 (see Table 3) and the expected accumulated number of deaths 3,734,025*0,02336=87,227 by November 2022. Registered numbers of deaths in Ukraine agree with the theoretical estimation for 13th wave (compare the magenta "triangles" and the dashed magenta line in Fig. 2).

According to the predictions for the 12th wave (posted in [13]], the numbers of infectious persons and average daily new cases will stop to increase around 17 and 14 October 2021, respectively (see blue dashed and dotted lines in Fig. 2). The registered smoothed daily number of new cases in Ukraine really achieved a local maximum on October 10, 2021, but started to increase very rapid after October 17, 2022 (see the red "crosses" in Figs. 1 and 2).

Fig. 1. The COVID-19 pandemic waves in Ukraine and in the whole world in the summer and autumn of 2021

The results of SIR simulations of the 11th (see [11]), 12th, and 13th waves in Ukraine are shown by black, blue, and brown lines, respectively. Green lines represent the 6th pandemic wave in the whole world. Numbers of victims $V(t) = I(t) + R(t)$ — solid lines (for the world divided by 60); numbers of infected and spreading $I(t)$ multiplied by 5 – dashed; derivatives dV/dt (eq. (2), multiplied by 100 for Ukraine and by 2 for the world) — dotted. "Circles" correspond to the accumulated numbers of cases registered during the periods of time taken for SIR simulations (for the world divided by 60). "Stars" corresponds to V_j values beyond these time periods (for the world divided by 60). "Crosses" show the first derivative (3) multiplied by 100 for Ukraine and by 2 for the world.

Unfortunately, the general SIR model cannot predict the emergence of new epidemic waves. It simulates the dynamics for only the period with constant epidemic conditions. Therefore, permanent monitoring of the number of new cases is needed to determine changes in the epidemic dynamics. After that it is possible to do new simulations by means of the generalized SIR model with calculation and use of new values of its parameters.

We can only point out the three possible reasons for the new 13th wave in Ukraine:

1. The long weekend of October 14–17, 2021 without significant quarantine restrictions led to a significant increase in travels and contacts. This period accounted for the maximum number of infected (see the blue dashed curve in Fig. 2). We observed a similar situation in Ukraine in May 2020, when the lockdown was lifted during the period of the maximum number of infectious people, which led to the emergence of the second epidemic wave before the end of the first one [5, 10]. An increase in contacts during the holidays in early May 2021

also led to an increase in the number of infectious persons (see the black dashed line in Fig. 1). But during this period there was a tendency to reduce the daily number of new cases, so the increase in contacts only slowed down this trend (see red "crosses" in Fig. 1).

2. Due to a large number of asymptomatic patients, many COVID-19 cases are not detected and registered [26–31]. The ratio of real to detected cases in Ukraine was estimated to be between 4 and 20 for different periods of time [9, 11]. Such large numbers of undetected cases may suddenly change the number of reported cases, if the population frightened by the increase in mortality begins to seek medical care more often.

3. Appearance of new coronavirus strains.

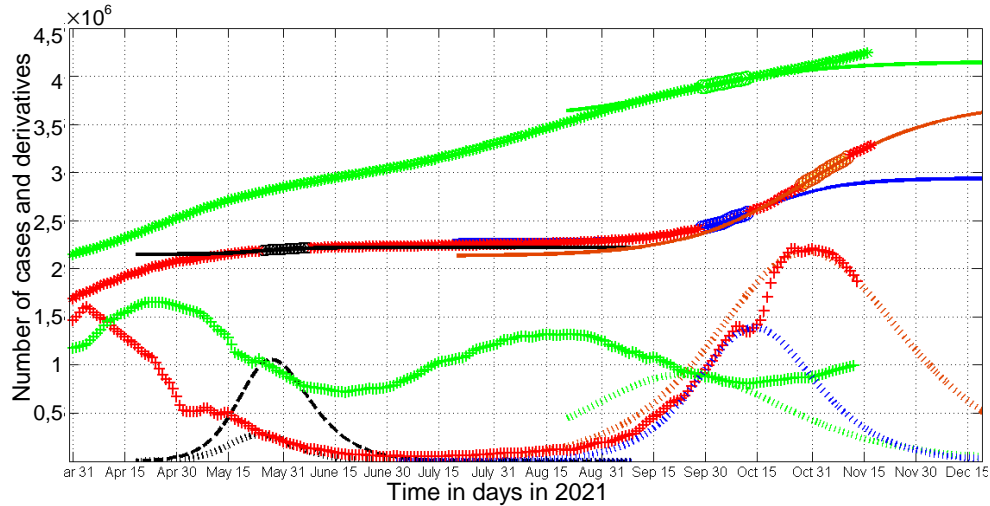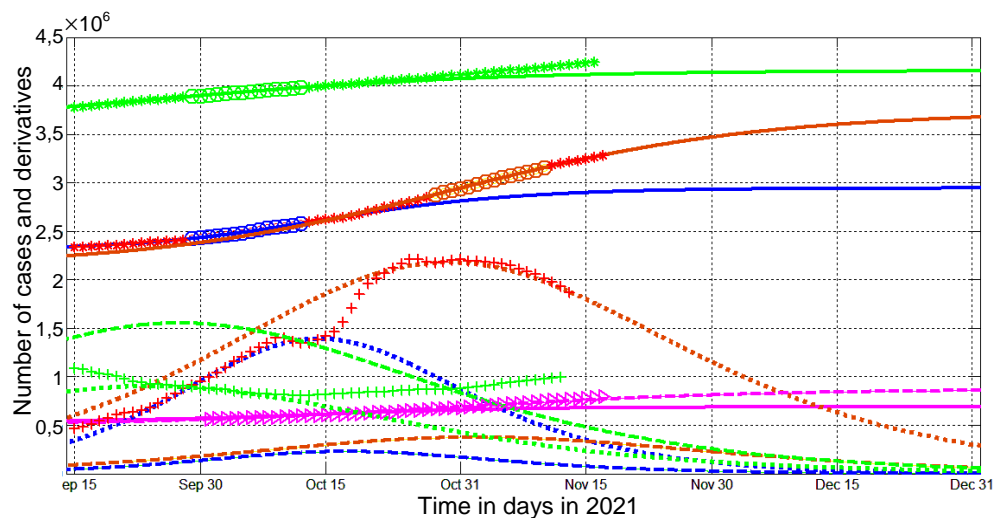*Fig. 2.* The COVID-19 pandemic waves in Ukraine and in the whole world in the autumn of 2021

The results of SIR simulations of the 12th and 13th waves in Ukraine are shown by blue and brown lines, respectively. Green lines represent the 6th pandemic wave in the whole world. Numbers of victims $V(t) = I(t) + R(t)$ — solid lines (for the world divided by 60); numbers of infected and spreading $I(t)$ (multiplied by 5 for Ukraine) – dashed; derivatives dV/dt (eq. (2), multiplied by 100 for Ukraine and by 2 for the world) — dotted. The magenta lines represent the estimation of the accumulated number of deaths during the 12th (solid) and 13th (dashed) epidemic waves in Ukraine multiplied by 10. Magenta "triangles" represent the accumulated numbers of death in Ukraine form Table 1 multiplied by 10. "Circles" correspond to the accumulated numbers of cases registered during the periods of time taken for SIR simulations (for the world divided by 60). "Stars" corresponds to V_j values beyond these time periods (for the world divided by 60). "Crosses" show the first derivative (3) multiplied by 100 for Ukraine and by 2 for the world.

"Stars" and "crosses" in Figs. 1 and 2 illustrate the accuracy of simulations for the accumulated number of cases and the averaged daily numbers of new cases (eq. (3)). Comparisons with corresponding blue solid and dotted lines in Fig. 2 show that the theoretical estimations for 12th wave in Ukraine were consistent with observations before October 15, 2021. After October 18 the results of observations are very close to the theoretical estimations for the 13th wave (see brown solid and dotted lines in Fig. 2). As of November 17, 2021 the

number of infectious persons (the brown dashed line) and the daily number of new cases were decreasing. Premature lifting of quarantine restrictions, a significant increase in contacts during the New Year and Christmas holidays or/and the appearance of a new coronavirus strain could disrupt these positive trends.

Unfortunately, the general SIR model cannot predict the emergence of new epidemic waves. It simulates the dynamics for only the period with constant epidemic conditions. Therefore, permanent monitoring of the number of new cases is needed to determine changes in the epidemic dynamics. After that it is possible to do new simulations by means of the generalized SIR model with calculation and use of new values of its parameters.

The global number of new cases is also characterized by wave-like behavior (see green "crosses" in Fig. 1). But unlike Ukraine and many other countries, the difference between the minimum and maximum values of the derivative (3) is much smaller for the world dynamics. The minima of new global cases also do not go to zero (compare green and red "crosses" in Figs. 1 and 2). All this limits the use of the SIR model for the long-term predictions. In particular, the increase in daily number of new cases (see green "crosses" in Figs. 1 and 2) indicate the beginning of a new global wave after October 15, 2021 (this fact makes the predictions for the 6th wave no more relevant). It should be noted that the COVID-19 pandemic is characterized by a very slow decline in the number of infectious $I(t)$. In particular, according to the results of modeling of the 6th world wave (shown in Table 3), the number of infectious persons worldwide may be less than 100 in May 2021. This small number is enough to continue the pandemic for almost 10 years.

CONCLUSIONS

The generalized SIR-model and corresponding parameter identification procedure was used to simulate and predict the dynamics of two new epidemic waves in Ukraine and one in the whole world. Results of calculations show that new cases in Ukraine will not stop to appear before November 2022. If the global situation with vaccination, testing and treatment will not change, the pandemic could continue for another ten years.

REFERENCES

1. I. Nesteruk, I.Kudybyn, and G. Demelmair, "Global stabilization trends of COVID-19 pandemic", *KPI Science News*, no. 2, pp. 55–62, 2020. doi: 10.20535/kpi-sn.2020.2.205124.
2. I. Nesteruk, "Simulations and predictions of COVID-19 pandemic with the use of SIR model", Innov Biosyst Bioeng, vol. 4, no. 2, pp. 110–121, 2020. doi: 10.20535/ibb.2020.4.2.204274. Available: http://ibb.kpi.ua/article/view/204274
3. Yu.N. Kyrychko, K.B. Blyuss, and I. Brovchenko, "Mathematical modelling of the dynamics and containment of COVID-19 in Ukraine", *Scientific Reports*, 10:19662, 2020. Available: https://doi.org/10.1038/s41598-020-76710-1
4. I. Nesteruk, *Coronasummer in Ukraine and Austria. [Preprint]*. ResearchGate, June 2020. doi: 10.13140/RG.2.2.32738.56002.

5. I. Nesteruk, *COVID-19 pandemic dynamics.* Springer Nature, 2021. doi: 10.1007/978-981-33-6416-5. Available: https://link.springer.com/book/10.1007/978-981-33-6416-5

6. S. Pardhan and N. Drydakis, "Associating the Change in New COVID-19 Cases to GDP per Capita in 38 European Countries in the First Wave of the Pandemic", *Front Public Health*, 8:582140, 2021. doi: 10.3389/fpubh.2020.582140.

7. S. Chintala, R. Dutta, and D. Tadmor, "COVID-19 spatiotemporal research with workflow-based data analysis", *Infect Genet Evol.*, 88:104701, 2021. doi: 10.1016/j.meegid.2020.104701.

8. I. Nesteruk and N. Benlagha, "Predictions of COVID-19 pandemic dynamics in Ukraine and Qatar based on generalized SIR model", *Innov. Biosyst. Bioeng.*, vol. 5, no. 1, pp. 37–46, 2021. doi: 10.20535/ibb.2021.5.2.230487. Available: http://ibb.kpi.ua/article/view/230487

9. I. Nesteruk, "Visible and real sizes of new COVID-19 pandemic waves in Ukraine", *Innov. Biosyst. Bioeng.*, vol. 5, no. 2, pp. 85–96, 2021. doi: 10.20535/ibb.2021.5.2.230487. Available: http://ibb.kpi.ua/article/view/230487

10. I. Nesteruk, "Detections and SIR simulations of the COVID-19 pandemic waves in Ukraine", *Comput. Math. Biophys.*, 9, pp. 46–65, 2021. Available: https://doi.org/10.1515/cmb-2020-0117

11. I. Nesteruk, "Influence of Possible Natural and Artificial Collective Immunity on New COVID-19 Pandemic Waves in Ukraine and Israel", *Explor. Res. Hypothesis. Med.*, 2021. doi: 10.14218/ERHM.2021.00044.

12. I. Nesteruk, O. Rodionov, A.V. Nikitin, and S. Walczak, "Influences of seasonal and demographic factors on the COVID-19 pandemic dynamics", *EAI Endorsed Transactions on Bioengineering and Bioinformatics*, 2021. doi: 10.4108/eai.8-12-2021.172364.

13. I. Nesteruk, *Simulation and predictions of a new COVID-19 pandemic wave in Ukraine with the use of generalized SIR model*. Medrxiv, 2021. Available: https://doi.org/10.1101/2021.10.13.21264949

14. I. Nesteruk and O. Rodionov, "New COVID-19 Pandemic Waves Caused by Omicron and Efficiency of Vaccinations", *J. Biomed. Res. Environ. Sci.*, 3(1), pp. 114–139, 2022. doi: 10.37871/jbres1410. Available: https://www.jelsciences.com/ articles/jbres1410.pdf

15. W.O. Kermack and A.G. McKendrick, "A Contribution to the mathematical theory of epidemics", *J. Royal. Stat. Soc., Ser A.*, vol. 115, issue 700, 1927, 21 p.

16. J.D. Murray, *Mathematical Biology I/II*. New York: Springer, 2002.

17. D. Langemann, I. Nesteruk, and J. Prestin, "Comparison of mathematical models for the dynamics of the Chernivtsi children disease", *Mathematics in Computers and Simulation*, vol. 123, pp. 68–79. 2016. doi: 10.1016/j.matcom.2016.01.003.

18. I. Nesteruk, "Statistics based models for the dynamics of Chernivtsi children disease", *Naukovi Visti NTUU KPI*, no. 5, pp. 26–34, 2017. doi: 10.20535/1810-0546.2017.5.108577.

19. I. Nesteruk, "Identification of the New Waves of the COVID-19 Pandemic", in book *COVID-19 Pandemic Dynamics*. Springer Nature, 2021. doi: 10.1007/978-981-33-6416-5_8. Available: https://link.springer.com/chapter/10.1007/978-981-33-6416-5_8

20. I. Nesteruk, "General SIR Model and Its Exact Solution", in book *COVID-19 Pandemic Dynamics*. Springer Nature, 2021. doi: 10.1007/978-981-33-6416-5_9. Available: https://link.springer.com/content/pdf/10.1007%2F978-981-33-6416-5_9.pdf

21. I. Nesteruk, "Procedures of Parameter Identification for the Waves of Epidemics", in book *COVID-19 Pandemic Dynamics*. Springer Nature, 2021. doi: 10.1007/978-981-33-6416-5_10. Available: https://link.springer.com/chapter/10.1007%2F978-981-33-6416-5_10

22. *Coronavirus in Ukraine - Statistics - Map of infections, graphs*. [Internet]. 2021. Available: https://index.minfin.com.ua/ua/reference/coronavirus/ukraine/
23. *Cabinet of Ministers of Ukraine – Home.* [Internet]. Available: https://www.kmu.gov.ua/
24. *COVID-19 Data Repository by the Center for Systems Science and Engineering (CSSE) at Johns Hopkins University (JHU)*. Available: https://github.com/owid/covid-19-data/tree/master/public/data
25. I. Nesteruk, "The COVID-19 pandemic dynamic in India in the spring and summer of 2021", J. Bio. Med.: Open Access, vol.2, issue 2, pp. 1–13, 2021. Available: https://gnoscience.com/uploads/journals/articles/856271132747.pdf
26. "Coronavirus: 'strange pneumonia' seen in Lombardy in November, leading Italian doctor says", *South China Morning Post.* Available: https://www.scmp.com/news/china/society/article/3076334/coronavirus-strange-pneumonia-seen-lombardy-november-leading
27. "Wir sind alle erkrankt", *Frankfurter Allgemeine.* Available: https://m.faz.net/ aktuell/sport/mehr-sport/militaerweltspiele-2019-in-wuhan-damals-schon-corona-faelle-16758894.html
28. D.M. Weinberger et al., *Estimating the early death toll of COVID-19 in the United States. [Preprint.]*. MEDRXIV, 2020. Available: https://doi.org/10.1101/2020.04.15.2006643
29. "Slovakia tested most of the country in two days. Here's how they did it and what they found", *CNN.* Available: https://edition.cnn.com/2020/11/02/europe/slovakia-mass-coronavirus-test-intl/index.html
30. "Slovakia's Second Round of Coronavirus Tests Draws Large Crowds", *Reuters.* Available: https://www.voanews.com/covid-19-pandemic/slovakias-second-round-coronavirus-tests-draws-large-crowds
31. "An experiment with mass testing for COVID-19 was conducted in Khmelnytsky", *Podillya News.* Available: https://podillyanews.com/2020/12/17/u-shkolah-hmelnytskogo-provely-eksperyment-z-testuvannyam-na-covid-19/

INFORMATION ON THE ARTICLE

Igor G. Nesteruk, ORCID: 0000-0001-7250-2729, Institute of Hydromechanics, National Academy of Sciences of Ukraine, Ukraine, e-mail: inesteruk@yahoo.com

МОДЕЛЮВАННЯ НОВИХ ХВИЛЬ ПАНДЕМІЇ COVID-19 В УКРАЇНІ ТА СВІТІ ЗА УЗАГАЛЬНЕНОЮ МОДЕЛЛЮ SIR / І.Г. Нестерук

Анотація. Нові хвилі пандемії COVID-19 в Україні, що розпочалися влітку 2021 року та після свят у середині жовтня 2021 року, характеризувались майже експоненціальним зростанням згладженої щоденної кількості нових випадків. Це викликає велике занепокоєння та необхідність негайного прогнозування динаміки епідемії, щоб оцінити можливі максимальні значення нових випадків, ризику зараження та кількості смертей. Узагальнену SIR-модель та процедуру ідентифікації відповідних параметрів використано для моделювання і прогнозування динаміки двох нових епідемічних хвиль в Україні та однієї у світі. Результати розрахунків показують, що нові випадки в Україні не перестануть з'являтися до листопада 2022 року. Якщо глобальна ситуація з вакцинацією, тестуванням та лікуванням не зміниться, пандемія може тривати ще десять років.

Ключові слова: пандемія COVID-19, епідемічні хвилі, епідемічна динаміка в Україні, глобальна динаміка пандемії, математичне моделювання інфекційних захворювань, модель SIR, ідентифікація параметрів, статистичні методи.

AUTOMATIC PANCREAS SEGMENTATION USING RESNET-18 DEEP LEARNING APPROACH

S.N. KAKARWAL, P.M. PAITHANE

Abstract. The accurate pancreas segmentation process is essential in the early detection of pancreatic cancer. The pancreas is situated in the abdominal cavity of the human body. The abdominal cavity contains the pancreas, liver, spleen, kidney, and adrenal glands. Sharp and smooth detection of the pancreas from this abdominal cavity is a challenging and tedious job in medical image investigation. Top-down approaches like Novel Modified K-means Fuzzy clustering algorithm (NMKFCM), Scale Invariant Feature Transform (SIFT), Kernel Density Estimator (KDE) algorithms were applied for pancreas segmentation in the early days. Recently, Bottom-up method has become popular for pancreas segmentation in medical image analysis and cancer diagnosis. LevelSet algorithm is used to detect the pancreas from the abdominal cavity. The deep learning, bottom-up approach performance is better than another. Deep Residual Network (ResNet-18) deep learning, bottom-up approach is used to detect accurate and sharp pancreas from CT scan medical images. 18 layers are used in the architecture of ResNet-18. The automatic pancreas and kidney segmentation is accurately extracted from CT scan images. The proposed method is applied to the medical CT scan images dataset of 82 patients. 699 images and 150 images with different angles are used for training and testing purposes, respectively. ResNet-18 attains a dice similarity index value up to 98.29±0.63, Jaccard Index value up to 96.63±01.25, Bfscore value up to 84.65±03.96. The validation accuracy of the proposed method is 97.01%, and the loss rate value achieves up to 0.0010. The class imbalance problem is solved by class weight and data augmentation.

Keywords: Deep Learning, Dice Coefficient, Fully Connected Layer (FCN), Residual Network (ResNet-18), Visual Geometry Group (VGG).

INTRODUCTION

Image splitting task is rigorously act as vital character in image investigation [1]. Image splitting task is beneficial for many applications like clinical image analysis, disease detection of crop, traffic control observation, metallic surface crack detection, and Aerospace image analysis. CT, MRI, PET, and supplementary images are used in the clinical image diagnosis and cure of illnesses. Pancreas segmentation is challenging job in medical image investigation and analysis [2]. Accurate organ segmentation and rapid processing are the major challenges in the result of medical images. Computerized segmentation of several image subsections is useful to analyze anatomical organization as well as abdominal body. Segmentation is played major role in visualization and diagnosis of clinical images. Sub-grouping is an important subject to several image-processing research. Spleen, liver, kidney, pancreas is present in the abdominal CT images [3]. Bottom-up approach and Top-down approach are applied to image splitting process [4]. In Top-down approach, medical image segmentation is performed within minimum time- period but less accuracy of segmentation. Bottom-up approach is

efficient approach for medical image segmentation with high accuracy and minimum time-period. Semantic segmentation is one approach of deep learning which used for abdominal computed tomography. Deep learning model is popular approach of a machine learning methods. Deep learning model is dealing with algorithms with hierarchical procedure layers [5]. It is experimenting nonuniform transformations to view and gain data characteristics successfully [6]. Currently Deep learning model is popular in various domains such as medical image analysis, medical signal analysis, speech recognition, bio informatics, computer vision [4]. Convolution neural networks, Generative Adversarial Networks, networks with auto-encoder, and recurrent neural networks are prominent deep learning approaches. These approaches are introduced and used in various task to map with state-of-the-art results. In deep learning, network training is required with dataset. For network training, set of convolution network, annotated dataset, optimizer, minibatch size, epoch, loss function is used. Dataset can be divided into training, validation and testing purposed also. Fully convolution network (FCN) was introduced by Long et al. [5]. In FCN, fully convolution layer is used as the last fully convolution network layer. For more accuracy of dense pixelwise predication, the network is used fully convolution network. Semantic segmentation can be performed by FCN. FCN architecture is built with pooling, upsampling and convolution. FCN can perform predication of image within on single forward pass [7].

MATERIALS AND METHODS

Image Dataset and Ground Truth Labeling

Bottom-UP approaches are applying on a dataset of 80 patient, 53 male and 57 female patients high resolution (512*512) CT scan images of 3D abdominal with 1,5–2,5 mm slice thickness range using Philips and Siemens MDCT scanners [2]. The 63 patients CT scans abdominal images are erratic recommend by an expert radiologist from the Picture Archiving and Communications System (PACS). National Institutes of Health Clinical Center is providing database of CT dicom images for abdominal,78 to 79 years patient age series with a mean of 46.8±16.7 are used dataset [8]. DICOM medical images are converted to PNG image format. The view of scans images was axial, sagittal and coronoal with 1,5 mm or 3 mm thickness available [9]. Human expert labeling was performed under guideline of certified radiologist. 3 labels are created for manual labeling like background, pancreas, and kidney. Medical images are selected with different focal phase angle of CT. Size and shape of pancreas is varies in different view of CT. Image input size is $255 \times 255 \times 3,699$ images are used for and 150 for testing.

LevelSets Algorithm

Levelset algorithm was presented by Osher and Sethian. It can use zero corresponding exterior method [10]. Basic phenomena are to adjustment of portable pathway of a two-dimensional arc into portable path of a 3D surface. In this, level Set is actively participate toward indication of arcs as zero levelset of high dimension hyper-superficial [9]. Challenge of such exercise suggestions supplementary faultless algebraic execution also operates topological variation without any prob-

lems [8]. The predictable set edge is described zero levelset of an implicit symbol U of the evolving curve. In brief, evolve the implicit levelset function $\phi(x, y, t)$ to represent evolution of curve $\tau(t)$ with a speed $F(x, y)$ in normal direction. Time t, zero levelset $(x, y) / \phi(x, y, t) = 0$ defines evolved shape $\tau(t)$:

$$\phi(\tau(t), t) = 0 . \tag{1}$$

Differentiate equation (1) with respect to t and apply chain rule,

$$\frac{\partial \phi}{\partial t} + \nabla \phi . \frac{\partial \tau}{\partial t}, \tag{2}$$

F denotes speed of curve in normal direction, describe below

$$\frac{\partial \tau}{\partial t} . N = F , \tag{3}$$

where N denotes outwards normal, and elaborated by equation

$$N = \frac{\nabla \phi}{|\nabla \phi|} . \tag{4}$$

Substitute Equation (4) and (3) into (2), and calculate evolution equation for ϕ as

$$\phi_t + F|\nabla \phi| = 0 .$$

This is fundamental equation of the levelset [6], and zero levelset represents item shape curve:

$$\tau(t) = \{(x, y) / \phi(x, y, t) = 0\} .$$

Function ϕ is generally determined grounded on signed distance calculation to primary front. Relating to image field purely based on Euclidean distance between the curve and one image point. Describe below:

$$\phi(x, y) = \pm d(x, y) ,$$

where $d(x, y)$ — Euclidean distance from point to borderline. Sign: points inside borderline (–) sign and outside (+) sign.

Evolution of borderline is elaborated by partial differential equation on zero levelset of ϕ:

$$\frac{\partial \phi}{\partial t} = -F|\nabla \phi| ,$$

where F — known function, which calculated by the local curvature κ at the zero levelset, i.e., $F = F(\kappa)$, where κ:

$$\kappa = \nabla . \frac{\nabla \phi}{|\nabla \phi|} = \frac{\phi_{xx} \phi_y^2 - 2\phi_x \phi_y \phi_{xy} + \phi_{xy} \phi^2}{(\phi_x^2 + \phi_y^2)^{3/2}} .$$

Speed function F is represent as $F = F(L, G, I)$, where L — local information, which define by local geometric properties, G — global property of front depends on contour and location of front; I — independent properties that independent of front [11].

The propagating task is characterized as:

$$\frac{\partial \phi}{\partial t} = g_I(F_A + F_G)\,|\nabla\phi|.$$

The term *FA*, causing front to consistently multiply or bond with a speed of *FA* dependent on sign [12].

FG : portion that relate on geometry of front, such as own local curvature:

$$g_I(x,y) = \frac{1}{1 + \left|\nabla(G_\sigma \otimes I(x,y))\right|},$$

where $G_\sigma \otimes I$ — convolute image *I* with Gaussian smoothing filter G_σ with characteristic width of σ.

The form of speed function expressed as [9]: $F = FA + FG$. Via calculation control objects or different image force which stated in common but simple form:

$$F = A(F_A + F_G) + B\,;$$

$$A = \frac{1}{(1 + dist(C_{img}, C_{front})}\,;$$

$$B = \overrightarrow{dist}(C_{img}, C_{front})\,.$$

dist() — appropriate distance function which is used to calculate variance of image features between propagating front and propagated zones. *B* — additional forces from image content. *C* — image content model, including any of the color, shape, and texture features.

Automatic Seeded Region Growing Algorithms for LevelSet

General area developing algorithms determine pixel value physically from each mark region as seed. The seed point normally contains of great uniform to neighboring pixels and can be correspond to region [9]. The nature of seed point is very close together to cluster center in clustering algorithm. AP clustering algorithm is going to discover seed points in an image [13].

All data points as potential cluster centers, and computes accessibility and accountability data by equations below iteratively between every two data points to find characteristic centers of data points:

$$R(i,k) \leftarrow S(i,k) - \max_{k'\partial t, k'\neq k}\{a(i,k') + S(i,k)\}\,,$$

if $\qquad i \neq k, ai,\; k \leftarrow \min\left\{0, R(k,k') + \sum_{i'\partial t.i'\notin i,k}\max\{0, ri', k\}\right\},$

$$a(k,k) \leftarrow \sum_{i'\partial t.i'\neq k}(0, R(i',k))\,.$$

To receive the seed x_j by equation below and cluster this holds x_i :

$$\underset{1\leq j\leq N}{\operatorname{argmax}}\,[R(i,k) + a(i,k)]\,.$$

The simple linear iterative cluster (SLIC) algorithm is going for segmented pixel-level image before using AP clustering process by combining adjacent pixels with similar characteristics to some irregular pixel blocks [14].

The region growing is computed by continually assimilation of seed points also surrounding pixels and division of aim objects with background. Lastly design of ROIs is in rectangular boxes according to segmentation results [10].

Euclidean Distance runs to measure LAB color matches by equation

$$S = \sqrt{(L_0 - L_{0j})^2 + (a_0 - a_{0j})^2 + (b_0 - b_{oj})^2} \ .$$

PROPOSED METHOD

Residual Network (ResNet-18)

The training accuracy problem is solved by Residual Network-18 (ResNet-18). $H(x)$ is underlying mapping layer fit to new layer with x map inputs from previous layer. Residual function is stated that $f(x) = H(x) - x$ with same dimensions. So updated residual function $f(x) + x$ is use in deep network layer [15].

Residual function is used to improve training accuracy value with minimum time.

This residual function is used in every connected layer which formulated using following expression:

$$F = f(x, \{M_i\}) + x \ . \tag{5}$$

Fig. 1. ResNet-18 Relu Function
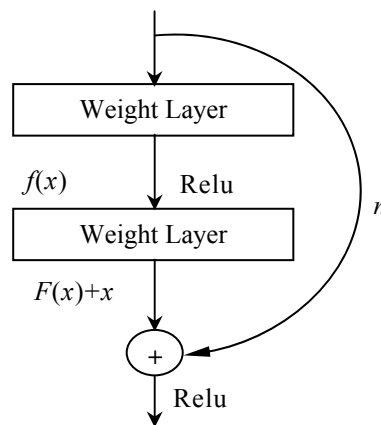
In this x and F are input and output dimensions, M_i is layer used for RELU. $F(x) + x$ is used as short connection in ResNet-18 (Fig. 1). Linear projection can be execute through M_s and add into eq. (5) when dimension will match. M_s is square matrix which address the training accuracy problem when matching dimensions condition satisfied [16]:

$$F_u = F + M_s x \ .$$

T a b l e 1. ResNet-18 model Network Layer Detail

Layer Name	Output Size	ResNet-18 Layer
Conv1	112×112	7×7.64 Stride,2
Conv2	56×56	3×3 max pool, stride 2
		$\begin{bmatrix} 3\times3,64 \\ 3\times3,64 \end{bmatrix}\times2$
Conv3	28×28	$\begin{bmatrix} 3\times3,128 \\ 3\times3,128 \end{bmatrix}\times2$
Conv4	14×14	$\begin{bmatrix} 3\times3,256 \\ 3\times3,256 \end{bmatrix}\times2$
Conv5	7×7	$\begin{bmatrix} 3\times3,512 \\ 3\times3,512 \end{bmatrix}\times2$
	1×1	

Table 1 is depicted detail about convolution network layer used in ResNet-18 approach.

Data Augmentation

Class imbalance is problem in deep learning image segmentation. An image data augmenter setup to an examine of pre-processing choices for image augmentation, such as resizing, rotation and reflection. Random *x* and *y* direction translation is performed by [−10,10] and random rotation by [−180,180]. Data augmentation is beneficial to enhance output and results of deep learning approaches using set novel and discrete examples to datasets [17]. Transformations in datasets by using data augmentation approaches authorize companies to minimize these experimental costs. In the system, data augmentation is using reflection, translation, and rotation to improve model prediction accuracy and reducing overfitting of data [18].

Loss Function

Cross Entropy. Cross -Entropy is used in ResNet-18 as loss function to relate binary classification problems that calculate the probability of specific class or not [19]. Let d and g represent the input image and related ground truth or manually annotated image respectively. The key aim of segmentation is to learn relation of *d* and *g*. Cross-entropy loss function L_{CET} is shown as

$$L_{CET} = \sum_{i=1}^{N} g_i \log(f_i(d,t)) + (1-g_i)\log(1-f_i(d,t)),$$

where i = pixel index, N = total pixel.

Dice Loss. To calculate overlap rate of predicated mask and ground-truth for segmentation results Dice Score Coefficient is used. DSC is formulated as below:

$$DSC(d,g) = \frac{2(d \cap g)}{|d| + |g|}.$$

Dice loss function can be formulated as per below expression:

$$L_{DSCL} = \sum_c (1 - DSC_c),$$

where C is number of iteration.

Categorical Cross-Entropy Loss. It is used for multi-class classification task. In this work 3 class are used liked background, pancreas, and kidney. This model helps to detect object belong to which class among other classes.

Categorical loss function computed using following expression:

$$L_{CCET} = \frac{1}{N} \sum_p^N -\log\left(\frac{e^{s_p}}{\sum_j^C e^{s_j}}\right),$$

where M is positive class, e^{s_p} is score of positive class.
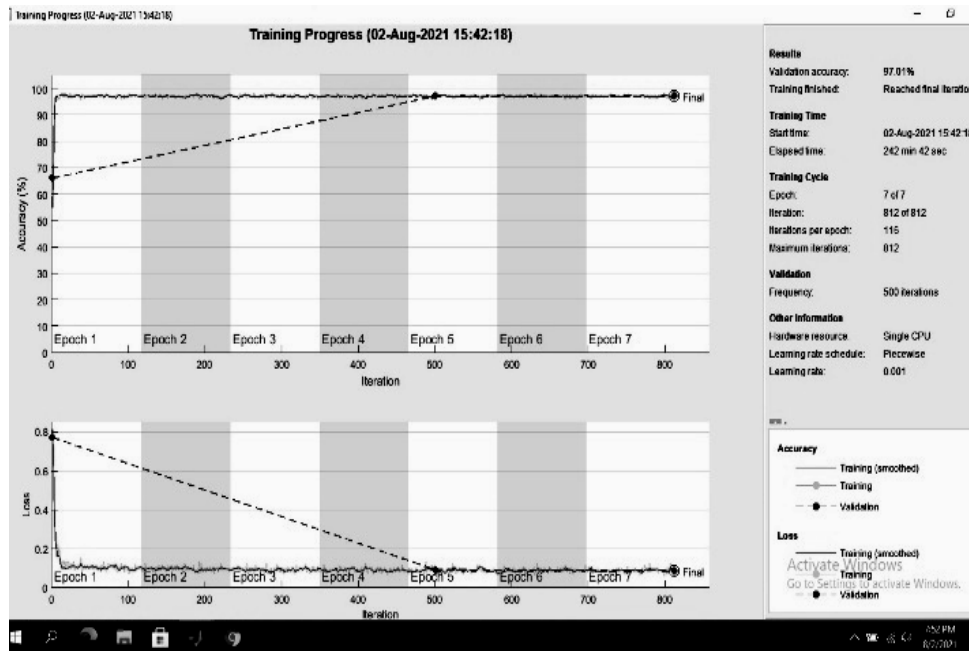
Fig. 2. ResNet-18 Validation Accuracy

RESULTS

Evaluation Parameter

Global Accuracy (*GA*): *GA* is the ratio of perfectly segmented pixels divided by the total number of pixels

$$GA = \frac{\sum_{i=0}^C p_i}{\sum_{i=0}^C \sum_{j=0}^C p_{ij}},$$

where p_{ij} is the number of pixels of class *i* segmented as belonging to class *j*.

Mean Accuracy (*MA*): Mean Accuracy is an next step of Global Accuracy, in which the ratio of match pixels are computed in a per-class pattern and then averaged over the total number of classes [19]:

$$MA = \frac{1}{C+1}\sum_{i=0}^{C}\frac{p_{ii}}{\sum_{j=0}^{C}p_{ij}}.$$

Interaction of Union (*IoU*): Jaccard index alias *IoU*, it is correlation between segmented image (S) and annotated image (B). The value of *IoU* lies between 0 to 1[20].

$$Jaccard(d,g) = \text{IoU} = \frac{|d \cap g|}{|d \cup g|}.$$

Mean Interaction of Union (*MIoU*): Mean *IoU* is calculated by the average *IoU* value of all classes.

$$MIoU = \frac{\sum_{C}IoU}{C},$$

where total number of classes value is denoted by C. 3 classes are used like pancrea, kidney and background.

Weighted Interaction of Union:

$$WIoU = \frac{\sum_{C}IoU * \sum_{i=0}^{C}p_{i}}{C}.$$

Weight value is number pixel in class. Average *IoU* of each class [19].

Bfscore. The bf score measure how close to the segmented boundary of an input image matched with the annotated image. The BF score is calculated with the help of the harmonic mean of the precision and recall values with a distance error tolerance to decide whether a point on the segmented boundary has a correlated to annotated boundary or not [20]:

$$score = \frac{2 * precision * recall}{(recall + precision)}.$$

Dice Coefficient. It is correlation between segmented image (S) and annotated image (B). The value of dice coefficient lies between 0 to 1 and easily converted into % for understanding purpose [20]:

$$dice(S,B) = 2 * \frac{|S \cap B|}{(|S| + |B|)}.$$

Sensitivity

$$Sensitivity = \frac{TP}{FN + TP},$$

where *TP* is true positive, *FN* is false negative [20].

Specificity

$$Specificity = \frac{TN}{FP + TN},$$

where *TN* is true negative, *FP* is false positive [20].

T a b l e 2. ResNet-18 Model Compare with VGG-16 and VGG-19

Approach	VA, %	Bf, %	Number of Layer	Time	MA, %
ResNet-18	97.01	84.06±3.96	18	242 min 42 sec	42.16
VGG-16	97.01	84.05±4.02	16	522 min 7 sec	42.439
VGG-19	96.90	56.62±2.48	19	632 min 44 sec	42.05

Table 2 is depicted performance of ResNet-18 as compared other deep learning approaches. Validation accuracy is more as compared to VGG-19. ResNet-18 is required less training time. The Bf score of ResNet-18 is higher as compared to VGG-16 and VGG-19. ResNet-18 is using 18 number of layer where 17 number are convolution layer used so accuracy is improved.

T a b l e 3. ResNet-18 Model Compare with VGG-16 and VGG-19 using Evaluation Parameter

Approach	IOU	Dice	Sensitivity	Precision
ResNet-18	96.63 ± 01.25	98.29 ± 00.63	96.78 ± 00.03	96.64 ± 00.12
ATLAS [19]	55.50 ± 17.10	69.60 ± 16.70	67.90 ± 18.20	74.10 ± 17.10
_U_-net Single Mode [20]		74.10 ± 00.13	74.30 ± 00.17	78.90 ± 00.13
Frame-1[2]	57.2 ± 25.40	68.80 ± 25.60	72.50 ± 27.20	71.50 ± 30.00
Frame-2[2]	57.9 ± 13.60	70.70 ± 13.00	74.40 ± 15.10	71.60 ± 10.50
LevelSET[1]	28.18 ± 14.07	42.26 ± 16.37	98.48 ± 00.03	98.70 ± 00.03

Table 3 is depicted the performance of ResNet-18 deep learning approach as compared to state-of-arts. ResNet-18 having more IoU value as compared to other approach. In Dice index, ResNet-18 is achieved higher value (Fig. 3).
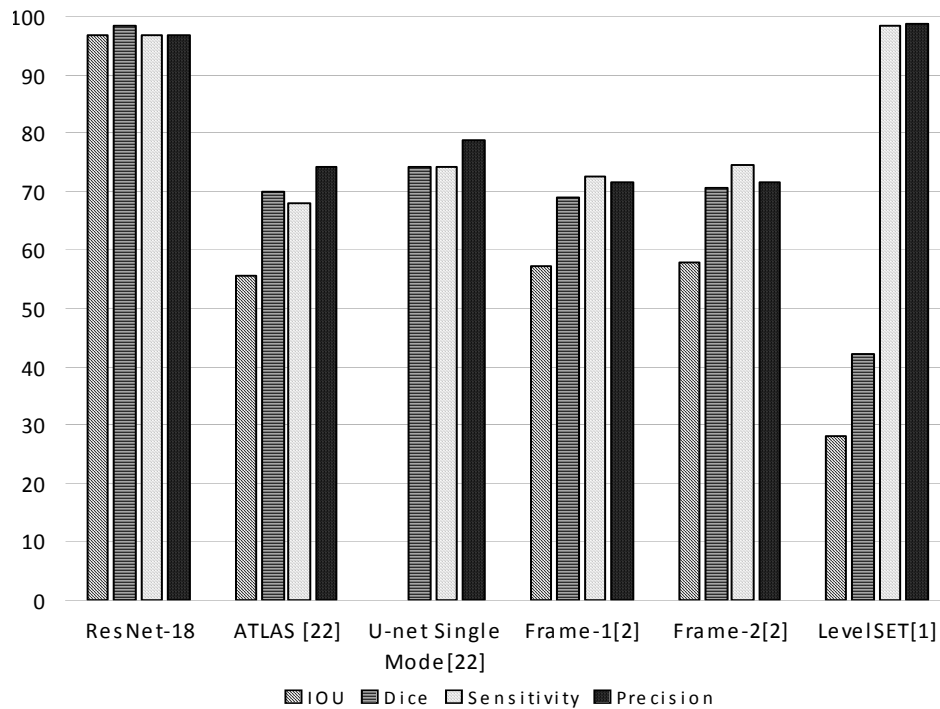
Fig. 3. ResNet-18 Result Comparison with State-of-Art

Above figure is showing the ResNet-18 result in detail in terms of IOU, Dice, Sensitivity and Precision (Fig. 4 and 5).
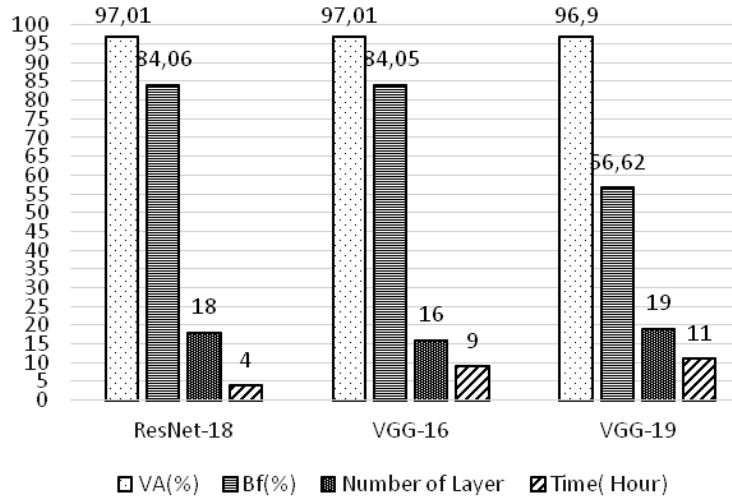
Fig. 4. ResNet-18 Result Comparison with State-of-Art using Performance Parameter
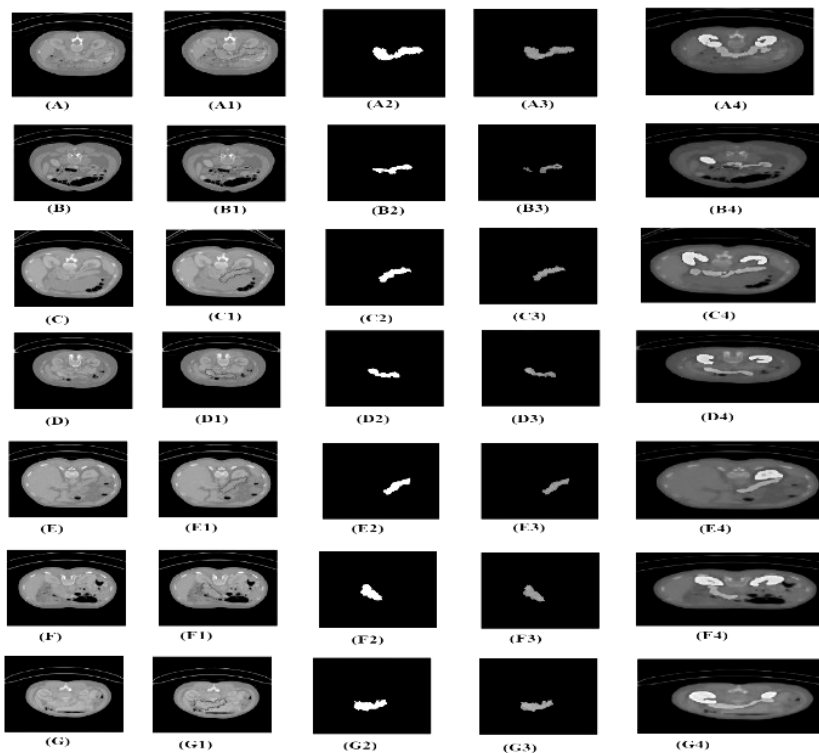
Fig. 5. ResNet-18 Result Comparison with State-of-Art using Performance

Above figure is consist of origan image (subfigure A, B, C, D, E, F, G), levelset boundary image (subfigure A1, B1, C1, D1, E1, F1, G1), binary levelset (subfigure A2, B2, C2, D2, E2, F2, G2), segmented image by levelset (subfigure A3, B3, C3, D3, E3, F3, G3) and Segmented image using ResNet-18 (subfigure A4, B4, C4, D4, E4, F4, G4).

CONCLUSION

ResNet-18 approach for automatic pancreas segmentation from CT scan images. 18 layers architecture is used for multiple organ segmentation from CT scan image. In VGG-16 method, 16 convolution layers are used, in VGG-19, 19 convolution layers are used. In deep learning, training of network layer is time consuming task. Levelset method is also used for pancreas segmentation but if seeded point is wrong then output image is not correct. Levelset algorithm takes more time to extract image with non-clear boundary of pancreas. Proposed method takes very less time as compared to other deep learning method. Bfscore value of proposed method is superior from VGG-19 method for same dataset. Sensitivity, Mean Accuracy and Mean-bfscore value are superior to other methods. Dice coefficient, jaccard Index are high as compared to state-of-art. Proposed method values as per evaluation matrix parameters are high as compared to state-of-art. Loss function value is less than other methods. In method, patch labeling is used so 64*64 patch channel used so only one organ segmentation can be performed. In proposed method, manually annotation process is performed by medical practitioner and two classes is generated for pancreas and kidney. With the help of proposed method many abdominal organ segmentations can be performed. Input image size is 255*255*3 used so maximum pixel information is available in convolution network. Noisy pixel image information can be easily omitted during dropout network layer. Accurate pancreas shape and size is detected by proposed method, but it fails to detect pancreas cancer affected areas in percentage. Pancreas size and shape is available in 2D image using proposed method. 3D pancreas image detection is future scope for proposed method.

AUTHOR CONTRIBUTIONS

Pradip Paithane: Conceptualization, Data curation, Methodology, Software, Roles/Writing-original draft. Dr.S.N. Kakarwal: Formal analysis, Investigation, Visualization, Project administration, Supervision, Validation, Writing - review and editing.

REFERENCES

1. Pradip M. Paithane, Dr.S.N.Kakarwal, and Dr.D.V.Kurmude, "Top-Down Method used for Pancreas Segmentation", *International Journal of Innovative and Exploring Engineering (IJITEE)*, 9-3, pp. 2278–3075, 2020.
2. Amal Farag, Le Lu, Holger R. Roth, Jiamin Liu, Evrim Turkbey, and Ronald M. Summers, "A Bottom-Up Approach for Pancreas Segmentation Using Cascaded Superpixels and (Deep) Image Patch Labeling", *IEEE Transactions on image processing*, 26-1, 2017. doi:10.1109/TIP.2016.2624198.
3. Pradip M. Paithane and S.A. Kinariwal, "Automatic Determination Number of Cluster for NMKFC-means algorithm on Image Segmentation", *IOSR-JCE*, 17-1, 2015.
4. Pradip M. Paithane and Dr.S.N. Kakarwal, "Automatic Determination Number of Cluster for Multi Kenel NMKFCM algorithm on image segmentation", *Intelligent System Design and Applications*, Springer Cham, 2017, pp. 80–89.
5. Justin Ker, Lipo Wang, Jai Rao, and Tchoyoson Lim, "Deep Learning Applications in Medical Image Analysis", *IEEE Transactions*, pp. 9375–9389, 2018.

6. Yingege Qu, Pheng Ann Heng, and Tien-Tsin Wong, *Image Segmentation using the levelset Method*. New York: Springer, 2004.

7. Xin-Jiang, Renjie-Zhang, and Shengdong-Nie, "Image Segmentation Based on Level set Method", *International conference on Medical Physics and Biomedical Engineering*, Elsevier, 2012.

8. Joris R Rommelse, Hai-Xiang Lin, and Tony F. Chann, *A Robust Level Set Algorithm for Image Segmentation and its Parallel Implementation*. Springer, 2014.

9. P.M. Paithane, S.N. Kakarwal, and D.V. Kurmude, "Automatic Seeded Region Growing with Level Set Technique Used for Segmentation of Pancreas", *Proceedings of the 12th International Conference on Soft Computing and Pattern Recognition (SoCPaR 2020)*, 1383.

10. Qianwen Li, Zhihua Wei, and Cairong Zhao, "Optimized Automatic Seeded Region Growing Algorithm with Application to ROI Extraction", *IJIG*, 17-4, 2017.

11. H.K. Abbas, A.H. Al-Saleh, H.J. Mohamad, and A.A. Al-Zuky, "New algorithms to Enhanced Fused Images from Auto-Focus Images", *Baghdad Sci. J.*, 10, 18(1):0124, 2021

12. R.J. Mitlif and I.H. Hussein, "Ranking Function to Solve a Fuzzy Multiple Objective Function", *Baghdad Sci. J.*, 10, 18(1):0144, 2021.

13. O. Bandyopadhyay, B. Chanda, and B.B. Bhattacharya, "Automatic Segmentation of bones in X-ray images based on entropy measure", *Int. J. Image Graph.*, 16-01, 2016.

14. I. Bankman, *Handbook of medical imaging: processing and analysis*. New York: Acdameic Press, 2000.

15. Shuo Cheng and Guohui Zhou, "Facial Expression Recognition Method Based on Improved VGG Convolution Neural Network", *IJPRAI*, vol. 34, no. 7, 2020.

16. Pikul Vejjanugraha, Kazunori Kotani, Waree Kongprawechnon, Toshiaki Kondo, and Kanokvate Tungpimolrut, "Automatic Screening of Lung Diseases by 3D Active Contour Method for Inhomogeneous Motion Estimation in CT Image Pairs", *Walailak J. Sci.Tech*, 18-2, 2021

17. Mizuho Nishio, Shunjiro Noguchi, and Koji Fujimoto, "Automatic Pancreas Segmentation Using Coarse-Scaled 2D Model of Deep Learning: Usefulness of Data Augmentation and Deep U-Net", *Appl. Sci.*, 2020. doi: 10.3390/app10103360.

18. Srikanth Tammina, "Transfer Learning using VGG-16 with deep convolution Neural Network for classifying Images", *IJSR Publications*, 9-10, 2019.

19. H.R. Roth et al., *Deep Organ: Multi-level Deep Convolutional Networks for Automated Pancreas Segmentation*. MICCAI, 2015.

20. Robin Wolz, Chengwen Chu, Kazunari Misawa, Michitaka Fujiwara, Kensaku Mori, and Daniel Rueckert, Automated Abdominal Multi-Organ Segmentation With Subject-Specific Atlas Generation, *IEEE Transactions On Medical Imaging*, 32-9, 2013.

INFORMATION ON THE ARTICLE

S.N. Kakarwal, PES Engineering College, Aurangabad, MH, India.

Pradip M. Paithane, Dr. Babasaheb Ambedkar Marathwada University, Aurangabad, MH, India, e-mail: paithanepradip@gmail.com

АВТОМАТИЧНА СЕГМЕНТАЦІЯ ПІДШЛУНКОВОЇ ЗАЛОЗИ З ВИКОРИСТАННЯМ RESNET-18 МЕТОДУ ГЛИБОКОГО НАВЧАННЯ / С.Н. Какарвал, П.М. Паітане

Анотація. Точний процес сегментації підшлункової залози є важливим процесом для раннього виявлення раку підшлункової залози. Підшлункова залоза

розташована в черевній порожнині тіла людини як і печінка, селезінка, нирки та наднирники. Чітке та плавне виявлення підшлункової залози у черевній порожнині є складною та виснажливою роботою у ході дослідження медичного зображення. Для сегментації підшлункової залози в перші дні застосовуються підходи «зверху-вниз», як-от новий модифікований алгоритм кластеризації K-середніх (NMKFCM), масштабно інваріантне перетворення ознак (SIFT), алгоритм оцінювання щільності ядра (KDE). Останнім часом популярний метод BottomUp для сегментації підшлункової залози в аналізі медичного зображення та діагностики раку. Алгоритм LevelSet використовується для виокремлення підшлункової залози серед черевної порожнини. Поглиблене навчання, підхід «знизу-вгору» кращий, ніж інші. Глибока залишкова мережа (ResNet-18) глибоке навчання, підхід «знизу-вгору» використовується для виявлення точної та чіткої підшлункової залози за медичними зображеннями КТ. В архітектурі ResNet-18 застосовується 18 шарів. Автоматична сегментація підшлункової залози та нирок виокремлюється із зображень КТ-сканування із високою точністю. Запропонований метод застосовано на медичній комп'ютерній томографії 82 пацієнтів. 699 зображень і 150 зображень із різними кутами застосовують для навчання та тестування відповідно. ResNet-18 досягає значення індексу подібності кубиків до 98,29±0,63, значення індексу Жакара до — 96,63±01,25, значення Bfscore — до 84,65±03,96. Точність валідації запропонованого методу становить 97,01%, а значення коефіцієнта втрат досягає 0,0010. Проблема дисбалансу класу вирішується за допомогою ваги класу та збільшення даних.

Ключові слова: глибоке навчання, коефіцієнт кубиків, повністю підключений шар (FCN), залишкова мережа (ResNet-18), група візуальної геометрії (VGG).

MODELLING NEGATIVE THERMOMECHANICAL EFFECTS IN REINFORCED ROAD STRUCTURES WITH THERMOELASTIC INCOMPATIBILITY OF COATING AND REINFORCEMENT MATERIALS

V.I. GULYAYEV, V.V. MOZGOVYI, N.V. SHLYUN, L.V. SHEVCHUK

Abstract. The phenomena of the formation of local defects and cracks in asphalt concrete pavements of roads and bridges are most often observed in climatic zones with large temperature differences during their seasonal and daily changes. To a large extent, this is due to the heterogeneity of the thermomechanical properties of the materials of the coating layers and the base. To prevent these phenomena, reinforcing rods and meshes are introduced into the coating structure. In this work, using the theory of thermoelasticity, it is shown by the method of mathematical modelling that in cases of incompatibility of the thermomechanical characteristics of asphalt concrete materials and reinforcement, additional localized thermal stresses arise in its small vicinity, which, even at moderate temperatures, can reach critical values and lead to local defects and cracks. Since these defects are latent, they cannot always be detected in practice. The presented results of analytic calculation validated these conclusions. They can be used in both road building and composite design.

Keywords: reinforced asphalt concretes, thermomechanical incompatibility, mathematical modelling, destruction prevention.

INTRODUCTION

The strength and durability of the roadway is largely determined by the intensity of traffic loads and the impact of climatic conditions. Noticeable destruction of road surfaces, bridges, tunnels and dams, as well as other infrastructure facilities in climatic zones with large temperature differences, as a rule, occurs during off-season periods, accompanied by high temperature gradients.

Among the most common types of thermal destruction of the roadway is the appearance of transverse cracks in it, caused by the limiting values of longitudinal stresses at low negative temperatures in the conditions of the impossibility of free shortening of the upper layers. To avoid this effect, so-called "unloading expansion joints" and reinforcement (longitudinal, mesh, etc.) are introduced into the road structure. Such a general strengthening of the roadway with reinforcement leads to an increase in its overall strength, a reduction of deformability, an enlargement of durability, and a decrease in the cost of repair work.

In the theoretical analysis of the effect of reinforcement on the structural strength and the study of the general thermomechanical properties of reinforced (composite) materials and road coatings, the reduced (effective) values of the parameters of combined systems containing inclusions in the form of particles, fibers or rods are mainly determined [4, 6]. In these cases, mainly, models of homogeneous and inhomogeneous spherical particles, including those coated with shell layers, are considered [4]. The cases of ordered [2] and stochastic [10] placement of grains of these particles are singled out, and the reduced values of Young's modulus, Poisson's ratio, thermal conductivity coefficient, and thermal expansion coefficient of the entire system are calculated for them.

Very complex processes of thermal deformation and thermal destruction are observed in the structures of asphalt concrete pavements of roads and bridges [3, 9, 13, 16, 17, 19, 20]. The issues of determining the reduced thermomechanical characteristics of asphalt concrete materials reinforced with particles, fibers and rods are considered in publications [5, 7, 12, 14]. Here, however, these tasks become more complicated, since it is possible to create materials with directional (anisotropic) properties.

In addition, it should be noted that the insertion of reinforcing inclusions from another material into one material can not only improve the generalized characteristics of the entire composite, but under thermal effects it can also be accompanied by the generation of noticeable additional local internal thermal stresses if the thermomechanical characteristics of the composite components are incompatible. For plastic materials, these stresses can lead to local plastic deformations and defects; for brittle materials, to local cracking. Since these defects are localized and latent, they are not always detectable. Therefore, the problem of their theoretical forecasting seems to be relevant.

To simulate these effects, in this work, on the basis of the theory of thermoelasticity, the problem is posed of a planar thermally deformed state of an elastic medium containing an elastic rod of a circular cross section with different thermomechanical parameters. For the case of a change in the temperature of the system by a constant value, an analytical solution of the constitutive equations is constructed, expressions for thermal deformations and thermal stresses are obtained. The general regularities of possible negative influence of the thermomechanical incompatibility of the system parameters on the internal fields of the additional stresses are found. It has been established that the maximum thermal stresses in the medium are realized on the surface of its contact with an elastic inclusion, and they decrease along the radial coordinate in proportion to the square of the distance to the rod axis. The conditions for thermomechanical compatibility of the properties of the medium and the rod are formulated, under which there are no additional thermal stresses in the system. It is shown that in a system with incompatible parameters, additional thermal stresses can be decreased by reducing the radial rigidity of the inclusion through insertion a cylindrical cavity into it.

STATEMENT OF THE PROBLEM

Let us formulate the problem of stationary thermal deformation of an infinite elastic medium 2 (matrix), which is reinforced with rod 1 of circular cross section of radius r_1. Fig. 1 shows a fragment of this system.

Let's use a cylindrical coordinate system $Or\varphi z$, axis Oz of which coincides with the axis of the rod. Let the thermomechanical characteristics of rod 1 and medium 2 be determined, respectively, by the Lame parameters λ_1, μ_1 and λ_2, μ_2 and coefficients of thermal linear expansion α_1 and α_2. The temperature of the system changes steadily by the value ΔT. Let us single out the case when the thermoelastic relative strains $\varepsilon_z^{(i)}(r,\varphi,z)$ of the bodies $i=1,2$ along the Oz axis are equal to zero and the system is in a plane axisymmetric thermally deformed state, described by the equilibrium equations [1, 8, 11, 15, 18]

$$\frac{d\sigma_r^{(i)}}{dr}+\frac{\sigma_r^{(i)}-\sigma_\varphi^{(i)}}{r}=0, \quad (i=1,2),\tag{1}$$
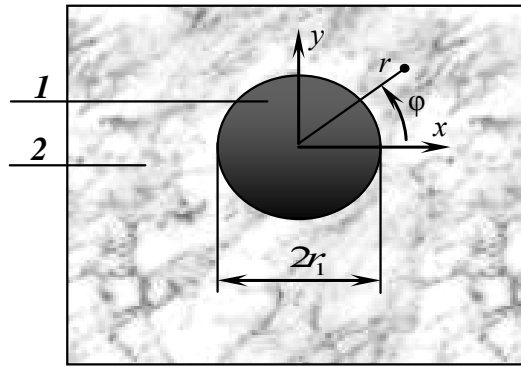
Fig. 1. Planar fragment of an elastic medium with a rod inclusion

where $\sigma_r^{(i)}$, $\sigma_\varphi^{(i)}$ are the normal radial and circumferential stresses of bodies 1 and 2 on the respective areas $r=\text{const}$ and $\varphi=\text{const}$. Let us express normal thermal stresses in terms of strains $\varepsilon_r^{(i)}$, $\varepsilon_\varphi^{(i)}$, $\varepsilon_z^{(i)}$:

$$\sigma_r^{(i)}(r)=(\lambda_i+2\mu_i)\varepsilon_r^{(i)}+\lambda_i(\varepsilon_\phi^{(i)}+\varepsilon_z^{(i)})-(3\lambda_i+2\mu_i)\lambda_i\Delta T\,;$$

$$\sigma_\phi^{(i)}(r)=(\lambda_i+2\mu_i)\varepsilon_\phi^{(i)}+\lambda_i(\varepsilon_r^{(i)}+\varepsilon_z^{(i)})-(3\lambda_i+2\mu_i)\alpha_i\Delta T\,;$$

$$\sigma_z^{(i)}(r)=(\lambda_i+2\mu_i)\varepsilon_z^{(i)}+\lambda_i(\varepsilon_r^{(i)}+\varepsilon_\phi^{(i)})-(3\lambda_i+2\mu_i)\alpha_i\Delta T,\quad (i=1,2).\tag{2}$$

Next, we take into account that $\varepsilon_z^{(i)}(r,\varphi,z)=0$. Then expressions (2) will be simplified

$$\sigma_r^{(i)}(r)=(\lambda_i+2\mu_i)\varepsilon_r^{(i)}+\lambda_i\varepsilon_\varphi^{(i)}-(3\lambda_i+2\mu_i)\alpha_i\Delta T;$$

$$\sigma_\phi^{(i)}(r)=(\lambda_i+2\mu_i)\varepsilon_\phi^{(i)}+\lambda_i\varepsilon_r^{(i)}-(3\lambda_i+2\mu_i)\alpha_i\Delta T;\tag{3}$$

$$\sigma_z^{(i)}(r)=\lambda_i(\varepsilon_r^{(i)}+\varepsilon_\phi^{(i)})-(3\lambda_i+2\mu_i)\alpha_i\Delta T,\quad (i=1,2).$$

The deformations used in (3) depend on the radial displacement $u(r)$:

$$\varepsilon_r^{(i)}(r)=\frac{\partial u^{(i)}}{\partial r},\quad \varepsilon_\varphi^{(i)}(r)=\frac{u^{(i)}}{r},\quad (i=1,2).\tag{4}$$

Taking into account (3), (4), equation (1) is reduced to the form

$$\frac{d^2 u^{(i)}}{dr^2} + \frac{1}{r}\frac{du^{(i)}}{dr} - \frac{1}{r^2}u^{(i)} = 0 \tag{5}$$

for each body $i = 1,2$.

Let us represent equation (5) in a more compact form:

$$\frac{d}{dr}\left[\frac{1}{r}\frac{d}{dr}(ru^{(i)})\right] = 0, \quad (i=1,2). \tag{6}$$

Integrating the left side of equation (6) twice over r, get his solutions

$$u^{(1)}(r) = rC_1 + \frac{1}{r}C_2 \text{ at } i=1;$$

$$u^{(2)}(r) = rC_3 + \frac{1}{r}C_4 \text{ at } i=2. \tag{7}$$

The unknown constants C_i $(i=\overline{1,4})$ included here are determined from the boundary conditions and the contact equation for $r = r_1$:

$$u^{(0)}(0) = 0; \tag{8}$$

$$u_r^{(1)}(r_1) = u_r^{(2)}(r_1); \tag{9}$$

$$\sigma_r^{(1)}(r_1) = \sigma_r^{(2)}(r_1); \tag{10}$$

$$\sigma_r^{(2)}(r) \to 0 \text{ at } r \to \infty. \tag{11}$$

Condition (8) implies

$$C_2 = 0.$$

Using equalities (7), we express the strains and stresses of bodies 1 and 2 in terms of C_i $(i=1,3,4)$:

$$\varepsilon_r^{(1)}(r) = C_1, \quad \varepsilon_\varphi^{(1)}(r) = C_1; \quad \varepsilon_r^{(2)}(r) = C_3 - \frac{1}{r^2}C_4, \quad \varepsilon_\varphi^{(2)}(r) = C_3 + \frac{1}{r^2}C_4;$$

$$\sigma_r^{(1)}(r) = 2(\lambda_1 + \mu_1)C_1 - (3\lambda_1 + 2\mu_1)\alpha_1\Delta T; \tag{12}$$

$$\sigma_r^{(2)}(r) = 2(\lambda_2 + \mu_2)C_3 - \frac{2\mu_2}{r_1^2}C_4 - (3\lambda_2 + 2\mu_2)\alpha_2\Delta T.$$

Condition (11) and the last equality of system (12) imply:

$$C_3 = \frac{3\lambda_2 + 2\mu_2}{2(\lambda_2 + \mu_2)}\alpha_2\Delta T.$$

Constants C_1 and C_4 are found from the system of equations (9), (10) transformed taking into account equalities (12),

$$C_1 = \frac{[(3\lambda_1 + 2\mu_1)(\lambda_2 + \mu_2)\alpha_1 + (3\lambda_2 + 2\mu_2)\mu_2\alpha_2]\Delta T}{2(\lambda_1 + \mu_1 + \mu_2)(\lambda_2 + \mu_2)},$$

$$C_4 = \frac{r_1^2[(3\lambda_1 + 2\mu_1)(\lambda_2 + \mu_2)\alpha_1 - (3\lambda_2 + 2\mu_2)(\lambda_1 + \mu_1)\alpha_2]\Delta T}{2(\lambda_1 + \mu_1 + \mu_2)(\lambda_2 + \mu_2)}.$$

Knowing constants C_i $(i = \overline{1,4})$, find the displacement functions:

$$u^{(1)}(r) = \frac{r[(3\lambda_1 + 2\mu_1)(\lambda_2 + \mu_2)\alpha_1 + (3\lambda_2 + 2\mu_2)\mu_2\alpha_2]\Delta T}{2(\lambda_1 + \mu_1 + \mu_2)(\lambda_2 + \mu_2)}, \quad (0 \le r \le r_1),$$

$$u^{(2)}(r) = r\frac{(3\lambda_1 + 2\mu_2)}{2(\lambda_2 + \mu_2)}\alpha_2\Delta T +$$

$$+ \frac{r_1^2[(3\lambda_1 + 2\mu_1)(\lambda_2 + \mu_2)\alpha_1 - (3\lambda_2 + 2\mu_2)(\lambda_1 + \mu_1)\alpha_2]\Delta T}{2(\lambda_1 + \mu_1 + \mu_2)(\lambda_2 + \mu_2)}, \quad (r \ge r_1).$$

Note that in the equation for $u^{(2)}(r)$ the first term is the radial displacement in a homogeneous medium 2 in the absence of rod 1, the second term is due to the influence of body 1. It decreases in proportion to radius r.

We also give expressions for the stresses in rod 1:

$$\sigma_r^{(1)}(r) = \sigma_\phi^{(1)} = -\frac{\mu_2[(3\lambda_1 + 2\mu_1)(\lambda_2 + \mu_2)\alpha_1 - (3\lambda_2 + 2\mu_2)(\lambda_1 + \mu_1`)\alpha_2]\Delta T}{(\lambda_1 + \mu_1 + \mu_2)(\lambda_2 + \mu_2)};$$

$$\sigma_z^{(1)}(r) =$$

$$= \frac{[-(3\lambda_1 + 2\mu_1)(\lambda_2 + \mu_2)(\mu_1 + \mu_2)\alpha_1 + (3\lambda_2 + \mu_2)\lambda_1\mu_2\alpha_2]\Delta T}{(\lambda_1 + \mu_1 + \mu_2)(\lambda_2 + \mu_2)}, \quad (0 \le r \le r_1) \quad (13)$$

and in medium 2:

$$\sigma_r^{(2)}(r) = -\frac{r_1^2}{r^2}\frac{\mu_2[(3\lambda_1 + 2\mu_1)(\lambda_2 + \mu_2)\alpha_1 - (3\lambda_2 + 2\mu_2)(\lambda_1 + \mu_1)\alpha_2]\Delta T}{(\lambda_1 + \mu_1 + \mu_2)(\lambda_2 + \mu_2)};$$

$$\sigma_\phi^{(2)}(r) = \frac{r_1^2}{r^2}\frac{\mu_2[(3\lambda_1 + 2\mu_1)(\lambda_2 + \mu_2)\alpha_1 - (3\lambda_2 + 2\mu_2)(\lambda_1 + \mu_1)\alpha_2]\Delta T}{(\lambda_1 + \mu_1 + \mu_2)(\lambda_2 + \mu_2)};$$

$$\sigma_z^{(2)}(r) = -\frac{\mu_2(3\lambda_2 + 2\mu_2)}{(\lambda_2 + \mu_2)}\alpha_2\Delta T, \quad (r \ge r_1). \quad (14)$$

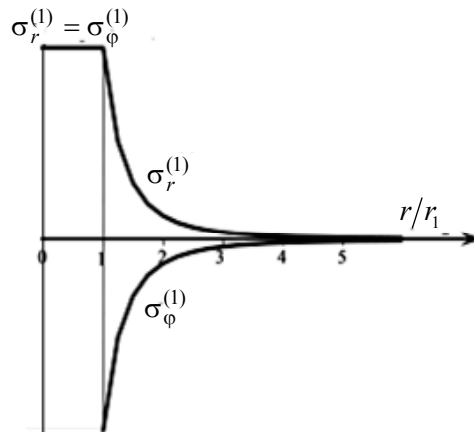Graphs of these functions are shown in Fig. 2. They indicate that additional

Fig. 2. Graphs of the thermal stresses distribution in the plane of the axial section of the reinforced system under planar thermal deformation

thermal stresses $\sigma_r^{(2)}(r)$, $\sigma_\phi^{(2)}(r)$, caused by the inclusion of reinforcing rod 1 into medium 2, are local in nature and decrease in proportion to the square of the radial coordinate. In addition, they are equal to each other in absolute value and differ in signs, which depend on the ratio of quantities α_1 and α_2. So if $\alpha_1 > \alpha_2$, then, as follows from the form of the numerators of formula (14) with $\Delta T > 0$, $\alpha_1 > \alpha_2$, there are inequalities $\sigma_r^{(2)}(r) < 0$, $\sigma_\phi^{(2)}(r) > 0$, and if $\alpha_1 < \alpha_2$, then vice versa, $\sigma_r^{(2)}(r) > 0$, $\sigma_\phi^{(2)}(r) < 0$. This means that, since asphalt concrete has a lower tensile strength than compressive strength, under any temperature ΔT changes, unfavorable thermal stresses will be realized for $\sigma_r^{(2)}(r)$ or $\sigma_\phi^{(2)}(r)$.

It is also obvious that the values of thermomechanical parameters, at which the numerators of fractions (14) of functions $\sigma_r^{(2)}(r), \sigma_\phi^{(2)}(r)$ are zero, are thermally compatible. Therefore, equality

$$(3\lambda_1 + 2\mu_1)(\lambda_2 + \mu_2)\alpha_1 - (3\lambda_2 + 2\mu_2)(\lambda_1 + \mu_1)\alpha_2 = 0 \tag{15}$$

represents a condition for the compatibility of the thermomechanical parameters of the matrix and the reinforcing rod.

Condition (15) can be simplified if to replace the Lame parameters λ and μ with modulus of elasticity E and Poisson's ratio υ, using formulas

$$\lambda = \frac{E\upsilon}{(1+\upsilon)(1-2\upsilon)}; \quad \mu = \frac{E}{2(1+\upsilon)}.$$

Then, instead of (15) we have a simpler record of this condition

$$\frac{\alpha_1}{1+\upsilon_2} = \frac{\alpha_2}{1+\upsilon_1}.$$

As an example, consider the case when a fiberglass reinforcing rod of radius r_1 with thermomechanical parameters $\lambda_1 = 30.2\,\text{GPa}$, $\mu_1 = 12.9\,\text{GPa}$, $\alpha_1 = 21 \cdot 10^{-6}\,\text{K}^{-1}$ is located in an asphalt concrete medium with parameters $\lambda_2 = 1.39$ GPa, $\mu_2 = 2.08$ GPa, $\alpha_2 = 10 \cdot 10^{-6}\,\text{K}^{-1}$. It is accepted that $\Delta T = -20°\text{K}$. With these data, the thermal stresses in the system amounted to

$\sigma_r^{(1)} = \sigma_\phi^{(1)} = 1.298$ MPa, $\sigma_z^{(1)} = 15.541$ MPa, $\sigma_r^{(2)} = 1.298\dfrac{r_1^2}{r^2}$ MPa,

$\sigma_z^{(2)} = -1.298\dfrac{r_1^2}{r^2}$ MPa, $\sigma_z^{(2)} = 0.9986$ MPa.

If we take into account that the ultimate strength of asphalt concrete in compression is $5 \div 20$ MPa, and in tension it turns out to be several times less than these values, then we can conclude that under the considered conditions, additional thermal stresses in asphalt concrete, caused by the insertion of a fiberglass reinforcing rod into it, can lead to the occurrence of local defects in its small neighbourhood.

REDUCING THE LEVEL OF ADDITIONAL THERMAL STRESSES ON TUBULAR REINFORCING RODS

As can be seen from equalities (13), (14), additional stresses $\sigma_r^{(i)}$, $\sigma_\phi^{(i)}$ $(i = 1, 2)$ are determined not only by the values of coefficients α_1, α_2, but also by elasticity parameters λ_i, μ_i $(i = 1, 2)$, which are included in the numerators of fractions (13), (14) in the third powers, and in the denominators — in the second ones. Therefore, additional thermal stresses in the system increase with increasing λ_i, μ_i $(i = 1, 2)$ or, for example, with an increase in the radial rigidity of rod 1 (while maintaining its axial strength and rigidity). Conversely, they decrease as this stiffness decreases. Given this property, we can propose to use tubular rods as reinforcement in asphalt concrete pavements (Fig. 3). Let us investigate the thermally stressed state in this case. Let r_1 and r_2 be the inner and outer radii of pipe 1, respectively, the dimensions of medium 2 are unlimited. Let us assume, as above, that λ_i, μ_i, α_i $(i = 1, 2)$ be the thermomechanical parameters of bodies 1 and 2, ΔT — difference in body temperature in the initial and final states. Let us find the functions of thermal stresses in the system for the case of its axisymmetric planar thermally deformed state.
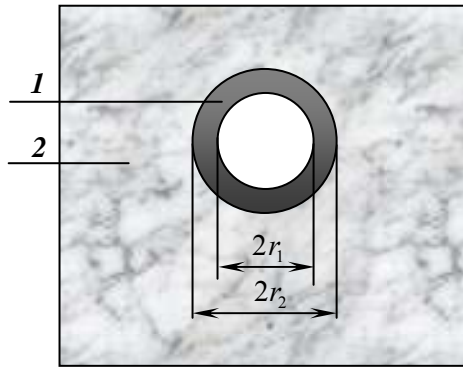
Fig. 3. Planar fragment of an elastic medium with a tubular inclusion

Similarly to the case of a solid rod, the equations of thermoelasticity of the system have form (1) – (6). The solution of these equations is again formulated in the form of functions of radial displacements of body 1

$$u_1(r) = rC_1 + \frac{1}{r}C_2 \quad (r_1 \le r \le r_2),$$

and for medium 2

$$u_2(r) = rC_3 + \frac{1}{r}C_4 \quad (r \ge r_2).$$

At the same time, constants C_i $(i = \overline{1,4})$ are found from the conditions:

$$\sigma_r^{(1)}(r_1) = 0; \quad u^{(1)}(r_2) = u^{(2)}(r_2);$$

$$\sigma_r^{(1)}(r_2) = \sigma_r^{(2)}(r_2); \quad \sigma_r^{(2)}(r) \to 0 \quad \text{at } r \to \infty.$$

After appropriate substitutions, these equations are reduced to the form:

$$2(\lambda_1 + \mu_1)C_1 - \frac{2\mu_1}{r_1^2}C_2 - (3\lambda_1 + 2\mu_1)\alpha_1\Delta T = 0;$$

$$C_1 + \frac{1}{r_2^2}C_2 - C_3 - \frac{1}{r_2^2}C_4 = 0;$$

$$2(\lambda_1 + \mu_1)C_1 - \frac{2\mu_1}{r_2^2}C_2 - (3\lambda_1 + 2\mu_1)\alpha_1\Delta T -$$

$$-2(\lambda_2 + \mu_2)C_3 + \frac{2\mu_2}{r_2^2}C_4 + (3\lambda_2 + 2\mu_2)\alpha_2\Delta T = 0;$$

$$2(\lambda_2 + \mu_2)C_3 - (3\lambda_2 + 2\mu_2)\alpha_2\Delta T = 0. \tag{16}$$

From the last equation of this system, we obtain

$$C_3 = \frac{(3\lambda_2 + 2\mu_2)}{2(\lambda_2 + \mu_2)}\alpha_2\Delta T.$$

Next, from the remaining equations of system (16) we find:

$$C_1 = \frac{\mu_1}{r_1^2}\frac{[-(3\lambda_1 + 2\mu_1)(\lambda_2 + \mu_2)\alpha_1 + (3\lambda_2 + 2\mu_2)(\lambda_1 + \mu_1)\alpha_2]\Delta T}{2(\lambda_1 + \mu_1)^2(\lambda_2 + \mu_2)\left[\dfrac{\mu_1}{r_1^2(\lambda_1 + \mu_1)} + \dfrac{1}{r_2^2} + \dfrac{\mu_1}{\mu_2}\left(\dfrac{1}{r_1^2} - \dfrac{1}{r_2^2}\right)\right]} +$$

$$+ \frac{(3\lambda_1 + 2\mu_1)}{2(\lambda_1 + \mu_1)}\alpha_1\Delta T;$$

$$C_2 = \frac{[-(3\lambda_1 + 2\mu_1)(\lambda_2 + \mu_2)\alpha_1 + (3\lambda_2 + 2\mu_2)(\lambda_1 + \mu_1)\alpha_2]\Delta T}{2(\lambda_1 + \mu_1)(\lambda_2 + \mu_2)\left[\dfrac{\mu_1}{r_1^2(\lambda_1 + \mu_1)} + \dfrac{1}{r_2^2} + \dfrac{\mu_1}{\mu_2}\left(\dfrac{1}{r_1^2} - \dfrac{1}{r_2^2}\right)\right]};$$

$$C_4 = \frac{r_2^2\mu_1}{\mu_2}\left(\frac{1}{r_1^2} - \frac{1}{r_2^2}\right)\frac{[(3\lambda_1 + 2\mu_1)(\lambda_2 + \mu_2)\alpha_1 - (3\lambda_2 + 2\mu_2)(\lambda_1 + \mu_1)\alpha_2]\Delta T}{2(\lambda_1 + \mu_1)(\lambda_2 + \mu_2)\left[\dfrac{\mu_1}{r_1^2(\lambda_1 + \mu_1)} + \dfrac{1}{r_2^2} + \dfrac{\mu_1}{\mu_2}\left(\dfrac{1}{r_1^2} - \dfrac{1}{r_2^2}\right)\right]}.$$

Using the found constants, you can build expressions for displacements

$$u(r) = rC_1 + \frac{1}{r}C_2, \ (r_1 \le r \le r_2); \quad u(r) = rC_3 + \frac{1}{r}C_4, \ (r \ge r_2)$$

and stresses

$$\sigma_r^{(1)}(r) = 2(\lambda_1 + \mu_1)C_1 - \frac{2\mu_1}{r^2}C_2 - (3\lambda_1 + 2\mu_1)\alpha_1\Delta T;$$

$$\sigma_\phi^{(1)}(r) = 2(\lambda_1 + \mu_1)C_1 + \frac{2\mu_1}{r^2}C_2 - (3\lambda_1 + 2\mu_1)\alpha_1\Delta T;$$

$$\sigma_z^{(1)}(r) = 2\lambda_1 C_1 - (3\lambda_1 + 2\mu_1)\alpha_1\Delta T, \quad (r_1 \le r \le r_2)$$

in rod 1 and

$$\sigma_r^{(2)}(r) = -\frac{2\mu_2}{r^2}C_4; \quad \sigma_\phi^{(2)}(r) = -\frac{2\mu_1}{r^2}C_2;$$

$$\sigma_z^{(2)}(r) = 2\lambda_2 C_3 - (3\lambda_2 + 2\mu_2)\alpha_2\Delta T, \ (r \ge r_1)$$

in medium 2.

Table shows the stress values $\sigma_r^{(1)}$, $\sigma_\phi^{(1)}$, $\sigma_z^{(1)}$ on surfaces $r = r_1$ and $r = r_2$ of fiberglass body 1 and stresses $\sigma_r^{(2)}$, $\sigma_\phi^{(2)}$, $\sigma_z^{(2)}$ on surface $r = r_2$ of asphalt

concrete medium 2 for relations $r_1 / r_2 = 0.5, 0.75,$ and 0.9 at the values of the thermomechanical parameters given above and the temperature difference $\Delta T = -20$ K.

Values of thermal stresses in the medium reinforced with a tubular rod

Types of thermal stresses	r_1 / r_2			
	0.0	0.5	0.75	0.9
$\sigma_r^{(1)}(r_1)$ MPa	1.2981	0	0	0
$\sigma_\phi^{(1)}(r_1)$ MPa	1.2981	3.2455	4.5766	7.3764
$\sigma_z^{(1)}(r_1)$ MPa	15.541	15.569	16.235	17.215
$\sigma_r^{(1)}(r_2)$ MPa	1.2981	1.2171	1.0011	0.7008
$\sigma_\phi^{(1)}(r_2)$ MPa	1.2981	2.0285	3.5742	6.6752
$\sigma_z^{(1)}(r_2)$ MPa	15.541	15.569	16.235	17.215
$\sigma_r^{(2)}(r_2)$ MPa	1.2981	1.2171	1.0011	0.7008
$\sigma_\phi^{(2)}(r_2)$ MPa	-1.2981	-1.2171	-1.0011	-0.7008
$\sigma_z^{(2)}(r_2)$ MPa	0.9986	0.9986	0.9986	0.9986

The question of the distribution in the radial direction of additional thermal stresses $\sigma_r^{(i)}(r)$, $\sigma_\phi^{(i)}(r)$ deserves a special interest. Fig. 4 shows the graphs of these functions for case $r_1 / r_2 = 0.75$.
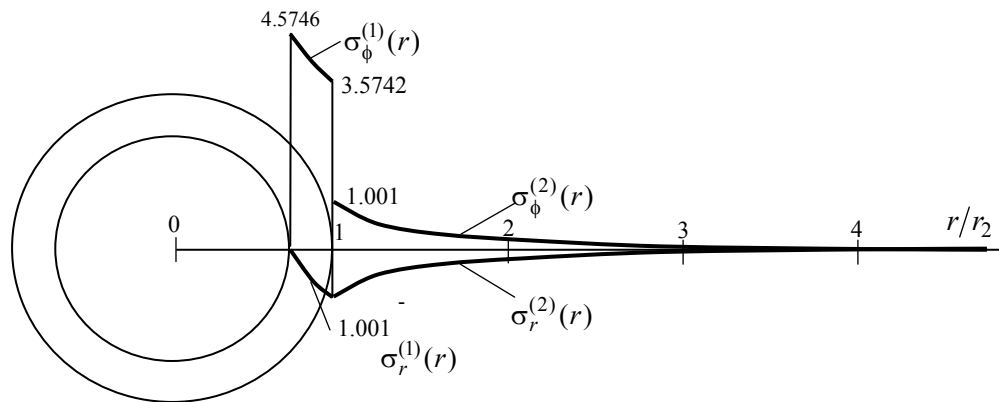
Fig. 4. Graphs of distribution of thermal stresses $\sigma_r^{(i)}(r)$, $\sigma_\phi^{(i)}(r)$ (MPa) for case $r_1 / r_2 = 0,75$

As can be seen, additional thermal stresses $\sigma_r^{(2)}(r)$, $\sigma_\phi^{(2)}(r)$ in the asphalt concrete have the highest values on the contact surface $r = r_2$ and they decrease rapidly in the radial direction.

An analysis of the above results indicates that the replacement of a solid reinforcing rod with a tubular one leads to a noticeable decrease in additional local thermal stresses in the matrix medium, although the thermal stresses in the rod increase somewhat. This effect becomes more noticeable as the thickness of the tube rod decreases.

CONCLUSION

1. The problem associated with the modelling of the formation of additional thermal stresses, defects and destructions in the medium of an asphalt concrete pavement with the insertion of a reinforcing rod into it is considered. On the basis of thermoelasticity methods, the system of differential equations is formed for a plane axisymmetric deformed state of an infinite cylindrical elastic body in an infinite elastic medium under condition of a change in the temperature of the system.

2. An analytical solution of the formulated equations is constructed in a closed form, which determines the additional thermal displacements, additional strains and stresses in the system. It is shown that additional thermal stresses have the highest values on the contact surface of the reinforcing rod and the coating array and decrease in inverse proportion to the square of the distance from this surface. It has been established that the values of these stresses enlarge with an increase in the thermomechanical incompatibility of the system materials and the radial stiffness of the rod. On the example of asphalt concrete reinforced with a fiberglass rod, it was demonstrated that even with moderate temperature changes, additional thermal stresses in asphalt concrete can reach critical values.

3. A method is proposed for reducing additional thermal stresses by reducing the radial stiffness of the reinforcement by replacing a solid rod with a hollow tube. Theoretical modelling of this effect showed that with a decrease in the tube wall thickness, the decrease in additional contact thermal stresses in asphalt concrete becomes significant.

REFERENCES

1. T.G. Beleicheva and K.K. Ziling, "Thermoelastic axisymmetric problem for a two-layer cylinder", *J. Appl. Mech. Technical Physics*, **19**, pp. 108–113, 1978.
2. Boubaker Fetiza Ali, Khedoudja Soudani, and Smail Haddadi, "Effect of waste plastic and crumb rubber on the thermal oxidative ageing of modified bitumen", *Road Mat. and Pav.*, vol. 23, issue 1, pp. 222–233, Dec. 2022.
3. Brian Hill et al., "Evaluation of low temperature viscoelastic properties and fracture behavior of bio-asphalt mixtures", *International Journal of Pavement Engineering*, vol. 19, issue 4, pp. 362–369, 2018.
4. R.M. Christensen and K.H. Lo, "Solutions for effective shear properties in three-phase sphere and cylinder models", *J. Mech. Phys. Solids.*, vol. 27, pp. 315–330, 1979.
5. Christian Karch, "Micromechanical analysis of thermal expansion coefficient", *Modeling and Numerical Simulation of Material Science*, vol. 3, pp. 1–15, 2014.
6. R.M. Christiansen, *Mechanics of Composite Materials*. Wiley: New York, NY, USA, 1979.
7. Gholamali Shafabakhsh, Mohammadreza Aliakbari Bidokhti, and Hassan Divandan, "Evaluation of the performance of SBS/Nano-Al2O3 composite-modified bitumen at high temperature", *Road Mat. and Paves*, vol. 22(11), pp. 2523–2537, 2021.
8. R.B. Hetnarski and J. Ignaczak, *Mathematical Theory of Elasticity*. New York: Taylor and Francis, 2004.
9. Jorge Pais et al., "The adjustment of pavement deflections due to temperature variations", *International Journal of Pavement Engineering*, vol. 21, issue 13, pp. 1585–1594, 2020.
10. J.W. Ju and T.M. Chen, "Effective elastic moduli of two-phase composites containing randomly dispersed spherical inhomogeneities", *Acta Mech.*, 103(1), pp. 123–144, 1994.
11. A.D. Kovalenko, *Thermoelasticity: Basic Theory and Applications*. The Netherlands: Wolters-Noordhoff Groningen, 1972.
12. Marcela Fiedlerova, Petr Jisa, and Kamil Stepanek, "Using various thermal analytical methods for bitumen characterization", *International Journal of Pavement Research and Technology*, vol. 14, issue 4, pp. 459–465, 2021.

13. Md Amanul Hasan and Rafiqul A. Tarefder, "Development of temperature zone map for mechanistic empirical (ME) pavement design", *Journal of Pavement Research and Technology*, vol. 11, issue 1, pp. 99–111, 2018.

14. Mirosław Graczyk, Józef Rafa, and Adam Zofka, "Pavement modelling using mechanical and thermal homogenization of layered systems", *Roads and Bridges - Drogi i Mosty*, 17(2), pp. 141–157, 2018.

15. W. Nowacki, *Thermoelasticity*; 2 nd ed. Oxford: PWN – Polish Scientific Publishers, Warsaw and Pergamon Press, 1986.

16. Dian M. Setiawan, "The role of temperature differential and subgrade quality on stress, curling, and deflection behavior of rigid pavement", *Journal of the Mechanical Behavior of Materials*, vol. 29, issue 5–6, id.10, 12 p.

17. Tarn Minh Phan, Tri Ho Minh Le, and Dae-Wook Park, "Evaluation of cracking resistance of healed warm mix asphalt based on air-void and binder content", *Road Materials and Pavement Design*, vol. 23, issue 1, pp. 47–61, 2022.

18. D.E. Carlson, "Thermoelasticity", in *Truesdell C. (ed) Encyclopedia of physics*, vol. Vla/2: mechanics of solids, Springer, Berlin, 1972.

19. Yang Liu, Zhendong Qian, and Dong Zheng, "Meng Zhang Interlaminar thermal effect analysis of steel bridge deck pavement during gussasphalt mixture paving", *International Journal of Pavement Engineering*, vol. 20, issue 11, pp. 1323–1335, 2019.

20. Yingjun Jiang, Changqing Deng, Zhejiang Chen, and Yuhang Tian, "Evaluation of the cooling effect and anti-rutting performance of thermally resistant and heat-reflective pavement", *International Journal of Pavement Engineering*, vol. 21, issue 4, pp. 447–456, 2020.

INFORMATION ON THE ARTICLE

Valery I. Gulyayev, ORCID: 0000-0002-5388-006X, National Transport University, Ukraine, e-mail: valery@gulyayev.com.ua

Volodymyr V. Mozgovyy, ORCID: 0000-0002-1032-8048, National Transport University, Ukraine, e-mail: mozgoviy@gmail.com

Nataliia V. Shlyun, ORCID: 0000-0003-1040-8870, National Transport University, Ukraine, e-mail: nataliyashlyun@gmail.com

Lyudmyla V. Shevchuk, ORCID: 0000-0002-5748-9527, National Transport University, Ukraine, e-mail: ludmilashevchuk25@gmail.com

НЕГАТИВНІ ТЕРМОМЕХАНІЧНІ ЕФЕКТИ В АРМОВАНИХ ДОРОЖНІХ КОНСТРУКЦІЯХ ЗА ТЕРМОПРУЖНОЇ НЕСУМІСНОСТІ МАТЕРІАЛІВ ПОКРИТТЯ ТА АРМАТУРИ / В.І. Гуляєв, В.В. Мозговий, Н.В. Шлюнь, Л.В. Шевчук

Анотація. Явища утворення локальних дефектів і тріщин в асфальтобетонних покриттях автомобільних доріг та мостів найчастіше спостерігаються у кліматичних зонах з великими перепадами температур за їх сезонних та добових змін. Значною мірою це зумовлено неоднорідністю термомеханічних властивостей матеріалів шарів покриттів та основи. Для попередження цих явищ в конструкції покриттів уводять армувальні стрижні і сітки. У роботі методами теорії термопружності показано, що у випадках несумісності термомеханічних характеристик матеріалів асфальтобетону та арматури в її малому околі виникають додаткові локалізовані термонапруження, які навіть за помірних значень перепадів температури можуть досягати критичних значень та призводити до локальних дефектів і тріщин. Оскільки ці дефекти мають прихований характер, їх не завжди можна виявляти.

Ключові слова: асфальтобетонне покриття, стрижнева арматура, термомеханічна несумісність, концентрація термонапруг.

RESEARCH OF AUTOENCODER-BASED USER BIOMETRIC VERIFICATION WITH MOTION PATTERNS

M.P. HAVRYLOVYCH, V.Y. DANYLOV

Abstract. In the current research, we continue our previous study regarding motion-based user biometric verification, which consumes sensory data. Sensory-based verification systems empower the continuous authentication narrative – as physiological biometric methods mainly based on photo or video input meet a lot of difficulties in implementation. The research aims to analyze how various components of sensor data from an accelerometer affect and contribute to defining the process of unique person motion patterns and understanding how it may express the human behavioral patterns with different activity types. The study used the recurrent long-short-term-memory autoencoder as a baseline model. The choice of model was based on our previous research. The research results have shown that various data components contribute differently to the verification process depending on the type of activity. However, we conclude that a single sensor data source may not be enough for a robust authentication system. The multimodal authentication system should be proposed to utilize and aggregate the input streams from multiple sensors as further research.

Keywords: motion patterns recognition, biometric verification, recurrent autoencoders.

INTRODUCTION

In the modern world, we strive to automate all the systems and processes but to keep stability, reliability, and trustworthiness of automatization on the highest possible level. Although there are still a lot of use cases, which are impossible to make fully automated due to ethical and other artificial intelligence issues (for example, in the medical area), automated ensuring of the system reliability and stability is critical in many real-world applications. There is a need for advanced monitoring and anomaly detection applications for this purpose. The appliance of such systems is very broad: financial operations, sensors or medical data, security sector, and many others.

All of such systems meet some challenges during development as there is a lot of uncertainty. First, you never know what anomaly data should look like, despite some apparent cases, especially if you have an inlier type of anomaly. Second, all the processes change over time, so the data – and if new data points are not similar to the previous ones – it does not mean they are anomalies. As well, real-world data frequently has a pretty complex structure and is heterogeneous, leading to the inefficiency of classic statistical and machine learning methods.

From the machine learning perspective, it is impossible to apply a classical supervised approach, as in most cases, only regular data examples are available. In this study, we will look at the user motion-based verification problem. In this application, it is not feasible to solve such a problem in a classic supervised man-

ner due to the huge population and inability to compare specific users with all others (as well, there could be personal information concerns). Therefore, only self-supervised or unsupervised approaches may fit for problem solutions.

The research object is motion-based user biometric verification based on sensor data.

The purpose is to research and analyze various components, which affect the result of verification and understanding how sensor data (accelerometer) and its components may express human behavioral patterns with different activity types.

LITERATURE REVIEW

According to [1], biometric data can be physiological: like iris, face, fingerprint, and behavioral: like motion or gate patterns, mouse or keyboard movements, or even both (voice data). For example, in [2], the authors propose interesting approaches for biometric identification systems based on circular kernel principal component analysis, Chebyshev transforms hashing, and Bose–Chaudhuri–Hocquenghem error-correcting codes for ear-based biometrics.

Nevertheless, many biometric-based verification systems are explicit and require specific actions by the person or from an external supervisor. Many biometric approaches utilize computer vision approaches like iris, ear, face, or gate-based, which require a camera sensor. A camera sensor is not convenient for continuous authentication, and for explicit authentication, somebody, for example, should take a photo. Usage of the camera for continuous and implicit authentication may cause problems: it should process a considerable amount of data (video or image streaming), there are issues with saving and processing personal data, and a person may feel uncomfortable as they are constantly watched. On the other hand, the motion-based or mouse/keyboard movement authentication, that can be implicit and be conducted all the time in the background without user intervention, such data is more lightweight, and in most cases do not need additional sensor installation, because most devices already have all the sensors for other purposes.

We can reformulate the motion-based user verification task as a time series classification problem. The anomaly detection on time series data has already been a research topic in many fields. As well, time-series data anomalies, according to [3], have their taxonomy: point outliers, subsequent, and time series. In user verification, the subsequent outliers are of the most significant interest, as we can reformulate the task from a pattern recognition and classification point of view. Worth mentioning that the time series classification task has a lot of applications, besides anomaly detection, especially in the field of motion sensory data.

In [4], we can see the survey on existing machine learning algorithms, both statistical and deep learning, for anomaly detection on univariate time series. In the case of univariate data – deep learning methods do not overperform classic machine learning and statistical methods in the survey. However, for multivariate and heterogeneous time series anomaly detection, according to [5], deep learning methods are the ones with the greatest accuracy. In [6], we can review the comparative study for anomaly detection on multivariate time series for LSTM and CNN-based (Temporal Convolutional Network) architectures, and the CNN-based solution even slightly outperformed the recurrent one. In [7], the CNN-

based and LSTM model are also compared for biometric motion-based verification on various datasets and activity types. The hybrid LSTM-CNN-based neural network was proposed, as it allows to capture of temporal dependencies on more complex features extracted with convolutional layers.

In [4], the authors measures not only predictions quality metrics but the computational time for model training and inference and conclude that amongst all deep learning approaches, the best combination of quality metrics and computational time has an autoencoder-based approach, which is very important in the angle of verification and security to achieve best results with the lowest latency.

In our previous research [8], we conducted a comparative analysis of various types of recurrent autoencoders for user biometric verification. We compared them to classical machine learning algorithms such as Isolation Forest and One-Class SVM. In [9], the authors designed the user personalization and biometric verification system based on geometric concepts on the convex hull. They mentioned the SVM as a state-of-the-art approach (in 2012), but the one which requires a lot of time for training, thus do not fit for on-the-fly verification model training. In our research, One-Class SVM showed the lowest and most unstable performance, though. In contrast, the variational autoencoders showed the best performance; even so, all types of autoencoders provide comparable results.

 It is essential to mention that despite the continuous authentication idea gaining popularity, some research shows that it still underperforms compared to explicit biometric systems. In the [10], authors mention that the multimodel authentication systems are a better choice. It allows achieving the highest level of system robustness, increasing flexibility, and mitigating drawbacks of every verification modality. In [11], authors propose multimodal authentication based on face, motion patterns, and touch stroke. Motion-based authentication systems can also be boosted using multiple sensors [10, 13], such as accelerometers and gyroscopes. The combination of multiple sensory data increases the accuracy of the motion-based authentication system.

It is relevant to note that the deep learning model, especially autoencoder-based, may be used as a single base model for many purposes and may have interesting applications – for example, activity classification, and more exotic things like detecting smoking events [12] or gender of the person [13]. Overall, having a single model for a couple of purposes is a tendency in the modern machine learning and data science field. It allows to reduce the cost and add additional context for every task-specific downstream model appliance at the same time.

In this study, we wanted to continue the in-depth analysis of biometric motion-based user verification and conduct detailed experiments and research regarding how accelerometer motion data and its components describe the person using recurrent autoencoders.

MATERIALS AND METHODS

Based on our previous research [8], we will use the undercomplete autoencoder as a baseline model architecture with recurrent LSTM layers types, as all types of autoencoders (undercomplete, variational, contractive) showed comparable results between each other.

Autoencoder architecture consists of an encoder and decoder. Autoencoders are learned to reconstruct the input data points from some hidden space. Therefore, the optimization task objective is to minimize reconstruction error:

$$E = \sqrt{\sum_{i=1}^{n} \left\| x_i - d_\varphi(e_\theta(x_i)) \right\|} , \qquad (1)$$

where $x_1, \ldots, x_n$ is data rows, d is the decoder, and e is the encoder with some parameters.

In the undercomplete autoencoder type, the data is encoded in lower-dimensional space. Such compression guarantees that the model will not blindly memorize the train set but will learn the proper feature space and data embedding, which later as well can be used for various purposes. The decoder's purpose is to recreate the sample from an encoded example.

The optimization process of encoder and decoder parameters is done with classic backpropagation using gradient descent-based algorithms to minimize (1) [14].

After model training, the decision threshold ε should be set. This threshold will be used at the model inference step: the data points that reconstruction error will be higher than this threshold would be considered anomaly or non-self class, and self otherwise. The threshold setting process is dependent on the use case and varies for different applications. It can be set manually by an expert or some knowledge keeper or automatically based on the error distribution on some predefined dataset.

We will use an autoencoder with LSTM layers. The LSTM layer contains cells with specific internal structures. The memory cell contains three gates: input, output, and forget. The input controls the input activations when the output controls the output flow. The forget gate controls what information memory cells should forget and what to pass further through the network, which theoretically may solve the problems of long sequences, which is a known problem for vanilla recurrent neural networks, which fail to learn from big sequences [15].

EXPERIMENTS

Dataset: open-source dataset [16] with accelerometer data (52 Hz) from 15 people with seven activity types. In [9], the original paper that presents the used dataset, the HAR (human activity recognition) task should be solved first, as training the algorithm on all types of activities will mostly bring additional noise to data and decrease the metrics due to not enough amount of data points per each activity. The problem can be understood as detecting the unique and distinguishing patterns of a specific person's motions.

For understanding accelerometer data and human movement patterns, we will train the model separately for each axis (x, y, z), axis pairs (xy, yz, xz), and all three axes — xyz for different types of activities.

For deep learning models, we split data in overlapping on 50 percent windows with a length of 52 (because of accelerometer frequency).

We split the original dataset into a 33% share for the test set and the rest for the train.

An accelerometer measures changes in velocity along one axis (Fig.1). The values reported by the accelerometers are measured in increments of the gravitational acceleration, with the value 1,0 representing an acceleration of 9,8 meters per second (per second) in the given direction. Depending on the direction of the acceleration, the sensor values may be positive or negative [17].

Fig. 1. Accelerometer axis demonstration on the general smartwatch/bracelet [12]

Autoencoder model architecture is in Table 1 below. As an activation function, the hyperbolic tangent was used. The model was trained in 10 epochs, with Adam optimizer and mean absolute error loss. We build autoencoders with python on Keras library and Tensorflow backend [17].

The dropout rate was 0,4.

T a b l e 1. The used model architecture with layers' type, shape, and amount of params

Type	Layer Shape	# of Params
LSTM	(None, 52, 20)	1760
LSTM	(None, 10)	1240
RepeatVector	(None, 52, 10)	0
Dropout	(None, 52, 10)	0
LSTM	(None, 52, 10)	840
LSTM	(None, 52, 20)	2480
TimeDistributed	(None, 52, 3)	21

The threshold formula was used as in [8]:

$$T = \sum_{i=1}^{N} MAE_i \Big/ n + std(MAE_i) ,$$

where *MAE* is the mean absolute error between ground truth and predicted sample; *std* – standard deviation, and *N* is the number of samples in the training dataset.

As model evaluation metrics [19], the *EER* (equal error rate), *FAR* (false accept rate) and *FRR* (false reject rate), and ROCAUC (area under the curve) were chosen, which are typical for assessing the biometric system quality:

$$FAR = FPR = \frac{FP}{FP + TN} ; \quad FRR = FNR = \frac{FN}{TP + FN} .$$

Equal error rate (*EER*) (illustrated in Fig. 2) is obtained by adjusting the system's detection threshold to equalize *FAR* and *FRR*. The *EER* is calculated using the following formula:

$$EER = \frac{FAR + FRR}{2} ,$$

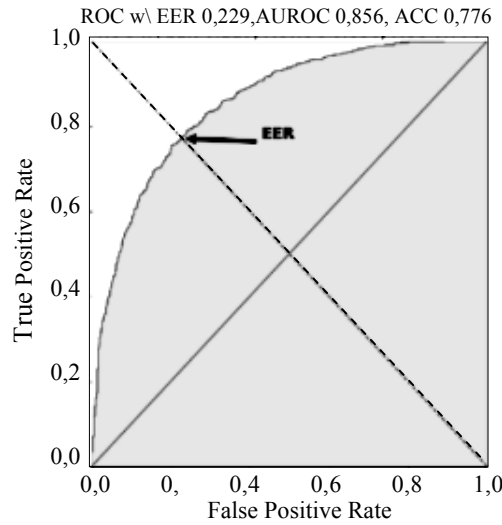where $| FAR + FRR |$ is the smallest value [20].

ROC w\ EER 0,229,AUROC 0,856, ACC 0,776

Fig. 2. Illustration of the *EER* calculation from [19]

RESULTS

For analysis, we considered only 1, 3, 4, and 7 types of activities. We filtered out 2,5, and 6 activities (Standing Up, Walking and Going updown stairs, Going UpDown Stairs, Walking and Talking with Someone) as less than 200 data points were presented in the train set and less than 100 in the median for 15 users (Table 2).

T a b l e   2 . Amount of samples in train set (median value for 15 users) for various activities

Activity	1	2	3	4	5	6	7
# in trainset (median for 15 users)	133	89	301	599	86	62	860

We can review the results for every metric in the tables below: *EER* and *AUC* (Table 3), *FAR*, and *FRR* (Table 4). We have 15 users in the dataset therefore we report the average performance metric.

T a b l e   3 . Average *EER* and *AUC* (on 15 users) for various activities

Axis data for train	1 activity	7 activity	3 activity	4 activity	1 activity	7 activity	3 activity	4 activity
	Mean *EER*				Mean *AUC*			
x-axis	0,202	0,350	0,407	0,318	0,837	0,671	0,617	0,714
y-axis	0,168	0,276	0,364	0,345	0,868	0,756	0,657	0,687
z-axis	0,161	0,358	0,394	0,237	0,873	0,669	0,631	0,791
x-axis_*y*-axis	0,084	0,200	0,346	0,280	0,938	0,833	0,680	0,759
x-axis_*z*-axis	0,101	0,254	0,358	0,191	0,924	0,777	0,673	0,841
y-axis_*z*-axis	0,081	0,223	0,349	0,225	0,938	0,807	0,680	0,807
x-axis_ *y*-axis_*z*-axis	0,074	0,189	0,334	0,197	0,949	0,846	0,689	0,830

T a b l e 4. Average *FAR* (on 15 users) for various activities

Axis data for train	1 activity	7 activity	3 activity	4 activity	1 activity	7 activity	3 activity	4 activity
	Mean *FAR*				Mean *FRR*			
x-axis	0,260	0,527	0,589	0,459	0,067	0,132	0,177	0,113
y-axis	0,207	0,388	0,526	0,517	0,058	0,101	0,160	0,108
z-axis	0,182	0,534	0,564	0,307	0,071	0,128	0,174	0,112
x-axis_y-axis	0,066	0,219	0,464	0,374	0,058	0,116	0,176	0,107
x-axis_z-axis	0,076	0,312	0,488	0,196	0,075	0,133	0,166	0,122
y-axis_z-axis	0,059	0,269	0,459	0,259	0,064	0,117	0,181	0,127
x-axis_ y-axis_z-axis	0,030	0,188	0,452	0,222	0,073	0,120	0,171	0,117

DISCUSSION

The obtained results show that all axes contribute to the final results and hold important information about human patterns. Therefore, training on all three axes shows the best performance.

Another interesting thing we can notice is that for different types of activities – different axis brings more value. For example, in walking (4-th activity), we can say that the model trained on the z-axis only or on another axis in combination with the z-axis has the best performance if looking at *EER* and *AUC*. On the other side, for the 7th activity (Talking While Standing), the y-axis brings the most value.

As well, if looking at the performance of models trained on the x-axis only, they always have the lowest performance compared to others. Still, in combination with the y-axis, the performance increases a lot.

The best results were shown for 1 activity (Working at Computer), but this can be related, that this type of activity has the highest amount of training samples.

Overall, the performance is highly correlated with the number of training samples (Table 1), which may point out for need in artificial synthetic data generation for model training, because for the personalization system is important to be able to work and be reliable as fast as possible. The continuous training of the model during the system is alive should be considered to prevent model and data drift and allow the system to prevent the cold start when there are not that many available training samples.

CONCLUSIONS

In this research, we conducted an in-depth analysis of different components on human motion patterns from sensory data (accelerometer in our case) and whether we can extract distinguishing person patterns from such data and use it for biometric verification systems.

The deep learning approaches have already proved their applicability and stable performance in such cases. Still, as already mentioned, the motion-based authentication shows lower accuracy than other biometric verification (e.g., physiological), but this does not mean that motion-based verification should not be used. The solution to overcome problems drawbacks of various types of verifi-

cation – is a multimodal authentication system, which increases stability, robustness, and flexibility for customization in different environments.

Looking at the metrics for different accelerometer data components and activities, we can see that every axis contributes to the final result not equally. Depending on the activity type, different features are important, proving that we probably need a multi-stage system with preliminary human activity classification in case of motion-based verification. The advantage of the autoencoder model is that single model can be used for both tasks without the need to train different models.

Further research should be done to create a sensory-based authentication system that utilizes multiple sensors. Such approach should increase the quality of the system but keep the continuous option.

Additional analysis of evaluation metrics should also be done, as there are raising concerns regarding commonly used metrics and biometric evaluation framework, as they may lead to incorrect decisions and be misleading.

REFERENCES

1. S. Minaee, A. Abdolrashid, H. Su, M. Bennamoun, and D. Zhang, *Biometrics Recognition Using Deep Learning: A Survey*. 2021. [Online]. Available: https://arxiv.org/abs/1912.00271. (Accessed on: Feb 15, 2022).

2. L. Olanrewaju, O. Oyebiyi, S. Misra, R. Maskeliunas, and R. Damasevicius, "Secure ear biometrics using circular kernel principal component analysis, Chebyshev transform hashing and Bose–Chaudhuri–Hocquenghem error-correcting codes", *Signal, Image and Video Processing*, vol. 14, no. 5, pp. 847–855, 2020. doi: 10.1007/s11760-019-01609-y.

3. A. Blázquez-García, A. Conde, U. Mori, and J.A. Lozano, "A Review on Outlier/Anomaly Detection in Time Series Data", *ACM Computing Surveys*, vol. 54, no. 3, pp. 1–33, 2021. doi: 10.1145/3444690.

4. M. Braei and S. Wagner, *Anomaly Detection in Univariate Time-series: A Survey on the State-of-the-Art*. 2020. [Online]. Available: https://arxiv.org/abs/2004.00433. (Accessed on: Feb 15, 2022).

5. M. Braei, "Anomaly detection of time series: A comparison of statistical vs classical machine learning vs deep learning approaches", *Unpublished*, 2019. doi: 10.13140/RG.2.2.17687.80801.

6. S. Gopali, F. Abri, S. Siami-Namini, and A. Namin, "A Comparative Study of Detecting Anomalies in Time Series Data Using LSTM and TCN Models", *arXiv.org*, 2021. [Online]. Available: https://arxiv.org/abs/2112.09293. (Accessed on Feb 15, 2022).

7. S. Mekruksavanich and A. Jitpattanakul, "Deep Learning Approaches for Continuous Authentication Based on Activity Patterns Using Mobile Sensing", *Sensors*, vol. 21, no. 22, pp. 7519, 2021. doi: 10.3390/s21227519.

8. M. Havrylovych, V. Danylov, and A. Gozhyi, "Comparative Analysis of using Recurrent Autoencoders for User Biometric Verification with Wearable Accelerometer", *Proceedings of the 9th International Conference "Information Control Systems & Technologies"*, pp. 358–370, Sept. 2020.

9. P. Casale, O. Pujol, and P. Radeva, "Personalization and user verification in wearable systems using biometric walking patterns", *Personal and Ubiquitous Computing*, vol. 16, no. 5, pp. 563–580, 2011. doi: 10.1007/s00779-011-0415-z.

10. M. Abuhamad, A. Abusnaina, D. Nyang, and D. Mohaisen, "Sensor-Based Continuous Authentication of Smartphones' Users Using Behavioral Biometrics: A Contemporary Survey", *IEEE Internet of Things Journal*, vol. 8, no. 1, pp. 65–84, 2021. doi: 10.1109/jiot.2020.3020076.

11. Z. Akhtar, A. Buriro, B. Crispo, and T.H. Falk, "Multimodal smartphone user authentication using touchstroke, phone-movement and face patterns", *2017 IEEE Global Conference on Signal and Information Processing (GlobalSIP)*, 2017. doi: 10.1109/globalsip.2017.8309185.

12. C.A. Cole, D. Anshari, V. Lambert, J.F. Thrasher, and H. Valafar, "Detecting Smoking Events Using Accelerometer Data Collected Via Smartwatch Technology: Validation Study", *JMIR mHealth and uHealth*, vol. 5, no. 12, pp. e189, 2017. doi: 10.2196/mhealth.9035.

13. A. Mostafa, T. Barghash, A. Assaf, and W. Gomaa, "Multi-sensor Gait Analysis for Gender Recognition", *Proceedings of the 17th International Conference on Informatics in Control, Automation and Robotics*, 2020. doi: 10.5220/0009792006290636.

14. I. Goodfellow, Y. Bengio, and A. Courville, *Deep Learning Adaptive Computation and Machine Learning series*. 2016. 775 p.

15. H. Sak, A. Senior, and F. Beaufays, "Long short-term memory recurrent neural network architectures for large scale acoustic modeling", *Interspeech 2014*, 2014. doi: 10.21437/interspeech.2014-80.

16. *UCI machine learning repository*. [Online]. Available: https://archive.ics.uci.edu/ml/datasets/Activity+Recognition+from+Single+Chest-Mounted+Accelerometer. (Accessed on: Feb 15, 2022).

17. F. Chollet, *Building Autoencoders in Keras*. 2016. [Online]. Available: https://blog.keras.io/building-autoencoders-in-keras.html. (Accessed on: Feb 15, 2022).

18. *Getting Raw Accelerometer Events*. [Online]. Available: https://developer.apple.com/documentation/coremotion/getting_raw_accelerometer_events\

19. S. Sugrim, C. Liu, M. McLean, and J. Lindqvist, "Robust Performance Metrics for Authentication Systems", *Proceedings 2019 Network and Distributed System Security Symposium*, 2019. doi: 10.14722/ndss.2019.23351.

20. Y. Hong and R. Kumar, *Performance Evaluation Metrics for Biometrics-based Authentication Systems*. 2021. [Online]. Available: http://hdl.handle.net/10066/23535. (Accessed on: Feb 15, 2022).

INFORMATION ON THE ARTICLE

Mariia P. Havrylovych, ORCID: 0000-0002-9797-2863, Institute for Applied System Analysis of the National Technical University of Ukraine "Igor Sikorsky Kyiv Polytechnic Institute", Ukraine, e-mail: mariia.havrylovych@gmail.com

Valeriy Ya. Danylov, ORCID: 0000-0003-3389-3661, Institute for Applied System Analysis of the National Technical University of Ukraine "Igor Sikorsky Kyiv Polytechnic Institute", Ukraine, e-mail: danilov1950@ukr.net

ДОСЛІДЖЕННЯ БІОМЕТРИЧНОЇ ВЕРИФІКАЦІЇ КОРИСТУВАЧА НА ОСНОВІ АВТОКОДЕРІВ З ПЕРЕВІРКАМИ РУХУ / М.П. Гаврилович, В.Я. Данилов

Анотація. Продовжено попереднє дослідження щодо біометричної перевірки користувача на основі руху з використанням сенсорних даних. Системи сенсорної верифікації розширюють можливості неперервної автентифікації, оскільки фізіологічні біометричні методи, в основному засновані на фото- або відеоданих, стикаються з багатьма труднощами під час реалізації. Мета дослідження — проаналізувати як різні компоненти сенсорних даних від акселерометра впливають і сприяють визначенню процесу унікальних моделей руху людини та розуміння того, як вони можуть виражати моделі поведінки людини з різними видами активності. Як базову модель використано рекурентний автокодувальник довгої-короткої пам'яті. Вибір моделі ґрунтується на попередніх дослідженнях. Результати дослідження показали, що залежно від виду діяльності різноманітні компоненти даних мають різний внесок. Зроблено висновок, що одного джерела даних датчика може бути недостатньо для надійної системи автентифікації. Для подальших досліджень слід запропонувати мультимодальну систему автентифікації, яка повинна використовувати та об'єднувати вхідні потоки від кількох датчиків.

Ключові слова: розпізнавання образів руху, біометрична верифікація, рекурентні автокодувальники.

AN EXPLANATION OF THE J. HUBER EFFECT, WHICH DOES NOT CONTRADICT THE LAWS OF PHYSICS AND EXPERIMENTAL RESEARCH

A. SILVESTROV, D. ZIMENKOV, L. SPINUL, V. SVYATNENKO

Abstract.. An explanation of any physical phenomenon is essential, both theoretically and practically. The phenomenon discovered by the Austrian engineer J. Huber, the so-called "Huber effect," posits that if an electric current passes through an already moving wheelset of wheels of a railroad train from one rail of a railway to another, an additional accelerating mechanical force arises in the direction of travel. From 1951 to the present, scientists have tried to explain and utilize this effect. A brief overview of these explanations and their contradictions in theory and experiment is given. However, they have become important for finding an explanation that does not contradict the laws of classical electrodynamics and experimental data.

Keywords: Huber effect, Kosyrev–Milroy engine, Biot–Savart–Laplace law, systemic approach, electricity flow, super-capacitor, ferromagnetism

INTRODUCTION

In 1951, the Austrian engineer J. Huber discovered the following physical phenomenon: if during the existing movement at speed V of a railroad train or a separate pair of wheels (Fig. 1) one connects a source 4 of voltage U_s to the rails, then, under the action of current I passing from one rail to another 3 through the wheels 2 and the axle, an additional force F is created, which increases the speed of rectilinear motion V or that of rotational motion Ω of the wheels. This effect was used at the railway sorting station. The same phenomenon was observed in a bearing pair (Fig. 2) by Kosyrev–Milroy [1]. Here, instead of wheels and rails, there were balls and bearing clips.
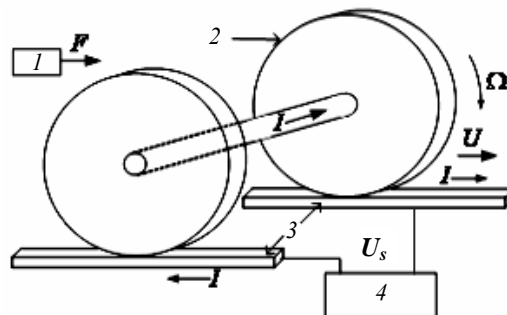

Fig. 1. Wheelset

The ambiguity of the effect and the low efficiency of the Kosyrev–Milroy engine required scientists to further study to explain the Huber effect and identify areas for its effective use.
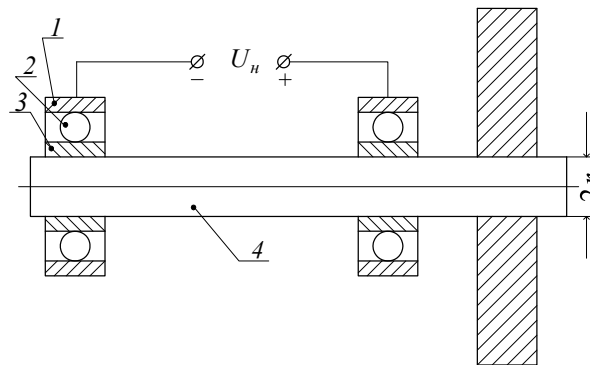
Fig. 2. Kosyrev–Milroy electric motor: *1, 3* — clips; *2* — ball; *4* — shaft; $U_{\text{н}}$ — source voltage

BRIEF OVERVIEW OF THE EFFORTS TO EXPLAIN THE HUBER'S EFFECT

It was considered [2, 3] that the interaction of electric currents in accordance to Ampere's law in the wheel and rail, which are positioned at an acute angle due to motion, creates a torque (Fig. 3). However, in the second wheel of the wheel set or on the opposite side of the bearing ball, it will be of the opposite direction.
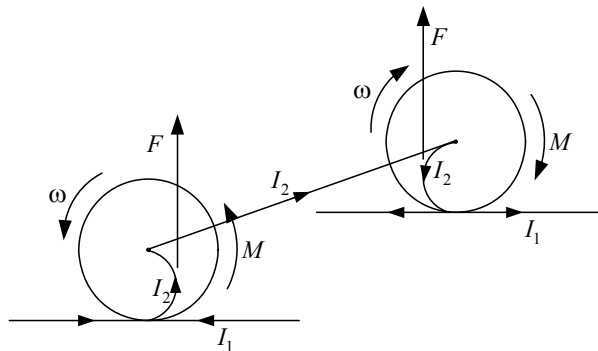

Fig. 3. Kuzmin–Shpatenko's oversight

Nonetheless, the curvature of current I_2 trajectories was further developed in our studies.

It was also believed [3] that the torque arises from sparking on the falling side of the contact.

Indeed, when the bearing was placed in a vacuum chamber [4], after a while the movement stopped. But, as we found out (and confirmed by experiment), this was due to the significant heating of the balls without heat dissipation in vacuum, and, as a result, the mechanical jamming of the almost non-existent clearance between the ball and the clip. In 1973, the author of [4] claimed that the spark is the cause, and in 1982, already points [5] to the negative impact of the spark.

Thermodynamic explanation [6] of motion caused by thermal deformation contradicts the thermal inertia of bearing bodies. Some studies [7] suggest propositions that generally contradict the laws of physics. Additional ambiguities were introduced by [8, 9], where the J. Huber effect is conflated with an unexplained effect of J. Searle ("flying saucers") and "non-physical" laws [7] of G. Nikolaev,

in which the directions of current I and magnetic flux Φ coincide. This is possible only for the longitudinal along the shaft axis current component I through the cross-section of the shaft rotating with frequency Ω (Fig. 4).
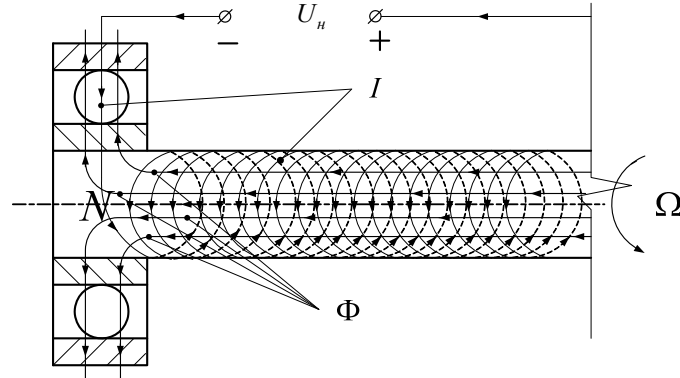

Fig. 4. The trajectory of "streams" of electrons in a rotating shaft

MULTI-STEP PROCESS FOR SOLVING THE PROBLEM EXPLAINING THE J. HUBER'S EFFECT

Thus, on the basis of the analysis of efforts to explain the effect rather simplistically (in one step), one should find an explanation for it through a multi-step truth-oriented algorithm, preserving the results that do not contradict the laws of physics, as well as finding new course of search.

In mathematics, this resembles the search for the extremum of a function in a multidimensional space of constrained variables [10].

Step 1. Analysis within the statics of the contact zone of the wheel and rail, or balls and clips.

As a rule, in any electric contact, one, first and foremost, points out its active resistance R_κ. However, the contact is not a point or a line: it has a finite area S_κ, an extremely small clearance δ with dielectric conductivity ε. And, as a result, it is determined by the final electrical resistance R_κ and capacitance C_κ. The power supply circuit additionally has a resistance R and an inductance L (Fig. 5).
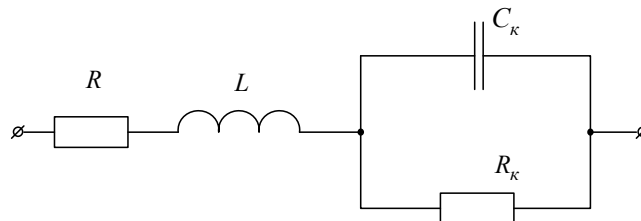

Fig. 5. Current circuit replacement scheme in the contact zone

Resistance R is much lower than R_κ. Therefore, in a pair of wheels, almost half U_κ of the voltage of the source U_s falls on the contact, creating a current I in the resistance R_κ, and a charge q_κ on the capacitance C_κ. For example [10],

for the contact of the wheel and the rail of the railroad car capacity of $C_{\kappa} = (0,02 \div 0,03)\mu F$, the charge of q_{κ} at voltage of $U_{\kappa} = 10V$ is $(0,2 \div 0,3) \cdot 10^{-6} C$. This is posited for a clearance of one micron. But in the central zone of contact of the polished surfaces of a wheel and a rail under a force of pressure under car's weight the clearance δ can be even smaller (effect of the super-capacitor).

Therefore, at the first step, an important result of the study is the opening of the contact capacitance C_{κ}.

Step 2. Analysis of electricity flow through a moving contact.

Let us present the flow of electricity I as a sum of the currents $j_{\kappa}\Delta S_{\kappa}$ of each kth tube:

$$I = \sum j_{\kappa} \Delta S_{\kappa},$$

where j_{κ} is the density, and ΔS_{κ} is the cross-sectional area of the kth tube Ω.

If a wheel (or a ball) rotates with frequency and speed V_0, then to the left of the contact will be the area whose clearance δ decreases, and to the right — increases (Fig. 6).
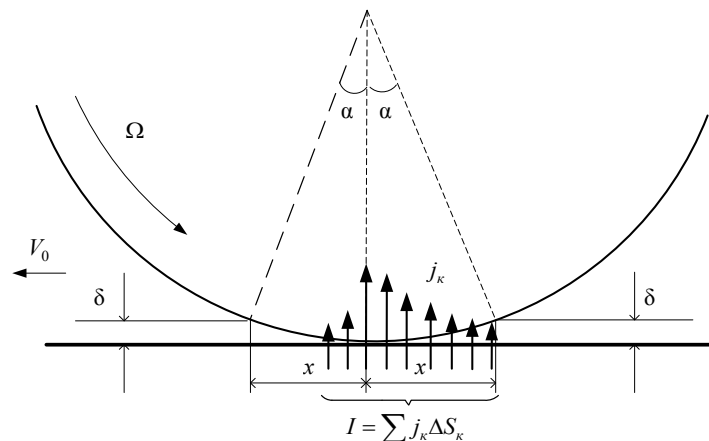

Fig. 6. Asymmetric distribution of density j_{κ} of current I

Then, taking into account the active inductive nature of the power supply circuit (Fig. 5), the current through the clearance on the left will increase exponentially [11].

$$I_{\kappa}(t) = I_{\kappa y}[1 - e^{-\int_0^t \frac{d\theta}{\tau_{\kappa}(\theta)}}],$$

where $I_{\kappa y}$ is the default value, $\tau_{\kappa} = \dfrac{L_{\kappa}}{R_{\kappa}(0)}$ is the time constant; to the right — decreasing exponentially

$$I_{\kappa}(t) = I_{\kappa y} \cdot e^{-\int_0^t \frac{d\theta}{\tau_{\kappa}(\theta)}}.$$

The greater the V_0 or Ω, the fewer current tubes there is to the left (lesser time t the current does not reach $I_{\kappa y}$). Next, in the area of mechanical contact a current $I_{\kappa y}$ is set, which will decrease exponentially to the right of the contact,

creating sparks due to EMF of self-induction of $\varepsilon_\kappa = -\dfrac{dI_\kappa}{dt}$. As a result, the flow q of electricity I shifts, as V increases to the right.

Step 3. Bilateral action of the Biot–Savart–Laplace law.

The product of the voltage U_κ and the capacitor C_κ is the charge q_κ. During movement, the charge q_κ moves in the body of the wheel and rail at a speed V equal to the angular velocity Ω times the radius r_κ of the wheel.

Then, according to Biot–Savart–Laplace law, (if we apply the product of q_κ and V as the product of the conditional current I_κ and the path component Δx, where Δx equals to the product of V and the time component Δt of time t) we obtain the magnetic field of induction ΔB at the point M (Fig.7):

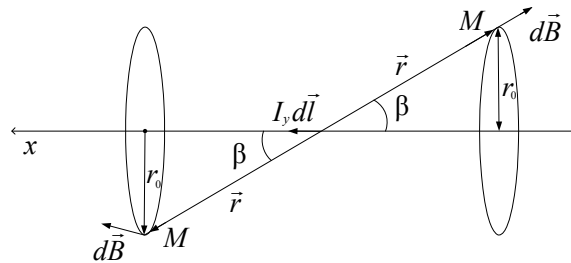$$\Delta B = \frac{\mu_0}{4\pi}\frac{I_y\,\Delta x\sin\beta}{r}\,.$$

Fig. 7. Biot–Savart–Laplace law

Due to the ferromagnetism of the wheel and rail bodies (ball and clip), the magnetic field is amplified and, according to the property of minimizing the loss of magnetic energy W_M [11] in the air clearance, creates a force P_M derived from W_M along δ, which reduces the clearance δ.

The Biot–Savart–Laplace law has a bilateral effect (Fig. 1), and, with the movement of the wheel (the ball) and the presence of at least inductance of L in the supply circuit, the flow of electricity I will shift towards the falling part of the contact zone, forming sparks. This leads to the arm of force P_M and the torque on the falling side increase as the speed goes up, and slowing down of the movement.

Therefore, as the current I passes through the moving contact, the initial movement speed V_0 should not increase, but instead decrease until complete cessation of movement.

This was observed in the bearing pair at low currents I, or at a minor moment of inertia of the flywheel on the shaft of the Kosyrev–Milroy engine.

Step 4. Transition from instantaneous values of moments to pulses of mechanical energy.

Given the specifics of the electrodynamics of moving bodies [12] with time-varying parameters (clearance δ to the left over time Δt decreases, to the right — increases), it is not difficult to show that the momentum of the energy of motion over time Δt, taking into account the influence of the dynamic moment from the mass or moment of inertia of the moving bodies of the system will be greater than the braking to the time at which the displacement of electricity flows in the

direction of the falling part of the contact, is set at the appropriate speed V balance. In this case, the greater the dynamic moment of inertia, the greater the speed.

CONCLUSION

This explanation is fully consistent with the laws of electrodynamics and the results of experimental studies of the Huber effect.

REFERENCES

1. V.V. Kosyrev, V.D. Rabko, and N.I. Velman, "Electric motor. A.s. № 155216 (USSR)", *Inventions. Prom. samples. Trademarks*, no. 12, 1963.
2. A.N. Silvestrov and D.K. Zimenkov, "On the nature of the Huber effect", *Bulletin of the Ostrogradsky CDRU*, no. 4, pp. 33–38, 2010.
3. V.V. Kuzmin and V.S. Shpatenko, "On the nature of the appearance of the torque in the Kosyrev–Milroy engine", *Bulletin of the Ostrogradsky CDRU*, no.3, pp. 41–47, 2008
4. A.V. Netushil, "J. Searl's invention as a development of the Huber effect", Electricity, no. 4, pp. 50–53, 1994.
5. K.M. Polivanov, N.V. Tatarinova, and A.V. Netushil, "Electromechanical Huber effect", *Electricity*, no. 8, pp. 72–76, 1973.
6. K.M. Polivanov, *Electrodynamics of moving bodies*. M.: Energoizdat, 1982, 192 p.
7. D.I. Penner and V.A. Ugarov, *Electrodynamics and special theory of relativity*. M.: Prosveschenie, 1980, 272 p.
8. G.V. Nikolaev, *Modern electrodynamics and the reasons for its paradox*. Tomsk: Tverdynya, 2003, 149 p.
9. S.S. Voronkov, "Electrodynamic forces of Nikolaev", *Scientific and technical library, articles and publications*. Available: http://www.sciteclibrary.ru/rus/ catalog/arts/
10. P. Demin, "Huber effect and flying saucers", *Science and Life*, no. 7, 1991.
11. A.M. Silvestrov and D.K. Zimenkov, *Monograph "The effect of J. Huber (labyrinths of scientific research)"*. Kyiv 2020, 132 p.
12. I.E. Tamm, *Fundamentals of electricity theory*. M: Nauka, 1976, 616 p.

INFORMATION ON THE ARTICLE

Anton M. Silvestrov, ORCID: 0000-0002-2511-5029, National Technical University of Ukraine "Igor Sikorsky Kyiv Polytechnic Institute", Ukraine, e-mail: silvestrovanton@gmail.com

Dmytro K. Zimenkov, ORCID: 0000-0002-1345-3637, National Technical University of Ukraine "Igor Sikorsky Kyiv Polytechnic Institute", Ukraine, e-mail: zimenkovdk@ukr.net

Liudmyla Yu. Spinul, ORCID: 0000-0002-4234-6072, National Technical University of Ukraine "Igor Sikorsky Kyiv Polytechnic Institute", Ukraine, e-mail: spinul20@gmail.com

Vadym A. Svyatnenko, ORCID: 0000-0002-0518-1045, National Technical University of Ukraine "Igor Sikorsky Kyiv Polytechnic Institute", Ukraine, e-mail: vadiksv@gmail.com

ПОЯСНЕННЯ ЕФЕКТУ ГУБЕРА, ЯКЕ НЕ СУПЕРЕЧИТЬ ЗАКОНАМ ФІЗИКИ Й ЕКСПЕРИМЕНТАЛЬНИМ ДОСЛІДЖЕННЯМ / А.М. Сильвестров, Д.К. Зіменков, Л.Ю. Спінул, В.А. Святненко

Анотація. Пояснення того чи іншого фізичного явища конче важливе як у теоретичному, так і в практичному аспекті. Виявлене австрійським інженером Ж. Губером явище, так званий «ефект Губера», полягало в тому, що якщо від рейки до рейки залізничної колії через уже рухому колісну пару коліс залізничного потяга пропускати електричний струм, то виникає додаткова механічна сила в напрямку руху, яка збільшує швидкість. Із 1951 р. і дотепер учені багато разів намагались пояснити і використати цей ефект. Наведено короткий огляд цих пояснень та їх суперечностей теорії та експерименту, однак вони стали важливими для відшукання пояснення, яке не суперечить законам класичної електродинаміки й експериментальним даним.

Ключові слова: ефект Губера, двигун Косирєва–Мілроя, закон Біо–Савара–Лапласа, системний підхід, потік електрики, надконденсатор, феромагнетизм.

EXPERT SYSTEM FOR DEPRESSION DETECTION
IN TEENAGERS

B. RAHARJA, E.B. SAMUDERA, F. LAY, S. HANSUN

Abstract. Depression (major depressive disorder) is a common and serious medical illness that negatively affects how you feel, think, and act. Fortunately, it is treatable. Depression causes sadness and/or a loss of interest in activities once enjoyed. It can lead to various emotional and physical problems and decrease a person's ability to function at work and home. Teenagers often experience this disorder because their emotions are still unstable. They also don't have many chances to consult with a psychologist and doctor. Through this research, an expert system was created that implements knowledge from experts related to depression so that teenagers can do a self-test when needed. The expert system was developed using the Certainty Factor method for the knowledge inference engine. The system was tested iteratively and could achieve similar results with a domain expert. We hope that the system can detect early symptoms of depression among teenagers and minimize the negative impact it may cause.

Keywords: certainty factor, depression, detection, expert system, teenagers.

INTRODUCTION

The life of a human being goes through several phases change. This phase starts from when humans are babies until humans die. In human growth, there is an adolescent phase, namely the transitional phase of children to maturity in the age range of 12 years to 20 years [1].

Adolescence in a child can have various dynamic changes, one of which is emotion. Therefore, a teenager must be able to adapt to any changes that exist. When a teenager cannot adapt or control himself over his emotions and thoughts, it is not uncommon for a teenager to be depressed due to negative thoughts. Depression experienced by a teenager is not just a temporary feeling of stress and sadness, but there is a serious condition that can permanently affect behaviour, emotions, ways of thinking, and character that must be given special treatment to overcome it [2].

For teenagers who are in that phase, they may find it difficult and confused about who to go and consult to. This expert system that we designed aims to help teenagers and parents to make an early diagnosis of depression that may occur in a teenager. Our expert system is designed in the form of a website due to the ease of internet access, particularly in Indonesia.

By conducting this research, we hope to help teenagers to find out the level of depression they are experiencing. The other purpose of this system is to facilitate communication between parents and children regarding depression. With this expert system, it is hoped that parents can facilitate further treatment for their child if needed. To support this goal, the prediction results must have good accuracy. Here, we implement the Certainty Factor method in inferencing the knowledge base to the final decision shown to the user.

With this expert system, we hope that teenagers will have the courage to carry out self-diagnosis with good accuracy so that they can communicate with their parents for further treatment. For parents who are also worried about their child, they can monitor the child's actions and carry out a diagnosis with the child. This system can also help psychologists in carrying out their duties more quickly.

THEORETICAL BASIS

A. Expert System

An expert system is a computer-based system that can replace experts in solving problems by using knowledge, facts, and reasoning techniques [3].The definition of an expert system is a computer program that has expert knowledge of a specific field. From these two definitions, it can be concluded that an expert system is a program designed to have the knowledge to solve problems in a specific field like an expert.

In the development of an expert system, there are two main structures, namely the development environment and the consultation environment. The development environment is useful for entering expert knowledge into the expert system and the consultation environment is used by users to get results from the knowledge of an expert via the system [4].

B. Scrum Method

Software Development Life Cycle (SDLC) is a cycle in making a system with the aim of solving a problem effectively. With the proper use of SDLC, the resulting system can be of high quality and in accordance with the wishes or objectives of the formation of the system. According to Mulyani [5], SDLC is a set of logical processes applied by a systems analyst to develop an information system that involves requirements, validation, training, and discussion with system owners.

Scrum is basically one of the lightest Agile methods but can provide advantages in setting the stages and control in the development of a system or product [6]. This method relies on a collection of methods and practices that apply the values and principles of the Agile Manifesto [7]. With the use of Scrum, there is a sprint component which is a series of stages carried out in one process simultaneously. The main purpose of using Scrum is to get the Minimum Viable Product (MVP) value at the end of each sprint [8].

C. Depression

Depression is a condition in which a person's daily life is filled with feelings of pain, disappointment, sadness, and emotional confusion. Depression can be caused by trauma, guilt, isolation, and deep pain [9]. Depression can be concluded as a continuous feeling of sadness that a person feels and impacts on a person's thoughts and actions that can be caused by the environment around them and themselves.

In this study, we used 29 symptoms of depression in teenagers as mentioned by Burns in Widians et al. [10]. Table 1 shows the list of those symptoms used in this study.

T a b l e 1. Depression symptoms [10]

Code	Symptom	Code	Symptom
G001	Sad	G016	Feeling lonely
G002	Tiredness in doing activities	G017	Feeling guilty
G003	Difficulty to focus	G018	Often feel being punished
G004	Feeling bored	G019	Self-hatred
G005	Daydreaming	G020	Easily offended
G006	Not excited	G021	Loss of appetite
G007	Often upset	G022	Worried about one appearance
G008	Pessimistic about the future	G023	Very sensitive
G009	Often cries without explainable reasons	G024	Prefer to be alone
G010	Insomnia	G025	Having thoughts of suicide
G011	Often anxious	G026	Difficulty to make a decision
G012	Disappointed with oneself	G027	Difficulty to do activities well
G013	Often disturbed	G028	Weight gain or loss
G014	Looks gloomy	G029	Less confident
G015	Loss of interest in hobbies that used to be liked		

D. Certainty Factor

Certainty Factor (CF) is a method proposed by Shortliffe and Buchanan in 1975 to accommodate the exact reasoning of an expert [11]. An expert (for example: doctor) often analyses information with the expressions "probably", "most likely", "almost certain". So that with the Certainty Factor method, it can describe the level of confidence of an expert on the problem at hand. The basic formula to calculate the confidence level of a rule is shown in [12]:

$$CF[h,e] = MB[h,e] - MD[h,e]$$

where $CF[h,e]$ is the certainty factor, $MB[h,e]$ is the measure of belief of hypothesis (h) given evidence (e), and $MD[h,e]$ is the measure of disbelief of hypothesis (h) given evidence (e).

Moreover, Certainty Factor formula for one premise is shown in CF[h,e] = = CF[t]*CF[rule] = CF[user]*CF[expert], while for two or more premises is shown in [13]–[15]:

$$CFc(CF_1, CF_2) = \begin{cases} CF_1 + CF_2(1 - CF_1), & \text{if } CF_1, CF_2 > 0, \\ CF_1 + CF_2(1 + CF_1), & \text{if } CF_1, CF_2 < 0, \\ \dfrac{CF_1 + CF_2}{(1 - \min\{|CF_1|, |CF_2|\})}, & \text{if } CF_1 < 0 \text{ xor } CF_2 < 0, \end{cases} \quad (1)$$

where $CF[e]$ is the certainty factor of given evidence which can be represented as certainty factor given by user, $CF[rule]$ is the certainty factor rule given by an expert, CFc is the combined certainty factor from the other two known certainty factor following the rules (1).

METHODOLOGY

In this research, we use Scrum method. Scrum itself uses an approach from another method, namely Agile. Scrum helps teams to solve problems, by having strong communication between team members [16]. Steps in the Scrum Method are follows:

1. Define the team.
2. Determine the processing time.
3. Define roles in the team.
4. Collect various problems.
5. Start a sprint. Sprint is a series of work carried out to solve a problem, especially the creation of a new product.

Our research is assisted by qualitative data collection methods. Qualitative research is a type of research whose findings are not obtained through statistical procedures or other forms of calculation and seeks to understand and interpret the meaning of an event of human behavior interaction in certain situations according to the researcher's own perspective [17]. We use interviews and literature study as data collection tools.

1. **Interview.** In addition to observations, direct interviews were also conducted with experts who have special knowledge about depression in adolescence.

2. **Literature Study.** In this method, searches and learning are carried out from various kinds of literature, and documents that can support the work of this project, including from books, scientific articles, scholarly journals, and also from various internet websites that provide information that is relevant with the study.

RESULTS AND DISCUSSION

A. Implementation Results

Based on the research and iterative development procedure, there are several further development from the initial design of the system which is finalize as follows. Firstly, there is homepage as main display when the site is accessed (Fig. 1). There is a "Get Started" button which will lead to the Identification menu to perform a diagnosis.

Fig. 1. Homepage of the system

On the Identification page as shown in Fig. 2, users can fill in the symptoms provided for the calculation process to be carried out using the Certainty Factor method. There is a total of 29 questions being used in this study. When finished inputting symptoms, the user can click the button with the magnifying glass icon at the bottom right of the screen to display the results of the diagnosis (Fig. 3).
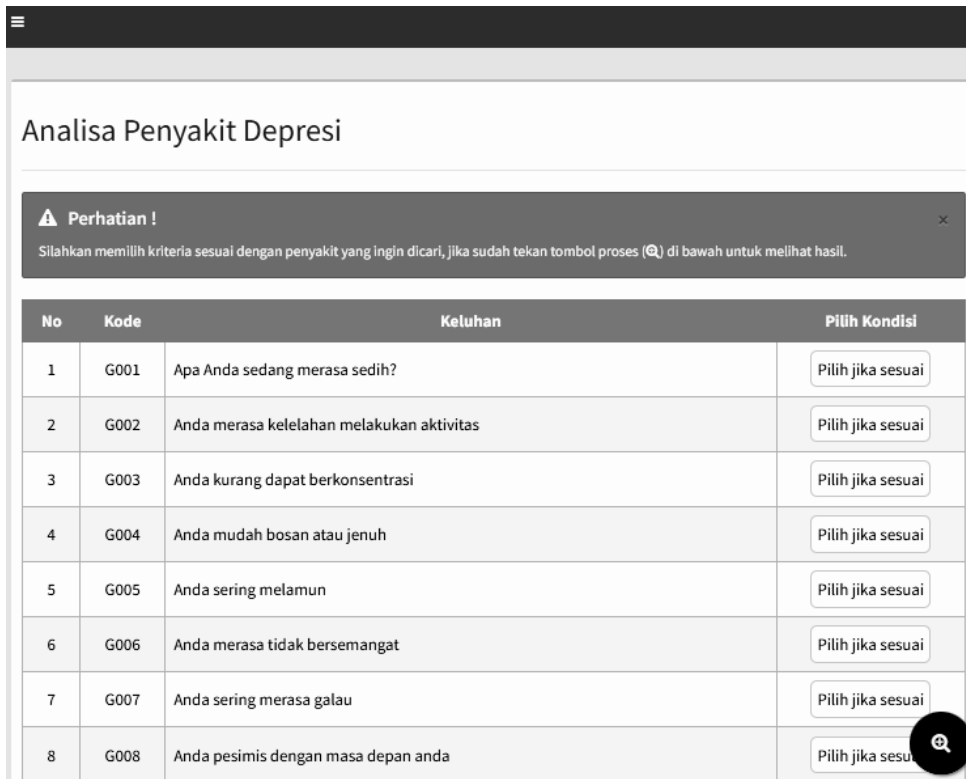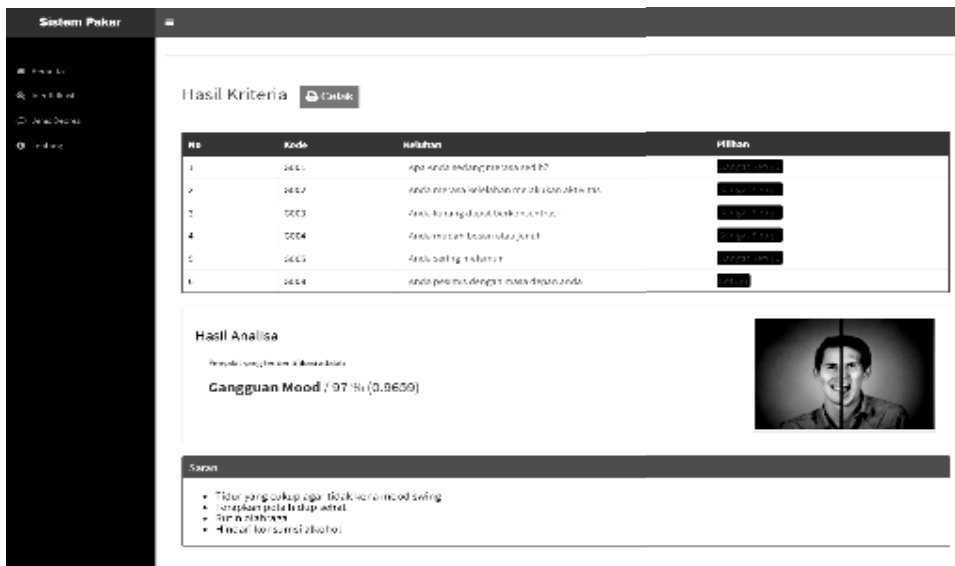
Fig. 2. Identification page

Fig. 3. Analysis result

There is also a page which show the basic information about depression as shown in Fig. 4. On this page, users can read information about the level of depression, details of the depression level, and some suggestions that have been provided. The system prototype may be found at https://uasexpertsystem. 000webhostapp.com/.
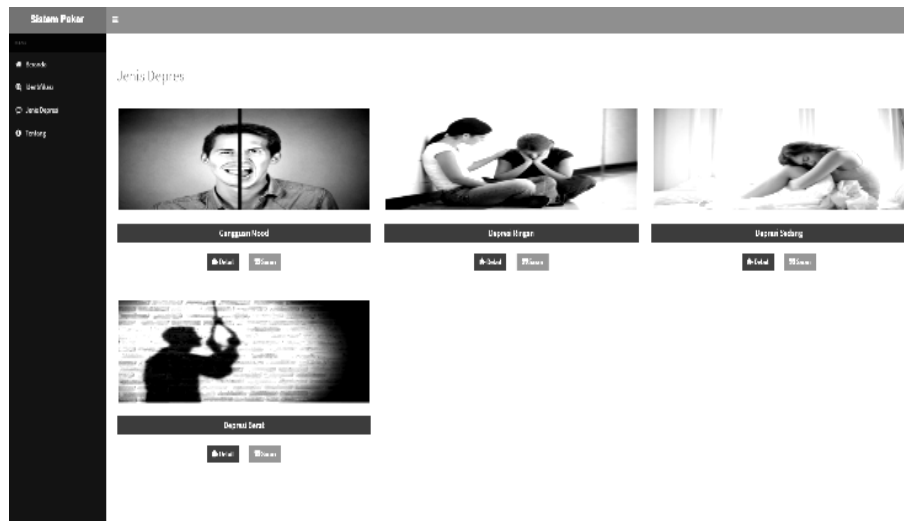
Fig. 4. Types of depression

B. Evaluation and Discussion

We conducted several evaluation methods, including the usability test of the built system and expert evaluation from a psychologist who has a legal license to perform his practice as an expert in this domain. Table 2 shows the usability test results on three main functionalities provided in the system.

T a b l e 2 . Usability test results

System component	Results
Main menu	The main menu is simple and easy to use where when the user wants to identify depression, they can click the "Get Started" or "Identify" button on the menu bar on the left
Identification menu	Has clear instructions for identification and easy-to-read writing. After identifying the user, he gets information about the identified depression and gets suggestions that can be applied by the user
Depression Type menu	It has an easy-to-understand display where there are types of depression, a "Details" button that displays a description of depression, and a "Suggestion" button that displays suggestions for selected depression sufferers

The evaluation with experts was carried out for the first time on November 17th, 2021. During the evaluation process, a calculation test was carried out three times with the following results as shown in Table 3.

T a b l e 3 . First evaluation result

Iteration #	Result	Expectation
1	Severe Depression (1%)	Middle Depression
2	Severe Depression (12%)	Mood Disorder
3	Severe Depression (1%)	Severe Depression

From the results of the calculation test above, it was found that there was an error in the calculation formula and a mismatch of the Certainty Factor value for the knowledge based used in this study. Therefore, several changes were made so that the calculation results got the final value as shown in Table 4.

T a b l e 4. Optimization result

Iteration #	Result	Expectation
1	Middle Depression (98%)	Middle Depression
2	Mood Disorder (100%)	Mood Disorder
3	Severe Depression (100%)	Severe Depression

CONCLUSION

In this study, we have successfully built an expert system for diagnosing depression in teenagers. The system knowledge is inferenced by the Certainty Factor method and could diagnose the level of depression based on the existing knowledge base that is quite accurate. Based on the evaluation results, the system gives results that are in line with expert expectations.

In the future, this research can still be developed by increasing the level of complexity and variations in the value of trust and the value of distrust that is more specific with the latest symptoms in the depression level detection. Other inference methods, ranging from Forward and Backward Chaining [18] to Fuzzy-based [19] or even Machine Learning-based such as the Long Short-Term Memory [20], might be applied in comparison with this study result.

ACKNOWLEDGEMENTS

REFERENCES

1. L. Mandasari and D. L. Tobing, "Tingkat Depresi dengan Ide Bunuh Diri pada Remaja", *J. Keperawatan*, vol. 2, no. 1, pp. 1–7, 2020.
2. K. Dianovinina, "Depresi pada Remaja: Gejala dan Permasalahannya", *J. Psikogenes*, vol. 6, no. 1, pp. 69–78, 2018. doi: 10.24854/jps.v6i1.634.
3. M.K. Jasmir, S. Kom, "Rancangan Sistem Pakar Dengan Metode Forward Chaining Dan Heteroassocoative Memory Untuk Mendeteksi Tingkat Depresi Seseorang", *J. Process. STIKOM Din. Bangsa-Jambi*, vol. 6, no. 1, pp. 1–17, 2011.
4. M. Dahria, "Pengembangan Sistem Pakar Dalam Membangun Suatu Aplikasi", *J. Saintikom*, vol. 10, no. 3, pp. 199–205, 2011.
5. S. Mulyani, *Metode Analisis dan Perancangan Sistem*; 1st ed. Bandung: Abdi Sistematika, 2016.
6. Z. Ereiz and D. Music, "Scrum Without a Scrum Master", *2019 IEEE Int. Conf. Comput. Sci. Educ. Informatiz. CSEI 2019*, pp. 325–328, 2019. doi: 10.1109/CSEI47661.2019.8938877.
7. A. Perdana, "Apa Itu Scrum Master? Simak Pengertian, Peran, dan Skill-nya di Sinitle", *glints.com*, 2021.
8. N. Garzaniti, S. Briatore, C. Fortin, and A. Golkar, "Effectiveness of the Scrum Methodology for Agile Development of Space Hardware", *IEEE Aerosp. Conf. Proc.*, vol. 2019-March, pp. 1–8, 2019. doi: 10.1109/AERO.2019.8741892.
9. A. Dirgayunita, "Depresi: Ciri, Penyebab dan Penangannya", *J. An-Nafs Kaji. Penelit. Psikol.*, vol. 1, no. 1, pp. 1–14, 2016. doi: 10.33367/psi.v1i1.235.
10. J.A. Widians, M. Wati, and J. Juriah, "Aplikasi Sistem Pakar Tingkat Depresi pada Remaja Menggunakan Certainty Factor", in *Seminar Nasional Teknologi Informasi dan Multimedia 2017*, pp. 1–6. [Online]. Available: https://ojs.amikom.ac.id/index.php/semnasteknomedia/article/view/1851/1574.
11. E.H. Shortliffe and B.G. Buchanan, "A model of inexact reasoning in medicine", *Math. Biosci.*, vol. 23, no. 3–4, pp. 351–379, 1975. doi: 10.1016/0025-5564(75)90047-4.

12. R.A. Widyatama and S. Hansun, "Expert System for Chili Plants Disease Detection using Certainty Factor Method", *Int. J. Innov. Technol. Explor. Eng.*, vol. 9, no. 1, pp. 1145–1151, 2019. doi: 10.35940/ijitee.A4440.119119.
13. D. Heckerman, "The Certainty-Factor Model," in Encyclopedia of Artificial Intelligence, 1992, pp. 131–138.
14. S. Sumiati, H. Saragih, T. Abdul Rahman, and A. Triayudi, "Expert system for heart disease based on electrocardiogram data using certainty factor with multiple rule", *IAES Int. J. Artif. Intell.*, vol. 10, no. 1, pp. 43–50, 2021. doi: 10.11591/ijai.v10.i1.pp43-50.
15. S.D. Putra, M.B. Ulum, and D. Aryani, "Expert System for Diagnosis of Uterine Myomas using the Certainty Factor Method", *Int. J. Eng. Sci. Inf. Technol.*, vol. 1, no. 4, pp. 103–108, 2021. doi: 10.52088/ijesty.v1i4.177.
16. N.D. Wirasbawa, M.D.R. Wibawanto, A. Kosasi, and S. Hansun, "Scalable Building Management System for Offices and Co-Working Spaces", *Indian J. Econ. Bus.*, vol. 20, no. 2, pp. 451–461, 2021. [Online]. Available: http://www.ashwinanokha.com/ resources/ijeb v20-2-30.Ijeb.pdf.
17. A.B. Hamilton and E.P. Finley, "Qualitative methods in implementation research: An introduction", *Psychiatry Res.*, vol. 280, p. 112516, 2019. doi: 10.1016/j.psychres.2019.112516.
18. J.W. Moore and L.M. Quintero, "Comparing forward and backward chaining in teaching Olympic weightlifting", *J. Appl. Behav. Anal.*, vol. 52, no. 1, pp. 50–59, 2019. doi: 10.1002/jaba.517.
19. M. Toseef and M.J. Khan, "An intelligent mobile application for diagnosis of crop diseases in Pakistan using fuzzy inference system", *Comput. Electron. Agric.*, vol. 153, pp. 1–11, 2018. doi: 10.1016/j.compag.2018.07.034.
20. S. Hansun and J.C. Young, "Predicting LQ45 Financial Sector Indices using RNN-LSTM", *J. Big Data*, vol. 8, no. 1, p. 104, 2021. doi: 10.1186/s40537-021-00495-x.

INFORMATION ON THE ARTICLE

Bintang Raharja, Multimedia Nusantara University, Tangerang, Indonesia, e-mail: bintang.raharja@student.umn.ac.id

Elfajar Bintang Samudera, Multimedia Nusantara University, Tangerang, Indonesia, e-mail: elfajar.bintang@student.umn.ac.id

Ferry Lay, Multimedia Nusantara University, Tangerang, Indonesia, e-mail: ferry.lay@student.umn.ac.id

Seng Hansun, ORCID: 0000-0001-6619-9751, Multimedia Nusantara University, Tangerang, Indonesia, e-mail: seng.hansun@lecturer.umn.ac.id

ЕКСПЕРТНА СИСТЕМА ВИЯВЛЕННЯ ДЕПРЕСІЇ У ПІДЛІТКІВ / Б. Рахарджа, Е.Б. Самудера, Ф. Лей, С. Хансун

Анотація. Депресія (великий депресивний розлад) є поширеним і серйозним медичним захворюванням, яке негативно впливає на самопочуття, на те, як думаєте і як дієте. На щастя, це піддається лікуванню. Депресія викликає почуття смутку та/або втрату інтересу до діяльності, яка колись приносила насолоду. Це може призвести до різноманітних емоційних і фізичних проблем і знизити здатність людини функціонувати на роботі та вдома. Цей розлад часто трапляється у підлітків, оскільки їхні емоції більш нестабільні. У них також не так багато шансів проконсультуватися з психологом і лікарем. Завдяки цьому дослідженню створено експертну систему, яка реалізує знання експертів, пов'язаних з депресією, щоб підлітки могли проводити самоперевірку, коли це необхідно. Експертну систему розроблено з використанням методу фактора визначеності для механізму виведення знань. Систему перевірено ітеративно, подібних результати отримано і за допомогою експерта в галузі. Сподіваємося, що система зможе виявити ранні симптоми депресії серед підлітків і мінімізувати негативний вплив, який вона може спричинити.

Ключові слова: фактор визначеності, депресія, виявлення, експертна система, підлітки.

ВІДОМОСТІ ПРО АВТОРІВ

Байрамова Тамілла Аділ кизи,

головний спеціаліст Інституту інформаційних технологій Національної Академії Наук Азербайджану, Баку

Бояринова Катерина Олександрівна,

професор, доктор економічних наук, завідувач кафедри економічної кібернетики КПІ ім. Ігоря Сікорського, Україна, Київ

Гаврилович Марія Павлівна,

аспірантка ІПСА КПІ ім. Ігоря Сікорського, Україна, Київ

Гамідов Галіб,

доктор філософії, керівник департаменту інформаційних технологій «Azerishiq», Баку, Азербайджан

Гуляєв Валерій Іванович,

професор, доктор технічних наук, завідувач кафедри вищої математики Національного транспортного університету, Україна, Київ

Данилов Валерій Якович,

професор, доктор технічних наук, професор КПІ ім. Ігоря Сікорського, Україна, Київ

Дроздович Ірина Геннадіївна,

кандидат технічних наук, старший науковий співробітник Інституту телекомунікацій та глобального інформаційного простору НАН України, Київ

Зайченко Юрій Петрович,

професор, доктор технічних наук, професор кафедри математичних методів системного аналізу ІПСА КПІ ім. Ігоря Сікорського, Україна, Київ

Згуровський Михайло Захарович,

академік НАН України, професор, доктор технічних наук, ректор КПІ ім. Ігоря Сікорського, Україна, Київ

Зіменков Дмитро Костянтинович,

старший викладач КПІ ім. Ігоря Сікорського, Україна, Київ

Іляш Ольга Ігорівна,

професор, доктор економічних наук, професор кафедри економічної кібернетики КПІ ім. Ігоря Сікорського, Україна, Київ

Копішинська Катерина Олександрівна,

доцент, кандидат економічних наук, доцент кафедри менеджменту підприємств КПІ ім. Ігоря Сікорського, Україна, Київ

Корочкін Олександр Володимирович,

доцент, кандидат технічних наук, заступник завідувача кафедри обчислювальної техніки з навчально-методичної роботи КПІ ім. Ігоря Сікорського, Україна, Київ

Кравченко Марина Олегівна,

професор, доктор економічних наук, декан факультету менеджменту і маркетингу КПІ ім. Ігоря Сікорського, Україна, Київ

Курєннов Сергій Сергійович,

доцент, доктор технічних наук, професор кафедри вищої математики і системного аналізу Національного аерокосмічного університету імені М.Є. Жуковського «Харківський авіаційний інститут», Україна, Харків

Кязімов Тофік Гасанага огли,

доцент, доктор філософії з фізико-математичних наук, завідувач відділу Інституту інформаційних технологій Національної Академії Наук Азербайджану, Баку

Мартелл Валерій Валентинович,

аспірант КПІ ім. Ігоря Сікорського, Україна, Київ

Мозговий Володимир Васильович,

професор, доктор технічних наук, завідувач кафедри дорожньо-будівельних матеріалів і хімії Національного транспортного університету, Україна, Київ

Надеран Марьям,

доктор філософії, кафедра математичних методів системного аналізу ІПСА КПІ ім. Ігоря Сікорського, Україна, Київ

Нестерук Ігор Георгійович,

доцент, доктор фізико-математичних наук, провідний науковий співробітник Інституту гідромеханіки НАН України, Київ

Пишнограєв Іван Олександрович,

доцент, кандидат фізико-математичних наук, доцент кафедри штучного інтелекту КПІ ім. Ігоря Сікорського, Україна, Київ

Русанова Ольга Веніамінівна,

доцент, кандидат технічних наук, вчений секретар кафедри обчислювальної техніки КПІ ім. Ігоря Сікорського, Україна, Київ

Святненко Вадим Анатолійович,

старший викладач КПІ ім. Ігоря Сікорського, Україна, Київ

Сільвестров Антон Миколайович,

професор, доктор технічних наук, професор КПІ ім. Ігоря Сікорського, Україна, Київ

Солдатова Марія Олександрівна,

кандидат технічних наук, доцент кафедри інформаційних систем і технологій КПІ ім. Ігоря Сікорського, Україна, Київ

Спінул Людмила Юріївна,

доцент, кандидат технічних наук, доцент КПІ ім. Ігоря Сікорського, Україна, Київ

Стенін Олександр Африканович,

професор, доктор технічних наук, професор кафедри технічної кібернетики КПІ ім. Ігоря Сікорського, Україна, Київ

Трофимчук Олександр Миколайович,

професор, доктор технічних наук, професор Інституту телекомунікацій та глобального інформаційного простору НАН України, Київ

Шевчук Людмила Володимирівна,

доцент, кандидат технічних наук, доцент кафедри вищої математики Національного транспортного університету, Україна, Київ

Шлюнь Наталія Володимирівна,

доцент, кандидат технічних наук, доцент кафедри вищої математики Національного транспортного університету, Україна, Київ

Bintang Raharja,

Informatics Department, Universitas Multimedia Nusantara, Tangerang, Indonesia

Elfajar Bintang Samudera,

Informatics Department, Universitas Multimedia Nusantara, Tangerang, Indonesia

Ferry Lay,

Informatics Department, Universitas Multimedia Nusantara, Tangerang, Indonesia

Pradip M. Paithane,

Research Scholar, Dr. Babasaheb Ambedkar Mararathawada University, Aurangabad, MH, India

Sangeeta N. Kakarwal,

Professor, PES Engineering College, Aurangabad, MH, India

Seng Hansun,

Informatics Department, Universitas Multimedia Nusantara, Tangerang, Indonesia